

APPROVAL SHEET

Title of Dissertation: Developing Novel Tools Toward β -Amyloid-Neuron
Interaction Discovery

Name of Candidate: Natasha Patrice Wilson
Doctorate of Philosophy, 2016

Dissertation and Abstract Approved: _____
Mariajosé Castellanos, PhD
Assistant Professor
Department of Chemical, Biochemical and
Environmental Engineering

Theresa A. Good, PhD
Adjunct Professor
Department of Chemical, Biochemical and
Environmental Engineering

Date Approved: _____

ABSTRACT

Title of Document: DEVELOPING NOVEL TOOLS TOWARD β -AMYLOID-NEURON INTERACTION DISCOVERY.

Natasha Patrice Wilson, Doctorate of Philosophy, 2016

Directed By: Mariajosé Castellanos, Assistant Professor and Theresa A. Good, Adjunct Professor, Department of Chemical, Biochemical and Environmental Engineering

β -amyloid(A β) is the primary protein component of senile plaques associated with Alzheimer's disease (AD) histopathology. Because of A β 's longstanding implication in the initiating events leading to AD pathology in *in vitro* and *in vivo* experimental preparations, it is commonly considered the causative agent of AD. Yet, though well studied, there still exists a lack of consensus concerning A β 's interactions with neurons and resulting alterations in neuronal signaling. We hypothesize that this lack of consensus is due to an incomplete framework for interpreting experimental data and discriminating between different hypotheses for A β -neuron interactions. In our work, we propose two changes to this framework in order to design better experiments to elucidate A β 's interactions with neurons: 1) using computational models to discriminate between different hypotheses of A β -neuron interactions by making predictions and comparing them to experimental data,

and 2) assume a complex intracellular signaling network model instead of a linear pathway hypothesis. By developing our models with these two changes in mind, our results demonstrate the ability of an electrophysiological neuron model to make discriminating predictions under experimentally testable conditions. Our results also show that a complex, intracellular signaling model reveals that 20 years of experimental data collected investigating A β -induced intracellular signaling are not self-consistent. With data that is more consistent internally and with a complex, intracellular network, the methodology we developed has the potential to discriminate between hypotheses of A β -neuron interactions. Finally, we demonstrate, using network analysis, the need to move away from a simple, linear pathway hypothesis toward a more complex system and how the inconsistencies in our dataset collected from the literature could have arisen. We make recommendations of discriminating experiments using path length analysis and our Signal Flow Method that we developed. With further development of these computational tools, we can move closer to designing experiments to identify A β -neuron interactions with greater discriminatory power. With this understanding of A β 's deleterious effects on neurons, better treatments can be designed. Furthermore, these methods could be applied to other misfolded protein (amyloid) diseases, such as Parkinson's disease, or other diseases where a known agent interacts extracellularly via an unknown receptor in neurons to cause cellular dysfunction.

DEVELOPING NOVEL TOOLS TOWARD β -AMYLOID-NEURON
INTERACTION DISCOVERY

By

Natasha Wilson

Dissertation submitted to the Faculty of the Graduate School of the
University of Maryland, Baltimore County, in partial fulfillment
of the requirements for the degree of
Doctorate of Philosophy
2016

© Copyright by
Natasha Wilson
2016

Dedication

*Glory be to the Father, and to the Son, and to the Holy Spirit
as it was in the beginning, it is now and ever shall be,
world without end. Amen. Alleluia. To James and Alice Wilson, “Honor your father
and mother so that you may have a long life in the land that the Lord your God has
given to you.” – Exodus 20:12*

Acknowledgements

First, I would like to thank God through Jesus Christ. I could not have done any of this without His leading, guiding, and wisdom from above. ‘What shall I return to the Lord for all his goodness to me? (Psalm 116:12)’ All I can offer is my life.

To my advisors, Drs. Mariajosé Castellanos and Theresa Good, you both had enough faith and trust in me to allow me to embark on this project. I thank you both for this opportunity and for your constant encouragement.

To my committee members, Drs. Jennie Leach (CBEE), Mark Marten (CBEE), and Ivan Erill (Biological Sciences), I admire you for not only being excellent researchers in your field, but for your willingness to help, to challenge me, and for your graciousness. Special thanks to Dr. Erill from Biological Sciences at UMBC for essentially adopting me into his lab for about a year or two.

Thanks to the CBEE faculty, both those who knew me as an undergraduate and as a graduate student. Thanks for making my tenure here both challenging and rewarding. To the CBEE staff (Denise Kedzierski, Kathryn Mattingly, and Victor Fulda), thanks for always being efficient and kind. Everything always ran smoothly because of your care for your work. Thanks especially to Denise and Victor, and especially for all of our good conversations over the years.

To my fellow graduate students, I wish I could name you all, but it would be a very long list. You have all had some impact, big or small, on me during my time here. I just really want to thank this graduate student community for being so supportive, nurturing, and willing to help in any way possible. Thanks for all of the laughs, tears, 6pm conversations (that took place at many other times during the day), and for sharing your lives with me and with each other. Any time I am surveyed about my graduate school experience, this community tops my list because of how supportive and familial it is. I hope the torch can continued to be passed to the next generation so that many others can have the experience that I did with you all.

To the Meyerhoff Graduate Fellowship program, I would like to thank all those who are in attendance from the program, but most especially Justine Johnson (Assistant Director of the Meyerhoff Graduate Fellowship program) for always being there for me, providing an ear to listen, and being an advocate for students. I do not think you will know on this side of eternity the impact that you have had on many lives.

I would like to express similar sentiments to Dr. Renetta Tull (Associate Vice Provost of Graduate Student Development and Postdoctoral Affairs) and the PROMISE/ BD program. Dr. Tull is a phenomenal woman and I am amazed at the energy she puts into the success of graduate students at UMBC. I also would like to thank Dr. Wendy Carter-Veale (program coordinator) and put a plug in for

Dissertation House – it really is very helpful for making progress on writing a thesis or dissertation, proposal, or journal articles.

To my lab members, both past and present, thank you for all of your help, encouragement, and example. I would especially like to acknowledge Dr. Arundhathi Venkatasubramaniam, Neil Agarwal, and Jonathan Bollinger, and undergraduates that I mentored: Zack Bailey, Stephen Vicchio, and Angela Norton.

I would like to acknowledge the Erill lab in the Biological Sciences Department at UMBC for allowing me to attend and present at their lab meetings and learn from them. I especially would like to thank Patrick O’Neill (soon-to-be Dr. O’Neill as I write this), especially for his help in the Bayes algorithm from my future work section.

I would like to thank the UMBC Psychology Training Clinic for providing needed help at the right time.

To my friends, both near and far, thank you for all of your love and support. I met you all from various places as I show here. Thank you so much very every little thing you have done to enrich my life and make my journey a little brighter. I would especially like to acknowledge my best friend Melissa Vyfhuis, her husband Kevin and her son (my godson) Elijah, and their families, for their consummate support.

To my parents, James and Alice Wilson, I would like to thank to my dad who was and still is a computer nerd and introduced me to the world of mathematics and science. Thanks to my mom for teaching me how to be organized, particularly when it comes to work. Thanks to you both and to all of my family (especially, Celeste, Harry, and Jan Burton, Tamille Hawkins, and Samuel Wilson) for instilling in me the importance of education. I am here because you made that a priority in my life from since I was a little child.

I would also like to acknowledge my deceased relatives and friends, especially my grandfather and mother, Charles and Geneva Jones, my great aunt Val Jones, and my friend Connie Fowler. Thanks for all your prayers and I am praying for you as well.

Table of Contents

Dedication	ii
Table of Contents	vii
List of Tables	x
List of Figures	xii
Chapter 1: Introduction	1
1.1 The Role of β -Amyloid in Alzheimer's Disease Etiology	1
1.1.1 Overview	1
1.1.2 The Amyloid Cascade Hypothesis	4
1.1.3 In vitro studies of $A\beta$ -neuron interactions in primary culture neurons	7
1.2 Computational Approaches for Modeling $A\beta$'s Early Action on Neurons	20
1.2.1 Overview	20
1.2.2 Electrophysiology Models	22
1.2.3 Intracellular Signaling Networks	23
1.3 This work	25
1.3.1 Overview	25
1.3.2 Electrophysiological Model of $A\beta$'s Action on a Neuron	26
1.3.3 Identifying $A\beta$ -Neuron Interactions by Inferring Network Topology from Experimental Data	27
1.3.4 Using Network Analysis to Identify Network Motifs for Experimental Design to Identify $A\beta$ -Neuron Interactions	29
1.3.5 Significance of This Research	30
1.4 Conclusions	33
1.5 References	35
Chapter 2: Modeling the short-time scale dynamics of β -amyloid-neuron interactions.	52
2.1 Introduction	52
2.2: Methods	55
2.2.1 Model Overview	55
2.2.2 Current-clamped Neuron Model	55
2.2.3 Voltage-clamped Neuron Model	57
2.2.4 High $[K^+]$ Membrane Depolarized Neuron Model	58
2.2.5 Ca^{2+} Diffusion	58
2.2.6 Mechanisms of $A\beta$ interactions with neuronal membrane	60
2.2.7 Choice of experimental data used to analyze predictions from the model	62
2.3: Results and Discussion	63
2.3.1 Voltage-clamp simulations in the presence of $A\beta$	63
2.3.2 Current-clamp simulations of a single AP, membrane excitability and $[Ca^{2+}]_i$	68
2.3.3 Simulations of high $[K^+]$ membrane depolarization and intracellular $[Ca^{2+}]$	75
2.3.4 Implications of this computational study	81
2.4 Conclusions	84

2.5 Appendix: Initial Conditions.....	85
2.6 References.....	86
Chapter 3: Toward inferring A β -neuron interactions using CellNOptR: a case study	98
3.1 Introduction.....	98
3.2 Methods.....	102
3.2.1 <i>Model description</i>	102
3.2.2 <i>Statistical analysis</i>	110
3.2.3 <i>Choice of Aβ-neuron interactions</i>	111
3.3 Results and Discussion	114
3.4 Conclusions.....	128
3.5 Future Work	128
3.6 References.....	135
Appendix 3A: Keyword search.....	153
Appendix 3B: A β -neuron interaction lists	154
Appendix 3C: Results from Kruskal-Wallis & Mann-Whitney U tests	159
Chapter 4: Identifying network motifs from network structure: impact on experimental design for inference of A β -neuron interactions	166
4.1 Introduction.....	166
4.2 Methods.....	170
4.2.1 <i>Signal Flow Method</i>	170
4.2.2 <i>Identification of Feedback Motifs Via Path Length Analysis</i>	172
4.2.3 <i>Kinetic Model</i>	172
4.3 Results and Discussion	173
4.3.1 <i>Intrinsic Topological Properties of CA1 Hippocampal Neuronal Signaling Network Challenge the Linear Pathway Hypothesis (LPH)</i>	173
4.3.2 <i>Signal Flow Method is Used to Identify Signaling Motifs Based on Network Topology</i>	181
4.3.3 <i>Kinetic Model of Receptor Trans-activation and Feedback in a Small Hippocampal Network</i>	197
4.3.4 <i>Experimental Rubric Based on Identified Feedback Loop in CA1 Hippocampal Network</i>	206
4.3.5 <i>Network properties of Nodes from Literature-Derived Experimental Data of In Vitro Experiments with Aβ</i>	209
4.4 Conclusions.....	213
4.5 Future Work	214
4.6 References.....	224
Appendix 4A Reaction List	234
Appendix 4B List of Compounds	235
Appendix 4C Reaction Equations.....	237
Appendix 4D Initial Conditions.....	241
Appendix 4E Nodes in CA1 Hippocampal Neuron Not Involved in Feedback Loops.....	242
Chapter 5: Conclusions and Future Work.....	243
5.1 Conclusions.....	243
5.2 Future Work	255
5.3 References.....	256

Appendix.....	259
---------------	-----

List of Tables

Table 1.1 Mechanisms of $A\beta$'s action on neurons observed by various investigators using different $A\beta$ species and aggregation states.

10

Table 1.2: Mechanisms of $A\beta$'s action on neurons observed by various investigators using different $A\beta$ concentrations.

13

Table 1.3: Mechanisms of $A\beta$'s action on neurons observed by various investigators at different timescales.

18

Table 3.1: Description of datasets used for CellNOptR optimization.

105

Table 3.2: Table of $A\beta$ -neuron interactions and “pseudo-controls” tested in this study.

112

Table 4.1 List of nodes involved in feedback loops (positive, negative, and positive/negative) in a CA1 hippocampal signaling network.

195

Table 4.2 Number of feedback loops per path length of nodes measured in literature-derived experiments.

210

Table 4.3 Number of in-, out-, and total degrees for nodes measured in literature-derived experiments.

211

List of Figures

Figure 1.1: A diagram of AD's effect on individuals, caregivers, and the nation.

3

Figure 1.2: A diagram describing $A\beta$ as a trigger for cognitive decline characteristic of AD.

6

Figure 2.1: The effect of $A\beta$ -ion channel and $A\beta$ -membrane interactions on the I_A channel under voltage-clamp conditions.

66

Figure 2.2: Comparison $A\beta$ -induced I_A channel block and membrane conductance increase under current-clamp conditions.

70

Figure 2.3: Effect of $A\beta$ I_A channel block and the membrane conductance increase on basal intracellular $[Ca^{2+}]$.

73

Figure 2.4: The effect of $A\beta$ under membrane depolarized conditions for the $A\beta$ block of the I_A channel and the $A\beta$ -induced membrane conductance increase.

76

Figure 2.5: Intracellular Ca^{2+} levels under high $[K^+]$ membrane depolarized conditions.

79

Figure 3.1: Prior knowledge network of a CA1 hippocampal network with a $A\beta$ node.

104

Figure 3.2: Flow chart for CellNOptR.

109

Figure 3.3: Histogram and box plots of the best objective function for ionotropic mechanisms versus the randomized prior knowledge network (rPKN) from CellNOptR.

116

Figure 3.4: $A\beta$ -ionotropic mechanisms optimized on different dataset sizes and types using CellNOptR.

119

Figure 3.5: Box plots of various A β -neuron interactions tested against the larger and scrambled datasets.

120

Figure 3.6: Single pathway hypothesis versus network as experimental prior knowledge.

124

Figure 3.7: Hypothesis space containing partitions indicating the space in which Boolean network states tend to fall into a particular attractor *ad infinitum*.

133

Figure 4.1 Histograms of the in- and out-degrees of nodes in the CA1 hippocampal neuronal network.

176

Figure 4.2 Example networks – trees, connected network with one cycle and a complex network.

179

Figure 4.3 Signal through selected receptors for an interaction of A β with the integrin receptor.

183

Figure 4.4 Signal through selected receptors for an interaction of A β with the EGF receptor.

185

Figure 4.5 Signal through selected receptors for an interaction of A β with the NMDA receptor.

188

Figure 4.6 Signal through selected receptors for an interaction of A β with the MGLUR7 receptor.

189

Figure 4.7 Signal through selected receptors for an interaction of A β with the LTYPECA channel.

191

Figure 4.8 Percentage of nodes involved in feedback loops in a CA1 hippocampal neuronal network.

194

Figure 4.9 Time-course profiles of PLC and PLC* in hippocampal network from[5].

199

Figure 4.10 Time-course profiles of PKC and PKC* in hippocampal network from[5].

200

Figure 4.11 Time-course profiles of RHO and RHO* in hippocampal network from[5].

201

Figure 4.12 Time-course profiles of ERK and ERK* in hippocampal network from[5].

202

Figure 4.13 Time-course profiles of SRC and SRC* in hippocampal network from[5].

203

Figure 4.14 Proteins in Small Kinetic Model with sign change in derivative.

204

Figure 4.15 Experimental rubric based on feedback in CA1 hippocampal neuronal network.

207

Figure 4.16 Signal through hub protein, Protein kinase A (PKA), given different inputs.

216

Figure 4.17 Signal through hub protein, Protein kinase C (PKC), given different inputs.

217

Figure 4.18 Signal through hub protein, G protein $\beta\gamma$ ($G_{\beta\gamma}$), given different inputs.

218

Figure 4.19 Signal through hub protein, Calmodulin, given different inputs.

219

Figure 4.20 Signal through hub protein, N-methyl-D-aspartate receptor (NMDAR), given different inputs.

220

Figure 4.21 Signal through hub protein, proto-oncogene tyrosine-protein kinase (SRC), given different inputs.

221

Figure 4.22 Signal through hub protein, cyclic adenosine monophosphate response element-binding (CREB) protein, given different inputs.

222

Figure 5.1 Flow chart of general experimental design.

244

Figure 5.2 Flow charts of experimental design using the general approach and with a discriminatory step (Chapter 2).

247

Figure 5.3 Flow chart of discriminatory step for discriminating between various hypotheses of A β -neuron interactions using a signaling network model (Chapter 3).

250

Figure 5.4 Flow chart of integrated methodology for experimentation and hypothesis discrimination.

253

Chapter 1: Introduction

1.1 The Role of β -Amyloid in Alzheimer's Disease Etiology

1.1.1 Overview

Alzheimer's disease (AD) is a neurodegenerative disease that causes learning and memory dysfunction. Approximately 5.3 million Americans are living with AD in 2015[1]. The current healthcare cost associated with AD and other dementias (of which AD is the most prevalent) is \$226 billion dollars and is expected to rise over the next 35 years to \$1.1 trillion dollars[1]. AD is the “sixth leading cause of death in the U.S.” and out of the top ten causes of death is the only one that “cannot be prevented, cured or attenuated”[1]. The histopathological features of AD are senile plaques and neurofibrillary tangles[2]. These senile plaques are found in the extracellular space; while the neurofibrillary tangles are found in the intracellular space. Senile plaques are comprised primarily of a 39-43 amino acid peptide widely known as β -amyloid ($A\beta$); neurofibrillary tangles are primarily composed of hyperphosphorylated tau. AD was discovered in 1907 by Alois Alzheimer, who studied the behavior of two patients who were subsequently found, upon autopsy, to have senile plaques and neurofibrillary tangles in areas of massive neuronal loss[3]. However, it was not until 1984 when Glenner and Wong[4] isolated and characterized the $A\beta$ peptide[4]. It was at this point that $A\beta$ became associated with AD pathogenesis.

AD is a highly complex disease. There are two types of AD, familial and sporadic. Only 5% of AD sufferers have the familial variety of the disease, which is inheritable due to genetic defects in the amyloid precursor protein (APP), presenilin 1 and 2 genes[5]. Familial AD (FAD) gives rise to an early onset of the neurodegenerative processes of the disease (around age 40). The other 95% of cases are sporadic AD, which has a similar symptomatology as FAD, for which inheritable genetic pre-determinants are still under investigation[6]. The etiology of AD remains unknown, but there are a host of genetic, epigenetic and cellular responses that have been implicated in the pathogenesis of this disease.

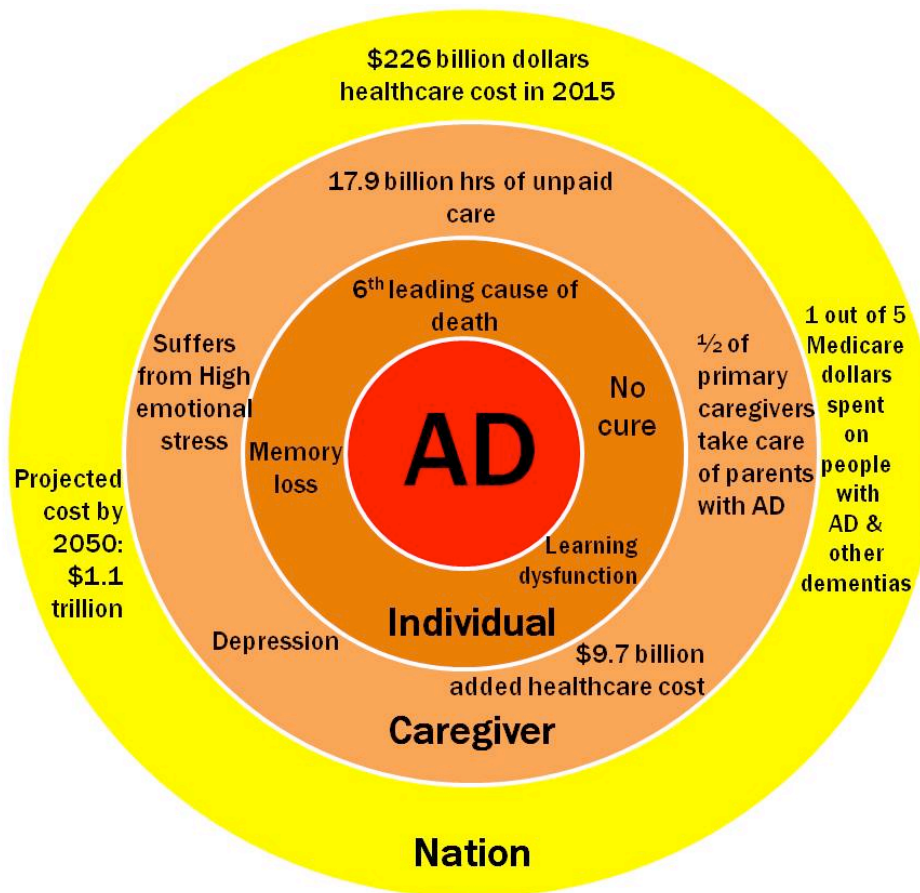


Figure 1: A diagram of AD's effect on individuals, caregivers, and the nation.

Information contain in this diagram from[1].

1.1.2 The Amyloid Cascade Hypothesis

After close to a decade of research, Hardy and Higgins first proposed the Amyloid Cascade Hypothesis (ACH) as an explanation for the pathogenesis of AD[7]. The ACH posits that an over-accumulation of A β occurs due to mutations in the Amyloid Precursor Protein (APP). In this seminal paper, Hardy and Higgins describe the proteolytic cleavage of APP that produces A β . Once formed from APP, A β , in the extracellular space, adversely interacts with neurons, which causes aberrant intracellular signaling. In 2002, Hardy and Selkoe offered a more refined and detailed presentation of the ACH[8], which especially included more genetic evidence that mutations in presenilins 1 and 2 result in the over-accumulation of A β . These presenilin genes directly affect γ -secretase, one of two proteins responsible for cleaving A β from APP, resulting in altered APP metabolism and overproduction of A β [8]. Hardy and Selkoe go on to describe the cascade begetting a number of detrimental processes, including apoptosis. This aberrant signaling also produces hyper-phosphorylated tau. As cell death takes place, this causes widespread neuronal dysfunction across the affected brain areas. Though the development of the ACH stems from discoveries about the etiology of familial AD, researchers have generally assumed a similar etiology for sporadic case of AD. However, in the cases of sporadic AD the initiating cause of the disease progression is still under investigation. There are multiple proposed etiologies, primarily having to do with age-related A β accumulation and clearance[5]; in some cases, having to do with the possible effect of

head injury[9]. Therefore, the ACH has become the prevailing hypothesis for A β 's role in AD etiology, though it is not without its opponents[9-14].

A constant challenge to the ACH has been A β 's central causative role. This is due primarily to a lack of correlation between plaque burden and cognitive impairments[8-11, 13-16]. It has been observed that changes senile plaque and even neurofibrillary tangle accumulation occur decades prior to symptoms of cognitive decline and cellular death[16]. Therefore, researchers have proposed refinements to the ACH in order to reconcile A β 's seemingly disjointed role in disease progression. For example, it has been postulated that the presence of highly toxic, oligomeric A β species may explain the discrepancy between plaque burden and cognitive decline[8, 17]. Difficulties in isolating and identifying these soluble oligomeric toxic structures of A β has made it difficult to examine this refinement of the ACH[17]. Another proposed refinement to the hypothesis states that A β "is necessary, but not sufficient"[16] for AD pathogenesis, and that other processes such as ageing, reactive oxidation and tauopathies work in concert with A β in AD progression[11, 14-16, 18]. However, A β may act as a trigger for these processes[16], in which case the failure of many A β drug therapies could be due to not treating the patients early enough to avoid the trigger initiated by A β . This is a therapeutic challenge since the early stages of the disease are not readily identifiable and the early mechanisms of A β 's actions on neurons still remains unknown. Despite the many challenges in proving the Amyloid Cascade Hypothesis, this hypothesis was the catalyst of continued efforts to identify A β 's specific role and its mechanism of action on neurons.

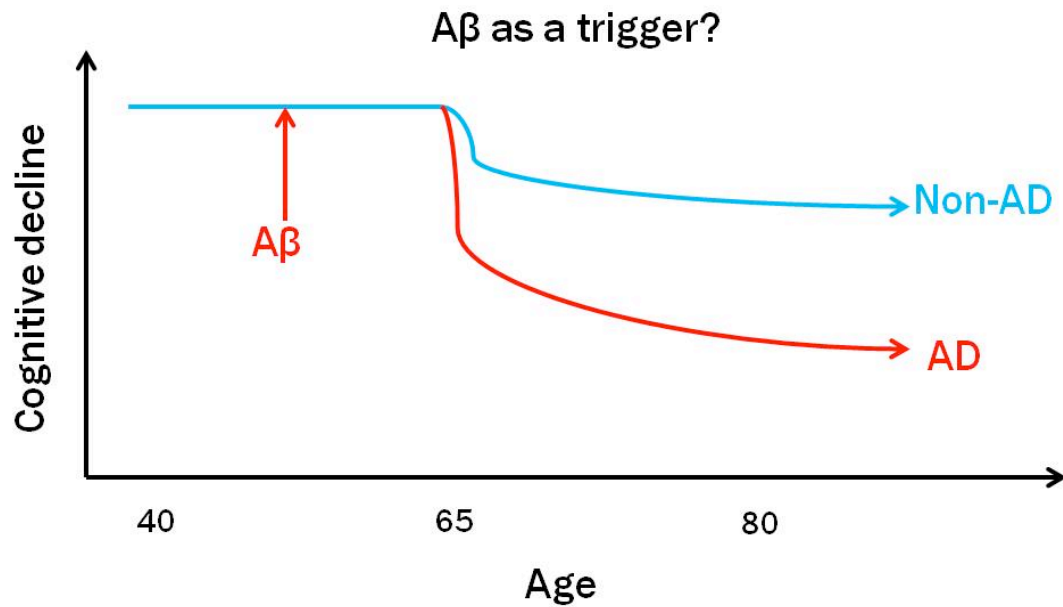


Figure 2: A diagram describing A β as a trigger of cognitive decline characteristic of AD. Karran et al[16] propose that A β may not be the primary initiator of AD progression, but rather acts as a trigger for cognitive decline. When other potential factors, such as aging, environment, presence of reactive oxidation species, etc, are present, and A β levels reach a certain threshold in the brain, A β triggers the pathology of AD, particularly cognitive decline.

The majority of research efforts since this seminal paper[7] has used the Amyloid Cascade Hypothesis as a *de facto* hypothesis for experimental programs. In particular, *in vitro* experimentation focuses almost exclusively on identifying A β 's early action on neurons. In challenging the veracity of the ACH, some researchers put forth the objection to the clinical relevance of an *in vitro* system[8, 14, 16]. In general, the concern is that the concentrations used for A β in *in vitro* experiments are not biologically relevant. While concentrations of A β in the brain tend to be in the picomolar range, experimentalists have used concentrations between 1nM-100 μ M[19, 20]. These higher concentrations may cause the acute effects of neurotoxicity observed, but because they are not physiologically relevant concentrations, the results may not translate well to the *in vivo* system[16, 18]. Another concern with *in vitro* experiments is time scale. AD progression takes place over decades, whereas *in vitro* experiments demonstrate neurotoxicity and neuronal death in a period of hours to days. However, the need for understanding the results of *in vitro* experiments is becoming more apparent with the newer refinements in the ACH. If A β is triggering a litany of other processes early on in the disease process, then it is likely that understanding the short-time scale interaction of A β with the neuron might open up other avenues for drug therapy design early in the disease progression. Though oft challenged, *in vitro* experiments do provide evidence of A β 's neurotoxic effects and continues to provide evidence for the ACH.

1.1.3 In vitro studies of A β -neuron interactions in primary culture neurons

In order to elucidate the underlying mechanisms of A β -induced neurotoxicity proposed by the ACH, researchers have observed changes in intracellular processes using *in vitro* experiments on neurons exposed to A β . More than two decades worth of *in vitro* experiments have not produced a consensus on a mechanism of action for A β [17, 18, 21-23]. A multi-factorial problem, there are multiple potential factors for this non-consensus: different A β -species and aggregation states used by various laboratory preparations, a large A β concentration range, and differing timescales of A β exposure to cells prior to measurement of cellular processes. However, with these factors potentially confounding the comparison of results from reports in the field, one could conclude that if it is a mixture of these factors that are providing divergent data that within any particular factor there might still be some consensus. However, this is not what is evidenced by the data from the literature. Instead, when the data are collected and categorized by the aforementioned factors, there still exists a non-consensus even within the factors. Therefore, there must be another reason for this non-consensus, which will be raised toward the end of this section.

1.1.3.1 A β species and aggregation state

A β is a 39-43 amino acid peptide and it exists in the brain and cerebral spinal fluid as a mixture of peptide lengths[21]. It is believed that A β (1-40) is the most abundant peptide length found in the brain and then A β (1-42). A β (1-42) is considered the more toxic of the two species (1-40 and 1-42) and that an increase in the ratio of A β (1-42):A β (1-40) may trigger neurotoxicity in the

brain associated with AD. Other species are used by experimentalists, on occasion: A β (25-35), A β (1-38) and A β (1-39). A β (25-35) is used because it is believed that the active portion of the peptide is found within these 10 amino acids. With respect to aggregation state, fibrils have been primarily used because their preparation and characterization are well-defined, and it is mature fibrils that make up the plaques that are identifiable upon autopsy[3]. However, monomers and various types of oligomers are also used. Monomers are usually considered not to be neurotoxic, and in some cases may be neuroprotective[24]. On the other hand, both oligomers and fibrils have shown neurotoxicity in neuronal cultures with oligomers being more neurotoxic than fibrils[17]. The solubility and multi-meric state of oligomers, makes stable oligomers difficult to reproducibly prepare and to characterize in experimentation. Here, experiments in which each species type was used will be discussed, with aggregation state being discussed within as a subtopic.

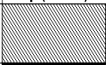

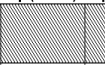
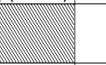
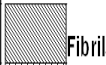

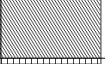








Categories of mechanisms	A β (1-40)	A β (1-42)	A β (1-38)	A β (1-39)	A β (25-35)	References	
Ion channel-mediated						[27-32]	 Fibrils
Receptor-mediated (non-ionic)						[33-36]	 Oligomers
Membrane-mediated						[37]	 Both
A β ion channel/pore						[38]	
Other (cholesterol, GSK-3 β , PIP2, etc)						[41-53]	

Table 1.1: Mechanisms of A β 's action on neurons observed by various investigators using different A β species and aggregation states. This table shows the different mechanisms that have been observed in experiments using A β (1-40), A β (1-42), A β (1-38), A β (1-39), and A β (25-35) species; fibrils (diagonal-lined box), oligomers (checkered box), or both (black box). No category of mechanisms has a consensus of all of the species types or aggregation states.

In general, the mechanisms of A β -neuron interactions proposed in the literature can be placed into five categories: ion channel-mediated, receptor-mediated (excluding ion channels and ion-conducting receptors such as NMDA receptors), membrane-mediated, A β ion channel or pore, and other (**Table 1.1**). Various laboratories have used A β (1-40), A β (1-42), A β (25-35), A β (1-38), and A β (1-39) species in their experiments. In the first decade of research in this area, controlling A β structure and aggregation state was difficult. With fibrils being the more stable aggregate, these were used most often in experimental preparations. In the next decade, more sophisticated techniques for isolating particular structures of A β , as well as isolating soluble oligomers, were developed[25]. The greater availability of synthetic A β peptides of various lengths also added in greater control over A β species. The species used in the first decade of research were primarily A β (1-40), A β (1-42) and A β (25-35). In the second decade of research, more emphasis was placed on the greater toxicity of A β (1-42) than A β (1-40)[26], and so A β (1-42) was used predominantly, followed by A β (1-40). So, for example, in **Table 1.1**, it would make sense, given the predominant use of A β (1-40) and A β (1-42), especially in the second decade of research, the oligomeric states are observed only for A β (1-40) and A β (1-42). In the second decade of research, other A β species, such as A β (1-39) and A β (1-38), are not used with much frequency.

Of the five categories of mechanisms in **Table 1.1**, four of them have been observed by different groups as potential mechanisms by which A β (1-

40) and A β (1-42) interacts with neurons. Other species, which are used less in most preparations (A β (1-38), A β (1-39), A β (25-35)) each have been observed in only one category of mechanisms. Again, this is likely due to the infrequent use of these species in experimental preparations. Ion channel-mediated mechanisms in experimental preparations using fibrillar A β (1-40)[27-31], A β (1-39)[27] and A β (25-35)[29, 32], and both fibrillar[30, 32] and oligomeric A β (1-42), have been observed. The species and aggregation states used in cases where a receptor-mediated mechanism was postulated were A β (1-40)[33-35], A β (1-42)[35, 36] fibrils and oligomers. A β (1-42)[37] oligomers were used in preparations where membrane-mediated mechanisms were hypothesized. A β (1-40)'s[38] action on neurons has been postulated, also, through a A β channel or pore. This mechanism has also been observed often in acellular membranes[39, 40]. Other mechanisms have been reported involving A β (1-40), A β (1-42), A β (1-39), and A β (25-35). Some of these mechanisms have involved changes in glucose uptake[41], attenuation of A β -related neurodegeneration via a GSK-3 β pathway[42, 43], impairment of long-term potentiation[44], increased transcription factor[45] and gene expression[46], among others[20, 47-53]. The variety of mechanisms amongst experimental preparations involving different A β species and aggregation states indicates that it is unlikely that the lack of consensus on A β -neuron interactions is due to the use of different species and aggregation states of A β .

Categories of mechanisms				References
	nM	Low μ M	High μ M	
Ion channel-mediated				[27-32]
Receptor-mediated (non-ionic)				[34,35,59;60-62]
Membrane-mediated				[37, 65, 66]
A β ion channel/pore				
Other (cholesterol, GSK-3 β , PIP2, etc)				[36,41-44, 46, 47, 50-53, 63, 64]

Table 1.2: Mechanisms of A β 's action on neurons observed by various investigators using different A β concentrations. This table shows the different mechanisms that have been observed in experiments using nanomolar, low and high micromolar concentrations of A β . Each grey box represents the proposed hypothesis for A β -neuron interactions based on results from experimental data at each concentration range. In this figure, the specific aggregation states are not identified since A β concentrations are reported for the monomer, and the active states are not reported. The data here suggest possible promiscuity of A β , as at least three different mechanisms (ion-channel-mediated, receptor-mediated, and other) are proposed across the concentration range.

1.1.3.2 Concentration

The concentration of A β monomer used in experiments ranges, in general, between 1nM-100 μ M[19, 20]. Picomolar concentrations of A β have been shown to act positively on synapses[54, 55]. There have been questions about the physiological relevance of high micromolar concentrations of A β [16]. Rarely, or if at all, are the concentration of active aggregates reported. Therefore, though the intended aggregate might be fibrils or oligomers, it is likely that all three states: monomer, oligomers and fibril, exist in the preparation in equilibrium[56, 57]. Though there are mechanisms that are observed across the concentration range (ion channel-, receptor-mediated, and other) (**Table 1.2**), this would be more suggestive of the promiscuity of the A β peptide, rather than a consensus on its mechanism of action. It has been suggested that A β might act in a more promiscuous manner on neurons, possibly affecting multiple receptors and/or receptor-types[17, 58].

For preparations in which fibrils were the intended species, across the concentration range, ion channel-mediated mechanisms are observed[27-32]. However, receptor-mediated mechanisms are also observed for fibrils in the nanomolar[34, 59] and low micromolar[35, 60-62] range. Other mechanisms have also been proposed for experiments involving fibrils in the low[36, 41-43, 46, 47, 52, 63] and high micromolar range[36, 41, 50, 53]. With respect to

preparations in which oligomers were the intended species, for the nanomolar range, other mechanisms have been observed. For example, A β oligomers have been shown to inhibit long-term potentiation[44] and cause PAK signaling deficits[64]. At low micromolar concentration, A β oligomers act via membrane-mediated mechanisms according to reports by various investigators[37, 65, 66]. Finally, at high micromolar concentrations, oligomers have been shown to interact with neurons via receptor-mediated mechanisms, such as interactions with the cellular prion protein[61]. Again, noting that these preparations do not necessarily represent a pure concentration of each aggregate, these data do not suggest a consensus, but possibly give credence to hypotheses describing the promiscuity of A β .

1.1.3.3 Time scale

The timescales for experiments done with A β vary widely from milliseconds to days (**Table 1.3**). This is strongly a function of the type of experimental tools being used and the outcome the experimentalist desires to measure. Many investigators are interested in the link between A β and neurotoxicity, and so cell viability measurements are frequently employed. The neurotoxic effects of A β take place within hours to days[67, 68] .

The temporal progression for most signaling events starts with the extracellular cue acting on a receptor or channel. This occurs during the milliseconds to seconds time frame[69]. In the literature data, A β -induced

mechanisms, such as ion channel-mediated mechanisms[28-32] and receptor-mediated mechanisms[62, 70-72] have been observed at this time scale.

Receptor-[33, 62], membrane-mediated[37, 73] and other mechanisms[43, 44, 46, 53, 71] have been reported in the literature to occur at the seconds to days timescale; however, at times greater than 60 minutes, changes in gene expression will occur, resulting in changes in protein expression[74]. This is significant when analyzing these data from the literature on A β and attempting to determine the initiating event. At the shorter time scale (< 60 minutes), it is possible to connect signaling events with the initial extracellular cue, albeit not a trivial task due to the complexity of intracellular signaling. However, as the timescale moves into hours or days, genetic and even epigenetic changes occur that can change the state of the neuron from the original state[18]. This may be a result of the initiating event, but not necessarily directly correlated, as a host of other processes may take place simultaneously. Therefore, the closer in time that a signaling event is measured to the initiating event, the more likely that the measured event is attributable to the initiating event[69]. With that being said, the data collected on the longer timescale (> 60 minutes) may not correlate directly to the hypothesized initiating event because what is being measured is the result of downstream processes (gene and protein expression changes). But even for shorter timescale (< 60 minutes) data, there is still a lack of consensus on A β

mechanism of action, although ion channel-mediated mechanisms seem to predominate.



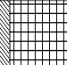



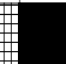
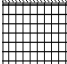

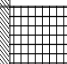
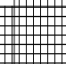


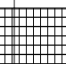
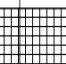
Categories of mechanisms	ms	secs	mins	hrs	days	References	
Ion channel-mediated						[28-32]	 Fibrils
Receptor-mediated (non-ionic)						[33, 62, 70-73]	 Oligomers
Membrane-mediated						[37, 73]	 Both
A β ion channel/pore							
Other (cholesterol, GSK-3 β , PIP2, etc)						[43, 44, 46, 53, 71]	

Table 1.3: Mechanisms of A β 's action on neurons observed by various investigators at different timescales. This table shows the different mechanisms that have been observed in experiments at different timescales of A β incubation time, again, with fibrils (diagonal-lined box), oligomers (checkered box), or both (black box). No consensus is observed across the timescales.

As this discussion shows, there are factors in the experiments that are controllable. Each laboratory, in preparing their experiments, chooses these factors differently. It is possible that these non-standardized experimental preparations each contributes to the lack of consensus, but are not the primary factors. We propose that methods for discriminating between hypotheses, especially given a complex system, is the missing factor which could bring consensus to the widely disparate data in the literature.

Because intracellular signaling does not occur as a series of linear pathways, but rather as a highly connected network of interacting proteins[75], many of the proteins being measured in the field are interconnected. This interconnectedness means that a significant number of proteins in a neuronal signaling network can receive a signaling from multiple pathways. It is important, therefore, to explore areas of signaling that are discriminatory. By utilizing computational tools, we can explore these systems, and their associated data, *in silico* and determine the best experimental methods that would allow for discrimination between hypotheses, whether *a priori* or *a posteriori*. We will do this, first, *a priori* by recreating, *in silico*, experimentally testable conditions and discriminating between hypotheses by testing the model's results against literature-derived data. We call this *a priori* because the assumption about A β -neuron interactions *in silico* are made beforehand (*a priori*), following the same methodology as would the experimentalist. Secondly, we will do this *a posteriori* by inferring A β -neuron interactions from literature-derived data on a complex system. This is *a posteriori* because we are inferring A β -neuron interactions from the data. Here, we also depart from a simplistic, linear view of intracellular

signaling in order to embrace the actual complexity of the system. In our final analysis, we attempt to justify this departure. In the next section, we will describe in greater depth the computational approaches available and the rationale for our computational strategy.

1.2 Computational Approaches for Modeling A β 's Early Action on Neurons

1.2.1 Overview

Computational and mathematical modeling has been introduced to the biological world, allowing for the exploration of the complex mechanisms underlying biological processes. This type of modeling allows for what could be deemed *in silico* experimentation. The interface between modeling and experiments will always be a dynamic one within the field of biology, whereby experimental results are needed in order to build, refine and test the model and its predictions. The mathematical and computational tools for modeling are almost as varied as the types of systems to be modeled.

When designing a mathematical model, the complexity of the system, the spatial and temporal details of the system, the computability and computational expense of the proposed mathematical framework are typically taken into account. Beginning with the fullness of spatial and temporal complexity, partial differential equations can be used in order to simulate both the spatial and temporal changes in

metabolite concentration or protein activity, for example[76, 77]. Ordinary differential equations are oft employed when little to no spatial information is required or available for use in order to simulate temporal changes[76-78]. These two methods mentioned so far, depending on the complexity of the system, may require many parameters that have to be experimentally determined under specific conditions. This is problematic as the size of the system increases, such as when modeling complex systems.

There are other modeling paradigms that allow for an increase in model size without an increase in the number of parameters. These modeling paradigms lose temporal detail or are without it at all. Boolean modeling assumes that each component of a system can take on a state value, usually on (=1) or off (=0)[78, 79]. Then, a transfer function is created (a linear combination of the input variables) that makes a prediction about the current state value of a set of components from the previous state of the inputs. This methodology has been used for modeling intracellular signaling because of the lack of need for parameters, and because the activity of intracellular proteins can be approximated to be on/off (Hill kinetics). Flux balance analysis makes an assumption about the system being at steady state and estimates the flux of (or the rates of) reactions via a global, constrained optimization[77, 80]. Again, because of the steady-state assumption, the number of parameters are reduced, but not absent as thermodynamic data are widely used as constraints on reaction fluxes. In addition, flux balance analysis is more compatible with metabolic modeling than modeling intracellular signaling because flux

information through pathways in metabolism can be constrained via conservation of mass[81]. However, intracellular signaling consists of reversible changes in the state of a protein, which is neither accumulated nor depleted. Thus, it is of greater importance to predict the state of a signaling protein (whether it is activated or inhibited) than to predict the flux of a signal through the pathway. Finally, topological analysis requires only knowledge of the components and their interacting partners in order to analyze the possible paths that could be traveled through chemical space[75, 82]. Choosing an appropriate modeling schema and its implementation requires a detailed understanding of the underlying system and experimental data either for training, testing, and/or verification of the model's predictions.

The follow sections will describe some of the modeling paradigms used to model A β -neuron interactions.

1.2.2 Electrophysiology Models

In 1952, A.L. Hodgkin and A.F. Huxley published their seminal paper describing a mathematical model for the membrane conductance in the giant axon of a squid[83]. This mathematical formulation, borrowed from the mathematics of electrical circuit design, has since been used in electrophysiology to model and predict membrane conductances due to various types of ion channels present in biological membranes[84]. There having been few computational models that have examined the mechanisms of A β -neuron interactions, and they have mostly been electrophysiological models of the Hodgkin and Huxley type[85-87]. These models primarily focused on the interaction between A β and the fast-inactivating potassium

channel[85-88] or a $A\beta$ pore[89]. They also focus on excitability of neurons due to $A\beta$, which means they modeled only one type of electrophysiology experiment – current clamp. In a current-clamp experiment, the current applied to a neuron is held constant while the change in voltage across the neuron is measured. Once a threshold current is applied, an action potential (or several) occurs. The strength of the applied current needed to evoke an action potential and the frequency of these potentials are what determine the neuron’s excitability, with and without the presence of $A\beta$.

In **Section 1.3.2**, we describe how our work with an electrophysiological neuronal model expands on work done in this area in order to test multiple $A\beta$ -neuron interactions under three experimentally testable conditions.

1.2.3 Intracellular Signaling Networks

In 1970, Martin Rodbell won the Nobel Prize in physiology or medicine in 1994 for his discovery of G-proteins[90]. This began the era of research into intracellular signaling. From his simplistic, three component model of G-protein signaling, the field advanced to multi-component models with more complex interactions such as cross-talk and feedback. A well-known example of such a model is the Kholodenko MAPK pathway[91], a nine-component pathway with 6 feedback loops. With the advent of the proteomics era and high-throughput experimentation, in less than a decade the number of components in a model of intracellular signaling had increase 10-100 fold[75]. Now, there is enough experimental data to construct,

complex, systems-level models, rather than single pathways, for intracellular signaling.

Over the past 15 years, investigations into A β 's effect on intracellular signaling began to predominate the literature. The search had begun for a pathway to target pharmacologically in order to attenuate or treat AD. As this data became more abundant, the number of hypotheses for A β -neuron interactions also began to increase. It would appear that A β has effects on multiple pathways, instead of through a single pathway[17, 58]. In order to better understand the potential pathways that A β could affect, models of intracellular signaling have been used.

To date, there have been no reports of using intracellular signaling network models to identify A β -neuron interactions. Of reports on intracellular signaling networks used in AD research, AlzPathway[92] and AlzPlatform[93] stand out as highly comprehensive databases of information on AD. However, neither of these databases is used to bring consensus to nor to identify A β -neuron interactions based on known intracellular pathways in neurons and literature-derived experimental data.

In **Sections 1.3.3**, we describe how we used a CA1 hippocampal neuronal signaling network to attempt to infer A β -neuron interactions that would explain the data found in the literature. In **Section 1.3.4**, we describe how we use this network to identify signaling motifs, their potential impact on experimental design, and interpretation of available experimental data in the literature.

1.3 This work

1.3.1 Overview

The work of this dissertation entails the development and evaluation of computational tools that were designed to identify A β -neuron interactions. Developing and utilizing such tools allows us to generate and test hypotheses of a complex system, and to identify potential confounding factors in an experiment so as to improve experimental design. The goal of this work was to produce experimentally testable results from various simulations such that, once tested, would provide experimental data that could discriminate between hypotheses of the A β -neuron interactions. Discrimination between hypotheses is the key. Currently, experiments are being designed and tested in a manner in which each investigator might prove his or her hypothesis (and thereby reject the null hypothesis of his or her experiment) but does not necessarily confirm or reject the results of another laboratory (see **Section 1.1.3**). This has left the field full of experimental data from *in vitro* experiments without convergence or consensus. Since the first formulation of the Amyloid Cascade Hypothesis, the results of *in vitro* experiments have fueled the conviction that A β is directly toxic to neurons, but those same experiments have failed to neither lead to a consistent mechanism of action for A β responsible for its toxicity nor yield actionable targets for therapeutic strategies.

In order to accomplish the aforementioned goal, it was necessary to bring together the current literature data appropriate for the type of computational models available. Then, the approach was taken to develop further and/or utilize already compiled computational algorithms suitable for the type of modeling required. This was to avoid re-inventing the wheel and instead either re-purposing the model to give the experimentally testable outputs required or applying an algorithm developed for one application to another, more complex problem. Subsequently, relevant hypotheses were tested to demonstrate the feasibility of utilizing each tool. For each tool, there were complications and drawbacks to their usefulness toward identifying A β -neuron interactions. However, in no case was the computational model proven insufficient for the applied problem, but rather that the modeling program was severely data-limited.

1.3.2 Electrophysiological Model of A β 's Action on a Neuron

In this work (found in **Chapter 2**), an electrophysiological model neuron[86] was used to test A β -neuron interactions under three experimentally testable conditions. These experimental conditions are: current-clamp, voltage-clamp and high potassium membrane depolarization. These are three typical experimental designs for electrophysiology experiments. As discussed in **Section 1.2.2**, most electrophysiology models of neurons used to test A β -neuron interactions focus on modeling current-clamp experiments because of the action potential. The shape and frequency of action potentials are extremely important for fast inter-neuronal communication. However, the other two types of experiments, voltage-clamp and high potassium membrane

depolarization, are also used in the area of electrophysiology, in general, in order to identify and study the dynamics of channel opening and closing. This information is important, especially the dynamic information of channel opening and closing from voltage-clamp experiments, because changes in those dynamics in the presence of another compound, such as A β , can provide a detailed mechanism for its action on an ion channel and/or the membrane. Being able to model these three different experimental designs also provides various means of discriminating between the potential effects of A β on a neuron (pending that A β interacts either with an ion channel or the membrane) in well-understood, experimentally testable ways. In this work, we were able to identify the high potassium membrane depolarization experiment as being the most discriminatory of the three experimental conditions simulated for two common hypotheses of A β -neuron interactions. Though there were some observable differences in the results from simulations of the other experimental conditions, these differences were not able to distinguish one mechanism from the other.

1.3.3 Identifying A β -Neuron Interactions by Inferring Network Topology from Experimental Data

The aim of this work (found in **Chapter 3**) was to identify A β -neuron interactions by inferring network topology from literature-derived *in vitro* experimental data with primary culture neurons exposed to A β . This work was a departure from the electrophysiological neuronal model in order to utilize data that had been collected in the field on the activity of proteins involved in intracellular

signaling. In order to accomplish this aim, CellNOptR[94] was utilized. CellNOptR is a reverse engineering algorithm that infers network topology from a prior knowledge network[94] and experimental data. A prior knowledge network contains all of the information about interacting pairs of proteins involved in intracellular signaling. CellNOptR uses experimental data to test different network configurations using Boolean logic in order to make predictions about the state of proteins in the network. The state of a protein is determined by a Boolean function, which is a function of the state of its adjacent inputs that takes on a value of either 0 (off) or 1 (on). These predicted values of the state are compared to the normalized experimental data to determine which network configuration best describes the data. The prior knowledge network for this work was a CA1 hippocampal neuronal network[95]. CA1 hippocampal neurons are the neuronal population most affected in AD. Therefore, this network was most applicable to the system.

Again, discrimination between hypotheses is necessary here for testing multiple hypotheses for how A β could potentially interact with a neuron. Different A β -neuron interactions were included in the prior knowledge network prior to inputting the network into CellNOptR. In this way, the results from CellNOptR for each hypothesis could be compared to those of another hypothesis. The hypothesis with the best fit to the data would be the most likely candidate for further study. Therefore, consensus could be found by placing the experimental data in the proper context of its more complex, interacting system. In this work, we collected data from over the past two decades of *in vitro* experimentation on A β 's early action on

neurons. We found in using CellNOptR to discriminate between different hypotheses of A β -neuron interactions utilizing a CA1 hippocampal neuronal signaling network that the data are not self-consistent. Many of the data points collected in the literature thus far have been collected from areas of the network that are not discriminatory due to their presence in multiple signaling pathways and/or in network motifs, such as feedback loops. This is discussed in greater detail in the work done in **Chapter 4**.

1.3.4 Using Network Analysis to Identify Network Motifs for Experimental Design to Identify A β -Neuron Interactions

The goal of this work (found in **Chapter 4**) was to demonstrate that the complexity of the CA1 hippocampal network precludes the use of a linear pathway hypothesis for A β 's action on neurons. At the cellular level, the intracellular signaling landscape is quite complex. Each protein exists within a particular network context; which determines, along with the kinetics of the system, the activity of that particular protein. On the one hand, a linear pathway hypothesis would assume that a protein has a single modulator and in turn modulates the activity of only one other substrate. On the other hand, a protein within a complex network may be modulated by multiple proteins, may modulate more than one substrate, and/or be involved in feedback or feedforward mechanisms[69, 75]. The cellular contexts in both of these cases are different for each protein. In this work, we utilize network analysis tools, such as path length analysis, signal flow, and counting feedback loops, to demonstrate that the linear pathway hypothesis insufficiently describes the cellular context for many proteins in a CA1 hippocampal neuron[95]; in particular, for those proteins

commonly measured in *in vitro* experiments aimed at identifying the mechanisms of A β -neuron interactions. In this work, we assessed general network properties of a CA1 hippocampal neuronal network to determine that a linear pathway hypothesis would be insufficient to describe the cellular context of most proteins in the network. Then, we developed tools to be used to design discriminatory experiments, providing the necessary information about the cellular context of a particular protein in the network. The Signal Flow Method provides an approximate time-course behavior of individual proteins given a particular set of inputs. Path length analysis allows for determining the number and type of feedback loops in which a particular protein participates. Knowing this information prior to designing an experiment can aid in either choosing the number of time points to collect, as in the case of proteins in feedback loops, and choosing the right sets of proteins to measure given a particular set of inputs.

1.3.5 Significance of This Research

Our goal in the work of this dissertation was to provide tools for improving experimental design toward finding consensus on A β 's early action on neurons. In this dissertation, we revealed two primary issues leading to this lack of consensus in the data from *in vitro* experimentation in this field: the need for methods with discriminatory power to distinguish between hypotheses from experimental results and the need to move away from a linear pathway hypothesis toward a complex, systems-level network to describe the underlying neuronal system. We proposed that computational modeling be a solution for both of these issues; for the first issue, the

model's predictions for each hypothesis can be compared to experimental results in order to select the hypothesis that best describes the data. The computational model also allows for further refinements in the understanding of the system to be made, which can better inform experimental design. Our work in **Chapters 2 and 3**, were toward demonstrating the discriminatory power of each computational model on literature-derived data on A β 's action on neurons. For the second issue, in **Chapter 4**, we used a computational model of a CA1 hippocampal neuron to demonstrate the inadequacy of a linear pathway hypothesis to fully describe signaling in neuronal populations used in *in vitro* experimentation, and developed tools to design more discriminatory experiments. Therefore, such a model can be used as an alternative set of prior knowledge to inform hypothesis generation and experimental design.

In developing these tools, another goal was to make them as generic as possible such that they might apply to other similar problems and systems. In **Chapter 2**, the neuronal model adapted from the Good and Murphy model[86], can be used to compare any ion channel or receptor-based mechanism present in a hippocampal neuron under electrophysiology experimental conditions. Even the type of neuron can be changed by the identification of the types of ion channels and ion-conducting receptors that exist in its membrane, adjusting the capacitance, and perhaps also the surface area of the membrane. This modeling methodology may be applicable to other neurological diseases such as Parkinson's disease[96], a disease which may have similar misfolded protein (amyloid)-related etiology as Alzheimer's disease[97, 98].

In **Chapter 3**, the algorithm that was used, CellNOptR[94], can take as inputs any signaling network and associated data, and hence why we found it to be applicable to our system. Given an intracellular signaling network, an associated dataset, and hypotheses for how a given molecule or protein interacts with that network, ideally one should be able to discriminate between hypotheses based on goodness-of-fit to the data (objective function). And this was the subject of our work in **Chapter 3**.

In **Chapter 4**, again, our goal was to create tools that were generic to an extent. The Signal Flow Method and path length analysis could all be done with any network in which the adjacency matrix was available. Given a list of interactions, in the proper format, we created an algorithm that could populate the adjacency matrix needed for these methods. These methods are especially useful for large networks in which following the signal propagation through the various proteins in the network would be difficult to do by human intuition alone. Also, we were able to use path length analysis to identify all feedback loops that started and ended with the same protein. This could be useful for many types of networks as feedback is a common motif in many real networks[75, 82, 99]. The Signal Flow Method, for example, could be useful for studying the effect of cross-talk on particular proteins in pathways of interest, such as cross-talk in protein phosphorylation events collected using phosphoproteomics[100]. For instance, phosphorylation events, such as those associated with the mitogen-activated protein kinase (MAPK) pathway, have been shown to arise from multiple pathways via cross-talk, but were previously thought to

be specific to a particular stimulus[100] (linear pathway hypothesis). The Signal Flow Method can highlight all of the input pathways that could give rise to phosphorylation of MAPK.

1.4 Conclusions

To understand the mechanisms of A β -neuron interactions has been a major experimental driving force for more than two decades in the field of AD research. Though recent failures of drug therapies targeting A β has called for a re-evaluation of the Amyloid Cascade Hypothesis (and some propose to reject it all together), the role of A β in the disease progression is still considered to be an important role, even if it is not the sole initiating factor. However, a continual impediment in understanding the mechanisms of A β 's neurotoxic effects on neurons via *in vitro* experimentation has been a lack of experimental consensus on the mechanisms of A β 's early action on neurons. In our discussion of the experimental data, we argue that the controllable differences in experimental preparations between laboratories, such as A β species and aggregation state, A β concentration, and timescale of the experiments, are not the primary reasons for a lack of consensus (although they probably do contribute to uncertainty in the field). This is because within each controllable factor of the laboratory preparations, there is not a consensus with respect to any particular mechanism of A β -neuron interaction (see **Tables 1.1-1.3**).

We proposed that computational approaches could be applied to the system in order to analyze the current experimental data against a model for the system and then test different hypotheses for A β -neuron interactions. We introduced our work using a computational electrophysiological model neuron to test A β 's action on ion channels in the membrane. We also introduced our work with a CA1 hippocampal neuronal signaling network, utilizing a reverse-engineering algorithm to identify A β -neuron interactions from experimental data. Finally, we introduced our work using network analysis to identify the cellular context of proteins in a CA1 hippocampal neuronal signaling network, and to show that the cellular context of proteins commonly measured in *in vitro* experiments with A β are involved in complex interactions, such as a feedback.

Given these approaches, we hope to further guide experiments in this area of AD research toward the end of finding consensus on A β 's early action on neurons. Though a standardized methodology for preparing experiments would greatly aid this endeavor (standardized A β species and aggregation state, concentration and timescale used), we have shown that these are not the only confounding factors. Instead, we propose that the system is complex and that by assuming a more complex model for the system, we could identify A β -neuron interactions that explain the current literature data.

1.5 References

1. Association As. 2015 Alzheimer's Disease Facts and Figures 2016 [cited 2016 January 15].
2. Small D, Cappai R. Alois Alzheimer and Alzheimer's disease: a centennial perspective. *Journal of Neurochemistry*. 2006;99(3):708-10. doi: DOI 10.1111/j.1471-4159.2006.04212.x. PubMed PMID: ISI:000241345100002.
3. Moller H, Graeber M. The case described by Alois Alzheimer in 1911 - Historical and conceptual perspectives based on the clinical record and neurohistological sections. *European Archives of Psychiatry and Clinical Neuroscience*. 1998;248(3):111-22. PubMed PMID: ISI:000075335600001.
4. Glenner GG, Wong CW. Alzheimer's disease: initial report of the purification and characterization of a novel cerebrovascular amyloid protein. *Biochem Biophys Res Commun*. 1984;120(3):885-90. doi: S0006-291X(84)80190-4 [pii]. PubMed PMID: 6375662.
5. Vinters HV. Emerging concepts in Alzheimer's disease. *Annu Rev Pathol*. 2015;10:291-319. doi: 10.1146/annurev-pathol-020712-163927. PubMed PMID: 25387055.
6. Weiner M. Further insights into Alzheimer disease pathogenesis. *Nature Reviews Neurology*. 2013;9(2):65-6. doi: 10.1038/nrneurol.2012.275. PubMed PMID: WOS:000315250400002.
7. Hardy JA, Higgins GA. Alzheimer's disease: the amyloid cascade hypothesis. *Science*. 1992;256(5054):184-5. PubMed PMID: 1566067.

8. Hardy J, Selkoe D. Medicine - The amyloid hypothesis of Alzheimer's disease: Progress and problems on the road to therapeutics. *Science*. 2002;297(5580):353-6. PubMed PMID: ISI:000176892600038.
9. Armstrong RA. The Pathogenesis of Alzheimer's Disease: A Reevaluation of the "Amyloid Cascade Hypothesis". *International Journal of Alzheimer's Disease*. 2011;2011.
10. Davis JN, Chisholm JC. The 'amyloid cascade hypothesis' of AD: decoy or real McCoy? *Trends Neurosci*. 1997;20(12):558-9. PubMed PMID: 9416666.
11. Reitz C. Alzheimer's Disease and the Amyloid Cascade Hypothesis: A Critical Review. *International Journal of Alzheimer's Disease*. 2012;2012.
12. Drachman DA. The amyloid hypothesis, time to move on: Amyloid is the downstream result, not cause, of Alzheimer's disease. *Alzheimers Dement*. 2014;10(3):372-80. doi: 10.1016/j.jalz.2013.11.003. PubMed PMID: 24589433.
13. Herrup K. The case for rejecting the amyloid cascade hypothesis. *Nature Neuroscience*. 2015;18(6):794-9. doi: 10.1038/nn.4017. PubMed PMID: WOS:000355218300006.
14. Mullane K, Williams M. Alzheimer's therapeutics: Continued clinical failures question the validity of the amyloid hypothesis-but what lies beyond? *Biochemical Pharmacology*. 2013;85:289-305.
15. Hardy J. The amyloid hypothesis for Alzheimer's disease: a critical reappraisal. *J Neurochem*. 2009;110(4):1129-34. doi: JNC6181 [pii] 10.1111/j.1471-4159.2009.06181.x. PubMed PMID: 19457065.

16. Karran E, Mercken M, De Strooper B. The amyloid cascade hypothesis for Alzheimer's disease: an appraisal for the development of therapeutics. *Nat Rev Drug Discov.* 2011;10(9):698-712. doi: 10.1038/nrd3505. PubMed PMID: 21852788.
17. Kaye R, Lasagna-Reeves C. Molecular Mechanisms of Amyloid Oligomers Toxicity. *J Alzheimers Dis.* 2012. doi: Q5167K4JP4351322 [pii] 10.3233/JAD-2012-129001. PubMed PMID: 22531422.
18. De Strooper B, Karran E. The Cellular Phase of Alzheimer's Disease. *Cell.* 2016;164(4):603-15. doi: 10.1016/j.cell.2015.12.056. PubMed PMID: WOS:000369998300008.
19. Chen C. beta-amyloid increases dendritic Ca²⁺ influx by inhibiting the A-type K⁺ current in hippocampal CA1 pyramidal neurons. *Biochemical and Biophysical Research Communications.* 2005;338(4):1913-9. doi: 10.1016/j.bbrc.2005.10.169|10.1016/j.bbrc.2005.10.169. PubMed PMID: WOS:000233815900036.
20. Shelat PB, Chalimoniuk M, Wang JH, Strosznajder JB, Lee JC, Sun AY, et al. Amyloid beta peptide and NMDA induce ROS from NADPH oxidase and AA release from cytosolic phospholipase A2 in cortical neurons. *J Neurochem.* 2008;106(1):45-55. doi: JNC5347 [pii] 10.1111/j.1471-4159.2008.05347.x. PubMed PMID: 18346200.
21. Benilova I, Karran E, De Strooper B. The toxic A beta oligomer and Alzheimer's disease: an emperor in need of clothes. *Nature Neuroscience.* 2012;15(3):349-57. doi: 10.1038/nn.3028. PubMed PMID: WOS:000300793100006.

22. LaFerla F. Calcium dyshomeostasis and intracellular signalling in Alzheimer's disease. *Nature Reviews Neuroscience*. 2002;3(11):862-72. doi: DOI 10.1038/nrn960. PubMed PMID: ISI:000179041700017.
23. Demuro A, Parker I, Stutzmann G. Calcium Signaling and Amyloid Toxicity in Alzheimer Disease. *Journal of Biological Chemistry*. 2010;285(17):12463-8. doi: DOI 10.1074/jbc.R109.080895. PubMed PMID: ISI:000276787800001.
24. Giuffrida ML, Caraci F, Pignataro B, Cataldo S, DeBona P, Bruno V, et al. beta-Amyloid Monomers are Neuroprotective. *The Journal of Neuroscience*. 2009;29(34).
25. Ryan DA, Narrow WC, Federoff HJ, Bowers WJ. An improved method for generating consistent soluble amyloid-beta oligomer preparations for in vitro neurotoxicity studies. *J Neurosci Methods*. 2010;190(2):171-9. doi: 10.1016/j.jneumeth.2010.05.001. PubMed PMID: 20452375; PubMed Central PMCID: PMC2902796.
26. El-Agnaf OMA, Mahil DS, Patel B, Austen BM. Oligomerization and Toxicity of beta-Amyloid-42 Implicated in Alzheimer's Disease. *Biochemical and Biophysical Research Communications*. 2000;273.
27. Good T, Smith D, Murphy R. beta-amyloid peptide blocks the fast-inactivating K⁺ current in rat hippocampal neurons. *Biophysical Journal*. 1996;70(1):296-304. PubMed PMID: ISI:A1996TY68300024.
28. MacManus A, Ramsden M, Murray M, Henderson Z, Pearson HA, Campbell VA. Enhancement of (45)Ca(2+) influx and voltage-dependent Ca(2+) channel activity by beta-amyloid-(1-40) in rat cortical synaptosomes and cultured cortical

neurons. Modulation by the proinflammatory cytokine interleukin-1 β . *J Biol Chem*. 2000;275(7):4713-8. PubMed PMID: 10671502.

29. Rovira C, Arbez N, Mariani J. A β (25-35) and A β (1-40) act on different calcium channels in CA1 hippocampal neurons. *Biochem Biophys Res Commun*. 2002;296(5):1317-21. PubMed PMID: 12207918.

30. Plant LD, Webster NJ, Boyle JP, Ramsden M, Freir DB, Peers C, et al. Amyloid beta peptide as a physiological modulator of neuronal 'A'-type K⁺ current. *Neurobiol Aging*. 2006;27(11):1673-83. doi: 10.1016/j.neurobiolaging.2005.09.038. PubMed PMID: 16271805.

31. Sun XD, Mo ZL, Taylor BM, Epps DE. A slowly formed transient conformer of A β (1-40) is toxic to inward channels of dissociated hippocampal and cortical neurons of rats. *Neurobiol Dis*. 2003;14(3):567-78. PubMed PMID: 14678772.

32. Yu SP, Farhangrazi ZS, Ying HS, Yeh CH, Choi DW. Enhancement of outward potassium current may participate in beta-amyloid peptide-induced cortical neuronal death. *Neurobiol Dis*. 1998;5(2):81-8. doi: 10.1006/nbdi.1998.0186. PubMed PMID: 9746905.

33. Yankner BA, Caceres A, Duffy LK. Nerve growth factor potentiates the neurotoxicity of beta amyloid. *Proc Natl Acad Sci U S A*. 1990;87(22):9020-3. PubMed PMID: 2174172; PubMed Central PMCID: PMC55092.

34. Yaar M, Zhai S, Pilch P, Doyle S, Eisenhauer P, Fine R, et al. Binding of beta-amyloid to the p75 neurotrophin receptor induces apoptosis - A possible mechanism for Alzheimer's disease. *Journal of Clinical Investigation*.

1997;100(9):2333-40. doi: 10.1172/JCI119772. PubMed PMID: WOS:A1997YF66000024.

35. Vigo F, Kedikian G, Heredia L, Heredia F, Anel A, Rosa A, et al. Amyloid-beta precursor protein mediates neuronal toxicity of amyloid beta through Go protein activation. *Neurobiology of Aging*. 2009;30(9):1379-92. doi: DOI 10.1016/j.neurobiolaging.2007.11.017. PubMed PMID: ISI:000268783200004.

36. Koh JY, Yang LL, Cotman CW. Beta-amyloid protein increases the vulnerability of cultured cortical neurons to excitotoxic damage. *Brain Res*. 1990;533(2):315-20. PubMed PMID: 2289145.

37. Williamson R, Usardi A, Hanger DP, Anderton BH. Membrane-bound beta-amyloid oligomers are recruited into lipid rafts by a fyn-dependent mechanism. *FASEB J*. 2008;22(5):1552-9. doi: 10.1096/fj.07-9766com. PubMed PMID: 18096814.

38. Whitson JS, Appel SH. Neurotoxicity of A beta amyloid protein in vitro is not altered by calcium channel blockade. *Neurobiol Aging*. 1995;16(1):5-10. doi: 0197458095800029 [pii]. PubMed PMID: 7723935.

39. Arispe N, Pollard HB, Rojas E. Giant multilevel cation channels formed by Alzheimer disease amyloid beta-protein [A beta P-(1-40)] in bilayer membranes. *Proc Natl Acad Sci U S A*. 1993;90(22):10573-7. PubMed PMID: 7504270; PubMed Central PMCID: PMC47819.

40. Kawahara M, Arispe N, Kuroda Y, Rojas E. Alzheimer's disease amyloid beta-protein forms Zn(2+)-sensitive, cation-selective channels across excised

membrane patches from hypothalamic neurons. *Biophys J.* 1997;73(1):67-75. doi: S0006-3495(97)78048-2 [pii]

10.1016/S0006-3495(97)78048-2. PubMed PMID: 9199772; PubMed Central PMCID: PMCPMC1180909.

41. Mark RJ, Pang Z, Geddes JW, Uchida K, Mattson MP. Beta-amyloid-Peptide Impairs Glucose Transport in Hippocampal and Cortical Neurons: Involvement of Membrane Lipid Peroxidation. *The Journal of Neuroscience.* 1997;17(3).

42. Alvarez G, Muñoz-Montaña JR, Satrustegui J, Avila J, Bogónez E, Díaz-Nido J. Lithium protects cultured neurons against beta-amyloid-induced neurodegeneration. *FEBS Lett.* 1999;453(3):260-4. PubMed PMID: 10405156.

43. Alvarez AR, Godoy JA, Mullendorff K, Olivares GH, Bronfman M, Inestrosa NC. Wnt-3a overcomes beta-amyloid toxicity in rat hippocampal neurons. *Exp Cell Res.* 2004;297(1):186-96. doi: S0014482704000837 [pii]

10.1016/j.yexcr.2004.02.028. PubMed PMID: 15194435.

44. Wang HW, Pasternak JF, Kuo H, Ristic H, Lambert MP, Chromy B, et al. Soluble oligomers of beta amyloid (1-42) inhibit long-term potentiation but not long-term depression in rat dentate gyrus. *Brain Res.* 2002;924(2):133-40. PubMed PMID: 11750898.

45. Pugazhenth S, Wang M, Pham S, Sze CI, Eckman CB. Downregulation of CREB expression in Alzheimer's brain and in A β -treated rat hippocampal neurons. *Mol Neurodegener.* 2011;6:60. doi: 1750-1326-6-60 [pii]

10.1186/1750-1326-6-60. PubMed PMID: 21854604; PubMed Central PMCID: PMCPMC3174124.

46. Fogarty M, Downer E, Campbell V. A role for c-Jun N-terminal kinase 1 (JNK1), but not JNK2, in the beta-amyloid-mediated stabilization of protein p53 and induction of the apoptotic cascade in cultured cortical neurons. *Biochemical Journal*. 2003;371:789-98. doi: 10.1042/BJ20021660. PubMed PMID: WOS:000182733400016.
47. Alvarez A, Muñoz JP, Maccioni RB. A Cdk5-p35 stable complex is involved in the beta-amyloid-induced deregulation of Cdk5 activity in hippocampal neurons. *Exp Cell Res*. 2001;264(2):266-74. doi: S0014-4827(01)95152-3 [pii] 10.1006/excr.2001.5152. PubMed PMID: 11262183.
48. Lacor PN, Buniel MC, Chang L, Fernandez SJ, Gong Y, Viola KL, et al. Synaptic targeting by Alzheimer's-related amyloid beta oligomers. *J Neurosci*. 2004;24(45):10191-200. doi: 24/45/10191 [pii] 10.1523/JNEUROSCI.3432-04.2004. PubMed PMID: 15537891.
49. Zempel H, Thies E, Mandelkow E, Mandelkow E-M. Beta-amyloid Oligomers Cause Localized Calcium Elevation, Missorting of Endogenous Tau into Dendrites, Tau Phosphorylation, and Destruction of Microtubules and Spines. *Journal of Neuroscience*. 2010;30(36).
50. Abramov AY, Ionov M, Pavlov E, Duchon MR. Membrane cholesterol content plays a key role in the neurotoxicity of β -amyloid: implications for Alzheimer's disease. *Aging Cell*. 2011;10(4):595-603. doi: 10.1111/j.1474-9726.2011.00685.x. PubMed PMID: 21332922.

51. Jung C-G, Uhm K-O, Miura Y, Hosono T, Horike H, Khanna KK, et al. Beta-amyloid increases the expression level of ATBF1 responsible for death in cultured cortical neurons. *Molecular Neurodegeneration*. 2011;6(47).
52. Yang S, Hsieh W, Liu D, Tsai L, Tung C, Wu J. The involvement of nitric oxide in synergistic neuronal damage induced by beta-amyloid peptide and glutamate in primary rat cortical neurons. *Chinese Journal of Physiology*. 1998;41(3):175-9. PubMed PMID: WOS:000077697700008.
53. Mattson MP, Cheng B, Davis D, Bryant K, Lieberburg I, Rydel RE. beta-Amyloid peptides destabilize calcium homeostasis and render human cortical neurons vulnerable to excitotoxicity. *J Neurosci*. 1992;12(2):376-89. PubMed PMID: 1346802.
54. Palop J, Mucke L. Amyloid-beta-induced neuronal dysfunction in Alzheimer's disease: from synapses toward neural networks. *Nature Neuroscience*. 2010;13(7):812-8. doi: 10.1038/nn.2583. PubMed PMID: WOS:000279173900011.
55. Rammes G, Hasenjaeger A, Sroka-Saidi K, Deussing JM, Parsons CG. Therapeutic significance of NR2B-containing NMDA receptors and mGluR5 metabotropic glutamate receptors in mediating the synaptotoxic effects of β -amyloid oligomers on long-term potentiation (LTP) in murine hippocampal slices. *Neuropharmacology*. 2011;60(6):982-90. doi: 10.1016/j.neuropharm.2011.01.051. PubMed PMID: 21310164.
56. Murphy RM, Pallito MM. Probing the Kinetics of beta-Amyloid Self-Association. *Journal of Structural Biology*. 2000;130.

57. Broersen K, Rousseau F, Schymkowitz J. The culprit behind amyloid beta peptide related neurotoxicity in Alzheimer's disease: oligomer size or conformation. *Alzheimer's Research & Therapy*. 2010;2(12).
58. Patel A, Jhamandas J. Neuronal receptors as targets for the action of amyloid-beta protein (A beta) in the brain. *Expert Reviews in Molecular Medicine*. 2012;14. doi: 10.1017/S1462399411002134. PubMed PMID: WOS:000300516400001.
59. Yankner B, Lu T. Amyloid beta-Protein Toxicity and the Pathogenesis of Alzheimer Disease. *Journal of Biological Chemistry*. 2009;284(8):4754-8. doi: 10.1074/jbc.R800018200. PubMed PMID: WOS:000263416600002.
60. Inestrosa NC, Godoy JA, Quintanilla RA, Koenig CS, Bronfman M. Peroxisome proliferator-activated receptor gamma is expressed in hippocampal neurons and its activation prevents beta-amyloid neurodegeneration: role of Wnt signaling. *Exp Cell Res*. 2005;304(1):91-104. doi: 10.1016/j.yexcr.2004.09.032. PubMed PMID: 15707577.
61. Laurén J, Gimbel DA, Nygaard HB, Gilbert JW, Strittmatter SM. Cellular prion protein mediates impairment of synaptic plasticity by amyloid-beta oligomers. *Nature*. 2009;457(7233):1128-32. doi: 10.1038/nature07761. PubMed PMID: 19242475; PubMed Central PMCID: PMC2748841.
62. Chacon PJ, Garcia-Mejias R, Rodriguez-Tebar A. Inhibition of RhoA GTPase and the subsequent activation of PTP1B protects cultured hippocampal neurons against amyloid β toxicity. *Mol Neurodegener*. 2011;6(1):14. doi: 1750-1326-6-14 [pii]

10.1186/1750-1326-6-14. PubMed PMID: 21294893; PubMed Central PMCID: PMCPMC3038970.

63. Vossel KA, Zhang K, Brodbeck J, Daub AC, Sharma P, Finkbeiner S, et al. Tau reduction prevents Abeta-induced defects in axonal transport. *Science*. 2010;330(6001):198. doi: 10.1126/science.1194653. PubMed PMID: 20829454; PubMed Central PMCID: PMCPMC3024010.

64. Zhao L, Ma QL, Calon F, Harris-White ME, Yang F, Lim GP, et al. Role of p21-activated kinase pathway defects in the cognitive deficits of Alzheimer disease. *Nat Neurosci*. 2006;9(2):234-42. doi: 10.1038/nn1630. PubMed PMID: 16415866.

65. Lacor P. Advances on the understanding of the origins of synaptic pathology in AD. *Current Genomics*. 2007;8(8):486-508. doi: 10.2174/138920207783769530. PubMed PMID: WOS:000254654000002.

66. Berman D, Dall'Armi C, Voronov S, McIntire L, Zhang H, Moore A, et al. Oligomeric amyloid-beta peptide disrupts phosphatidylinositol-4,5-bisphosphate metabolism. *Nature Neuroscience*. 2008;11(5):547-54. doi: 10.1038/nn.2100. PubMed PMID: WOS:000255327300013.

67. Patel D, Good T. A rapid method to measure beta-amyloid induced neurotoxicity in vitro. *Journal of Neuroscience Methods*. 2007;161(1):1-10. doi: 10.1016/j.jneumeth.2006.10.004|10.1016/j.jneymeth.2006.10.004. PubMed PMID: WOS:000245490900001.

68. Wogulis M, Wright S, Cunningham D, Chilcote T, Powell K, Rydel R. Nucleation-dependent polymerization is an essential component of amyloid-mediated

- neuronal cell death. *Journal of Neuroscience*. 2005;25(5):1071-80. doi: 10.1523/JNEUROSCI.2381-04.2005. PubMed PMID: WOS:000226750600004.
69. Kholodenko B. Cell-signalling dynamics in time and space. *Nature Reviews Molecular Cell Biology*. 2006;7(3):165-76. doi: 10.1038/nrm1838. PubMed PMID: WOS:000235590500012.
70. Snyder EM, Nong Y, Almeida CG, Paul S, Moran T, Choi EY, et al. Regulation of NMDA receptor trafficking by amyloid-beta. *Nat Neurosci*. 2005;8(8):1051-8. doi: nn1503 [pii] 10.1038/nn1503. PubMed PMID: 16025111.
71. Li S, Jin M, Koeglsperger T, Shepardson NE, Shankar GM, Selkoe DJ. Soluble A β oligomers inhibit long-term potentiation through a mechanism involving excessive activation of extrasynaptic NR2B-containing NMDA receptors. *J Neurosci*. 2011;31(18):6627-38. doi: 31/18/6627 [pii] 10.1523/JNEUROSCI.0203-11.2011. PubMed PMID: 21543591; PubMed Central PMCID: PMC3100898.
72. Arispe N, Pollard HB, Rojas E. beta-Amyloid Ca(2+)-channel hypothesis for neuronal death in Alzheimer disease. *Mol Cell Biochem*. 1994;140(2):119-25. PubMed PMID: 7898484.
73. Sepulveda FJ, Parodi J, Peoples RW, Opazo C, Aguayo LG. Synaptotoxicity of Alzheimer beta amyloid can be explained by its membrane perforating property. *PLoS One*. 2010;5(7):e11820. doi: 10.1371/journal.pone.0011820. PubMed PMID: 20676404; PubMed Central PMCID: PMC2910737.

74. Chiang LW, Grenier JM, Ettwiller L, Jenkins LP, Ficenec D, Martin J, et al. An orchestrated gene expression component of neuronal programmed cell death revealed by cDNA array analysis. *Proc Natl Acad Sci U S A*. 2001;98(5):2814-9. doi: 98/5/2814 [pii] 10.1073/pnas.051630598. PubMed PMID: 11226323; PubMed Central PMCID: PMC30222.
75. Barabasi A, Oltvai Z. Network biology: Understanding the cell's functional organization. *Nature Reviews Genetics*. 2004;5(2):101-U15. doi: 10.1038/nrg1272. PubMed PMID: WOS:000188602400012.
76. Hughey JJ, Lee TK, Covert MW. Computational modeling of mammalian signaling networks. *WIREs Systems Biology and Medicine*. 2009.
77. Klipp E, Liebermeister W. Mathematical modeling of intracellular signaling pathways. *Bmc Neuroscience*. 2006;7. doi: 10.1186/1471-2202-7-S1-S10. PubMed PMID: WOS:000203525800010.
78. Kholodenko B, Yaffe M, Kolch W. Computational Approaches for Analyzing Information Flow in Biological Networks. *Science Signaling*. 2012;5(220). doi: 10.1126/scisignal.2002961. PubMed PMID: WOS:000303002700007.
79. Morris MK, Saez-Rodriguez J, Sorger PK, Lauffenburger DA. Logic-based models for the analysis of cell signaling networks. *Biochemistry*. 2010;49(15):3216-24. doi: 10.1021/bi902202q. PubMed PMID: 20225868; PubMed Central PMCID: PMC3022202.
80. Papin JA, Hunter T, Palsson BO, Subramaniam S. Reconstruction of Cellular Signalling Networks and Analysis of Their Properties. *Nature Reviews*. 2005;6.

81. Orth J, Thiele I, Palsson B. What is flux balance analysis? *Nature Biotechnology*. 2010;24:5-8. doi: DOI 10.1038/nbt.1614. PubMed PMID: ISI:000275288300022.
82. Albert R, Barabasi A. Statistical mechanics of complex networks. *Reviews of Modern Physics*. 2002;74(1):47-97. doi: 10.1103/RevModPhys.74.47. PubMed PMID: WOS:000174548700003.
83. Hodgkin AL, Huxley AF. A quantitative description of membrane current and its application to conduction and excitation in nerve. *J Physiol*. 1952;117(4):500-44. PubMed PMID: 12991237; PubMed Central PMCID: PMCPMC1392413.
84. Herz A, Gollisch T, Machens C, Jaeger D. Modeling single-neuron dynamics and computations: A balance of detail and abstraction. *Science*. 2006;314(5796):80-5. doi: DOI 10.1126/science.1127240. PubMed PMID: ISI:000241031200039.
85. Morse TM, Carnevale NT, Mutalik PG, Migliore M, Shepherd GM. Abnormal Excitability of Oblique Dendrites Implicated in Early Alzheimer's: A Computational Study. *Front Neural Circuits*. 2010;4. doi: 10.3389/fncir.2010.00016. PubMed PMID: 20725509; PubMed Central PMCID: PMCPMC2901152.
86. Good TA, Murphy RM. Effect of beta-amyloid block of the fast-inactivating K⁺ channel on intracellular Ca²⁺ and excitability in a modeled neuron. *Proc Natl Acad Sci U S A*. 1996;93(26):15130-5. PubMed PMID: 8986775; PubMed Central PMCID: PMCPMC26368.
87. Zou X, Coyle D, Wong-Lin K, Maguire L. Beta-amyloid induced changes in A-type K(+) current can alter hippocampo-septal network dynamics. *J Comput Neurosci*. 2011. doi: 10.1007/s10827-011-0363-7. PubMed PMID: 21938438.

88. Culmone V, Migliore M. Progressive effect of beta amyloid peptides accumulation on CA1 pyramidal neurons: a model study suggesting possible treatments. *Frontiers in Computational Neuroscience*. 2012;6:1-9. doi: 10.3389/fncom.2012.00052. PubMed PMID: WOS:000306605600001.
89. Ullah G, Demuro A, Parker I, Pearson JE. Analyzing and Modeling the Kinetics of Amyloid Beta Pores Associated with Alzheimer's Disease Pathology. *PLoSOne*. 2015.
90. Rodbell M. Martin Rodbell - Biographical Stockholm, Sweden: Nobel Foundation; 1995 [cited 2016 February 12].
91. Kholodenko BN. Negative feedback and ultrasensitivity can bring about oscillations in the mitogen-activated protein kinase cascades. *Eur J Biochem*. 2000;267(6):1583-8. PubMed PMID: 10712587.
92. Mizuno S, Iijima R, Ogishima S, Kikuchi M, Matsuoka Y, Ghosh S, et al. AlzPathway: a comprehensive map of signaling pathways of Alzheimer's disease. *BMC Syst Biol*. 2012;6:52. doi: 10.1186/1752-0509-6-52. PubMed PMID: 22647208; PubMed Central PMCID: PMC3411424.
93. Liu H, Wang L, Lv M, Pei R, Li P, Pei Z, et al. AlzPlatform: An Alzheimer's Disease Domain-Specific Chemogenomics Knowledgebase for Polypharmacology and Target Identification Research. *Journal of Chemical Information and Modeling*. 2014;54(4):1050-60. doi: 10.1021/ci500004h. PubMed PMID: WOS:000335201200004.
94. Saez-Rodriguez J, Alexopoulos L, Epperlein J, Samaga R, Lauffenburger D, Klamt S, et al. Discrete logic modelling as a means to link protein signalling networks

with functional analysis of mammalian signal transduction. *Molecular Systems Biology*. 2009;5. doi: 10.1038/msb.2009.87. PubMed PMID: WOS:000273359200002.

95. Ma'ayan A, Jenkins SL, Neves S, Hasseldine A, Grace E, Dubin-Thaler B, et al. Formation of regulatory patterns during signal propagation in a Mammalian cellular network. *Science*. 2005;309(5737):1078-83. doi: 309/5737/1078 [pii] 10.1126/science.1108876. PubMed PMID: 16099987; PubMed Central PMCID: PMC3032439.

96. Oliveira LM, Falomir-Lockhart LJ, Botelho MG, Lin KH, Wales P, Koch JC, et al. Elevated α -synuclein caused by SNCA gene triplication impairs neuronal differentiation and maturation in Parkinson's patient-derived induced pluripotent stem cells. *Cell Death Dis*. 2015;6:e1994. doi: 10.1038/cddis.2015.318. PubMed PMID: 26610207; PubMed Central PMCID: PMC4670926.

97. Bucciantini M, Giannoni E, Chiti F, Baroni F, Formigli L, Zurdo J, et al. Inherent toxicity of aggregates implies a common mechanism for protein misfolding diseases. *Nature*. 2002;416(6880):507-11. doi: 10.1038/416507a. PubMed PMID: 11932737.

98. Knowles TP, Vendruscolo M, Dobson CM. The amyloid state and its association with protein misfolding diseases. *Nat Rev Mol Cell Biol*. 2014;15(6):384-96. doi: 10.1038/nrm3810. PubMed PMID: 24854788.

99. Sauro HM, Kholodenko BN. Quantitative analysis of signaling networks. *Progress in Biophysics & Molecular Biology*. 2004;86.

100. Riley NM, Coon JJ. Phosphoproteomics in the Age of Rapid and Deep Proteome Profiling. *Anal Chem.* 2016;88(1):74-94. doi: 10.1021/acs.analchem.5b04123. PubMed PMID: 26539879; PubMed Central PMCID: PMC4790442.

Chapter 2: Modeling the short-time scale dynamics of β -amyloid-neuron interactions.¹

2.1 Introduction

“Do not despise these small beginnings...” ~Zechariah 4:10 (The Bible)

Beta-amyloid ($A\beta$) is a 39-43 amino acid peptide that accumulates in the extracellular matrix of hippocampal and cortical regions of Alzheimer diseased brains[3]. $A\beta$ is suspected to play a key role in initiating a cascade of intracellular reactions that lead to neuronal dysfunction and cell death associated with Alzheimer’s disease (AD)[4], the most common form of dementia[5]. Exogenous exposure of neurons to $A\beta$, during *in vitro* experiments, have shown that $A\beta$ elicits a variety of intracellular responses including increased calcium influx[6, 7], altered kinase and phosphatase activities[8-10], disrupted regulation of transcriptions factors[11, 12], and alterations in ion channel and receptor gene expression[13]. Because intracellular functions are altered in the presence of extracellular $A\beta$, it has been hypothesized that $A\beta$ interacts with neuronal surfaces. Monomeric $A\beta$ may interact with certain features of cellular membranes acting as a locus for attachment, oligomerization and eventual fibril formation. The resulting toxic structures alter membrane morphology[14] via

¹ Wilson NP, Gates B, Castellanos M. Modeling the short time-scale dynamics of β -amyloid-neuron interactions. J Theor Biol. 2013. doi: 10.1016/j.jtbi.2013.02.012. PubMed PMID: 23454082.

protein-protein[15] or protein-lipid interactions[16]. After over twenty-years of research, there is no consensus on the exact mechanisms of A β -neuron interactions.

A mechanistic description of A β 's interaction with neurons requires reconciling a wealth empirical data performed under various conditions, making comparison of relevant mechanisms challenging. Computational modeling offers avenues for discriminating between mechanisms under experimentally testable conditions. Although experimentalists have faced challenges with the use of different species and aggregation states of A β [2, 17-25], thereby causing debate around the exact nature of the toxic A β species[26], in a computational model, A β can be treated as generalized toxic aggregate that binds to the neuron with some affinity and elicits a response. Though a simplified depiction of quite complex phenomena, this allows for comparison of results from the model to experimental data from various laboratories in order to identify trends in neuronal response that may be common to all species; while delineating probable mechanistic explanations for differing responses in the presence of a particular A β species or aggregation state. Computational modeling also allows for the determination of the type of response and its time-scale *a priori*, giving flexibility to examine the short time-scale (ms-sec) response of neurons to A β exposure, which may proceed the induction of intracellular processes associated with neurotoxicity[27]. Capturing short time-scale responses can often be tedious or limited by the experimental design. And so, while experimental literature on A β 's interaction with neurons *in vitro* abounds, there is still a need for a tool that allows for comparison across experiments in order to begin developing a mechanistic model for

A β -neuron interactions. Computational modeling is a powerful tool for analyzing the results of multiple hypotheses under controlled conditions.

Herein, we present a computational study where short time-scale interactions of A β with the neuronal membrane are compared. Utilizing a mathematical model of a hippocampal neuron[28], we input mathematical expressions for two proposed mechanisms of A β -neuron interaction: A β 's block of fast-inactivating potassium (I_A) channels and the membrane conductance increase by A β .

A fairly well-studied hypothesis, *in vitro* experiments with both hippocampal and cortical neurons suggest that A β blocks I_A channels in a [A β]-dependent manner, increases membrane excitability, and calcium influx[1, 17, 29, 30]. On the other hand, the membrane conductance increase mechanism posits that through A β 's interaction with the neuronal membrane, the dielectric constant is increased and the membrane becomes more permeable to ions and other compounds[24, 25, 31-33]. Though investigators have observed that A β evokes a current in artificial bilayers consistent with an increase in general membrane permeability[31, 32] and increases Ca^{2+} entry into hippocampal neurons[24], other physiological responses important to neuronal signaling, such as action potential (AP) generation and membrane excitability have not yet been examined for this mechanism.

For each mechanism presented, we report the effects of A β on voltage properties of the membrane, membrane excitability, action potential generation and the

dynamics of Ca^{2+} entry; all measurable outputs that can be experimentally tested. Each mechanism was simulated under voltage-clamp, current-clamp and high $[\text{K}^+]$ membrane depolarized experimental conditions. In comparing these two A β -neuron interactions via computational modeling, we demonstrate the model's potential for hypothesis generation and comparison, which could be used to guide the rational design of experiments.

2.2: Methods

2.2.1 Model Overview

A rat hippocampal neuron model was used to demonstrate the effects of the I_A channel block by A β on intracellular Ca^{2+} levels, under current-clamp conditions[28]. We adapted this model to simulate voltage-clamp and high $[\text{K}^+]$ membrane depolarization experiments, and can include multiple possible mechanisms of A β -neuron interactions. The neuron is modeled as a wrinkled sphere with a radius of $12\mu\text{m}$ and a surface area of $4 \times 10^{-5} \text{ cm}^2$ [28].

2.2.2 Current-clamped Neuron Model

The general form of the current-clamped model[28] describes the voltage-time trajectory of ionic conductances in the neuronal membrane:

$$C_m \frac{\partial V}{\partial t} = \Sigma I_{ions} + I_{AMPA} + I_{inject} + I_{leak} \quad (1)$$

The expressions for the currents (I ; μA), membrane capacitance (C_m ; μF) and the membrane potential (V ; mV) are described in detail here[28]. $I_{AMPA} = 0$ for all simulations as current density for this receptor is low in the soma and requires the neurotransmitter, glutamate, for activation[34]. Each ion channel takes on a Hodgkin and Huxley[35] form. The leak current is adjusted such that a quiescent cell is achieved in the absence of any stimulus.

We replaced the original I_A channel current in the Good and Murphy model [28] with an I_A channel current equation from[36] that better describes the dynamics of I_A channel gating observed experimentally since the publication of the Good and Murphy model. This current is represented by the following equation:

$$I_A = g_A * m^N * h * (V - V_K) \quad (2)$$

where N is the order of the activation ($N = 3$ or $f(V)$; 3 in our model)[36] and V_K is the Nernst Potential for the K^+ ion. The parameters m and h are the activation and deactivation parameters, respectively, which represent probabilities of an open I_A channel based on the measured kinetics of channel gating[36]. The functions for m and h are given by $m = 1 - \exp(-t/\tau_t)$ and $h = \exp(-t/\tau_d)$, respectively. τ_t and τ_d are the

time to peak (ms) and the delay constants (ms), respectively, and are functions of the membrane potential (V)[36].

2.2.3 Voltage-clamped Neuron Model

To create the voltage-clamped model, the following equation is the steady-state solution to Eq. 1:

$$\sum I_{ions} + I_{AMPA} + I_{leak} + I_{inject} = 0 \quad (3)$$

Therefore, in Equation 3, the magnitude of I_{inject} , the current required in voltage-clamp experiment to maintain a constant voltage, is equal to the magnitude of the total ionic currents. In each simulation, two holding potentials (V_H , before and after the command potential) and a command potential (V_C) are invoked. The holding potential period allows ion channels to come to a closed and inactivated state. The command potential is a voltage set higher than resting potential of the cell ($V_R = -67.5$ mV) thereby opening channels and allowing each current to reach steady state. For our simulations, V_H is held at -100 mV; V_C is held at potentials between -60 and 60 mV, which represent the membrane potential range exhibited during an AP in hippocampal neurons.

2.2.4 High $[K^+]$ Membrane Depolarized Neuron Model

For the high $[K^+]$ membrane depolarized neuron model, the current-clamped model[28] is applied except that $I_{\text{inject}} = 0$ and a depolarizing concentration of 30 mM extracellular $[K^+]$ was simulated by changing the K^+ Nernst potential (V_K) from -89 to -32 mV.

2.2.5 Ca^{2+} Diffusion

The general equation governing intracellular Ca^{2+} diffusion and dynamics is[28]:

$$\frac{\partial [Ca^{2+}]}{\partial t} = D \nabla^2 [Ca^{2+}]_r - r_{\text{Buffer}} \quad (4)$$

where terms are $[Ca^{2+}]_r$, the Ca^{2+} concentration at a radial distance r (M), D , the diffusivity(cm^2/s) of Ca^{2+} inside the neuron and r_{Buffer} , the rate at which the buffer uptakes Ca^{2+} (M/s). Ca^{2+} buffering is modeled as a reversible reaction governed by mass action kinetics[28].

In order to solve Eq. 4, two boundary conditions are required. The boundary condition at the neuron center ($r = 0$) is given by[28]:

$$\frac{\partial[Ca^{2+}]_0}{\partial r} = 0 \quad (5)$$

where $[Ca^{2+}]_0$ is the concentration of Ca^{2+} at $r = 0$. This boundary condition accounts for symmetry. The second boundary condition describing Ca^{2+} flux across the membrane ($r = R$) is given by[28]:

$$DA \frac{\partial[Ca^{2+}]_R}{\partial r} + \frac{\Sigma I_{Ca}}{2F} + r_{pump} - r_{leak} = 0 \quad (6)$$

where terms are $[Ca^{2+}]_R$, the Ca^{2+} concentration at the intracellular cell membrane, ΣI_{Ca} , the sum of the current through Ca^{2+} channels, r_{pump} , the rate at which Ca^{2+} is pumped out of the cell by the Na^+ -dependent Ca^{2+} pump, and r_{Leak} , the rate at which Ca^{2+} leaks into the cell at the resting membrane potential. $r_{Leak} = r_{pump}$ when $[Ca^{2+}]$ is equal to the initial intracellular $[Ca^{2+}]$ given at $t = 0$ (not shown here). Governing equations for the Ca^{2+} pump were taken from[28]. The differential equations were solved using fourth order Runge-Kutta method with a variable time step, and programmed in Visual C++. The partial differential equation for $[Ca^{2+}]_r$ was solved numerically using the method of lines and the resultant $[Ca^{2+}]_i$ is given as a function

of radial distance and time. $[Ca^{2+}]_i$ presented were averaged over the entire volume of the neuron.

2.2.6 Mechanisms of A β interactions with neuronal membrane

We are modeling two hypothetical A β -neuron interactions to discriminate their effects on ion conductances and alterations in Ca^{2+} transients.

2.2.6.1 A β 's block of I_A channels mechanism

The A β -induced I_A channel block is represented by a kinetic inhibition equation[28]:

$$x_{A\beta} = \frac{[A\beta]}{K_I + [A\beta]} \quad (7)$$

where the terms are $x_{A\beta}$, the fraction of channels blocked by A β , $[A\beta]$, the concentration of exogenous A β (μ M) (represented as an aggregate), and K_I , the inhibition constant for A β (μ M). The simulated K_I values were 0.5 and 1.5 μ M[1]. The expression, $1-x_{A\beta}$, then describes the number of open I_A channels. For this mechanism, the I_A channel current expression is[28]:

$$I_A = g_A * (1 - x_{A\beta}) * m^N * h * (V - V_K) \quad (8)$$

2.2.6.2 Membrane Conductance Increase Mechanism

We have represented the membrane conductance mechanism[31, 32] in the model as a $[A\beta]$ -dependent increase in capacitance and membrane conductance. The capacitance increase[31] is scaled by a difference in capacitance between a biological membrane[37] and a sparsely-tethered lipid bilayer such that when $[A\beta] = 0$, $C_m = 1$:

$$C_m = 0.05[A\beta] + 1 \quad (9)$$

where C_m is the membrane capacitance($\mu\text{F}/\text{cm}^2$).

In a similar fashion as Eq. 9, a dimensionless equation for membrane conductance as a function of $[A\beta]$ [31] is given by:

$$\frac{g_{A\beta}}{g_0} = f = 39.165[A\beta]^2 - 11.6285[A\beta] + 1 \quad (10)$$

where terms are $g_{A\beta}$, the membrane conductance as a function of $[A\beta](\mu M)$ and, g_o , the membrane conductance when no $A\beta$ is present. The f parameter simulates an increase in general membrane permeability due to a $A\beta$ -induced increase in the membrane dielectric constant.

2.2.7 Choice of experimental data used to analyze predictions from the model

Experimental data was collected from [1, 2, 11, 17, 20, 24, 29, 33, 38, 39]. In order to analyze the model's predictions, we chose experimental data where $A\beta$ incubation times were relatively short (30s – 1hr) and the responses measured were similar to simulation conditions (i.e., voltage-clamp, current-clamp and high $[K^+]$ membrane depolarization), to ensure the responses were representative of changes at the membrane surface and not other processes that occur on longer time-scales. Voltage-clamp responses measured in experimental data were percent original (peak) I_A current [1, 2, 17, 29, 38] and change in conductance relative to the control at various $[A\beta]$ [33]. Responses under current-clamp conditions collected were membrane excitability via basal/spontaneous activity of neurons [1, 2], which is inversely related to threshold current needed to elicit an AP, and relative levels of Ca^{2+} influx, usually measured as the change in fluorescence over the baseline fluorescence ($\Delta F/F$); though in the case of data from [39], we normalized the measured calcium concentration relative to the control (no $A\beta$ present). Phosphorylated CREB relative levels were compared to the model's predictions for

Ca^{2+} levels under high $[\text{K}^+]$ membrane depolarization since intermediate Ca^{2+} data was sparse in the literature. When at all possible, we used data from hippocampal or cortical neurons, which exist in brain areas affected by AD. However, data from Leão et al[2] and Demuro et al[20] were from medial septal neurons and SY5Y cells, respectively. Though medial septal neurons and SY5Y cells differ from hippocampal neurons, we chose to use experimental data from Demuro et al and Leão et al because the mechanisms of $\text{A}\beta$ -neuron interaction being examined were relevant to those we simulated. $\text{A}\beta$ species and aggregation state varied among all of the experimental data used for this paper. Nonetheless, in our model we treat $\text{A}\beta$ as a toxic aggregate independent of its specific structure and therefore species and aggregation state did not play a role in how we chose data to compare.

2.3: Results and Discussion

2.3.1 Voltage-clamp simulations in the presence of $\text{A}\beta$

We performed voltage-clamp simulations to ensure that each mathematical expression for $\text{A}\beta$'s action on a neuron would have the desired response in the model. **Figure 2.1** shows the results of voltage-clamp simulations of $\text{A}\beta$'s I_A channel block and the $\text{A}\beta$ -induced membrane conductance mechanism at various $[\text{A}\beta]$. $[\text{A}\beta]$ used in our simulations are within the typical $[\text{A}\beta]$ range used on primary culture hippocampal neurons (1nM-50 μM)[29, 40]. In **Figure 2.1A**, the $\text{A}\beta$ I_A channel block is shown. Inhibition of K^+ current through this channel, as observed in experimental literature[1, 2, 17, 38], results in a decrease in peak amplitude of the current in a

[A β]-dependent manner, but has no effect on the activation or deactivation kinetics of the channel. We modeled A β 's block of I_A channels using saturation kinetics (see Eqn. 7), where the K_I for these simulations was 1.5 μ M. This K_I was chosen as a reasonable estimate for inhibition of the channel observed in experimental literature[1, 29]. The inset of **Figure 2.1A** shows how the block of I_A channels by A β varies with [A β]. A decreasing trend with increasing [A β] is observed. As can be seen by comparing the solid line representing the model with the experimental data, the choice of $K_I = 1.5\mu$ M is a reasonable estimate for the I_A channel block, even though the simulated inhibition of I_A channels trends lower than the experimental data. Experimental data from Ye et al[1] at 1 μ M represents almost a complete abolition of the I_A current. Differences in the data amongst the experiments are likely due to varied A β preparations. The relative potencies and targets of specific A β aggregates is still an open question in the literature[41]. However, given the experimental data compared in the inset of **Figure 2.1A**, our model is able to replicate a general trend observed for the block of I_A channels by A β .

Voltage-clamp simulations of the membrane conductance increase mechanism show a [A β]-dependent increase in the leak current (**Figure 2.1B**). The large increase in the leak conductance, especially at [A β] > 0.1 μ M, is represented as an increasing polynomial function of [A β]. This large [A β]-dependent increase in membrane conductance has been observed experimentally[25, 31, 32]. As shown in the inset of **Figure 2.1B**, this general trend toward increased membrane conductance with increasing [A β] was demonstrated in rat hippocampal neurons[33], though the

experimentally measured membrane conductance in hippocampal neurons appears to increase linearly as a function of $[A\beta]$. Equation 10 was adapted from experimental observations in artificial bilayers[31, 32], which are simplified model systems of neuronal membranes[14, 21]. From experiments in artificial membranes, the degree to which $A\beta$ increases membrane conductance varies with phospholipid composition, with more negatively charged lipids reducing the effect of $A\beta$ compared to more neutral compositions[31, 32]. Therefore, calibration of the effects of $A\beta$ on a native neuronal membrane system, which tends to be more of a mixed composition of phospholipids, is necessary to more accurately depict the effect of this $A\beta$ -neuron interaction. An additional consideration is that, as described by Gentet et al[37], the membrane capacitance has been shown not change due to the addition of membrane proteins to the neuronal membrane. Therefore, though the membrane conductance mechanism described herein contains a linear increase in capacitance with respect to $[A\beta]$, it is very likely that there is no change in capacitance in an actual neuronal membrane. Though it is noteworthy that for the $[A\beta]$ range used in this particular study, the calculated difference in the membrane capacitance is 1.005-1.15 μ F (for $[A\beta]$ =0.01-3 μ M), which is within the experimental range demonstrated by Gentet et al for HeLa cells[37]. Importantly, as seen in **Figure 2.1B**, our model shows that a significant $[A\beta]$ -dependent leak is observed. Such a large $A\beta$ -induced leak current could be difficult to discriminate from an effect on a channel current.

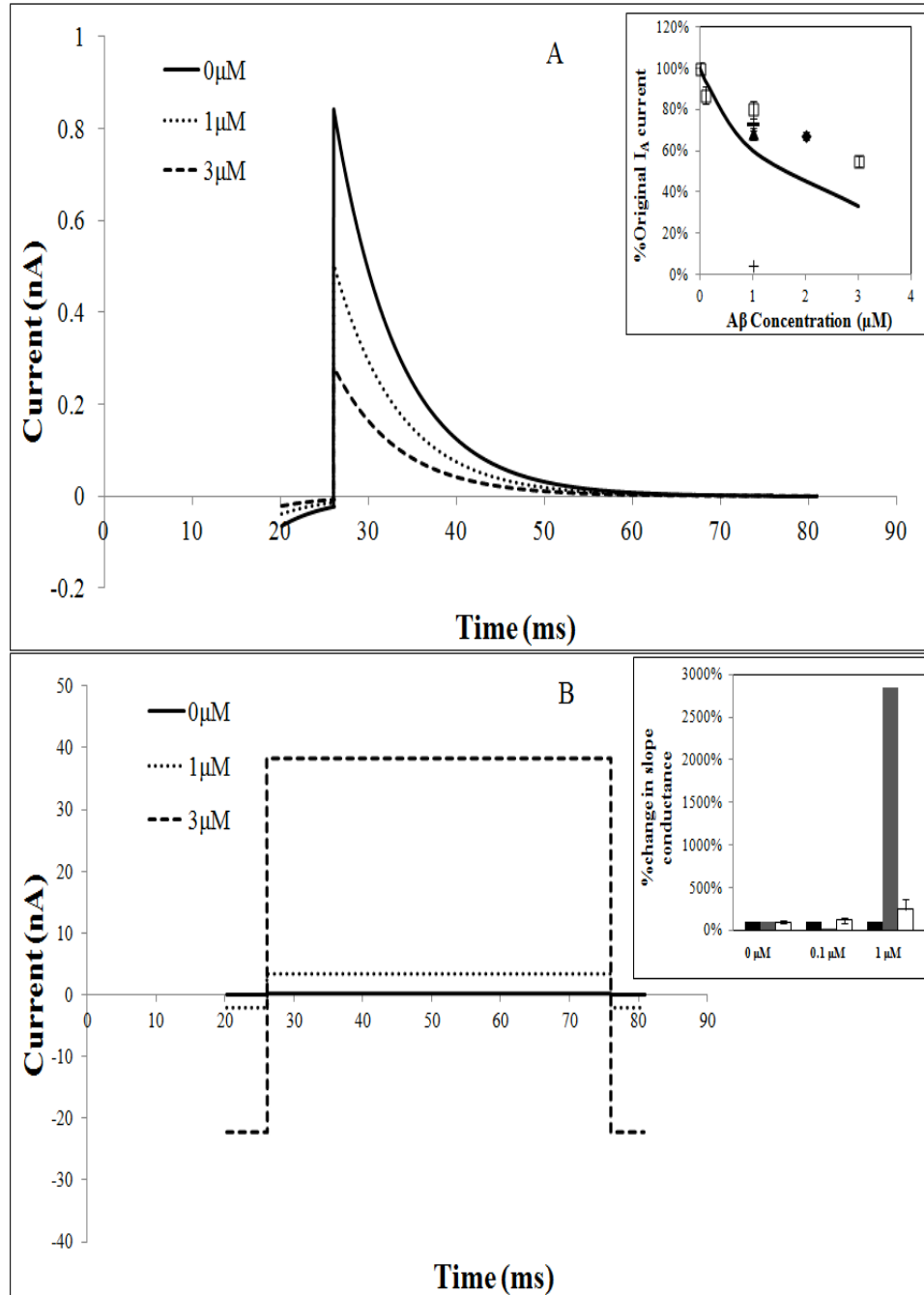


Figure 2.1: The effect of A β -ion channel and A β -membrane interactions on the I_A channel under voltage-clamp conditions. (A) I_A channel current is shown at various [A β]. Current inhibition was simulated using saturation kinetics to describe a block of the I_A channel pore (see Eq. 7) with an inhibition constant, K_I, of 1.5 μ M. *Inset*, percent peak current relative to the control ([A β] = 0) at various [A β]. Experimental data from Good et al[17] (*open squares*), Chen[29] (*closed triangle*), Leão et al[2] (*closed circle*), Jhamandas et al[38] (*dash*) and Ye et al[1] (*cross*) plotted for comparison. (B) The A β -induced increase in membrane conductance is represented by increases in both capacitance and membrane leak conductance (Eqs. 9 & 10). Plotted here is the leak current at various [A β]. *Inset*, percent change in conductance relative to the control, as measured by the slope of the I-V curve vs. [A β]. The black bars represent the simulated control; grey bar is the model results for the membrane conductance increase mechanism. Experimental data from[33] is represented by the white bars. For these voltage-clamp simulations, V_H = -100 mV for 26 ms before evoking V_C, and for 10 ms after the V_C; V_C = 60mV for 50 ms. All Ca²⁺ and sodium channels, the delayed-rectifying, Ca²⁺-dependent, and the long after hyperpolarization K⁺ channels were blocked during these simulations. [A β] = 0 (control), 1, and 3 μ M.

2.3.2 Current-clamp simulations of a single AP, membrane excitability and $[Ca^{2+}]_i$

We used current-clamp simulations to evaluate the effect of each mechanism on AP generation and membrane excitability. An inject current of 0.5nA is applied to simulate the effect of neurotransmitter release from the pre-synaptic cell to the model neuron sufficient enough to elicit an AP. Again, we simulated each mechanism's A β -induced effect for [A β] ranging between 0 and 3 μ M. The A β -induced I_A channel block decreases AP latency and increases AP height with a slight [A β]-dependence (**Figure 2.2A**), indicative of increased membrane excitability. These A β -induced alterations in firing properties of neurons have been examined both computationally and experimentally for the I_A channel block[29, 42]. Though alterations in APs that our model predicts are slight, these can lead to more dramatic increases in AP height in the dendrites due to back-propagation[29, 42]. Disturbances in dendritic signal propagation can result in loss of input-output control, which is essential for effective inter-neuronal signaling[43]. In contrast to the I_A channel block by A β , the A β -induced membrane conductance increase mechanism (**Figure 2.2B**) shows a strong non-linear [A β]-dependence on AP latency, height and shape as well as the hyperpolarization period following the AP. For [A β] < 0.1 μ M, AP latency is increased. Conversely, at [A β] > 0.1 μ M, AP latency is decreased, indicating greater membrane excitability. Furthermore, the AP peak is lower and broader for increased [A β] > 0.1 μ M. The depth of the hyperpolarization period also shows a non-linear correlation at [A β] < 0.1 μ M, but an inverse correlation at [A β] > 0.1 μ M.

This dichotomy in neuronal response to A β is due to the inverse relationship between capacitance and conductance, as both are increased by A β (Eqs. 9 & 10). Qualitatively, the implications of these opposite effects of the membrane conductance increase mechanism is that at lower concentrations (i.e., at [A β] < 0.1 μ M in our simulations), the neuron may be less responsive to external stimulus but at higher concentrations (i.e., [A β] > 0.1 μ M in our simulations) the neuron will become more responsive to external stimulus, and therefore more excitable, as compared to the case when no A β is present. Because information encoded in neurons is dependent on the height, shape and frequency of APs[44], then such changes in intrinsic membrane properties of neurons could be deleterious. To further examine the effects of A β on membrane excitability, the model neuron was given a subthreshold current ($I_{\text{inject}} < 0.5\text{nA}$), which would be insufficient to elicit an AP when no A β is present. A decrease in the threshold current required to evoke an AP would result in a neuron that is more excitable, or more responsive to a subthreshold external stimulus. When A β blocks I_A channels (**Figure 2.2C**), threshold current is decreased in a [A β]-dependent manner until the simulated concentration reaches around 2.5 μ M.

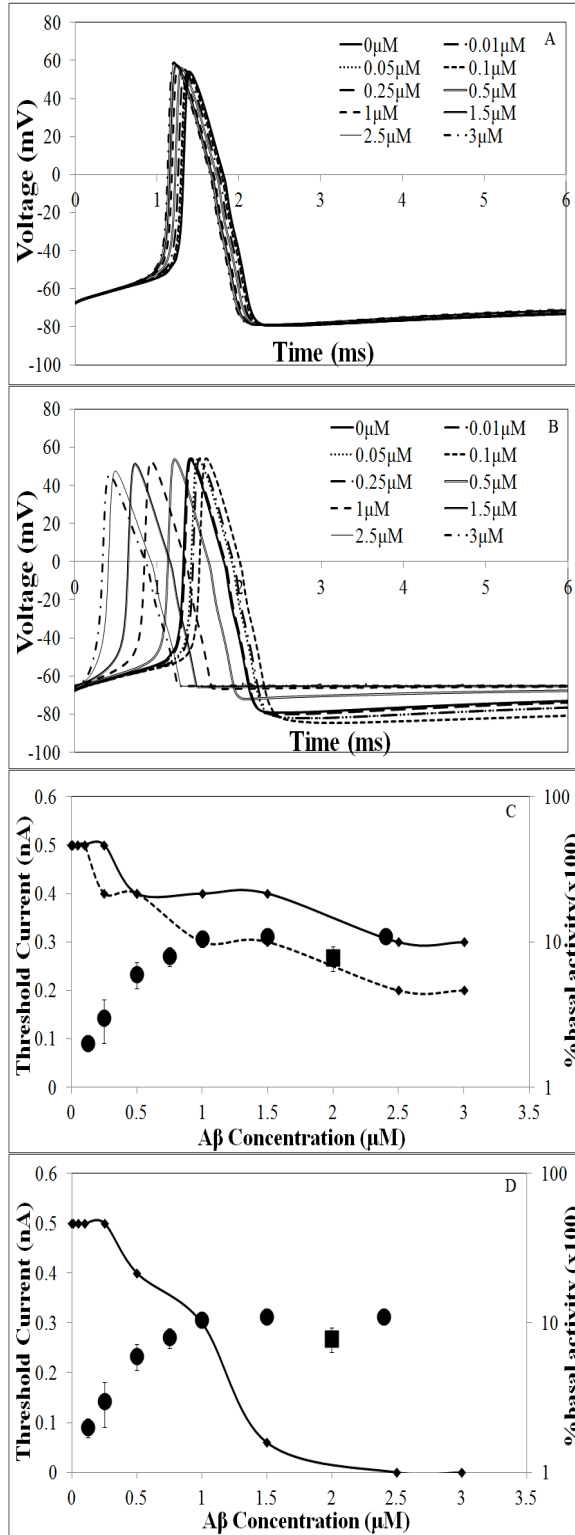


Figure 2.2: Comparison Aβ-induced I_A channel block and membrane conductance increase under current-clamp conditions. Top panel: Current was injected into the model neuron was sufficient to elicit an AP (0.5nA) when [Aβ] = 0. Shown are the I_A channel block by Aβ and (A) Aβ-induced membrane conductance increase (B). Bottom panel: Threshold current as a function of [Aβ] is plotted here for the I_A channel block (C) and the membrane conductance increase (D). K_I = 0.5 μM (dotted line/solid squares) and 1.5 (A and C, solid line/solid diamonds). [Aβ] = 0 (control), 0.01, 0.05, 0.1, 0.25, 0.5, 1, 1.5, 2.5 and 3 μM. Current-clamp electrophysiology data from [1, 2] (C and D; square, circle) are plotted as the percent basal activity or the ratio of the Aβ-stimulated activity of the control activity in [Aβ]-dependent manner. Basal activity and threshold current are inversely related.

Experimental data for basal activity of neurons as a function of $[A\beta]$ [1, 2], as shown in **Figures 2.2C and D**, is a measure of membrane excitability that is inversely related to the threshold current required to elicit an AP. Basal activity of neurons vs. $[A\beta]$ observed experimentally begins to plateau at $[A\beta] = 1\mu\text{M}$, and has saturated by time the $[A\beta] = 2.5\mu\text{M}$. Ye et al [1] attributed this $A\beta$ -induced increase in basal activity of neurons to reductions in the K^+ currents of the fast-inactivating type (A- and D-type), while Leão et al [2] reported increases in spontaneous (basal) activity due to the inhibition of I_A and I_M currents. The difference in the specific currents affected by $A\beta$ that Ye et al and Leão et al observed were most likely tissue specific. In **Figure 2.2D**, the threshold current for the membrane conductance increase mechanism decreases to zero as $[A\beta]$ increases, resulting in a spontaneously excitable neuron. Though our model shows that this spontaneously excitable neuron occurs at $[A\beta] = 3\mu\text{M}$, this result is a function of the parameters chosen to model the membrane conductance increase as discussed previously (see Section 3.1). Threshold current vs. $[A\beta]$ for the membrane conductance increase mechanism in **Figure 2.2D** was compared to the same experimental data as in **Figure 2.2C**. Again, the behavior of the trends in **Figures 2.2C and D** are distinct. For the block of I_A channels by $A\beta$, the $[A\beta]$ -dependent effect on threshold current saturates at a non-zero value; whereas, the trends for membrane conductance mechanism demonstrate a neuron that is spontaneously excitable at high $A\beta$ concentrations. The results from the threshold current vs. $[A\beta]$ simulations are important for two reasons: (1) it reveals a difference between the two mechanisms, under physiologically relevant conditions, that lends further credence to experimental observations and (2) a spontaneously excitable

neuron observed for the membrane conductance increase mechanism at high $A\beta$ concentrations is an experimentally testable result that differentiates these two mechanisms at a single $[A\beta]$ concentration.

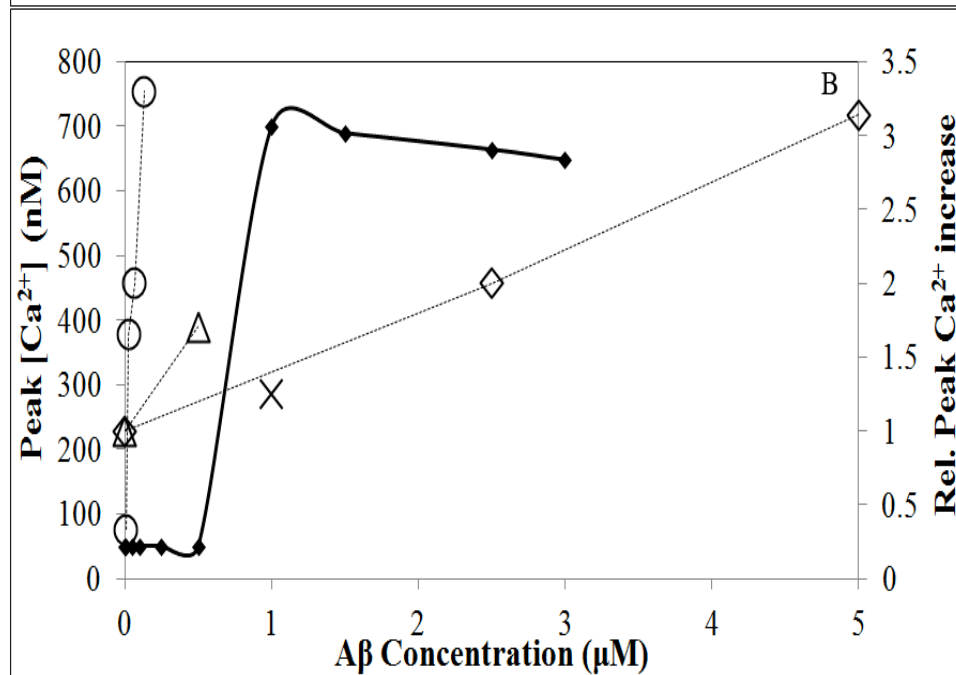
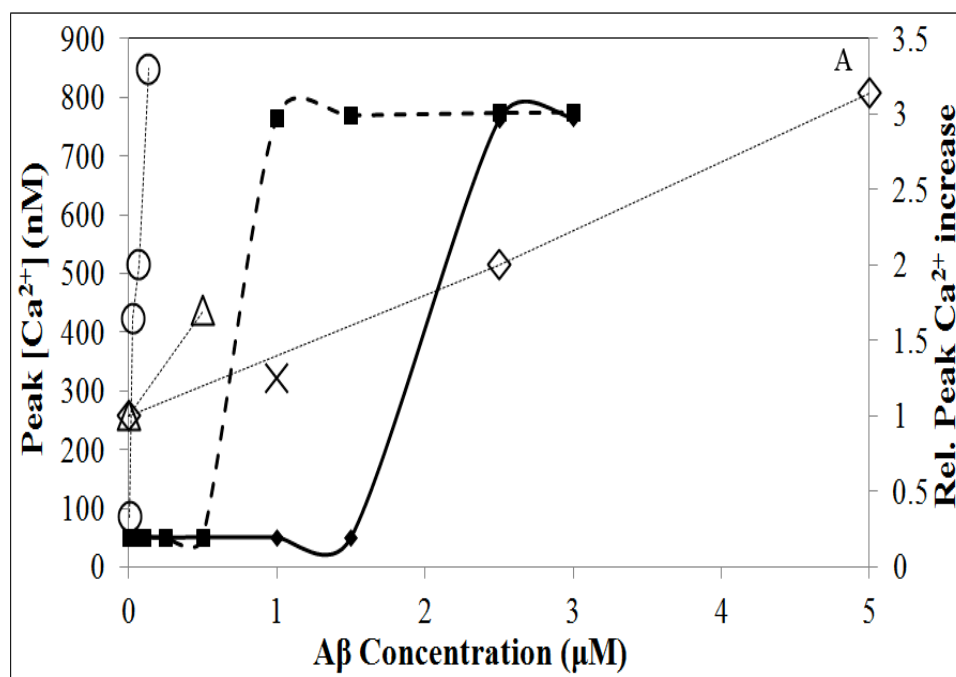


Figure 2.3: Effect of A β I_A channel block and the membrane conductance increase on basal intracellular [Ca²⁺]. The model neuron was subjected to a subthreshold current of 0.3nA ([A β] = 0). Intracellular Ca²⁺ levels were averaged over the entire model neuron volume and the log of the peak [Ca²⁺] as a function of [A β] is plotted for the I_A channel block (*A*) and membrane conductance increase (*B*). [A β] = 0 (control), 0.01, 0.05, 0.1, 0.25, 0.5, 1, 1.5, 2.5 and 3 μ M. In (*A*), K_I = 0.5 μ M and 1.5 μ M, represented by the dotted line and solid line, respectively. Experimental data of the relative (to baseline) peak increase in [Ca²⁺] from [39] (*open diamonds*), [29] (*X*), [20] (*open circles*) and [24] (*open triangles*) are included here for comparison.

Intracellular Ca²⁺ levels (**Figure 2.3**) are increased in the presence of A β (in general, at [A β] > 0.1 μ M) due to an increase in the neuron's response to an external stimulus for both mechanisms under current-clamp conditions. The increase in [Ca²⁺]_i levels is due to the induction of an AP at a subthreshold current of 0.3nA. As a result, for both mechanisms, a neuron exposed to a subthreshold stimulus, in the presence of A β , could experience an increase in basal [Ca²⁺]_i through membrane depolarization[45]. Interestingly for the block of I_A channels by A β , there is a notable difference between the [A β] at which a significant increase in Ca²⁺ influx takes place. For K_I = 0.5 μ M, the results show a sharp increase in Ca²⁺ at a [A β] that is 10 fold less than at K_I = 1.5 μ M. This makes sense because this effect is simulated by saturation kinetics and because K_I represents the concentration at which the half-maximal rate of

inhibition occurs. Therefore, a significant change in Ca^{2+} influx should occur at this value, due to an increase in membrane excitability (**Figure 2.2**). Also, there appears to be no qualitative difference between the dynamics of calcium entry for $K_I = 0.5\mu\text{M}$ for the I_A channel block and the membrane conductance increase by $A\beta$ mechanisms. Though these two hypothesized mechanisms have differing mathematical representations, under this specific experimental condition, depending on the actual value of K_I and the parameters for the membrane conductance, these two mechanisms could be indistinguishable. A general increasing trend in $[\text{Ca}^{2+}]_i$ with increasing $[A\beta]$ is also observed in the experimental data in **Figure 3**. However, between different experiments, the rate of increase in $[\text{Ca}^{2+}]_i$ as a function of $[A\beta]$ is very different. Another explanation for the lack of overlap between experimental and model results, is that calcium influx is a localized diffusional process; distribution of ion channels as well as calcium flux into and out of intracellular stores play a role in the precise response of a neuron to $A\beta$. Though our model does not take these two phenomena into account, our model is flexible enough for tuning as parameters for these two mechanisms are better evaluated experimentally or other potential mechanisms are proposed and tested.

2.3.3 Simulations of high $[K^+]$ membrane depolarization and intracellular $[\text{Ca}^{2+}]$

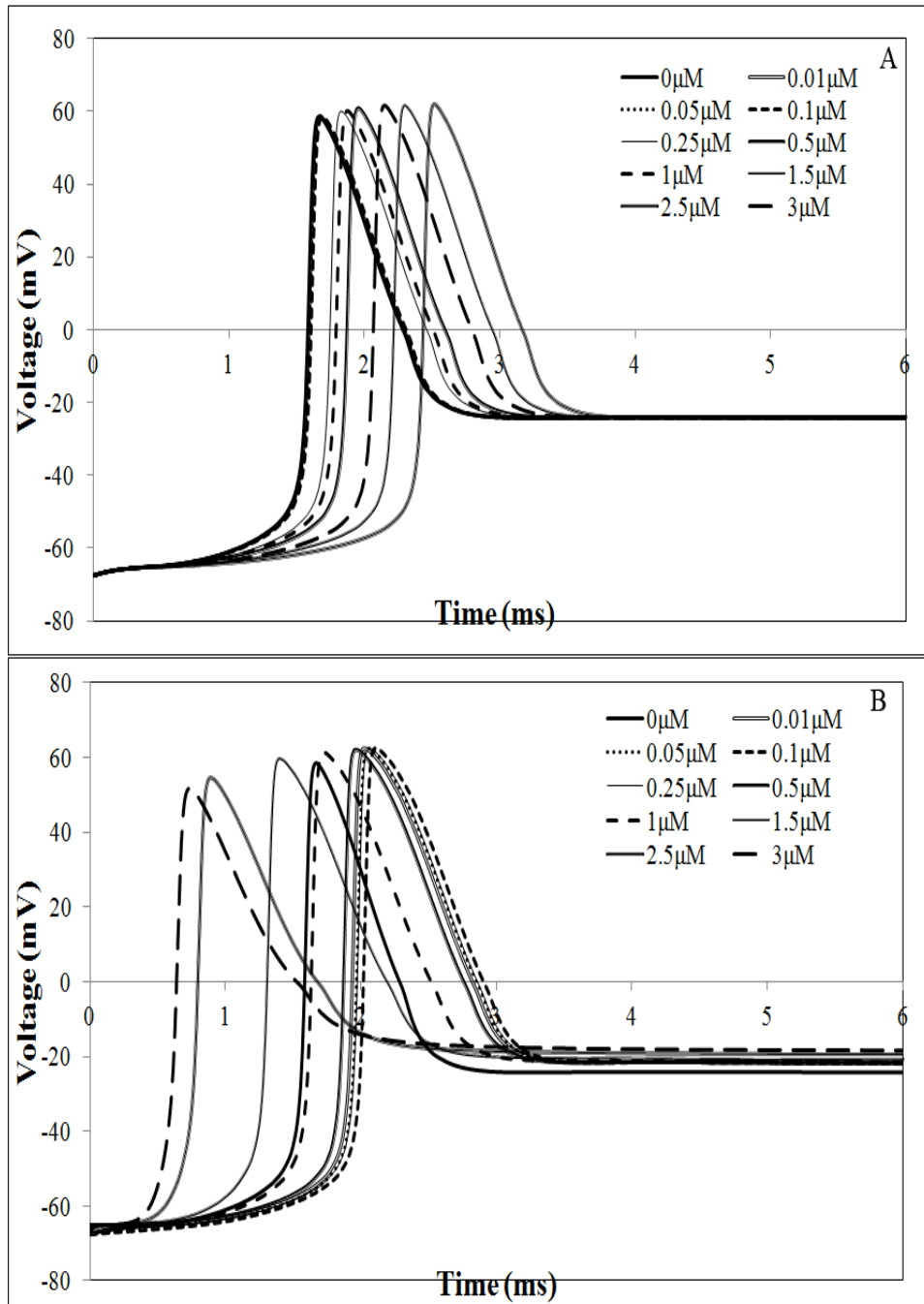


Figure 2.4: The effect of A β under membrane depolarized conditions for the A β block of the I_A channel and the A β -induced membrane conductance increase.

Membrane depolarization with 30mM [K⁺] was simulated by changing the Nernst potential of the K⁺ channels to -32 mV. [A β] = 0 (control), 0.01, 0.05, 0.1, 0.25, 0.5, 1, 1.5, 2.5 and 3 μ M. Plotted here: the A β I_A channel block and (A) A β -induced membrane conductance increase (B).

We simulate co-current application of 30mM [K⁺] and A β , at various concentrations, to the extracellular solution. In **Figure 2.4A**, when the membrane is depolarized with high [K⁺], the I_A channel block by A β increases AP latency in a [A β]-dependent manner. In **Figure 2.4B**, the A β -induced membrane conductance increase mechanism shows a non-linear correlation with [A β] of AP shape, height and latency, similar to the current-clamp results. At [A β] < 1 μ M, both mechanisms are predicted to increase AP latency. But, for the membrane conductance increase, at [A β] > 1 μ M, both AP latency and height are decreased. Unlike peak [Ca²⁺]_i under current-clamp conditions, high [K⁺] membrane depolarization simulations also reveal that the two mechanisms show very different correlations with respect to peak [Ca²⁺]_i (**Figures 2.5A and B**). A β 's block of I_A channels results in decreasing [Ca²⁺]_i with increasing [A β]. But, [Ca²⁺]_i for the membrane conductance increase mechanism a strong, non-linear response is observed. Because under high [K⁺] conditions, the neuron does not reset to its normal resting potential, as seen in **Figures 2.4A and B**, Ca²⁺ channels are still open. Therefore, there is a direct correlation between AP

latency and Ca^{2+} influx in our simulations; as AP latency increases, Ca^{2+} influx decreases. This is evident in the differences in the responses in **Figures 2.4 and 2.5** between the two mechanisms. Though the implication of such a result would be of interest experimentally, there have been few experiments designed to elucidate the $[\text{A}\beta]$ -dependent effect on $[\text{Ca}^{2+}]_i$ under high extracellular $[\text{K}^+]$ conditions at the short time-scale. Because intermediate Ca^{2+} data is sparse in the literature under these conditions, we wanted to demonstrate how simulating $[\text{Ca}^{2+}]_i$ under high $[\text{K}^+]$ conditions can provide potentially physiologically relevant information. Therefore, we compared our $[\text{Ca}^{2+}]_i$ results to experimental data on phosphorylated CREB (p-CREB) levels in the presence of $\text{A}\beta$. High $[\text{K}^+]$ membrane depolarization is commonly used to elicit and observe synaptic activity-dependent CREB phosphorylation[46, 47] and $\text{A}\beta$ has been shown to reduce phosphorylation of CREB in a $[\text{A}\beta]$ -dependent manner under high $[\text{K}^+]$ conditions[11, 48]. Investigators have described this reduction in p-CREB by $\text{A}\beta$ to be Ca^{2+} -dependent (primarily through L-type channels)[48, 49]. Therefore we compared both mechanisms to experimental data (**Figure 2.5A and B**) describing reduced p-CREB levels observed in neurons exposed to $\text{A}\beta$ under high extracellular $[\text{K}^+]$ [11]; since trends in p-CREB levels may be suggestive of trends in intracellular Ca^{2+} levels, though we acknowledge that other intracellular mechanisms may affect p-CREB levels[50].

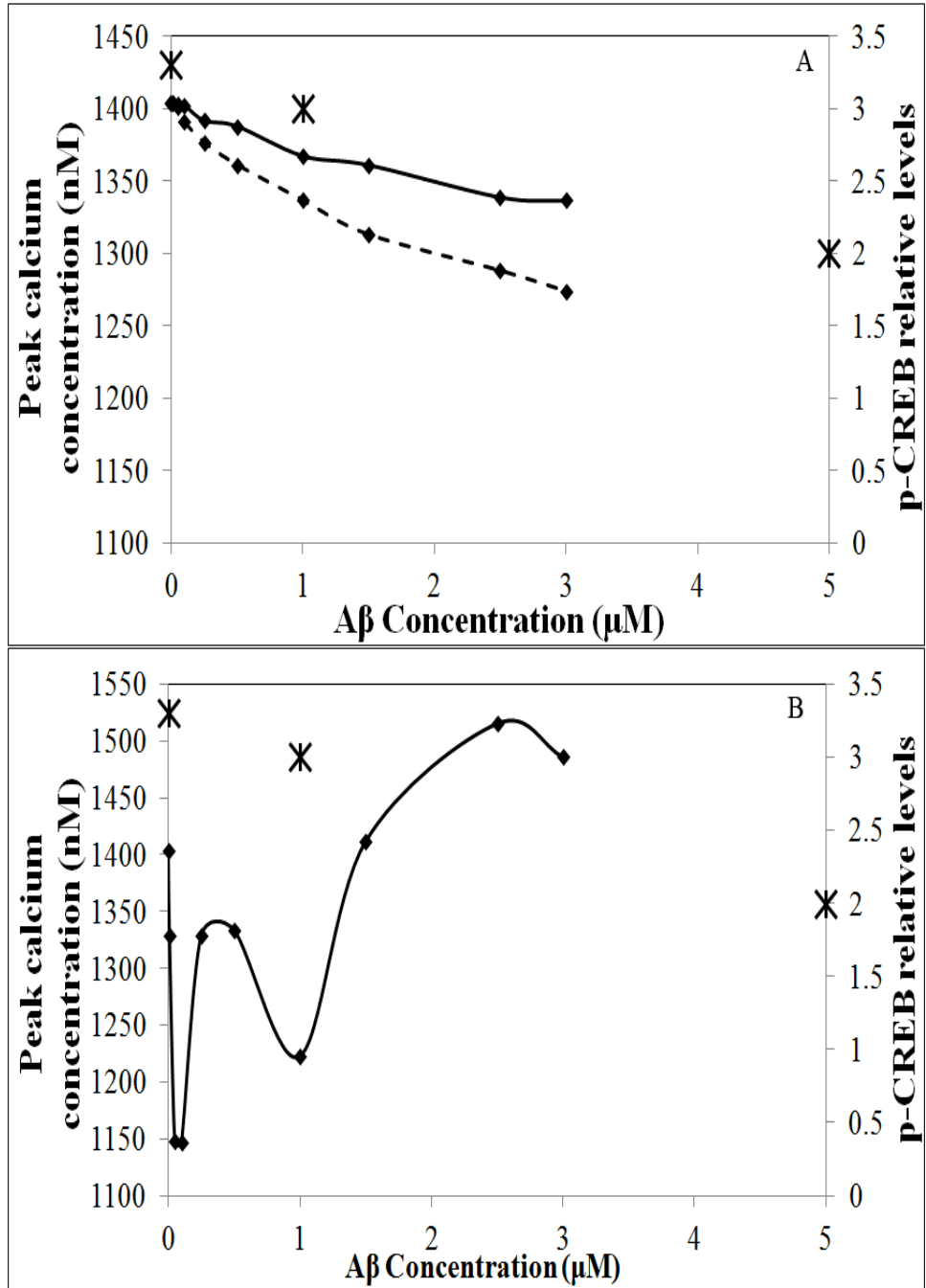


Figure 2.5: Intracellular Ca^{2+} levels under high $[\text{K}^+]$ membrane depolarized conditions. Changing the Nernst potential of the K^+ channels to -32 mV, we simulated high $[\text{K}^+]$ membrane depolarization with 30mM $[\text{K}^+]$. $[\text{A}\beta] = 0$ (control), 0.01, 0.05, 0.1, 0.25, 0.5, 1, 1.5, 2.5 and 3 μM . Intracellular Ca^{2+} levels were averaged over the model neuron volume and the peak Ca^{2+} level as a function of $[\text{A}\beta]$ is plotted for the I_A channel block (A) and membrane conductance increase (solid line/solid diamonds) (B). In (A), $\text{K}_I = 0.5$ and 1.5 μM are represented by the dotted line/solid squares and solid line/solid diamonds, respectively. Phosphorylated CREB (p-CREB) relative levels at elevated extracellular $[\text{K}^+]$ are plotted as a function of $[\text{A}\beta]$ [11] (asterisks).

In the presence of $\text{A}\beta$ and high $[\text{K}^+]$, p-CREB levels decrease in a $[\text{A}\beta]$ -dependent manner as experimental data shows in **Figures 2.5A and B**. Even though p-CREB levels were measured 1 hr after $\text{A}\beta$ addition, Bito et al[47] showed that changes in the phosphorylation state of p-CREB can occur in less than 30 sec after applied stimulus. Since increased Ca^{2+} influx is related to increased p-CREB levels under high $[\text{K}^+]$ conditions, then, hypothetically, reduced $[\text{Ca}^{2+}]$ would correlate to reduced p-CREB levels. In **Figures 2.5A and B**, the I_A channel block follows this decreasing trend, whereas the membrane conductance increase mechanism does not. If $\text{A}\beta$ increased membrane conductance, then p-CREB relative levels should show a strong, non-linear trend as well. Yet, not only does this not occur in the experimental

data shown in **Figure 2.5B**, but the decreasing trend in the experimental data for p-CREB levels of A β exposed neurons continues to decrease, linearly, at [A β] > 5 μ M (data not shown)[11, 48].

2.3.4 Implications of this computational study

Herein we tested the hypothesis that a computational neuron model can resolve the nature of short time-scale modifications of neuronal electrophysiology due to A β . Our neuron model was originally developed to examine the effects of the I_A channel block by A β under current-clamp conditions[28]. Including voltage-clamp and high [K⁺] membrane depolarization experimental conditions into the model makes it more broadly useful because its predictions about the differences between each proposed mechanism of A β -neuron interaction gives results that are comparable to and expound upon data from experimental literature. Though we included just two hypothetical A β -neuron interactions, our model can yield predictions for any A β -induced action on a neuron that is initiated by a A β -protein or -lipid interaction. Therefore, the model acts as a tool for both hypothesis generation and comparison. Importantly, the predictions from our model can be used to guide experimentation for discriminating between mechanisms of A β -neuron interaction, which to date has proven experimentally difficult[51].

From the comparison of A β 's block of I_A channels and A β -induced increase in membrane conductance mechanisms, we observed differences in [A β]-dependence of

AP generation and membrane excitability in current-clamp (**Figure 2.2**) and membrane depolarization experimental conditions (**Figure 2.4**), and determined that threshold current experiments could differentiate the two mechanisms at a single $[A\beta]$ (**Figure 2.2C and D**). Since many *in vitro* experiments with $A\beta$ are typically performed at one $[A\beta]$, this result is significant in that only a single point of data would be needed to distinguish these mechanistic effects. Though high $[K^+]$ membrane depolarization experiments do not represent a physiologically relevant condition, it is commonly used to study certain intracellular pathways[52], such as CREB phosphorylation[50, 53], that are synaptic activity-dependent. Through these high $[K^+]$ simulations, our model predicts trends in intermediate Ca^{2+} influx that could be integral in not only identifying a possible mechanism for $A\beta$ -neuron interaction, but provides a link to its effects on downstream intracellular processes. Because of the distinct effects observed from our computational study under this infrequently used experimental condition, we recommend this as a hypothesis to be tested experimentally.

There are many computational models of hippocampal neurons[54], which have been developed in-house[55, 56] or utilizing simulation programs such as NEURON[42, 57] and GENESIS[55, 58]. These models range from single compartment models[28, 56] to models with hundreds of compartments[42, 58]. Fewer models have been developed to simulate $A\beta$'s action on single neurons[42, 59-61]. Moreover, no existing modeling paradigms examine more than one mechanism of $A\beta$ -neuron interaction at a time. We report similar ion conductances as models

developed using NEURON[42, 62] or GENESIS[58, 63]. In addition, Ca^{2+} influx into our model neuron is described by Fickian diffusion providing spatio-temporal predictions of Ca^{2+} dynamics in the cell based on a theoretical framework. Neuron simulators, such as GENESIS[64] and NEURON[65], build-in a structure for creating morphologically detailed neurons. The addition of detailed morphology to the methodology presented in this paper would help us assess how different A β -neuron interactions could augment neuronal functions that are highly controlled spatially, such as input-output control[57, 66] and synaptic activity[29, 42].

A concern for all modeled systems is parameter choice. Parameters in our model for ion channel conductances, gating kinetics, initial conditions, and calcium dynamics have been taken from the Good and Murphy model[28]. Because it is known that I_A channels are not homogenously distributed across the neuron[66], some sensitivity analysis was done around the ratio of the delayed-rectifying to the I_A channel maximum conductance. The model is sensitive to this ratio, but the perturbation due to the block of the I_A channel is not (data not shown). A sensitivity analysis was also performed around K_I , the inhibition constant for the I_A channel block. Previously, it was described by Good et al[17] that 10 μM is an upper limit on the true value of the inhibition constant. In this sensitivity analysis, we used $K_I = 0.5$, 1.5 and 10 μM [1]. The sensitivity analysis showed that the model is sensitive to this parameter (data not shown), and therefore determining the value of this parameter experimentally would be useful for providing greater accuracy to our predictions. The parameters in the expressions used to describe the increase in capacitance and

conductance associated with A β from the membrane conductance mechanism were not tested for sensitivity of the model. Although, it is known that these parameters were derived, originally, from sparsely-tethered membranes[31], it is likely that there would be significant error associated with these parameters when comparing our results to empirical data performed on native membranes. Therefore, future work could incorporate a more detailed description of the parameter space involved with the membrane conductance increase mechanism through parameter sampling and experimental validation.

2.4 Conclusions

The ultimate goal of AD research is for a cure or adequate treatment for the disease. Most treatments have not been successful in ameliorating AD in patients[4]. Developing a wide variety of tools towards developing a mechanistic description of how A β interacts with the neuronal surface could be an avenue for drug design. One of the issues in this understanding is the lack of consensus around how A β interacts with the neuronal surface. We have developed a computational tool that allows us to discriminate between proposed A β -neuron interactions at the short time-scale, across three electrophysiology experimental systems. From examining the I_A channel block and the membrane conductance increase by A β , we have compared the distinct behavior of these two mechanisms under various experimentally testable conditions. Importantly, our model provides information about the types of experiments which might distinguish these two mechanisms further; information that is not currently

available in the literature. This methodology can be used to make predictions about multiple hypotheses of $A\beta$'s early action on neurons that would be experimentally testable. Implementing this comparative modeling for other mechanisms that have been implicated in the literature for $A\beta$'s action on a neuron and testing those predictions experimentally could be an important step toward defining $A\beta$'s early role in AD progression.

2.5 Appendix: Initial Conditions

The initial conditions are as follows[28]:

Initial Conditions	
V_0 (mV)	-67.5
$[Ca^{2+}]_r$ (nM)	50
$[B]_r$ (mM)	0.225
$[Ca^{2+}+B]_r$ (μ M)	1.87
m_i	0
h_i	1

Table 1: Initial Conditions

2.6 References

1. Ye C, Selkoe D, Hartley D. Protofibrils of amyloid beta-protein inhibit specific K⁺ currents in neocortical cultures. *Neurobiology of Disease*. 2003;13(3):177-90. doi: 10.1016/S0969-9961(03)00068-8|10.1016/S0969-9961(03)00068-8. PubMed PMID: WOS:000184559400001.
2. Leão RN, Colom LV, Borgius L, Kiehn O, Fisahn A. Medial septal dysfunction by A β -induced KCNQ channel-block in glutamatergic neurons. *Neurobiol Aging*. 2011. doi: S0197-4580(11)00297-1 [pii] 10.1016/j.neurobiolaging.2011.07.013. PubMed PMID: 21907458.
3. Kang J, Lemaire HG, Unterbeck A, Salbaum JM, Masters CL, Grzeschik KH, et al. The precursor of Alzheimer's disease amyloid A β protein resembles a cell-surface receptor. *Nature*. 1987;325(6106):733-6. doi: 10.1038/325733a0. PubMed PMID: 2881207.
4. Hardy J, Selkoe D. Medicine - The amyloid hypothesis of Alzheimer's disease: Progress and problems on the road to therapeutics. *Science*. 2002;297(5580):353-6. PubMed PMID: ISI:000176892600038.
5. [Anon], Assoc A. Alzheimer's Association Report 2011 Alzheimer's disease facts and figures. *Alzheimers & Dementia*. 2011;7(2):208-44. doi: DOI 10.1016/j.jalz.2011.02.004. PubMed PMID: ISI:000288930400010.
6. Khachaturian ZS. Calcium, membranes, aging, and Alzheimer's disease. Introduction and overview. *Ann N Y Acad Sci*. 1989;568:1-4. PubMed PMID: 2629579.

7. Demuro A, Parker I, Stutzmann G. Calcium Signaling and Amyloid Toxicity in Alzheimer Disease. *Journal of Biological Chemistry*. 2010;285(17):12463-8. doi: DOI 10.1074/jbc.R109.080895. PubMed PMID: ISI:000276787800001.
8. Alvarez A, Muñoz JP, Maccioni RB. A Cdk5-p35 stable complex is involved in the beta-amyloid-induced deregulation of Cdk5 activity in hippocampal neurons. *Exp Cell Res*. 2001;264(2):266-74. doi: S0014-4827(01)95152-3 [pii] 10.1006/excr.2001.5152. PubMed PMID: 11262183.
9. Alvarez AR, Godoy JA, Mullendorff K, Olivares GH, Bronfman M, Inestrosa NC. Wnt-3a overcomes beta-amyloid toxicity in rat hippocampal neurons. *Exp Cell Res*. 2004;297(1):186-96. doi: S0014482704000837 [pii] 10.1016/j.yexcr.2004.02.028. PubMed PMID: 15194435.
10. Chacon PJ, Garcia-Mejias R, Rodriguez-Tebar A. Inhibition of RhoA GTPase and the subsequent activation of PTP1B protects cultured hippocampal neurons against amyloid β toxicity. *Mol Neurodegener*. 2011;6(1):14. doi: 1750-1326-6-14 [pii] 10.1186/1750-1326-6-14. PubMed PMID: 21294893; PubMed Central PMCID: PMC3038970.
11. Tong L, Thornton P, Balazs R, Cotman C. beta-Amyloid-(1-42) impairs activity-dependent cAMP-response element-binding protein signaling in neurons at concentrations in which cell survival is not compromised. *Journal of Biological Chemistry*. 2001;276(20):17301-6. doi: 10.1074/jbc.M010450200. PubMed PMID: WOS:000168730400094.

12. Fogarty M, Downer E, Campbell V. A role for c-Jun N-terminal kinase 1 (JNK1), but not JNK2, in the beta-amyloid-mediated stabilization of protein p53 and induction of the apoptotic cascade in cultured cortical neurons. *Biochemical Journal*. 2003;371:789-98. doi: 10.1042/BJ20021660. PubMed PMID: WOS:000182733400016.
13. Kim S, Rhim H. Effects of Amyloid-beta Peptides on Voltage-Gated L-Type Ca(V)1.2 and Ca(V)1.3 Ca(2+) Channels. *Molecules and Cells*. 2011;32(3):289-94. doi: 10.1007/s10059-011-0075-x. PubMed PMID: WOS:000297627300011.
14. Williams T, Serpell L. Membrane and surface interactions of Alzheimer's A beta peptide - insights into the mechanism of cytotoxicity. *Febs Journal*. 2011;278(20):3905-17. doi: 10.1111/j.1742-4658.2011.08228.x. PubMed PMID: WOS:000295335500012.
15. Askarova S, Yang X, Lee JC. Impacts of membrane biophysics in Alzheimer's disease: from amyloid precursor protein processing to a β Peptide-induced membrane changes. *Int J Alzheimers Dis*. 2011;2011:134971. doi: 10.4061/2011/134971. PubMed PMID: 21547213; PubMed Central PMCID: PMC3087431.
16. Bokvist M, Lindstrom F, Watts A, Grobner G. Two types of Alzheimer's beta-amyloid (1-40) peptide membrane interactions: Aggregation preventing transmembrane anchoring Versus accelerated surface fibril formation. *Journal of Molecular Biology*. 2004;335(4):1039-49. doi: 10.1016/j.jmb.2003.11.046|10.1016/j.jmb.2003.11.046. PubMed PMID: WOS:000188067000014.

17. Good T, Smith D, Murphy R. beta-amyloid peptide blocks the fast-inactivating K⁺ current in rat hippocampal neurons. *Biophysical Journal*. 1996;70(1):296-304. PubMed PMID: ISI:A1996TY68300024.
18. Mattson MP, Cheng B, Davis D, Bryant K, Lieberburg I, Rydel RE. beta-Amyloid peptides destabilize calcium homeostasis and render human cortical neurons vulnerable to excitotoxicity. *J Neurosci*. 1992;12(2):376-89. PubMed PMID: 1346802.
19. Whitson JS, Appel SH. Neurotoxicity of A beta amyloid protein in vitro is not altered by calcium channel blockade. *Neurobiol Aging*. 1995;16(1):5-10. doi: 0197458095800029 [pii]. PubMed PMID: 7723935.
20. Demuro A, Mina E, Kayed R, Milton S, Parker I, Glabe C. Calcium dysregulation and membrane disruption as a ubiquitous neurotoxic mechanism of soluble amyloid oligomers. *Journal of Biological Chemistry*. 2005;280(17):17294-300. doi: DOI 10.1074/jbc.M500997200. PubMed PMID: ISI:000228615500093.
21. Glabe CG. Amyloid Oligomers Structures and Toxicity. *The Open Biology Journal*. 2009;2:222-7.
22. Lee S, Fernandez E, Good T. Role of aggregation conditions in structure, stability, and toxicity of intermediates in the A beta fibril formation pathway. *Protein Science*. 2007;16(4):723-32. doi: DOI 10.1110/ps.062514807. PubMed PMID: ISI:000245161800017.
23. Lacor P. Advances on the understanding of the origins of synaptic pathology in AD. *Current Genomics*. 2007;8(8):486-508. doi: 10.2174/138920207783769530. PubMed PMID: WOS:000254654000002.

24. Sepulveda FJ, Parodi J, Peoples RW, Opazo C, Aguayo LG. Synaptotoxicity of Alzheimer beta amyloid can be explained by its membrane perforating property. PLoS One. 2010;5(7):e11820. doi: 10.1371/journal.pone.0011820. PubMed PMID: 20676404; PubMed Central PMCID: PMCPMC2910737.
25. Lioudyno MI, Broccio M, Sokolov Y, Rasool S, Wu J, Alkire MT, et al. Effect of synthetic $\alpha\beta$ Peptide oligomers and fluorinated solvents on kv1.3 channel properties and membrane conductance. PLoS One. 2012;7(4):e35090. doi: PONE-D-11-16828 [pii] 10.1371/journal.pone.0035090. PubMed PMID: 22563377; PubMed Central PMCID: PMCPMC3338507.
26. Pimplikar S. Reassessing the amyloid cascade hypothesis of Alzheimer's disease. International Journal of Biochemistry & Cell Biology. 2009;41(6):1261-8. doi: 10.1016/j.biocel.2008.12.015. PubMed PMID: WOS:000264669300008.
27. Cappai R, Barnham KJ. Delineating the mechanism of Alzheimer's disease A beta peptide neurotoxicity. Neurochem Res. 2008;33(3):526-32. doi: 10.1007/s11064-007-9469-8. PubMed PMID: 17762917.
28. Good TA, Murphy RM. Effect of beta-amyloid block of the fast-inactivating K⁺ channel on intracellular Ca²⁺ and excitability in a modeled neuron. Proc Natl Acad Sci U S A. 1996;93(26):15130-5. PubMed PMID: 8986775; PubMed Central PMCID: PMCPMC26368.
29. Chen C. beta-amyloid increases dendritic Ca²⁺ influx by inhibiting the A-type K⁺ current in hippocampal CA1 pyramidal neurons. Biochemical and Biophysical Research Communications. 2005;338(4):1913-9. doi:

10.1016/j.bbrc.2005.10.169|10.1016/j.bbrc.2005.10.169. PubMed PMID:
WOS:000233815900036.

30. Zhang C, Yang P. Zinc-induced aggregation of A beta (10-21) potentiates its action on voltage-gated potassium channel. *Biochemical and Biophysical Research Communications*. 2006;345(1):43-9. doi:
10.1016/j.bbrc.2006.04.044|10.1016/j.bbrc.2006.04.044. PubMed PMID:
WOS:000237877700007.

31. Valincius G, Heinrich F, Budvytyte R, Vanderah DJ, McGillivray DJ, Sokolov Y, et al. Soluble amyloid beta-oligomers affect dielectric membrane properties by bilayer insertion and domain formation: implications for cell toxicity. *Biophys J*. 2008;95(10):4845-61. doi: S0006-3495(08)78623-5 [pii]
10.1529/biophysj.108.130997. PubMed PMID: 18515395; PubMed Central PMCID:
PMC2576380.

32. Sokolov Y, Kozak A, Kayed R, Chanturiya A, Glabe C, Hall JE. Soluble Amyloid Oligomers Increase Bilayer Conductance by Altering Dielectric Structure. *The Journal of General Physiology*. 2006;128(6):10.

33. Li WY, Czilli DL, Simmons LK. Neuronal membrane conductance activated by amyloid beta peptide: importance of peptide conformation. *Brain Res*. 1995;682(1-2):207-11. doi: 0006-8993(95)00264-Q [pii]. PubMed PMID: 7552313.

34. Cottrell JR, Dubé GR, Egles C, Liu G. Distribution, density, and clustering of functional glutamate receptors before and after synaptogenesis in hippocampal neurons. *J Neurophysiol*. 2000;84(3):1573-87. PubMed PMID: 10980028.

35. Hodgkin AL, Huxley AF. A quantitative description of membrane current and its application to conduction and excitation in nerve. *J Physiol.* 1952;117(4):500-44. PubMed PMID: 12991237; PubMed Central PMCID: PMCPMC1392413.
36. Bekkers JM. Properties of voltage-gated potassium currents in nucleated patches from large layer 5 cortical pyramidal neurons of the rat. *J Physiol.* 2000;525 Pt 3:593-609. doi: PHY_0058 [pii]. PubMed PMID: 10856115; PubMed Central PMCID: PMCPMC2269964.
37. Gentet L, Stuart G, Clements J. Direct measurement of specific membrane capacitance in neurons. *Biophysical Journal.* 2000;79(1):314-20. PubMed PMID: ISI:000088048500025.
38. Jhamandas JH, Cho C, Jassar B, Harris K, MacTavish D, Easaw J. Cellular mechanisms for amyloid beta-protein activation of rat cholinergic basal forebrain neurons. *J Neurophysiol.* 2001;86(3):1312-20. PubMed PMID: 11535679.
39. Kawahara M, Arispe N, Kuroda Y, Rojas E. Alzheimer's disease amyloid beta-protein forms Zn(2+)-sensitive, cation-selective channels across excised membrane patches from hypothalamic neurons. *Biophys J.* 1997;73(1):67-75. doi: S0006-3495(97)78048-2 [pii] 10.1016/S0006-3495(97)78048-2. PubMed PMID: 9199772; PubMed Central PMCID: PMCPMC1180909.
40. Shelat PB, Chalimoniuk M, Wang JH, Strosznajder JB, Lee JC, Sun AY, et al. Amyloid beta peptide and NMDA induce ROS from NADPH oxidase and AA release from cytosolic phospholipase A2 in cortical neurons. *J Neurochem.* 2008;106(1):45-55. doi: JNC5347 [pii]

10.1111/j.1471-4159.2008.05347.x. PubMed PMID: 18346200.

41. Kaye R, Pensalfini A, Margol L, Sokolov Y, Sarsoza F, Head E, et al. Annular protofibrils are a structurally and functionally distinct type of amyloid oligomer. *J Biol Chem*. 2009;284(7):4230-7. doi: M808591200 [pii]

10.1074/jbc.M808591200. PubMed PMID: 19098006; PubMed Central PMCID: PMC2640961.

42. Morse TM, Carnevale NT, Mutalik PG, Migliore M, Shepherd GM. Abnormal Excitability of Oblique Dendrites Implicated in Early Alzheimer's: A Computational Study. *Front Neural Circuits*. 2010;4. doi: 10.3389/fncir.2010.00016. PubMed PMID: 20725509; PubMed Central PMCID: PMC2901152.

43. Williams S, Stuart G. Role of dendritic synapse location in the control of action potential output. *Trends in Neurosciences*. 2003;26(3):147-54. doi: 10.1016/S0166-2236(03)00035-3|10.1016/S0166-2236(03)00035-3. PubMed PMID: WOS:000181351900008.

44. Bean BP. The action potential in mammalian central neurons. *Nat Rev Neurosci*. 2007;8(6):451-65. doi: nrn2148 [pii] 10.1038/nrn2148. PubMed PMID: 17514198.

45. Blanchard B, Thomas V, Ingram V. Mechanism of membrane depolarization caused by the Alzheimer A beta 1-42 peptide. *Biochemical and Biophysical Research Communications*. 2002;293(4):1197-203. doi: 10.1016/S0006-291X(02)00346-7. PubMed PMID: WOS:000175911900008.

46. Saura C, Valero J. The role of CREB signaling in Alzheimer's disease and other cognitive disorders. *Reviews in the Neurosciences*. 2011;22(2):153-69. doi:

10.1515/RNS.2011.018|10.1515/RNS.2011.018. PubMed PMID:
WOS:000300088800003.

47. Bito H, Deisseroth K, Tsien R. CREB phosphorylation and dephosphorylation: A Ca^{2+} - and stimulus duration-dependent switch for hippocampal gene expression. *Cell*. 1996;87(7):1203-14. doi: 10.1016/S0092-8674(00)81816-4. PubMed PMID: WOS:A1996WA54100009.

48. Espana J, Valero J, Minano-Molina A, Masgrau R, Martin E, Guardia-Laguarta C, et al. beta-Amyloid Disrupts Activity-Dependent Gene Transcription Required for Memory through the CREB Coactivator CRTC1. *Journal of Neuroscience*. 2010;30(28):9402-10. doi: 10.1523/JNEUROSCI.2154-10.2010. PubMed PMID: WOS:000279899100008.

49. Ma Q, Harris-White M, Ubeda O, Simmons M, Beech W, Lim G, et al. Evidence of A beta- and transgene-dependent defects in ERK-CREB signaling in Alzheimer's models. *Journal of Neurochemistry*. 2007;103(4):1594-607. doi: 10.1111/j.1471-4159.2007.04869.x|10.1111/j.1471-4159.2007.04869.x. PubMed PMID: WOS:000250403500030.

50. Shaywitz A, Greenberg M. CREB: A stimulus-induced transcription factor activated by a diverse array of extracellular signals. *Annual Review of Biochemistry*. 1999;68:821-61. doi: 10.1146/annurev.biochem.68.1.821. PubMed PMID: WOS:000082693200026.

51. Williams TL, Serpell LC. Membrane and surface interactions of Alzheimer's A β peptide--insights into the mechanism of cytotoxicity. *FEBS J*. 2011;278(20):3905-17. doi: 10.1111/j.1742-4658.2011.08228.x. PubMed PMID: 21722314.

52. Yamada MK, Nakanishi K, Ohba S, Nakamura T, Ikegaya Y, Nishiyama N, et al. Brain-derived neurotrophic factor promotes the maturation of GABAergic mechanisms in cultured hippocampal neurons. *J Neurosci.* 2002;22(17):7580-5. doi: 22/17/7580 [pii]. PubMed PMID: 12196581.
53. Kobayashi T, Yamauchi R, Murata S. Effect of Ca^{2+} antagonists on high- K^{+} evoked increase in $[\text{Ca}^{2+}]_i$ in rat cerebral synaptosomes and hippocampal neurons. *Jpn J Pharmacol.* 1992;58(4):417-25. PubMed PMID: 1405039.
54. Demont-Guignard S, Benquet P, Gerber U, Wendling F. Analysis of intracerebral EEG recordings of epileptic spikes: insights from a neural network model. *IEEE Trans Biomed Eng.* 2009;56(12):2782-95. doi: 10.1109/TBME.2009.2028015. PubMed PMID: 19651549; PubMed Central PMCID: PMC3245744.
55. Orbán G, Kiss T, Erdi P. Intrinsic and synaptic mechanisms determining the timing of neuron population activity during hippocampal theta oscillation. *J Neurophysiol.* 2006;96(6):2889-904. doi: 01233.2005 [pii] 10.1152/jn.01233.2005. PubMed PMID: 16899632.
56. Golomb D, Yue C, Yaari Y. Contribution of persistent Na^{+} current and M-type K^{+} current to somatic bursting in CA1 pyramidal cells: combined experimental and modeling study. *J Neurophysiol.* 2006;96(4):1912-26. doi: 00205.2006 [pii] 10.1152/jn.00205.2006. PubMed PMID: 16807352.
57. Li X, Ascoli GA. Computational simulation of the input-output relationship in hippocampal pyramidal cells. *J Comput Neurosci.* 2006;21(2):191-209. doi: 10.1007/s10827-006-8797-z. PubMed PMID: 16871350.

58. Káli S, Freund TF. Distinct properties of two major excitatory inputs to hippocampal pyramidal cells: a computational study. *Eur J Neurosci.* 2005;22(8):2027-48. doi: EJN4406 [pii]
10.1111/j.1460-9568.2005.04406.x. PubMed PMID: 16262641.
59. Zou X, Coyle D, Wong-Lin K, Maguire L. Beta-amyloid induced changes in A-type K(+) current can alter hippocampo-septal network dynamics. *J Comput Neurosci.* 2011. doi: 10.1007/s10827-011-0363-7. PubMed PMID: 21938438.
60. Kidd JF, Sattelle DB. The effects of amyloid peptides on A-type K(+) currents of *Drosophila* larval cholinergic neurons: modeled actions on firing properties. *Invert Neurosci.* 2006;6(4):207-13. doi: 10.1007/s10158-006-0034-y. PubMed PMID: 17106756.
61. Tiveci S, Akin A, Cakir T, Saybaşili H, Ulgen K. Modelling of calcium dynamics in brain energy metabolism and Alzheimer's disease. *Comput Biol Chem.* 2005;29(2):151-62. doi: S1476-9271(05)00023-X [pii]
10.1016/j.combiolchem.2005.03.002. PubMed PMID: 15833443.
62. Migliore M, Ferrante M, Ascoli GA. Signal propagation in oblique dendrites of CA1 pyramidal cells. *J Neurophysiol.* 2005;94(6):4145-55. doi: 94/6/4145 [pii]
10.1152/jn.00521.2005. PubMed PMID: 16293591.
63. Menschik E, Finkel L. Cholinergic neuromodulation of an anatomically reconstructed hippocampal CA3 pyramidal cell. *Neurocomputing.* 2000;32:197-205. doi: 10.1016/S0925-2312(00)00164-8. PubMed PMID: WOS:000087897800029.

64. Bower JM, Beeman D. The book of GENESIS : exploring realistic neural models with the GEneral NEural SIMulation System. 2nd ed. Santa Clara, Calif.: TELOS; 1998. xxiv, 458 p. p.
65. Hines M, Carnevale N. The NEURON simulation environment. Neural Computation. 1997;9(6):1179-209. PubMed PMID: ISI:A1997XM55000001.
66. Hoffman DA, Magee JC, Colbert CM, Johnston D. K⁺ channel regulation of signal propagation in dendrites of hippocampal pyramidal neurons. Nature. 1997;387(6636):869-75. doi: 10.1038/43119. PubMed PMID: 9202119.

Chapter 3: Toward inferring A β -neuron interactions using CellNOptR: a case study²

3.1 Introduction

“The great tragedy of science – the slaying of a beautiful hypothesis by an ugly fact.” ~ Thomas Huxley, English Biologist (1825-1895)

β -amyloid (A β) is the primary protein component of senile plaques associated with Alzheimer’s disease (AD)[3]. Although highly studied, the details of the molecular mechanisms underlying A β ’s role in AD remains undetermined. It is widely accepted that A β plays a primary, albeit complex, role in AD pathology. A β , in the form of mature fibrils, is found in the extracellular matrix of AD post-mortem brains, surrounding areas of massive neuronal loss[67]. This finding led, in turn, to *in vitro* studies involving the addition of A β to cells exogenously in order to observe A β ’s direct effects on cell populations[4]. From initial studies, it was apparent that exogenously applied A β causes intracellular changes to cells that result in eventual cellular dysfunction and death. This suggests, then, a mechanism by which A β acts on the extracellular surface of neurons, thereby relaying aberrant intracellular signals to the cell causing dysfunction leading to cellular death [4, 68].

² Co-authors: Angela Norton, Patrick O’Neil, Ivan Erill, Mariajosé Castellanos, and Theresa A. Good

For over more than two decades, many hypotheses for A β 's interactions with neurons have been proposed. In general, they fall into three categories: A β -receptor, A β -lipid or some combination of the two, interactions. Earlier researchers proposed that A β 's interaction with the neuronal surface was fairly specific to a receptor or an ion channel[39, 69], or with the lipid membrane itself[20, 32]. However, as more signaling data became available, it was evident that the complex signaling phenomena observed could not be reconciled into just a specific interaction with a receptor or the lipid membrane[23, 70]. There may be multiple factors contributing to divergent responses of neurons to A β : A β aggregation state-dependent effects, A β species-dependent effects, tissue-specific effects, measured response time-scale and promiscuity of A β interactions[23, 71, 72]. Though there may be a multiplicity of independent factors leading to observed A β effects on neurons, we hypothesize that the combined effect of these factors would give rise to an identifiable signaling landscape, characterized by the results of various experimental preparations.

Extracellular signals are transduced via membrane receptors, ion channels and even the membrane itself to intracellular signals whose purpose is to alter cellular function in response to its environment. Physiologically favorable environments will favor a healthy cellular response while pathological environments may favor detrimental cellular responses, such as in some diseases[46, 73-76]. This makes understanding changes in cell signaling in the presence of a particular pathological state, such as exposure to A β , important to uncovering disease mechanisms. Because signaling networks must respond to a litany of extracellular cues in a noisy

environment, signaling networks are necessarily complex and integrative[77]. We, therefore, chose to examine computationally the effects of multiple proposed A β -neuron interactions with a CA1 hippocampal signaling network[78]. This network, expertly curated from 1200 literature sources, consists of over 500 nodes and 1200 interactions, with nodes being related to signaling molecules (kinases, phosphatases, receptors, G-coupled proteins, etc) and edges (interactions) related to the relationship between a pair of nodes (activation, inhibition, and binding)[78]. This network, hereby to be referred to as a prior knowledge network or PKN[79], was utilized in this study to attempt to deduce specific A β -induced network topologies based on hypothesized A β -neuron interactions.

Deriving network topologies for complex, systems-level signaling networks is challenging. There are top-down[80-83] and bottom-up[79, 84-86] techniques that can be utilized for building network topologies. Top-down techniques require knowledge of all signaling molecules and their states in the presence of a particular set of extracellular cues of interest. This problem becomes intractable quickly, both computationally and experimentally, for only moderately sized networks (i.e., number of nodes < 100). For instance, utilizing a fairly simplistic, albeit informative[87], Boolean approach with two states, a network with 100 nodes would have to be observed on 2^{100} states, which is an unrealistic number of experiments or computations of random networks to perform. In cases where enough is known about the particular molecular species and their interactions, classical kinetic modeling could be employed; however, the parameter space is typically not well-defined for

even small networks ($n < 50$)[88]. Thus, bottom-up techniques are preferable for larger networks ($n > 50$). In this case, network topologies are found by data-driven means utilizing statistical search algorithms such as Bayesian networks[87] or information-theoretic simulations[84, 89]. These methods, though proven to be useful for developing specific network topologies given a set of experimental data, are not able to incorporate “prior knowledge” of particular pathways in the system beyond those inferred directly from the experimental data.

In this work, we have chosen to utilize a bottom-up technique that is both data-driven and accounts for “prior knowledge” of signaling in the system of interest. This technique, implemented in the computational software CellNOptR, was developed by Saez-Rodriguez and coworkers[79]. Making use of a prior knowledge network, defined as a protein interaction map of signaling for a particular system, CellNOptR takes in experimental data as an input to infer network topologies specific to the inputted experimental data, or the training set. In this study, we utilized CellNOptR to attempt to infer network topologies that were consistent with literature-derived experimental data for neurons exposed to $A\beta$, where the network included different specific hypotheses concerning the first steps in $A\beta$'s interaction with neurons. Although CellNOptR has been utilized to infer cell-type specific network topologies under experimental conditions[79, 90], the prior knowledge networks used were relatively small in comparison to the one used in our study (< 100 nodes) and the dataset was very large (> 1000 data points in[79]). In this study, we tested various $A\beta$ -neuron interactions as part of the PKN against literature-derived datasets. We

found that with a relatively small dataset that increasing dataset size does not necessarily improve the fit of network topologies found by CellNOptR. We also found that CellNOptR was able to find network topologies that fit scrambled datasets better than the real data set, which was an unexpected result. Lastly, regardless of which set of A β -neuron interactions selected, the fit to the data varied little between them. We suggest that part of the challenge of inferring interactions using a somewhat sparse literature-derived dataset lies in the availability of data at informative nodes in the network versus data at integrating, non-discriminative nodes. These results may help define better methodologies both for experimental data collection and network topology inference for complex signaling networks involving A β , or any other ligand or cell activator of interest.

3.2 Methods

3.2.1 Model description

CellNOptR[79] is genetic algorithm-based software used to identify signaling network topology from experimental data by making use of a prior knowledge network (PKN). A PKN is a signaling network graph composed of all known signaling species and their interactions. For our purposes, a protein interaction map of a CA1 hippocampal neuronal signaling network with 545 species and 1235 interactions was used[78]. The network (**Figure 3.1**) consists of nodes that represent receptors, ion channels, kinases, phosphatases, adapter, scaffolding proteins, and transcription factors; and edges that represent specific interactions between two

species, such as activation, inhibition or binding. To visualize the network, the nodes and their interactions were uploaded into Cytoscape[91].

	Original Dataset	Larger Dataset
A β incubation time	≤ 60 mins	≤ 60 mins
Measured species	10	24
Stimulated/inhibited species	13	27
Number of literature sources (out of 868)	13	22
Number of nodes total (percent of nodes in network)	23 (4.2%)	51 (9.4%)

Table 3.1: Description of datasets used for CellNOptR optimization. Two datasets are used in this study. Both datasets were curated based on the following criteria: to minimize variations in data that may arise from differences in cell phenotype we only included data from *in vitro* studies performed on primary culture hippocampal or cortical neurons. To minimize inclusion of effects associated with gene expression as opposed to signaling effects, we restricted data inclusion to that from experiments where the A β incubation time (the time after the application of A β to the neurons before measurement is taken) of 60 minutes or less. No attempt was made to control for A β aggregation state or morphology. Results from two datasets were compared, original and larger. In this table, the number of measured species (or proteins), the number of stimulated/inhibited species, the number of literature sources used to curate data and the number of nodes (and percent of total) that were present in the data are presented here for both datasets.

Experimental data were collected from literature-based sources listed in **Table 3.1**. Data were chosen based on the following criteria: *in vitro* studies performed in primary cultures of hippocampal or cortical neurons, and A β incubation times of less than 60 minutes. Primary culture hippocampal or cortical neuronal preparations were chosen for this study because they are the primary neuronal population in the brain affected by A β . A β incubation time of less than 60 minutes was chosen in order to identify A β 's early action on neurons at the cell surface prior to any changes in gene expression, which tends to happen over longer periods of time[92]. A β species and aggregation state as well as concentration were not used as criteria for data selection. The following databases were searched: MEDLINE and Web of Science. Keywords utilized in the search are given in **Appendix 3A**. Numerical data were used wherever applicable; however, most data were curated directly from figures. Data were cross-checked by two independent observers to ensure that inclusion criteria were correctly applied. Experimental data were inputted into a MIDAS format[79] and loaded into the CellNOptR software (**Figure 3.2**). Because CellNOptR is based on Boolean logic, experimental data were normalized from 0 (off/not active) to 1 (on/active). In order to test the effects of dataset size, we used the original dataset from our first literature curation and then added in additional data that was found from a second curation step to create what we referred to as the larger dataset. CellNOptR performs a genetic algorithm-based optimization in order to identify a set of network topologies that most closely explains the inputted experimental data. The objective function (Eq. 3.2.1) compares the mean squared difference between the experimental data and the model predictions (Eq. 3.2.2).

The model's predictions are determined from the Boolean steady state response of each node. The objective function (Eq. 3.2.1) was minimized during the course of the optimization in order to find the best solution.

$$\Theta(P) = \Theta_f(P) + \alpha \cdot \Theta_s(P) \quad (3.2.1)$$

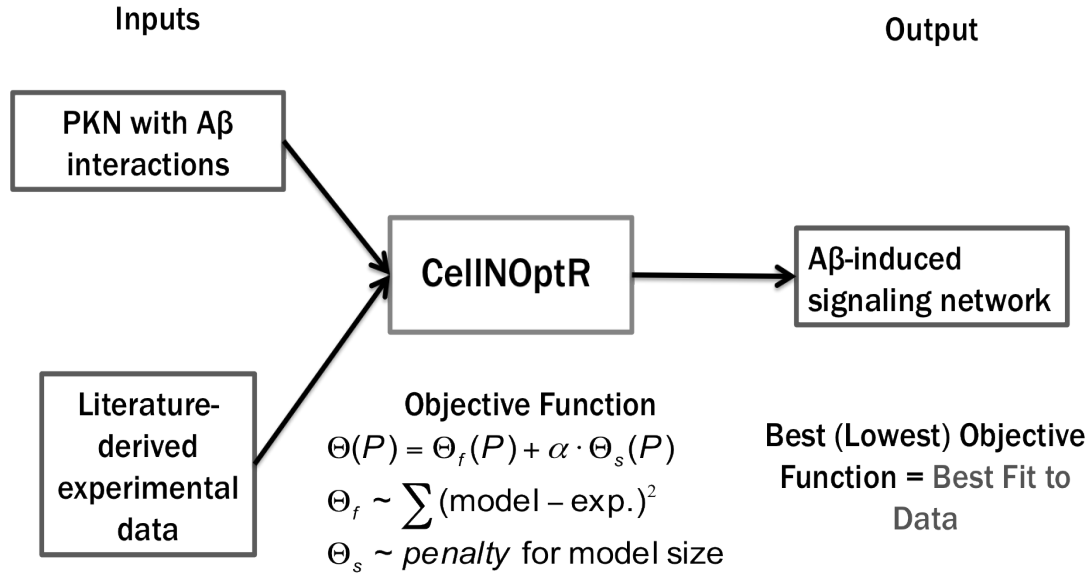
$$\Theta_f = \frac{1}{n_E} \sum_{k=1}^s \sum_{l=1}^m \sum_{t=1}^n (B_{k,l,t}^M(P) - B_{k,l,t}^E)^2 \quad (3.2.2)$$

$$\Theta_s(P) = \frac{1}{v_e} \sum_{e=1}^r v_e P_e \quad (3.2.3)$$

$\Theta(P)$ is the objective function, which is in terms of the vector of edges, P , and is bipartite. The first part of the objective function is Θ_f , the mean square error between the experimental data ($B_{k,l,t}^E$) and the model ($B_{k,l,t}^M$). The second part is Θ_s , a penalty for model size such that, as Eq. 3.2.3 shows, models with a large number of edges (v_e) are penalized more heavily than those with a smaller number of edges. Θ_s is scaled by α , an adjustable parameter set to its default value of 0.001 for the entirety of this study. Changing the size of α would change the relative magnitude of the contributions of the two parts of the objective function. The indices, k , l , and t , and the variables, s , m , and n represent the experimental condition, readout (measured node) and the time point (only initial and final in this study), respectively. The output from CellNOptR is a family of network solutions within a tolerance of the best solution (tolerance: 10%). The best solution is the solution with the overall minimum

objective function. Each interaction (or edge) is given a weight, which is the number of network topologies containing this interaction over the total solution set size. Therefore, a weight of 0 means that an interaction never occurs in the solution set and a weight of 1 means that the interaction always exists in the solution set.

How CellNOptR works



CellNOptR developed by: Saez-Rodríguez et al, Mol. Sys. Biol., 2009

Figure 3.2: Flow chart for CellNOptR. This flowchart shows the two inputs into CellNOptR, a prior knowledge network (PKN) with assumed Aβ-neuron interactions and literature-derived experimental data. The output is a family of networks, which in this study, would represent Aβ-induced signaling network topologies based on a particular set of Aβ-neuron interactions. The objective function is used to determine how well the best network topology matches the experimental data.

3.2.2 Statistical analysis

In order to make comparisons between the results from CellNOptR between different A β -neuron interactions, we ran CellNOptR multiple times on the same PKN and experimental data set. This allowed us to create a distribution of best objective functions that could be used for comparison. Because there is some stochasticity in the solution from the genetic algorithm (primarily due to the mutation rate), the same solution was not necessarily found at each instance of the algorithm, even if the same two inputs were given it. Therefore, it was necessary to run the algorithm multiple times to account for the variation in the solutions. We expected that better solutions should have a distribution with a lower median best objective function, a small percentage of overlap, and shifted toward the left on the abscissa. Comparisons of the solutions for each A β -neuron interaction tested were made by comparing the median and distributions of the best objective function. In order to determine statistical significance of the comparisons of multiple mechanisms, the Kruskal-Wallis test was used[93]. This is a statistical test similar to an ANOVA, except that it is non-parametric and does not require that the underlying distributions of the data be normally distributed. In order to perform pairwise comparisons, a Mann-Whitney U test was used with an *a priori* Bonferroni adjustment (see **Appendix 3C**)[93]. All statistical analysis, calculations of medians, associated plots were performed in the statistical program, Minitab[94].

3.2.3 Choice of $A\beta$ -neuron interactions

In this study, we chose $A\beta$ -neuron interactions to test using CellNOptR. Though hypothetically we could have selected any of the nodes for an $A\beta$ – cell interaction, we chose only cell surface receptors as hypothesized loci of $A\beta$ -cell interaction. This is because we made the assumption, based on *in vitro* observations[70, 72] that $A\beta$ initiates its action at the cell surface, and then relays aberrant signals through a pathway or sets of pathways affected by said receptors and/or ion channels. We tested two cases in which we selected the entire potential cell surface receptors/ion channels with which $A\beta$ could possibly interact; we either activated or inhibited them. This case allowed CellNOptR to sample all possible $A\beta$ -neuron interactions that might explain the data. $A\beta$'s induction of ion channels ($A\beta$ -Ionotropic) mechanism is based on the long standing calcium hypothesis of Alzheimer's disease[6, 7, 75], namely that $A\beta$ causes a disruption in calcium homeostasis in the cell by adverse interactions with calcium conducting ion channels or by forming an ion conducting pore (of which calcium has the largest concentration gradient). We also chose to add $A\beta$'s interaction with G-coupled protein receptors, a mechanism hypothesized by[95, 96]. Another set of mechanisms tested was $A\beta$'s interaction with G-protein coupled receptors and Integrin receptors, based on results out of our laboratory[97] with a different cell type than that included in our curated data.

Mechanism Code	Description	References
Iono_orig	A β is connected to ionotropic (conduct ions) receptors and channels (see Appendix 3B). This network was optimized on the original data set in CellNOptR.	[36, 37]
rPKN_orig	The PKN with the A β node connected to it is randomized, while maintaining a scale-free topology. This network was optimized on the original data set in CellNOptR.	--
Iono_larg	A β is connected to ionotropic (conduct ions) receptors and channels (see Appendix 3B). This network was optimized on the larger data set in CellNOptR.	[36, 37]
Iono_larg_scam	A β is connected to ionotropic (conduct ions) receptors and channels (see Appendix 3B). This network was optimized on a set of scrambled datasets in CellNOptR.	--
ABfullact_larg	A β is connected to all cell surface receptors and channels by activating edges. This network was optimized on the larger dataset in CellNOptR.	[41]
ABfull_act_scam	A β is connected to all cell surface receptors and channels by activating edges. This network was optimized on a set of scrambled datasets in CellNOptR.	--
ABfull_inhib_larg	A β is connected to all cell surface receptors and channels by inhibiting edges. This network was optimized on the larger dataset in CellNOptR.	[41]
ABfull_inhib_scam	A β is connected to all cell surface receptors and channels by inhibiting edges. This network was optimized on a set of scrambled datasets in CellNOptR.	--
ABGPCRs_larg	A β is connected to G-protein coupled receptors (GPCRs) by activation (see Appendix 3B). This network was optimized on the larger dataset in CellNOptR.	[40, 42]
ABGPCRInt_larg	A β is connected to G-protein coupled receptors (GPCRs) and the Integrin receptor by activation (see Appendix 3B). This network was optimized on the larger dataset in CellNOptR.	[40]
ABGPCRs_scam	A β is connected to G-protein coupled receptors (GPCRs) by activation (see Appendix 3B). This network was optimized on a set of scrambled datasets in CellNOptR.	--

As demonstrated experimentally in our lab with SH-SY5Y cells[97], it is hypothesized that A β might interact with both G-protein coupled receptors (GPCRs) and Integrin receptors, whereby aberrant signals from A β integrate at hub proteins, such as SRC or FYN. It is believed that A β -induced signaling through integrins, and GPCRs, followed by SRC and FYN may be the cause of neurotoxicity demonstrated in *in vitro* systems[97].

There are other hypotheses that could have been tested such as A β 's interaction with receptor tyrosine kinases[98], however, we chose a subset of these more specific interactions to test, while utilizing the cases in which all of the cell surface proteins were included so as to potentially capture any mechanisms we might have missed.

Table 3.2: Table of A β -neuron interactions and “pseudo-controls” tested in this study. In this table, the first column contains the code names given to each interaction or pseudo-control as an identifier throughout the rest of this chapter. In the middle column is a description of the A β -neuron interactions and pseudo-controls tested in the study. Included in the third column are the references for each interaction as they have been hypothesized in the literature.

Two ‘pseudo-controls’ were used, a randomized PKN and scrambled datasets. These are called ‘pseudo-controls’ because they do not function, in the strictest sense, like a positive or negative control, but act as worse case scenarios for the algorithm. In the case of the randomized PKN, this tests for biological significance of the network topologies found by the algorithm. If the network topologies are biologically significant, then they will perform better (have a lower best objective function) than those found by optimizing on the experimental data using the randomized PKN. The scrambled datasets test for the self-consistency of the experimental data itself. If the experimental data is self-consistent, then the expected result would be that network topologies found by CellNOptR should perform better than those found by optimizing on the scrambled datasets.

3.3 Results and Discussion

The goal of this work was to use a genetic algorithm-based method to test the likelihood that hypothesized A β -neuron interactions could give rise to experimental data from a fairly well characterized signaling network. To accomplish this goal, we performed simulations using CellNOptR on A β -ionotropic mechanisms against “pseudo-controls”. We chose ionotropic mechanisms, or channels/receptors that conduct ions such as calcium, potassium and sodium in and out of the cell, because of various experimental results in which A β was hypothesized to disrupt ion homeostasis through one or more of these channels or receptors[1, 13, 17, 29]. In **Figure 3.3**, the objective functions for the fit of experimental data to a signaling network including A β -ionotropic mechanisms were compared to randomized

PKNs(rPKN_orig); both were optimized on the same experimental dataset (original dataset). The rPKNs are sets of the original PKN along with A β , where the edges (or interactions) between nodes are randomized, while maintaining a power law distribution of the edges (scale-free). Here we observed that the median best objective function for the A β -ionotropic mechanisms was 0.24 and the median for the randomized PKN was 0.35. As the box plot (**Figure 3.3B**) shows, in addition to the median best objective function for the A β -ionotropic mechanisms being lower than that for the rPKN, it also has a smaller variation about the median. It was expected that the biological network should perform better on biological data than the rPKN in which biological significance is lost due to the interchange of protein-protein interactions. These first results indicated that a signaling model that included an A β interaction with a neuron that stimulated some ionotropic mechanism was more consistent with combined literature data than a random signaling network model that included no prior knowledge of signaling.

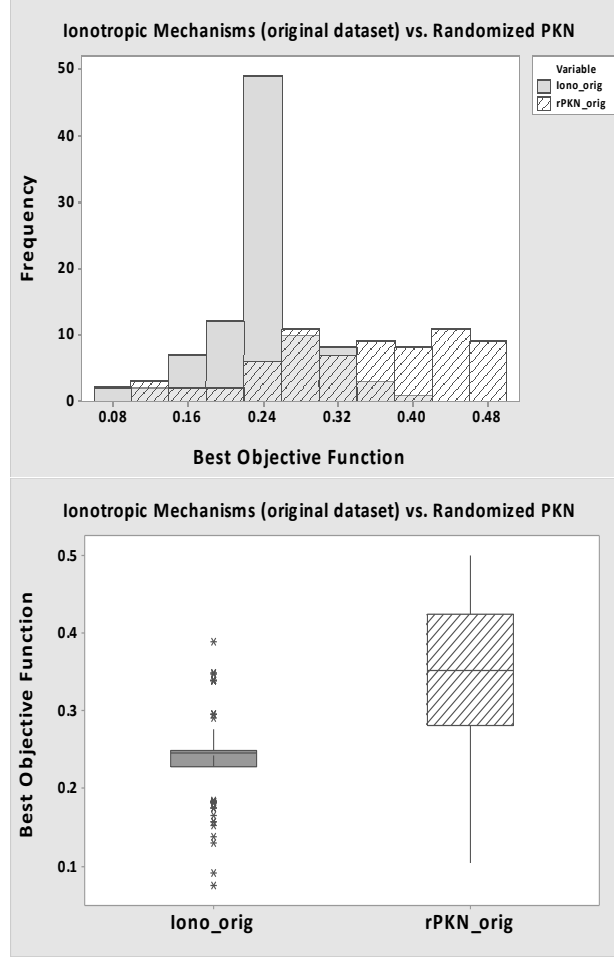


Figure 3.3: Histogram and box plots of the best objective function for ionotropic mechanisms versus the randomized prior knowledge network (rPKN) from CellNOptR. A) Histogram of the best objective function found from CellNOptR for the A β -Ionotropic mechanisms and the rPKN. Median for the A β -Ionotropic mechanisms was 0.24. Median for the rPKN was 0.35. B) Box plots of best objective function found from CellNOptR for the ionotropic mechanisms (left box plot) and the rPKN (right box plot). The median value is represented by the line in the middle of the box with the boundaries of the box representing the lower and upper 25% quartile. The lines above and below represent the minimum and maximum value of the best objective function and the stars are outliers.

Next, we examined if dataset size would have an influence on the ability of the CellNOptR algorithm to fit experimental data pulled from the literature to a signaling model that included A β activation of signaling through an ionotropic mechanism. We compared the fit of the network with the A β -ionotropic mechanisms to the original dataset, a larger dataset (about twice the size of the original) and scrambled datasets (“pseudo-control”). The objective function, a measure of the goodness-of-fit of the model to the data, is shown for each network/dataset comparison in **Figure 3.4**. With an increase in the size of the dataset, the expectation was that the algorithm would have more information about the state of the nodes in the network, thereby adding more constraints on the solutions found by CellNOptR. It was also expected that scrambled datasets would perform worse than both cases because of the disruption of the input/output relationships of the experimental dataset. Contrary to our expectations, what we observed (**Figure 3.4**) was that A β -ionotropic mechanism optimized on the original dataset had a lower median (0.24) than the larger dataset (0.33), and that the scrambled dataset (0.25) had a lower median value than the larger dataset. In addition, there was a significant overlap between their distributions. This suggests two things. First the increase in the dataset size may lead to less model reduction in the pre-processing step, particularly when more highly connected nodes are added to the dataset. CellNOptR performs a pre-processing step of network reduction by removing non-observable nodes, which is intended to reduce the search space in accord with the amount of data inputted into the algorithm. This reduction in search space might work with relatively small networks (<100 nodes)

with a low number of incoming interactions (less than 3), but with this much larger network and nodes that have high connectivity, the combinations of logic gates that must be tested increases dramatically with the addition of data or observations at new nodes in the network. With a larger search space, there may be more network configurations that only partially explain the data, but the majority of the search space is unlikely to be sampled. Second, the scrambled dataset performing better than the A β -ionotropic on the larger dataset can possibly be explained by certain configurations of the scrambled datasets may have been easier for the algorithm to optimize than others. This might suggest that when data from the literature on A β 's action on neurons are taken together as a set that the set may not be self-consistent, though this is not conclusive from our analysis. Self-consistency of a dataset could be described as each experimental data point being consistent with the whole when taken as part of a set. A third possible explanation would be that the experimental data taken from the literature do not support the hypothesis that A β interacts with a neuron and induces signaling via an ionotropic mechanism as a first step. There are many hypothesized mechanisms of A β -neuron interactions other than ionotropic mechanisms, therefore in further simulations, we explored some of these other mechanisms.

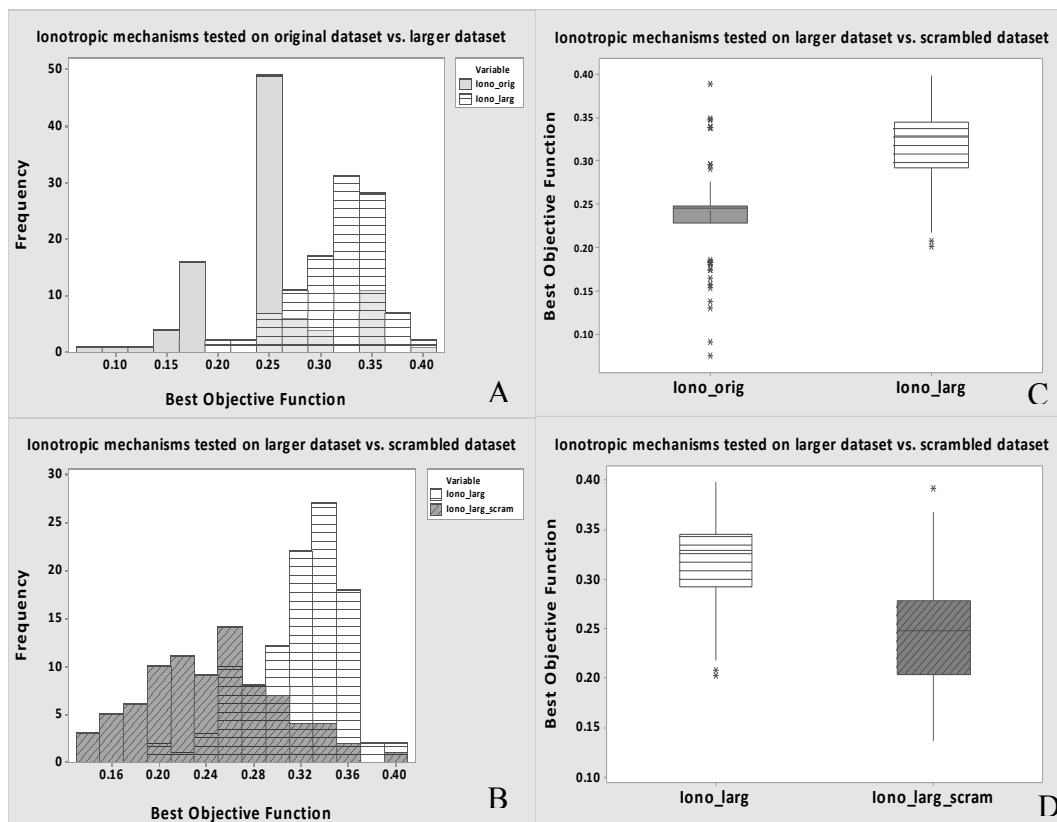


Figure 3.4: A β -ionotropic mechanisms optimized on different dataset sizes and types using CellNOptR. A) The A β -Ionotropic mechanisms were optimized on the original (solid gray bars) and larger dataset (horizontal lined bars). B) The larger dataset optimization (horizontal lined bars) was compared to the A β -Ionotropic mechanisms optimized on the scrambled dataset (diagonal lined gray bars). Box plots of C) A β -Ionotropic mechanisms on original (solid gray) versus larger dataset (horizontal lined bars) and D) larger dataset (horizontal lined bars) versus scrambled dataset (diagonal lined gray bars). The median value is represented by the line in the middle of the box with the boundaries of the box representing the lower and upper 25% quartile. The lines above and below represent the minimum and maximum value of the best objective function and the stars are outliers.

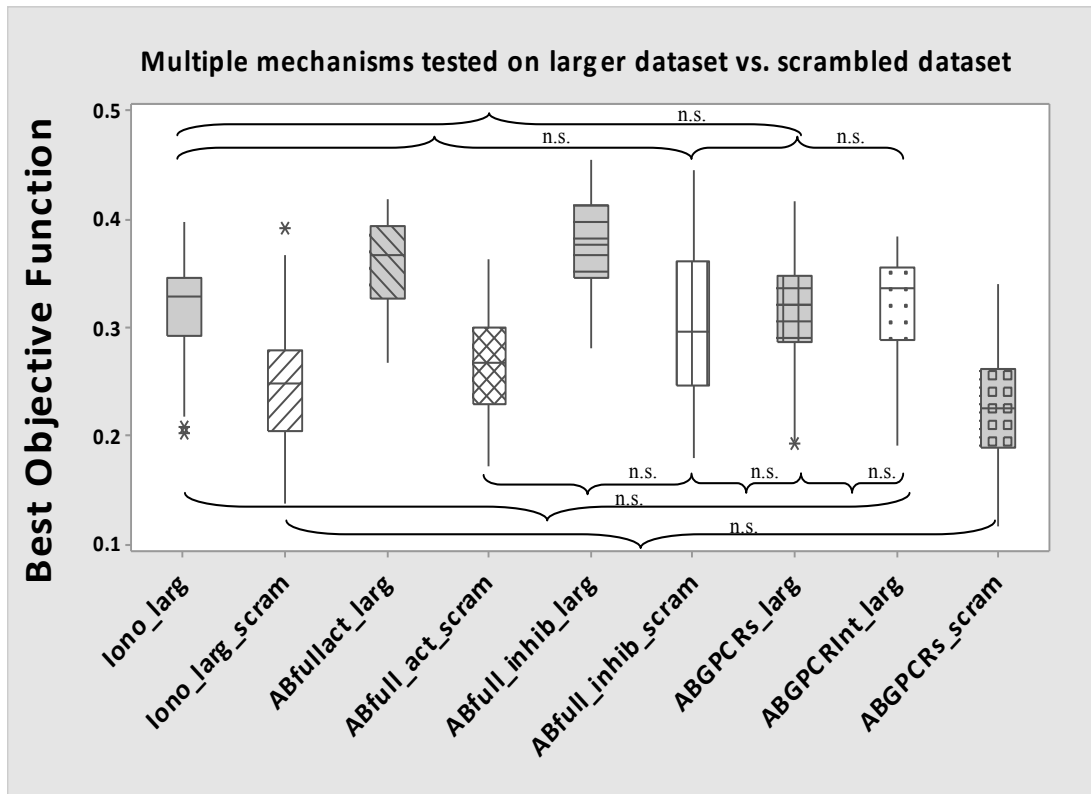


Figure 3.5: Box plots of various A β -neuron interactions tested against the larger and scrambled datasets. The A β -neuron interactions tested using CellNOptR on the larger and scrambled datasets are: Iono_large, Iono_large_scram, ABfullact_large, ABfull_act_scram, ABfull_inhib_large, ABGPCRs_large, ABGPCRInt_large and ABGPCRs_scram (see **Table 3.2**). Represented in these box plots are the median value is represented by the line in the middle of the box with the boundaries of the box representing the lower and upper 25% quartile. The lines above and below represent the minimum and maximum value of the best objective function and the stars are outliers. Statistical significance of the set was determined by Kruskal-Wallis test, since not all of the distributions met the normality test. Once it was found that there were statistically significant differences among the set, statistical hypothesis testing was done on pairwise comparisons. The brackets show those pairs that are not statistically significantly different (n.s.) based on a Mann-Whitney U test in Minitab.

We next constructed hypotheses of other A β signaling mechanisms to explore if hypotheses of those mechanisms (see **Table 3.2** for description of mechanisms) would prove to be more consistent with experimental data curated from the literature. In **Figure 3.5** we show the objective function for fits of the different hypotheses to the experimental data. We include models that described hypotheses of A β -induced neuron signaling via activation of all possible cell surface receptors/ion channels (ABfullact_large, ABfull_act_scram), inhibition of all cell surface receptors/ion channels (ABfull_inhib_large, ABfull_inhib_scram), activation of an ionotropic mechanism only (Iono_orig, Iono_large_scram), GPCRs and Integrin (ABGPCRInt_large), and GPCR mechanisms (ABGPCRs_large, ABGPCRs_large_scram) against the larger and scrambled datasets. To address sampling the entire space of possible A β -neuron interactions at the cell surface, we utilized the two hypotheses where A β activates/inhibits all cell surface receptors/channels in order to sample all of the potential A β -neuron interactions possible. Since CellNOptR samples the interaction space, then these two mechanisms, ideally, should be sufficient to sample the potential space of A β -neuron interactions using CellNOptR. We also chose particular sets of A β -neuron interactions based on certain hypotheses from the literature on A β (see **Table 3.2**). We did not test receptors with which A β hypothetically interacts that do not exist in this particular network structure. Perhaps in future work, we could add new receptors into the network, especially given some evidence of A β interacting with the PrP^C receptor[99], however, at this time, a well curated prior knowledge signaling network

including receptors such as PrP^C does not exist, which precluded our inclusion of extra receptors into our study.

In **Figure 3.5**, we observed that all of the distributions of the objective functions for the specific hypotheses (ionotropic, GPCR-Integrin and GPCRs) are not statistically significant from each other. We tested the statistical significance of the set using a Kruskal-Wallis test instead of an ANOVA because some of the distributions of objective functions were not normally distributed. A post-hoc test using the Mann-Whitney U test with a Bonferroni adjustment was performed to test pairwise comparisons (see **Appendix 3C**). Also, all of the hypotheses optimized on scrambled datasets, except for when A β is connected to all cell surface receptors/channels (ABfull_inhib_scram), had a lower objective function than their counterpart optimized on the real dataset, and this difference was statistically significant. Again, this is suggestive of a lack of self-consistency in the dataset. Researchers typically collect experimental data based upon a particular belief about the underlying behavior of the system. In effect, even if it is conceptual, an experimentalist would begin with a model of the system, and then run experiments in order to ascertain whether their (conceptual) model matches the empirical results from the system (see **Figure 3.6**). For example, if an experimentalist hypothesizes that a system has three components, where the output of two of the three components are coupled together, then the experimentalist might design an experiment to stimulate two components of the system and measure the output. If, in fact, the system is a three-component system with two coupled components, then the

hypothesis has been proven correct by the empirical data. If not, then the data will need to be reinterpreted into a new (conceptual) model and then retested. There are few examples[100, 101] where the hypothesis of A β -induced signaling in neurons has been assumed to be part of a highly interconnected intracellular network such as the one used in this study. Instead, most experimental hypotheses have assumed a linear pathway between A β and intracellular protein(s) of interest in the study. This suggests that there is a widening gap between our knowledge at the systems level (the interactions of various signaling pathways within a signaling network) and our experimental design.

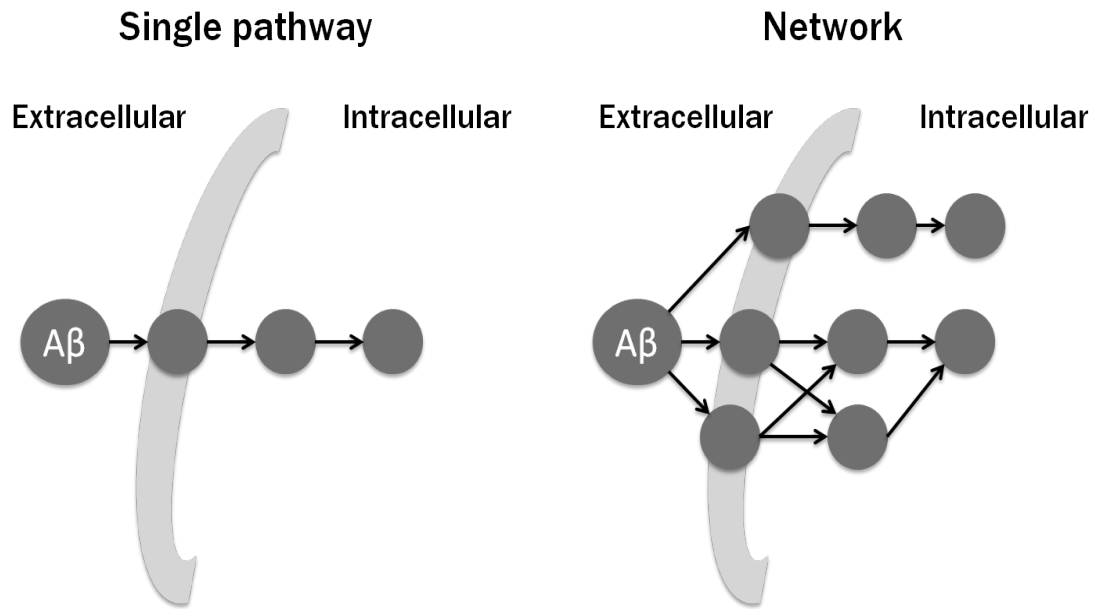


Figure 3.6: Single pathway hypothesis versus network as experimental prior knowledge. The single pathway or linear pathway hypothesis assumes that A β acts on a cell surface receptor and/or channel in such a way that a linear pathway is adversely affected by its signal. On the other hand, the network hypothesis or systems-level approach assumes that A β interacts with cell surface receptors and/or channels in such a way that it has a network-wide effect due to the strongly interconnected signaling network in neurons.

This lack of a standard experimental prior knowledge of the system could be an alternative explanation of the lack of consistency across data collected by various laboratories used in this study. Having a standard of experimental prior knowledge of the system would allow experimentalists to design their experiments in a context-dependent manner; that is, the experimentalist, with adequate knowledge of role that each protein plays in a number of pathways, could potentially design their experiment to minimize the effects of confounding factors such as cross-talk and feedback mechanisms (to be discussed in greater detail in **Chapter 4**).

Notwithstanding, CellNOptR makes a simplifying assumption about the system, namely by modeling the change in state of each node using a Boolean function. Boolean networks have been shown to produce biologically relevant predictions[87]. However, our ultimate goal would be to model the spatio-temporal dynamics of these complex systems. This requires the interplay between achieving a systems-level network topology via computational modeling and good experimental design. Given that data that is currently collected on A β 's action on neurons is usually at a single-time point, it suffices that a Boolean network assumption should be able to identify network configurations that explain the data (pending the data is self-consistent), and that this would help define the network topology that could be built upon with further kinetic and spatial information. Designing optimal experiments in which the data are self-consistent, but are also at a minimum presents a challenge, especially for large networks as that used in this case study. As mentioned previously,

there are few ways of estimating what might be the minimum dataset size for this type of optimization and what kind of experimental data would need to be collected for a system such as this[88]. This might be an area for future work (see **Section 3.5 Future Work**). In addition, upon examination of the experimental datasets, both original and large, greater than 80% of the nodes measured have four or more connections to other nodes with the highest number of total connections being 42. Nodes with higher number of connections would be less discriminating in the network than those that have fewer connections because highly connected nodes tend to be where extracellular signals integrate before continuing to downstream pathways. In this network, we also see that these highly connected nodes play a significant role in crosstalk between receptor-mediated pathways and also in feedback mechanisms. This indicates that the data requirements for such nodes will be greater than at sparser sections of the network and that current single-time point experimental design based on a linear pathway assumption may be insufficient for network inference using an algorithm such as CellNOptR.

In addition, these results suggest that there may be more to experimental design, in order to infer network topology from experimental data using a reverse engineering algorithm such as CellNOptR, than sheer size of the data. In the Saez-Rodriguez paper[79], from whence the algorithm came, their dataset consisted of many treatment combinations of receptor stimuli as well as inhibitors of various proteins in the network. The combinatorial nature of the experimental design tests a

greater combination of input-output relationships in the network than the data from our random literature search.

There exists very little literature that discusses the design of an optimal experimental dataset with a minimal number of treatment variables and/or measurements. Krupa[88] postulates an optimal experimental dataset design to identify a causal network. In his work, he derives an upper and lower bound on experimental dataset size, with the asymptotic lower bound being associated with a $(N, K, 2)$ -universal matrix, in the case of a two state system, where N is the number of nodes in the network and K is the number of in-degree edges. From his proof of this bound, he also establishes a corollary whereby he determines that the minimum number of experiments necessary to identify a causal network increases logarithmically with the numbers of nodes in the network (N) and exponentially with the number of in-degree edges (K) to each node. Evidence has shown that in many biological networks, K is no greater than 3 on average[102], and this is true for the network in this study. Though the minimum number of experiments could be estimated from the lower bound proposed by Krupa, the construction of a $(N, K, 2)$ -universal matrix was not included in Krupa's work. Therefore, the actual number of nodes that should be measured per experiment is not readily available from calculations of the minimum number of experiments.

3.4 Conclusions

In conclusion, the mechanisms underlying A β 's action on neurons remain unknown. We postulated that using a reverse engineering algorithm, CellNOptR, which would allow us to input a prior knowledge network relevant to the experimental system and experimental data collected from the literature, that we could identify a set of A β -neuron interactions that give rise to a network structure that explains the data. However, we observed that data collected from the literature as individual data points as a set may not be self-consistent. This lack of self-consistency in the data could be part of what is leading to a lack of consensus amongst researchers who are trying to make sense of all the data primarily by intuition alone. Utilizing 'experimental prior knowledge' such as the information contained in the network in this study might help with standardization of data collection in this field. Also, a greater understanding of the minimum dataset size needed for such network inference would aid in further advancement.

3.5 Future Work

Unfortunately, this case study was confounded not only by the complexity of the system, but also the difficulty of combining literature-derived data into a single dataset. Though this may have seemed naïve, at first, of an endeavor, this was not a

wasted effort because this procedure of surveying the currently literature, synthesizing data from various sources and drawing some conclusions about one's results from these data is quite common as it is usually the focus of most experimental discussion sections in journal articles. However, rarely is there a mechanism used to systematically determine how consistent these data are when taken as a whole. There are other methods, such as a meta-analysis, which could be utilized in order to determine self-consistency of the data (among other metrics) however, this type of analysis typically assumes that the same variable[103] is being studied across studies, which is rarely the case with data from biological experiments *in vitro*.

With this said, with respect to future work, there might be two potential areas: design of optimal experiments and determining the minimum dataset necessary to find a network topology using an algorithm such as CellNOptR. With regards to the latter, we have made some attempt (in collaboration with Patrick O'Neill in the laboratory of Dr. Ivan Erill in the Biological Sciences Department at UMBC) to develop an algorithm to map the hypothesis space given a partial data set. In order to illustrate, let's consider the question at hand. We have a PKN for which we want to determine the Boolean truth table at each node (this is effectively what CellNOptR is doing). Each instance of the network for which there is a set of truth tables for each node is considered a hypothesis, H . A dataset, D , is defined as a complete observation of the state of all nodes in the PKN under a set of conditions. We want to know what

the probability is of finding a particular set of truth tables (the hypothesis) given a dataset. For this we make use of Bayes' theorem (Eq. 3.6.1):

$$P(H | D) = P(D | H) \frac{P(H)}{P(D)} \quad (3.6.1),$$

where, $P(H|D)$ is the probability of the hypothesis, H , given the data, D , otherwise known as a conditional probability. $P(D|H)$ is the posterior distribution or the likelihood function of the data given the hypothesis. $P(H)$ and $P(D)$ are the probability of the hypothesis and the dataset, respectively, and correspond to $1/\text{size}$ of the hypothesis space or dataset. A pictorial view of the question is given in **Figure 3.7**. In order to make use of this theorem, it is necessary to find the posterior distribution ($P(D|H)$). In the case of observation of the full dataset, D , the posterior distribution can be found as follows:

$$P(D | H) = \begin{cases} 1, & \text{H is consistent with the data} \\ 0, & \text{otherwise} \end{cases} \quad (3.6.2)$$

However, in the case of this study, we have an incomplete dataset, where many of the nodes are unobserved (D_u) versus those that are observed (D_o). Therefore, for an incomplete dataset, we postulate that the posterior distribution be described as such:

$$P(D_o | H) = \sum_{D_u} P((D_o, D_u) | H) P(D_u) \quad (3.6.3)$$

$$\text{where, } P(D_u) = \frac{1}{|D_u|}$$

where, $P(D_o|H)$ is the posterior distribution for the observed data give the hypothesis, $P((D_o,D_u)|H)$ is the probability of the dataset (consistent of observed and unobserved node states) given a hypothesis. $P(D_u)$ is the probability of the unobserved data, which is 1/size of the unobserved data.

Another part of the problem that is again featured in **Figure 3.7** is that during an experiment when the cell is stimulated or inhibited, typically these perturbations last throughout the entirety of the experimental observation time. Therefore, when this is the case, it can be assumed that the network dynamics will settle into an attractor state. An attractor state is the state toward which a particular system tends to evolve over time. As seen in **Figure 3.7**, there can be several network states that tend to evolve into a single attractor state, shown by the partition of the hypothesis state space. If we assume that in each experiment in which we collect a particular set of data that an attractor state is reached, then it is only necessary to find the hypotheses corresponding to a particular attractor state (or multiple) to which the system evolves that overlap with the experimental dataset space (as seen by the dotted rectangle in **Figure 3.7**).

Given our current dataset, from this statistical algorithm, we could get an idea of the probability of finding a hypothesis that is consistent with the experimental data with only a partial observation of the entire network for any given experiment. This information could then be used to infer the size of the dataset required to maximize this probability.

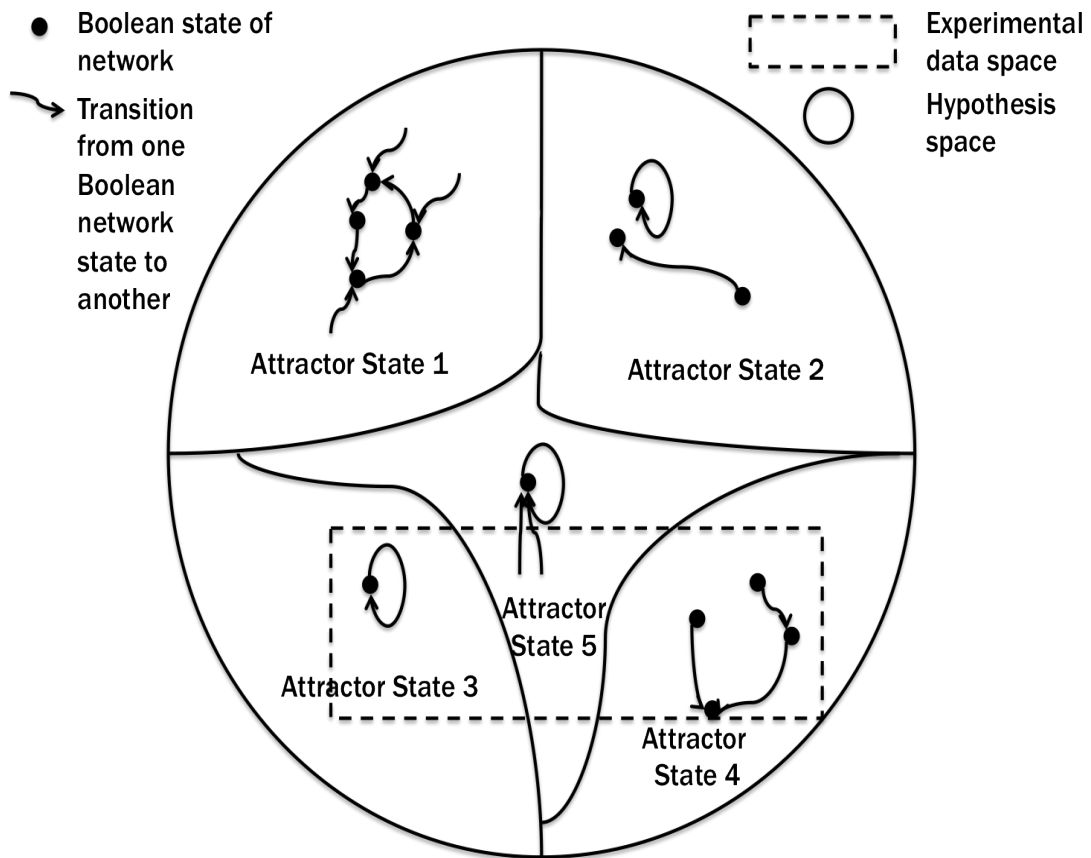


Figure 3.7: Hypothesis space containing partitions indicating the space in which Boolean network states tend to fall into a particular attractor *ad infinitum*. The larger circle represents a hypothetically hypothesis space where each dot represents a Boolean state of the network (hypothesis). The arrows represent a transition from one Boolean network state (usually the initial state) to another (usually the final state). The hypothesis space is partitioned by each attractor state which occupies that area, whereby multiple network states might evolve with time to an attractor state. The dotted rectangle represents the experimental data space wherein a subspace of the hypothesis space overlaps with this experimental data space and where the likelihood of the data given the hypothesis ($P(D|H)$) is high.

3.6 References

1. Ye C, Selkoe D, Hartley D. Protofibrils of amyloid beta-protein inhibit specific K⁺ currents in neocortical cultures. *Neurobiology of Disease*. 2003;13(3):177-90. doi: 10.1016/S0969-9961(03)00068-8|10.1016/S0969-9961(03)00068-8. PubMed PMID: WOS:000184559400001.
2. Leão RN, Colom LV, Borgius L, Kiehn O, Fisahn A. Medial septal dysfunction by A β -induced KCNQ channel-block in glutamatergic neurons. *Neurobiol Aging*. 2011. doi: S0197-4580(11)00297-1 [pii] 10.1016/j.neurobiolaging.2011.07.013. PubMed PMID: 21907458.
3. Kang J, Lemaire HG, Unterbeck A, Salbaum JM, Masters CL, Grzeschik KH, et al. The precursor of Alzheimer's disease amyloid A4 protein resembles a cell-surface receptor. *Nature*. 1987;325(6106):733-6. doi: 10.1038/325733a0. PubMed PMID: 2881207.
4. Hardy J, Selkoe D. Medicine - The amyloid hypothesis of Alzheimer's disease: Progress and problems on the road to therapeutics. *Science*. 2002;297(5580):353-6. PubMed PMID: ISI:000176892600038.
5. [Anon], Assoc A. Alzheimer's Association Report 2011 Alzheimer's disease facts and figures. *Alzheimers & Dementia*. 2011;7(2):208-44. doi: DOI 10.1016/j.jalz.2011.02.004. PubMed PMID: ISI:000288930400010.

6. Khachaturian ZS. Calcium, membranes, aging, and Alzheimer's disease. Introduction and overview. *Ann N Y Acad Sci.* 1989;568:1-4. PubMed PMID: 2629579.
7. Demuro A, Parker I, Stutzmann G. Calcium Signaling and Amyloid Toxicity in Alzheimer Disease. *Journal of Biological Chemistry.* 2010;285(17):12463-8. doi: DOI 10.1074/jbc.R109.080895. PubMed PMID: ISI:000276787800001.
8. Alvarez A, Muñoz JP, Maccioni RB. A Cdk5-p35 stable complex is involved in the beta-amyloid-induced deregulation of Cdk5 activity in hippocampal neurons. *Exp Cell Res.* 2001;264(2):266-74. doi: S0014-4827(01)95152-3 [pii] 10.1006/excr.2001.5152. PubMed PMID: 11262183.
9. Alvarez AR, Godoy JA, Mullendorff K, Olivares GH, Bronfman M, Inestrosa NC. Wnt-3a overcomes beta-amyloid toxicity in rat hippocampal neurons. *Exp Cell Res.* 2004;297(1):186-96. doi: S0014482704000837 [pii] 10.1016/j.yexcr.2004.02.028. PubMed PMID: 15194435.
10. Chacon PJ, Garcia-Mejias R, Rodriguez-Tebar A. Inhibition of RhoA GTPase and the subsequent activation of PTP1B protects cultured hippocampal neurons against amyloid β toxicity. *Mol Neurodegener.* 2011;6(1):14. doi: 1750-1326-6-14 [pii] 10.1186/1750-1326-6-14. PubMed PMID: 21294893; PubMed Central PMCID: PMC3038970.
11. Tong L, Thornton P, Balazs R, Cotman C. beta-Amyloid-(1-42) impairs activity-dependent cAMP-response element-binding protein signaling in neurons at concentrations in which cell survival is not compromised. *Journal of Biological*

Chemistry. 2001;276(20):17301-6. doi: 10.1074/jbc.M010450200. PubMed PMID: WOS:000168730400094.

12. Fogarty M, Downer E, Campbell V. A role for c-Jun N-terminal kinase 1 (JNK1), but not JNK2, in the beta-amyloid-mediated stabilization of protein p53 and induction of the apoptotic cascade in cultured cortical neurons. Biochemical Journal. 2003;371:789-98. doi: 10.1042/BJ20021660. PubMed PMID: WOS:000182733400016.

13. Kim S, Rhim H. Effects of Amyloid-beta Peptides on Voltage-Gated L-Type Ca(V)1.2 and Ca(V)1.3 Ca(2+) Channels. Molecules and Cells. 2011;32(3):289-94. doi: 10.1007/s10059-011-0075-x. PubMed PMID: WOS:000297627300011.

14. Williams T, Serpell L. Membrane and surface interactions of Alzheimer's A beta peptide - insights into the mechanism of cytotoxicity. Febs Journal. 2011;278(20):3905-17. doi: 10.1111/j.1742-4658.2011.08228.x. PubMed PMID: WOS:000295335500012.

15. Askarova S, Yang X, Lee JC. Impacts of membrane biophysics in Alzheimer's disease: from amyloid precursor protein processing to a β Peptide-induced membrane changes. Int J Alzheimers Dis. 2011;2011:134971. doi: 10.4061/2011/134971. PubMed PMID: 21547213; PubMed Central PMCID: PMC3087431.

16. Bokvist M, Lindstrom F, Watts A, Grobner G. Two types of Alzheimer's beta-amyloid (1-40) peptide membrane interactions: Aggregation preventing transmembrane anchoring Versus accelerated surface fibril formation. Journal of Molecular Biology. 2004;335(4):1039-49. doi:

10.1016/j.jmb.2003.11.046|10.1016/j.jmb.2003.11.046. PubMed PMID:
WOS:000188067000014.

17. Good T, Smith D, Murphy R. beta-amyloid peptide blocks the fast-inactivating K⁺ current in rat hippocampal neurons. *Biophysical Journal*. 1996;70(1):296-304. PubMed PMID: ISI:A1996TY68300024.

18. Mattson MP, Cheng B, Davis D, Bryant K, Lieberburg I, Rydel RE. beta-Amyloid peptides destabilize calcium homeostasis and render human cortical neurons vulnerable to excitotoxicity. *J Neurosci*. 1992;12(2):376-89. PubMed PMID: 1346802.

19. Whitson JS, Appel SH. Neurotoxicity of A beta amyloid protein in vitro is not altered by calcium channel blockade. *Neurobiol Aging*. 1995;16(1):5-10. doi: 0197458095800029 [pii]. PubMed PMID: 7723935.

20. Demuro A, Mina E, Kaye R, Milton S, Parker I, Glabe C. Calcium dysregulation and membrane disruption as a ubiquitous neurotoxic mechanism of soluble amyloid oligomers. *Journal of Biological Chemistry*. 2005;280(17):17294-300. doi: DOI 10.1074/jbc.M500997200. PubMed PMID: ISI:000228615500093.

21. Glabe CG. Amyloid Oligomers Structures and Toxicity. *The Open Biology Journal*. 2009;2:222-7.

22. Lee S, Fernandez E, Good T. Role of aggregation conditions in structure, stability, and toxicity of intermediates in the A beta fibril formation pathway. *Protein Science*. 2007;16(4):723-32. doi: DOI 10.1110/ps.062514807. PubMed PMID: ISI:000245161800017.

23. Lacor P. Advances on the understanding of the origins of synaptic pathology in AD. *Current Genomics*. 2007;8(8):486-508. doi: 10.2174/138920207783769530. PubMed PMID: WOS:000254654000002.
24. Sepulveda FJ, Parodi J, Peoples RW, Opazo C, Aguayo LG. Synaptotoxicity of Alzheimer beta amyloid can be explained by its membrane perforating property. *PLoS One*. 2010;5(7):e11820. doi: 10.1371/journal.pone.0011820. PubMed PMID: 20676404; PubMed Central PMCID: PMC2910737.
25. Lioudyno MI, Broccio M, Sokolov Y, Rasool S, Wu J, Alkire MT, et al. Effect of synthetic $\alpha\beta$ Peptide oligomers and fluorinated solvents on kv1.3 channel properties and membrane conductance. *PLoS One*. 2012;7(4):e35090. doi: PONE-D-11-16828 [pii] 10.1371/journal.pone.0035090. PubMed PMID: 22563377; PubMed Central PMCID: PMC3338507.
26. Pimplikar S. Reassessing the amyloid cascade hypothesis of Alzheimer's disease. *International Journal of Biochemistry & Cell Biology*. 2009;41(6):1261-8. doi: 10.1016/j.biocel.2008.12.015. PubMed PMID: WOS:000264669300008.
27. Cappai R, Barnham KJ. Delineating the mechanism of Alzheimer's disease A beta peptide neurotoxicity. *Neurochem Res*. 2008;33(3):526-32. doi: 10.1007/s11064-007-9469-8. PubMed PMID: 17762917.
28. Good TA, Murphy RM. Effect of beta-amyloid block of the fast-inactivating K^+ channel on intracellular Ca^{2+} and excitability in a modeled neuron. *Proc Natl Acad Sci U S A*. 1996;93(26):15130-5. PubMed PMID: 8986775; PubMed Central PMCID: PMC26368.

29. Chen C. beta-amyloid increases dendritic Ca²⁺ influx by inhibiting the A-type K⁺ current in hippocampal CA1 pyramidal neurons. *Biochemical and Biophysical Research Communications*. 2005;338(4):1913-9. doi: 10.1016/j.bbrc.2005.10.169|10.1016/j.bbrc.2005.10.169. PubMed PMID: WOS:000233815900036.
30. Zhang C, Yang P. Zinc-induced aggregation of A beta (10-21) potentiates its action on voltage-gated potassium channel. *Biochemical and Biophysical Research Communications*. 2006;345(1):43-9. doi: 10.1016/j.bbrc.2006.04.044|10.1016/j.bbrc.2006.04.044. PubMed PMID: WOS:000237877700007.
31. Valincius G, Heinrich F, Budvytyte R, Vanderah DJ, McGillivray DJ, Sokolov Y, et al. Soluble amyloid beta-oligomers affect dielectric membrane properties by bilayer insertion and domain formation: implications for cell toxicity. *Biophys J*. 2008;95(10):4845-61. doi: S0006-3495(08)78623-5 [pii] 10.1529/biophysj.108.130997. PubMed PMID: 18515395; PubMed Central PMCID: PMC2576380.
32. Sokolov Y, Kozak A, Kayed R, Chanturiya A, Glabe C, Hall JE. Soluble Amyloid Oligomers Increase Bilayer Conductance by Altering Dielectric Structure. *The Journal of General Physiology*. 2006;128(6):10.
33. Li WY, Czilli DL, Simmons LK. Neuronal membrane conductance activated by amyloid beta peptide: importance of peptide conformation. *Brain Res*. 1995;682(1-2):207-11. doi: 0006-8993(95)00264-Q [pii]. PubMed PMID: 7552313.

34. Cottrell JR, Dubé GR, Egles C, Liu G. Distribution, density, and clustering of functional glutamate receptors before and after synaptogenesis in hippocampal neurons. *J Neurophysiol.* 2000;84(3):1573-87. PubMed PMID: 10980028.
35. Hodgkin AL, Huxley AF. A quantitative description of membrane current and its application to conduction and excitation in nerve. *J Physiol.* 1952;117(4):500-44. PubMed PMID: 12991237; PubMed Central PMCID: PMCPMC1392413.
36. Bekkers JM. Properties of voltage-gated potassium currents in nucleated patches from large layer 5 cortical pyramidal neurons of the rat. *J Physiol.* 2000;525 Pt 3:593-609. doi: PHY_0058 [pii]. PubMed PMID: 10856115; PubMed Central PMCID: PMCPMC2269964.
37. Gentet L, Stuart G, Clements J. Direct measurement of specific membrane capacitance in neurons. *Biophysical Journal.* 2000;79(1):314-20. PubMed PMID: ISI:000088048500025.
38. Jhamandas JH, Cho C, Jassar B, Harris K, MacTavish D, Easaw J. Cellular mechanisms for amyloid beta-protein activation of rat cholinergic basal forebrain neurons. *J Neurophysiol.* 2001;86(3):1312-20. PubMed PMID: 11535679.
39. Kawahara M, Arispe N, Kuroda Y, Rojas E. Alzheimer's disease amyloid beta-protein forms Zn(2+)-sensitive, cation-selective channels across excised membrane patches from hypothalamic neurons. *Biophys J.* 1997;73(1):67-75. doi: S0006-3495(97)78048-2 [pii]
10.1016/S0006-3495(97)78048-2. PubMed PMID: 9199772; PubMed Central PMCID: PMCPMC1180909.

40. Shelat PB, Chalimoniuk M, Wang JH, Strosznajder JB, Lee JC, Sun AY, et al. Amyloid beta peptide and NMDA induce ROS from NADPH oxidase and AA release from cytosolic phospholipase A2 in cortical neurons. *J Neurochem*. 2008;106(1):45-55. doi: JNC5347 [pii]
10.1111/j.1471-4159.2008.05347.x. PubMed PMID: 18346200.
41. Kayed R, Pensalfini A, Margol L, Sokolov Y, Sarsoza F, Head E, et al. Annular protofibrils are a structurally and functionally distinct type of amyloid oligomer. *J Biol Chem*. 2009;284(7):4230-7. doi: M808591200 [pii]
10.1074/jbc.M808591200. PubMed PMID: 19098006; PubMed Central PMCID: PMC2640961.
42. Morse TM, Carnevale NT, Mutalik PG, Migliore M, Shepherd GM. Abnormal Excitability of Oblique Dendrites Implicated in Early Alzheimer's: A Computational Study. *Front Neural Circuits*. 2010;4. doi: 10.3389/fncir.2010.00016. PubMed PMID: 20725509; PubMed Central PMCID: PMC2901152.
43. Williams S, Stuart G. Role of dendritic synapse location in the control of action potential output. *Trends in Neurosciences*. 2003;26(3):147-54. doi: 10.1016/S0166-2236(03)00035-3|10.1016/S0166-2236(03)00035-3. PubMed PMID: WOS:000181351900008.
44. Bean BP. The action potential in mammalian central neurons. *Nat Rev Neurosci*. 2007;8(6):451-65. doi: nrn2148 [pii]
10.1038/nrn2148. PubMed PMID: 17514198.
45. Blanchard B, Thomas V, Ingram V. Mechanism of membrane depolarization caused by the Alzheimer A beta 1-42 peptide. *Biochemical and Biophysical Research*

Communications. 2002;293(4):1197-203. doi: 10.1016/S0006-291X(02)00346-7.
PubMed PMID: WOS:000175911900008.

46. Saura C, Valero J. The role of CREB signaling in Alzheimer's disease and other cognitive disorders. *Reviews in the Neurosciences*. 2011;22(2):153-69. doi: 10.1515/RNS.2011.018|10.1515/RNS.2011.018. PubMed PMID: WOS:000300088800003.

47. Bito H, Deisseroth K, Tsien R. CREB phosphorylation and dephosphorylation: A Ca^{2+} - and stimulus duration-dependent switch for hippocampal gene expression. *Cell*. 1996;87(7):1203-14. doi: 10.1016/S0092-8674(00)81816-4. PubMed PMID: WOS:A1996WA54100009.

48. Espana J, Valero J, Minano-Molina A, Masgrau R, Martin E, Guardia-Laguarta C, et al. beta-Amyloid Disrupts Activity-Dependent Gene Transcription Required for Memory through the CREB Coactivator CRTC1. *Journal of Neuroscience*. 2010;30(28):9402-10. doi: 10.1523/JNEUROSCI.2154-10.2010. PubMed PMID: WOS:000279899100008.

49. Ma Q, Harris-White M, Ubuda O, Simmons M, Beech W, Lim G, et al. Evidence of A beta- and transgene-dependent defects in ERK-CREB signaling in Alzheimer's models. *Journal of Neurochemistry*. 2007;103(4):1594-607. doi: 10.1111/j.1471-4159.2007.04869.x|10.1111/j.1471-4159.2007.04869.x. PubMed PMID: WOS:000250403500030.

50. Shaywitz A, Greenberg M. CREB: A stimulus-induced transcription factor activated by a diverse array of extracellular signals. *Annual Review of Biochemistry*.

1999;68:821-61. doi: 10.1146/annurev.biochem.68.1.821. PubMed PMID: WOS:000082693200026.

51. Williams TL, Serpell LC. Membrane and surface interactions of Alzheimer's A β peptide--insights into the mechanism of cytotoxicity. FEBS J. 2011;278(20):3905-17. doi: 10.1111/j.1742-4658.2011.08228.x. PubMed PMID: 21722314.

52. Yamada MK, Nakanishi K, Ohba S, Nakamura T, Ikegaya Y, Nishiyama N, et al. Brain-derived neurotrophic factor promotes the maturation of GABAergic mechanisms in cultured hippocampal neurons. J Neurosci. 2002;22(17):7580-5. doi: 22/17/7580 [pii]. PubMed PMID: 12196581.

53. Kobayashi T, Yamauchi R, Murata S. Effect of Ca²⁺ antagonists on high-K⁺ evoked increase in [Ca²⁺]_i in rat cerebral synaptosomes and hippocampal neurons. Jpn J Pharmacol. 1992;58(4):417-25. PubMed PMID: 1405039.

54. Demont-Guignard S, Benquet P, Gerber U, Wendling F. Analysis of intracerebral EEG recordings of epileptic spikes: insights from a neural network model. IEEE Trans Biomed Eng. 2009;56(12):2782-95. doi: 10.1109/TBME.2009.2028015. PubMed PMID: 19651549; PubMed Central PMCID: PMC3245744.

55. Orbán G, Kiss T, Erdi P. Intrinsic and synaptic mechanisms determining the timing of neuron population activity during hippocampal theta oscillation. J Neurophysiol. 2006;96(6):2889-904. doi: 10.1152/jn.01233.2005 [pii] 10.1152/jn.01233.2005. PubMed PMID: 16899632.

56. Golomb D, Yue C, Yaari Y. Contribution of persistent Na⁺ current and M-type K⁺ current to somatic bursting in CA1 pyramidal cells: combined experimental and modeling study. *J Neurophysiol.* 2006;96(4):1912-26. doi: 00205.2006 [pii] 10.1152/jn.00205.2006. PubMed PMID: 16807352.
57. Li X, Ascoli GA. Computational simulation of the input-output relationship in hippocampal pyramidal cells. *J Comput Neurosci.* 2006;21(2):191-209. doi: 10.1007/s10827-006-8797-z. PubMed PMID: 16871350.
58. Káli S, Freund TF. Distinct properties of two major excitatory inputs to hippocampal pyramidal cells: a computational study. *Eur J Neurosci.* 2005;22(8):2027-48. doi: EJN4406 [pii] 10.1111/j.1460-9568.2005.04406.x. PubMed PMID: 16262641.
59. Zou X, Coyle D, Wong-Lin K, Maguire L. Beta-amyloid induced changes in A-type K(+) current can alter hippocampo-septal network dynamics. *J Comput Neurosci.* 2011. doi: 10.1007/s10827-011-0363-7. PubMed PMID: 21938438.
60. Kidd JF, Sattelle DB. The effects of amyloid peptides on A-type K(+) currents of *Drosophila* larval cholinergic neurons: modeled actions on firing properties. *Invert Neurosci.* 2006;6(4):207-13. doi: 10.1007/s10158-006-0034-y. PubMed PMID: 17106756.
61. Tiveci S, Akin A, Cakir T, Saybaşili H, Ulgen K. Modelling of calcium dynamics in brain energy metabolism and Alzheimer's disease. *Comput Biol Chem.* 2005;29(2):151-62. doi: S1476-9271(05)00023-X [pii] 10.1016/j.combiolchem.2005.03.002. PubMed PMID: 15833443.

62. Migliore M, Ferrante M, Ascoli GA. Signal propagation in oblique dendrites of CA1 pyramidal cells. *J Neurophysiol.* 2005;94(6):4145-55. doi: 94/6/4145 [pii] 10.1152/jn.00521.2005. PubMed PMID: 16293591.
63. Menschik E, Finkel L. Cholinergic neuromodulation of an anatomically reconstructed hippocampal CA3 pyramidal cell. *Neurocomputing.* 2000;32:197-205. doi: 10.1016/S0925-2312(00)00164-8. PubMed PMID: WOS:000087897800029.
64. Bower JM, Beeman D. *The book of GENESIS : exploring realistic neural models with the GEneral NEural SIMulation System.* 2nd ed. Santa Clara, Calif.: TELOS; 1998. xxiv, 458 p. p.
65. Hines M, Carnevale N. The NEURON simulation environment. *Neural Computation.* 1997;9(6):1179-209. PubMed PMID: ISI:A1997XM55000001.
66. Hoffman DA, Magee JC, Colbert CM, Johnston D. K⁺ channel regulation of signal propagation in dendrites of hippocampal pyramidal neurons. *Nature.* 1997;387(6636):869-75. doi: 10.1038/43119. PubMed PMID: 9202119.
67. Glenner GG, Wong CW. Alzheimer's disease: initial report of the purification and characterization of a novel cerebrovascular amyloid protein. *Biochem Biophys Res Commun.* 1984;120(3):885-90. doi: S0006-291X(84)80190-4 [pii]. PubMed PMID: 6375662.
68. Hardy J. The amyloid hypothesis for Alzheimer's disease: a critical reappraisal. *J Neurochem.* 2009;110(4):1129-34. doi: JNC6181 [pii] 10.1111/j.1471-4159.2009.06181.x. PubMed PMID: 19457065.
69. Arispe N, Pollard HB, Rojas E. Giant multilevel cation channels formed by Alzheimer disease amyloid beta-protein [A beta P-(1-40)] in bilayer membranes. *Proc*

Natl Acad Sci U S A. 1993;90(22):10573-7. PubMed PMID: 7504270; PubMed Central PMCID: PMCPMC47819.

70. Patel A, Jhamandas J. Neuronal receptors as targets for the action of amyloid-beta protein (A beta) in the brain. *Expert Reviews in Molecular Medicine*. 2012;14. doi: 10.1017/S1462399411002134. PubMed PMID: WOS:000300516400001.

71. Stefani M. Structural features and cytotoxicity of amyloid oligomers: Implications in Alzheimer's disease and other diseases with amyloid deposits. *Progress in Neurobiology*. 2012;99:226-45. Epub March 23, 2012.

72. Kaye R, Lasagna-Reeves C. Molecular Mechanisms of Amyloid Oligomers Toxicity. *J Alzheimers Dis*. 2012. doi: Q5167K4JP4351322 [pii] 10.3233/JAD-2012-129001. PubMed PMID: 22531422.

73. del Sol A, Balling R, Hood L, Galas D. Diseases as network perturbations. *Current Opinion in Biotechnology*. 2010;21(4):566-71. doi: 10.1016/j.copbio.2010.07.010. PubMed PMID: WOS:000282717000019.

74. Barabasi A, Oltvai Z. Network biology: Understanding the cell's functional organization. *Nature Reviews Genetics*. 2004;5(2):101-U15. doi: 10.1038/nrg1272. PubMed PMID: WOS:000188602400012.

75. LaFerla F. Calcium dyshomeostasis and intracellular signalling in Alzheimer's disease. *Nature Reviews Neuroscience*. 2002;3(11):862-72. doi: DOI 10.1038/nrn960. PubMed PMID: ISI:000179041700017.

76. Yeager-Lotem E, Riva L, Su LJ, Gitler AD, Cashikar AG, King OD, et al. Bridging high-throughput genetic and transcriptional data reveals cellular responses to alpha-synuclein toxicity. *Nat Genet*. 2009;41(3):316-23. doi: ng.337 [pii]

10.1038/ng.337. PubMed PMID: 19234470; PubMed Central PMCID: PMCPMC2733244.

77. Rowland M, Fontana W, Deeds E. Crosstalk and Competition in Signaling Networks. *Biophysical Journal*. 2012;103(11):2389-98. doi: 10.1016/j.bpj.2012.10.006. PubMed PMID: WOS:000311963300018.

78. Ma'ayan A, Jenkins SL, Neves S, Hasseldine A, Grace E, Dubin-Thaler B, et al. Formation of regulatory patterns during signal propagation in a Mammalian cellular network. *Science*. 2005;309(5737):1078-83. doi: 309/5737/1078 [pii] 10.1126/science.1108876. PubMed PMID: 16099987; PubMed Central PMCID: PMCPMC3032439.

79. Saez-Rodriguez J, Alexopoulos L, Epperlein J, Samaga R, Lauffenburger D, Klamt S, et al. Discrete logic modelling as a means to link protein signalling networks with functional analysis of mammalian signal transduction. *Molecular Systems Biology*. 2009;5. doi: 10.1038/msb.2009.87. PubMed PMID: WOS:000273359200002.

80. Wu M, Yang X, Chan C. A Dynamic Analysis of IRS-PKR Signaling in Liver Cells: A Discrete Modeling Approach. *Plos One*. 2009;4(12). doi: 10.1371/journal.pone.0008040. PubMed PMID: WOS:000272828700006.

81. Ogunnaike B. Elucidating the digital control mechanism for DNA damage repair with the p53-Mdm2 system: single cell data analysis and ensemble modelling. *Journal of the Royal Society Interface*. 2006;3(6):175-84. doi: 10.1098/rsif.2005.0077. PubMed PMID: WOS:000235712600017.

82. Li F, Thiele I, Jamshidi N, Palsson B. Identification of Potential Pathway Mediation Targets in Toll-like Receptor Signaling. *Plos Computational Biology*. 2009;5(2). doi: 10.1371/journal.pcbi.1000292. PubMed PMID: WOS:000263924500007.
83. Birtwistle MR, Hatakeyama M, Yumoto N, Ogunnaike BA, Hoek JB, Kholodenko BN. Ligand-dependent responses of the ErbB signaling network: experimental and modeling analyses. *Mol Syst Biol*. 2007;3:144. doi: msb4100188 [pii] 10.1038/msb4100188. PubMed PMID: 18004277; PubMed Central PMCID: PMCPMC2132449.
84. Margolin AA, Nemenman I, Basso K, Wiggins C, Stolovitzky G, Dalla Favera R, et al. ARACNE: an algorithm for the reconstruction of gene regulatory networks in a mammalian cellular context. *BMC Bioinformatics*. 2006;7 Suppl 1:S7. doi: 10.1186/1471-2105-7-S1-S7. PubMed PMID: 16723010; PubMed Central PMCID: PMCPMC1810318.
85. Braunstein A, Pagnani A, Weigt M, Zecchina R. Inference algorithms for gene networks: a statistical mechanics analysis. *Journal of Statistical Mechanics: Theory and Experiment*. 2008;2-29. doi: 10.1088/1742-5468/2008/12/P12001.
86. Eduati F, De Las Rivas J, Di Camillo B, Toffolo G, Saez-Rodriguez J. Integrating literature-constrained and data-driven inference of signalling networks. *Bioinformatics*. 2012;28(18):2311-7. doi: 10.1093/bioinformatics/bts363. PubMed PMID: WOS:000308532300052.

87. Wang R, Saadatpour A, Albert R. Boolean modeling in systems biology: an overview of methodology and applications. *Physical Biology*. 2012;9(5). doi: 10.1088/1478-3975/9/5/055001. PubMed PMID: WOS:000309514900003.
88. Krupa B. On the number of experiments required to find the causal structure of complex systems. *Journal of Theoretical Biology*. 2002;219(2):257-67. doi: 10.1006/jtbi.2002.3119. PubMed PMID: WOS:000180138700008.
89. Liang S, Fuhuman S, Somogyi R, editors. REVEAL, A General Reverse Engineering Algorithm For Inference of Genetic Network Architectures. Pacific Symposium on Biocomputing; 1998; Hawaii.
90. Park J, Ogunnaike B, Schwaber J, Vadigepalli R. Identifying functional gene regulatory network phenotypes underlying single cell transcriptional variability. *Progress in Biophysics and Molecular Biology*. 2015;117:87-98.
91. Lopes C, Franz M, Kazi F, Donaldson S, Morris Q, Bader G. Cytoscape Web: an interactive web-based network browser. *Bioinformatics*. 2010;26(18):2347-8. doi: 10.1093/bioinformatics/btq430. PubMed PMID: WOS:000281714100059.
92. Chiang LW, Grenier JM, Ettwiller L, Jenkins LP, Ficene D, Martin J, et al. An orchestrated gene expression component of neuronal programmed cell death revealed by cDNA array analysis. *Proc Natl Acad Sci U S A*. 2001;98(5):2814-9. doi: 98/5/2814 [pii]
10.1073/pnas.051630598. PubMed PMID: 11226323; PubMed Central PMCID: PMCPMC30222.
93. Freund JE. Modern elementary statistics. 3d ed. Englewood Cliffs, N.J.,: Prentice-Hall; 1967. x, 432 p. p.

94. Minitab I. Minitab 17 Statistical Software. State College, PA2010.
95. Wang SS, Kazantzi V, Good TA. A Kinetic Analysis of the Mechanism of beta-Amyloid Induced G Protein Activation. *J Theor Biol.* 2003;221(2):269-78. doi: S0022519303931894 [pii]. PubMed PMID: 12628233.
96. Thathiah A, De Strooper B. The role of G-protein coupled receptors in the pathology of Alzheimer's Disease. *Nature Reviews.* 2011;12:73-87.
97. Venkatasubramaniam A. Engineering tools to analyze beta-amyloid's effect on cellular mechanisms linked to the neurodegeneration observed in Alzheimer's disease: University of Maryland, Baltimore County; 2014.
98. Bulbarelli A, Lonati E, Cazzaniga E, Re F, Sesana S, Barisani D, et al. TrkA pathway activation induced by amyloid-beta (Abeta). *Molecular and Cellular Neuroscience.* 2009;40(3):365-73. doi: 10.1016/j.mcn.2008.12.006. PubMed PMID: WOS:000263862000007.
99. Um J, Nygaard H, Heiss J, Kostylev M, Stagi M, Vortmeyer A, et al. Alzheimer amyloid-beta oligomer bound to postsynaptic prion protein activates Fyn to impair neurons. *Nature Neuroscience.* 2012;15(9):1227-U85. doi: 10.1038/nn.3178. PubMed PMID: WOS:000308072600013.
100. Hallock P, Thomas M. Integrating the Alzheimer's Disease Proteome and Transcriptome: A Comprehensive Network Model of a Complex Disease. *Omics-a Journal of Integrative Biology.* 2012;16(1-2):37-49. doi: 10.1089/omi.2011.0054. PubMed PMID: WOS:000300453800005.
101. Tagawa K, Homma H, Saito A, Fujita K, Chen X, Imoto S, et al. Comprehensive phosphoproteome analysis unravels the core signaling network that

initiates the earliest synapse pathology in preclinical Alzheimer's disease brain.
Human Molecular Genetics. 2014;1-19.

102. Albert R, Barabasi A. Statistical mechanics of complex networks. Reviews of
Modern Physics. 2002;74(1):47-97. doi: 10.1103/RevModPhys.74.47. PubMed
PMID: WOS:000174548700003.

103. Egger M, Smith GD, Phillips AN. Meta-analysis: Principles and procedures.
BMJ. 1997;315:1533-7.

Appendix 3A: Keyword search

MEDLINE

beta amyloid AND neurons

beta amyloid AND neurons NOT amyloid precursor protein

beta-amyloid AND neurons

beta-amyloid AND neurons NOT amyloid precursor protein

amyloid-beta AND neurons

amyloid-beta AND neurons NOT amyloid precursor protein

Web of Science

beta amyloid AND neurons

beta-amyloid AND neurons

amyloid-beta AND neurons

Appendix 3B: A β -neuron interaction lists

Ionotropic mechanisms (Iono_orig, Iono_large, Iono_large_scram)

AB	-1	NMR
AB	1	LTYPECA
AB	1	ABC
AB	-1	KV42
AB	1	ALPHA7NACHR
AB	-1	GIRK
AB	-1	KV12
AB	-1	KV11
AB	-1	KV41
AB	-1	KIR21
AB	-1	KIR23
AB	1	GABAAR
AB	1	RTYPECA
AB	1	PQCaCh
AB	1	NTYPECA

G-coupled protein receptors mechanism (ABGPCRs_larg,
ABGPCRs_larg_scram)

AB	1	PAR2
AB	1	BR1R
AB	1	CB1R
AB	1	ALPHA2AR
AB	1	D3R
AB	1	FIVEHT4R
AB	1	MGLUR1
AB	1	D2R
AB	1	MOPR
AB	1	BETA2AR
AB	1	A1R
AB	1	PAFR
AB	1	GABABR
AB	1	D1R
AB	1	SSTR1
AB	1	DOPR
AB	1	FIVEHT2AR
AB	1	M2R
AB	1	SSTR2
AB	1	NOPR
AB	1	MGLUR5
AB	1	MGLUR7
AB	1	M4R
AB	1	FIVEHT1AR
AB	1	CB2R
AB	1	M1R
AB	1	ALPHA1AR
AB	1	A2AR

G-protein coupled receptors and Integrin mechanisms (ABGPCRInt_large)

AB	1	INTEGRIN
AB	1	A2AR
AB	1	ALPHA1AR
AB	1	M1R
AB	1	CB2R
AB	1	FIVEHT1AR
AB	1	M4R
AB	1	MGLUR7
AB	1	MGLUR5
AB	1	NOPR
AB	1	SSTR2
AB	1	M2R
AB	1	FIVEHT2AR
AB	1	DOPR
AB	1	SSTR1
AB	1	PAR2
AB	1	D1R
AB	1	A1R
AB	1	BETA2AR
AB	1	MOPR
AB	1	D2R
AB	1	GABABR
AB	1	PAFR
AB	1	MGLUR1
AB	1	FIVEHT4R
AB	1	D3R
AB	1	ALPHA2AR
AB	1	CB1R
AB	1	BR1R

Activation of all cell surface receptors/channels mechanism (ABfullact_larg, ABfull_act_scram)

AB	1	EPHB2	AB	1	ALPHA2AR
AB	1	KV43	AB	1	DISHEVELED
AB	1	KV42	AB	1	AC5
AB	1	TNFR1	AB	1	BETA2AR
AB	1	NCADHERIN	AB	1	EGFR
AB	1	GIRK	AB	1	KV12
AB	1	AMPAR	AB	1	KV11
AB	1	GABAAR	AB	1	RYPECA
AB	1	KAL	AB	1	PDGFR
AB	1	MGLUR1	AB	1	A2AR
AB	1	MGLUR5	AB	1	M1R
AB	1	INTEGRIN	AB	1	BR1R
AB	1	PIP3	AB	1	ALPHA7NACHR
AB	1	PIP2	AB	1	PAR2
AB	1	PMCA	AB	1	KV41
AB	1	FIVEHT1AR	AB	1	KV14
AB	1	NMR	AB	1	M4R
AB	1	M2R	AB	1	KAR
AB	1	IR	AB	1	GAT1
AB	1	SSTR1	AB	1	FASCIN
AB	1	SSTR2	AB	1	GABABR
AB	1	FIVEHT2AR	AB	1	CHOLESTEROL
AB	1	PAFR	AB	1	LRP
AB	1	FIVEHT4R	AB	1	MGLUR7
AB	1	D2R	AB	1	LYPECA
AB	1	D1R	AB	1	KIR41
AB	1	RET	AB	1	PQCaCh
AB	1	FAS	AB	1	NYPECA
AB	1	TRKB	AB	1	D3R
AB	1	SYNDECAN	AB	1	KIR23
AB	1	L1	AB	1	ERBB
AB	1	CB1R	AB	1	DOPR
AB	1	A1R	AB	1	KOPR
AB	1	ALPHA1AR	AB	1	MOPR

Inhibition of all cell surface receptors/channels mechanism (ABfull_inhib_larg, ABfull_inhib_sram)

AB	-1	EPHB2	AB	-1	ALPHA2AR
AB	-1	KV43	AB	-1	DISHEVELED
AB	-1	KV42	AB	-1	AC5
AB	-1	TNFR1	AB	-1	BETA2AR
AB	-1	NCADHERIN	AB	-1	EGFR
AB	-1	GIRK	AB	-1	KV12
AB	-1	AMPA	AB	-1	KV11
AB	-1	GABAA	AB	-1	RTYPECA
AB	-1	KAL	AB	-1	PDGFR
AB	-1	MGLUR1	AB	-1	A2AR
AB	-1	MGLUR5	AB	-1	M1R
AB	-1	INTEGRIN	AB	-1	BR1R
AB	-1	PIP3	AB	-1	ALPHA7NACHR
AB	-1	PIP2	AB	-1	PAR2
AB	-1	PMCA	AB	-1	KV41
AB	-1	FIVEHT1AR	AB	-1	KV14
AB	-1	NMR	AB	-1	M4R
AB	-1	M2R	AB	-1	KAR
AB	-1	IR	AB	-1	GAT1
AB	-1	SSTR1	AB	-1	FASCIN
AB	-1	SSTR2	AB	-1	GABABR
AB	-1	FIVEHT2AR	AB	-1	CHOLESTEROL
AB	-1	PAFR	AB	-1	LRP
AB	-1	FIVEHT4R	AB	-1	MGLUR7
AB	-1	D2R	AB	-1	LTYPECA
AB	-1	D1R	AB	-1	KIR41
AB	-1	RET	AB	-1	PQCaCh
AB	-1	FAS	AB	-1	NTYPECA
AB	-1	TRKB	AB	-1	D3R
AB	-1	SYNDECAN	AB	-1	KIR23
AB	-1	L1	AB	-1	ERBB
AB	-1	CB1R	AB	-1	DOPR
AB	-1	A1R	AB	-1	KOPR
AB	-1	ALPHA1AR	AB	-1	MOPR

Appendix 3C: Results from Kruskal-Wallis & Mann-Whitney U tests

Identifier2	N	Median	Ave Rank	Z
ABfull_act_scram	48	0.2680	196.2	-4.91
ABfull_inhib_larg	48	0.3765	526.2	7.82
ABfull_inhib_scram	48	0.2960	305.6	-0.69
ABfullact_larg	60	0.3667	478.9	6.77
ABfullact_rPKN	48	0.3511	426.0	3.96
ABGPCRInt_larg	72	0.3367	358.3	1.68
ABGPCRs_larg	84	0.3214	345.6	1.16
ABGPCRs_scram	47	0.2261	113.8	-8.00
Iono_larg	107	0.3292	349.3	1.56
Iono_larg_scram	84	0.2477	153.7	-8.94
Overall	646		323.5	

H = 270.06 DF = 9 P = 0.000

H = 270.06 DF = 9 P = 0.000 (adjusted for ties)

Pairwise comparisons (Mann-Whitney U test)

Number of pairwise comparisons: 36

Significance level (α) adjusted for Bonferroni adjustment: 0.00139

	N	Median
Iono_larg	107	0.32920
Iono_larg_scram	84	0.24773

Point estimate for $\eta_1 - \eta_2$ is 0.07690

99.9 Percent CI for $\eta_1 - \eta_2$ is (0.05217,0.10012)

W = 13437.0

Test of $\eta_1 = \eta_2$ vs $\eta_1 \neq \eta_2$ is significant at 0.0000

The test is significant at 0.0000 (adjusted for ties)

	N	Median
Iono_larg	107	0.32920
ABfullact_larg	60	0.36675

Point estimate for $\eta_1 - \eta_2$ is -0.04235

99.9 Percent CI for $\eta_1 - \eta_2$ is (-0.06325,-0.02036)

W = 7294.0

Test of $\eta_1 = \eta_2$ vs $\eta_1 \neq \eta_2$ is significant at 0.0000

The test is significant at 0.0000 (adjusted for ties)

	N	Median
Iono_larg	107	0.32920
ABfull_act_scram	48	0.26800

Point estimate for $\eta_1 - \eta_2$ is 0.05191

99.9 Percent CI for $\eta_1 - \eta_2$ is (0.02743,0.07897)

W = 9928.0

Test of $\eta_1 = \eta_2$ vs $\eta_1 \neq \eta_2$ is significant at 0.0000

The test is significant at 0.0000 (adjusted for ties)

	N	Median
Iono_larg	107	0.32920
ABfull_inhib_larg	48	0.37650

Point estimate for $\eta_1 - \eta_2$ is -0.06144
 99.9 Percent CI for $\eta_1 - \eta_2$ is (-0.08450,-0.03368)
 W = 6568.0
 Test of $\eta_1 = \eta_2$ vs $\eta_1 \neq \eta_2$ is significant at 0.0000
 The test is significant at 0.0000 (adjusted for ties)

	N	Median
Iono_larg	107	0.32920
ABfull_inhib_scram	48	0.29601

Point estimate for $\eta_1 - \eta_2$ is 0.01806
 99.9 Percent CI for $\eta_1 - \eta_2$ is (-0.01836,0.05683)
 W = 8793.0
 Test of $\eta_1 = \eta_2$ vs $\eta_1 \neq \eta_2$ is significant at 0.0840
 The test is significant at 0.0840 (adjusted for ties)[n.s.]

	N	Median
Iono_larg	107	0.32920
ABGPCRs_larg	84	0.32141

Point estimate for $\eta_1 - \eta_2$ is 0.00070
 99.9 Percent CI for $\eta_1 - \eta_2$ is (-0.01821,0.02090)
 W = 10337.0
 Test of $\eta_1 = \eta_2$ vs $\eta_1 \neq \eta_2$ is significant at 0.8649
 The test is significant at 0.8649 (adjusted for ties)[n.s.]

	N	Median
Iono_larg	107	0.32920
ABGPCRInt_larg	72	0.33669

Point estimate for $\eta_1 - \eta_2$ is -0.00623
 99.9 Percent CI for $\eta_1 - \eta_2$ is (-0.02467,0.01530)
 W = 9275.0
 Test of $\eta_1 = \eta_2$ vs $\eta_1 \neq \eta_2$ is significant at 0.2970
 The test is significant at 0.2970 (adjusted for ties)[n.s.]

	N	Median
Iono_larg	107	0.32920
ABGPCRs_scram	47	0.22613

Point estimate for $\eta_1 - \eta_2$ is 0.09383
 99.9 Percent CI for $\eta_1 - \eta_2$ is (0.06409,0.12068)
 W = 10381.0
 Test of $\eta_1 = \eta_2$ vs $\eta_1 \neq \eta_2$ is significant at 0.0000
 The test is significant at 0.0000 (adjusted for ties)

	N	Median
Iono_larg_scram	84	0.24773
ABfullact_larg	60	0.36675

Point estimate for $\eta_1 - \eta_2$ is -0.11748

99.9 Percent CI for $\eta_1 - \eta_2$ is (-0.14574,-0.08701)
W = 3866.0
Test of $\eta_1 = \eta_2$ vs $\eta_1 \neq \eta_2$ is significant at 0.0000

	N	Median
Iono_larg_scram	84	0.24773
ABfull_act_scram	48	0.26800

Point estimate for $\eta_1 - \eta_2$ is -0.02356
99.9 Percent CI for $\eta_1 - \eta_2$ is (-0.05512,0.00901)
W = 5087.0
Test of $\eta_1 = \eta_2$ vs $\eta_1 \neq \eta_2$ is significant at 0.0184 [n.s.]

	N	Median
Iono_larg_scram	84	0.24773
ABfull_inhib_larg	48	0.37650

Point estimate for $\eta_1 - \eta_2$ is -0.13617
99.9 Percent CI for $\eta_1 - \eta_2$ is (-0.16772,-0.10312)
W = 3691.0
Test of $\eta_1 = \eta_2$ vs $\eta_1 \neq \eta_2$ is significant at 0.0000

	N	Median
Iono_larg_scram	84	0.24773
ABfull_inhib_scram	48	0.29601

Point estimate for $\eta_1 - \eta_2$ is -0.05758
99.9 Percent CI for $\eta_1 - \eta_2$ is (-0.09733,-0.01652)
W = 4621.0
Test of $\eta_1 = \eta_2$ vs $\eta_1 \neq \eta_2$ is significant at 0.0000

	N	Median
Iono_larg_scram	84	0.24773
ABGPCRs_larg	84	0.32141

Point estimate for $\eta_1 - \eta_2$ is -0.07523
99.9 Percent CI for $\eta_1 - \eta_2$ is (-0.10184,-0.04781)
W = 4701.0
Test of $\eta_1 = \eta_2$ vs $\eta_1 \neq \eta_2$ is significant at 0.0000

	N	Median
Iono_larg_scram	84	0.24773
ABGPCRInt_larg	72	0.33669

Point estimate for $\eta_1 - \eta_2$ is -0.08044
99.9 Percent CI for $\eta_1 - \eta_2$ is (-0.10758,-0.04774)
W = 4619.0

Test of $\eta_1 = \eta_2$ vs $\eta_1 \neq \eta_2$ is significant at 0.0000

	N	Median
Iono_larg_scram	84	0.24773
ABGPCRs_scram	47	0.22613

Point estimate for $\eta_1 - \eta_2$ is 0.01671
99.9 Percent CI for $\eta_1 - \eta_2$ is (-0.01783,0.05038)
W = 5880.5
Test of $\eta_1 = \eta_2$ vs $\eta_1 \neq \eta_2$ is significant at 0.1069
The test is significant at 0.1069 (adjusted for ties) [n.s.]

	N	Median
ABfullact_larg	60	0.36675
ABfull_act_scram	48	0.26800

Point estimate for $\eta_1 - \eta_2$ is 0.09375
99.9 Percent CI for $\eta_1 - \eta_2$ is (0.06371,0.12369)
W = 4491.0
Test of $\eta_1 = \eta_2$ vs $\eta_1 \neq \eta_2$ is significant at 0.0000

	N	Median
ABfullact_larg	60	0.36675
ABfull_inhib_larg	48	0.37650

Point estimate for $\eta_1 - \eta_2$ is -0.01890
99.9 Percent CI for $\eta_1 - \eta_2$ is (-0.04765,0.01083)
W = 2915.0
Test of $\eta_1 = \eta_2$ vs $\eta_1 \neq \eta_2$ is significant at 0.0284 [n.s.]

	N	Median
ABfullact_larg	60	0.36675
ABfull_inhib_scram	48	0.29601

Point estimate for $\eta_1 - \eta_2$ is 0.05933
99.9 Percent CI for $\eta_1 - \eta_2$ is (0.01837,0.10083)
W = 3987.0
Test of $\eta_1 = \eta_2$ vs $\eta_1 \neq \eta_2$ is significant at 0.0000

	N	Median
ABfullact_larg	60	0.36675
ABGPCRs_larg	84	0.32141

Point estimate for $\eta_1 - \eta_2$ is 0.04271
99.9 Percent CI for $\eta_1 - \eta_2$ is (0.01864,0.06708)
W = 5665.0
Test of $\eta_1 = \eta_2$ vs $\eta_1 \neq \eta_2$ is significant at 0.0000

	N	Median
ABfullact_larg	60	0.36675
ABGPCRInt_larg	72	0.33669

Point estimate for $\eta_1 - \eta_2$ is 0.03824
99.9 Percent CI for $\eta_1 - \eta_2$ is (0.01322,0.06246)
W = 5048.0

Test of $\eta_1 = \eta_2$ vs $\eta_1 \neq \eta_2$ is significant at 0.000

	N	Median
ABfullact_larg	60	0.36675
ABGPCRs_scram	47	0.22613

Point estimate for $\eta_1 - \eta_2$ is 0.13441
99.9 Percent CI for $\eta_1 - \eta_2$ is (0.10003,0.16637)
W = 4572.0
Test of $\eta_1 = \eta_2$ vs $\eta_1 \neq \eta_2$ is significant at 0.0000

	N	Median
ABfull_act_scram	48	0.26800
ABfull_inhib_larg	48	0.37650

Point estimate for $\eta_1 - \eta_2$ is -0.11273
99.9 Percent CI for $\eta_1 - \eta_2$ is (-0.14487,-0.08013)
W = 1243.0
Test of $\eta_1 = \eta_2$ vs $\eta_1 \neq \eta_2$ is significant at 0.0000

	N	Median
ABfull_act_scram	48	0.26800
ABfull_inhib_scram	48	0.29601

Point estimate for $\eta_1 - \eta_2$ is -0.03194
99.9 Percent CI for $\eta_1 - \eta_2$ is (-0.07755,0.00985)
W = 1978.0
Test of $\eta_1 = \eta_2$ vs $\eta_1 \neq \eta_2$ is significant at 0.0104 [n.s.]

	N	Median
ABfull_act_scram	48	0.26800
ABGPCRs_larg	84	0.32141

Point estimate for $\eta_1 - \eta_2$ is -0.05113
99.9 Percent CI for $\eta_1 - \eta_2$ is (-0.07914,-0.02289)
W = 2045.0
Test of $\eta_1 = \eta_2$ vs $\eta_1 \neq \eta_2$ is significant at 0.0000

	N	Median
ABfull_act_scram	48	0.26800
ABGPCRInt_larg	72	0.33669

Point estimate for $\eta_1 - \eta_2$ is -0.05554
99.9 Percent CI for $\eta_1 - \eta_2$ is (-0.08621,-0.02456)
W = 1937.0
Test of $\eta_1 = \eta_2$ vs $\eta_1 \neq \eta_2$ is significant at 0.0000

	N	Median
ABfull_act_scram	48	0.26800
ABGPCRs_scram	47	0.22613

Point estimate for $\eta_1 - \eta_2$ is 0.03972
99.9 Percent CI for $\eta_1 - \eta_2$ is (0.00468,0.07518)
W = 2794.5

Test of $\eta_1 = \eta_2$ vs $\eta_1 \neq \eta_2$ is significant at 0.0003
The test is significant at 0.0003 (adjusted for ties)

	N	Median
ABfull_inhib_larg	48	0.37650
ABfull_inhib_scram	48	0.29601

Point estimate for $\eta_1 - \eta_2$ is 0.08038
99.9 Percent CI for $\eta_1 - \eta_2$ is (0.03550,0.12081)
W = 3046.0
Test of $\eta_1 = \eta_2$ vs $\eta_1 \neq \eta_2$ is significant at 0.0000

	N	Median
ABfull_inhib_larg	48	0.37650
ABGPCRs_larg	84	0.32141

Point estimate for $\eta_1 - \eta_2$ is 0.06155
99.9 Percent CI for $\eta_1 - \eta_2$ is (0.03382,0.08928)
W = 4565.0
Test of $\eta_1 = \eta_2$ vs $\eta_1 \neq \eta_2$ is significant at 0.0000

	N	Median
ABfull_inhib_larg	48	0.37650
ABGPCRInt_larg	72	0.33669

Point estimate for $\eta_1 - \eta_2$ is 0.05808
99.9 Percent CI for $\eta_1 - \eta_2$ is (0.02569,0.08569)
W = 3988.0
Test of $\eta_1 = \eta_2$ vs $\eta_1 \neq \eta_2$ is significant at 0.0000

	N	Median
ABfull_inhib_larg	48	0.37650
ABGPCRs_scram	47	0.22613

Point estimate for $\eta_1 - \eta_2$ is 0.15214
99.9 Percent CI for $\eta_1 - \eta_2$ is (0.11765,0.18760)
W = 3413.0
Test of $\eta_1 = \eta_2$ vs $\eta_1 \neq \eta_2$ is significant at 0.0000

	N	Median
ABfull_inhib_scram	48	0.29601
ABGPCRs_larg	84	0.32141

Point estimate for $\eta_1 - \eta_2$ is -0.01688
99.9 Percent CI for $\eta_1 - \eta_2$ is (-0.05643,0.02292)
W = 2875.0
Test of $\eta_1 = \eta_2$ vs $\eta_1 \neq \eta_2$ is significant at 0.1343 [n.s]

	N	Median
ABfull_inhib_scram	48	0.29601
ABGPCRInt_larg	72	0.33669

Point estimate for $\eta_1 - \eta_2$ is -0.01844
99.9 Percent CI for $\eta_1 - \eta_2$ is (-0.06266,0.02464)

W = 2635.0
 Test of $\eta_1 = \eta_2$ vs $\eta_1 \neq \eta_2$ is significant at 0.1503 [n.s.]

	N	Median
ABfull_inhib_scram	48	0.29601
ABGPCRs_scram	47	0.22613

Point estimate for $\eta_1 - \eta_2$ is 0.07212
 99.9 Percent CI for $\eta_1 - \eta_2$ is (0.02849,0.11844)
 W = 3007.0
 Test of $\eta_1 = \eta_2$ vs $\eta_1 \neq \eta_2$ is significant at 0.0000

	N	Median
ABGPCRs_larg	84	0.32141
ABGPCRInt_larg	72	0.33669

Point estimate for $\eta_1 - \eta_2$ is -0.00597
 99.9 Percent CI for $\eta_1 - \eta_2$ is (-0.02855,0.01831)
 W = 6368.0
 Test of $\eta_1 = \eta_2$ vs $\eta_1 \neq \eta_2$ is significant at 0.4228 [n.s.]

	N	Median
ABGPCRs_larg	84	0.32141
ABGPCRs_scram	47	0.22613

Point estimate for $\eta_1 - \eta_2$ is 0.09192
 99.9 Percent CI for $\eta_1 - \eta_2$ is (0.06040,0.12171)
 W = 7121.0
 Test of $\eta_1 = \eta_2$ vs $\eta_1 \neq \eta_2$ is significant at 0.0000

	N	Median
ABGPCRInt_larg	72	0.33669
ABGPCRs_scram	47	0.22613

Point estimate for $\eta_1 - \eta_2$ is 0.09586
 99.9 Percent CI for $\eta_1 - \eta_2$ is (0.06046,0.12868)
 W = 5618.0
 Test of $\eta_1 = \eta_2$ vs $\eta_1 \neq \eta_2$ is significant at 0.0000

Chapter 4: Identifying network motifs from network structure: impact on experimental design for inference of A β -neuron interactions³

4.1 Introduction

“He that breaks a thing to find out what it is has left the path of wisdom.” – J.R.R. Tolkien

For many years, the community of researchers studying the effects of beta-amyloid (A β) on *in vitro* preparations of neurons has attempted to identify A β -neuron interactions. The primary assumption, given knowledge of intracellular signaling, was that A β interacts with some cell surface mechanism such that a linear pathway from a particular receptor was adversely affected. In some cases, it was assumed that A β caused some disruption in the cellular membrane itself, which would cause complete dysregulation of intracellular signaling (particularly, calcium signaling), resulting in the onset of apoptosis[1-3]. Given this linear pathway hypothesis, standard practice in the field was that hypotheses were tested experimentally by adding A β exogenously to neurons and then measuring the activity of a known protein in a pathway of interest, and not measuring the activity any other protein in potentially intersecting pathways. Many different hypotheses have been formulated based on what could be defined as a Linear Pathway Hypothesis (LPH)[6], but to date, no converging evidence of a particular set of A β -neuron interactions responsible for the signaling

³ Co-authors: Stephen Vicchio, Angela Norton, Theresa A. Good, and Mariajosé Castellanos

events observed has emerged. This has left the community, after over 20 years of research, without a strong consensus on A β 's early action on neurons.

With the advent of the proteomics era, there has been a great increase in the understanding of intracellular signaling. Particularly, intracellular signaling can no longer be viewed as a set of linear, non-intersecting pathways of just a few 10s of molecules, but has to be viewed as a highly interconnected network of hundreds and even thousands of signaling molecules[7, 8]. Intracellular networks are made up of many signaling motifs that give rise to the signaling landscape of the cell and its emergent behavior[9]. Each cell can have nearly 100 (or more) receptors or channels at the surface to transduce a signal from a complex milieu of extracellular cues through the network in order to produce any number of physiological responses. This landscape is becoming more highly complex as more and more interactions are being discovered.

Several researchers have studied the structure of networks in order to gain some fundamental knowledge of how networks develop and to infer network function[10-14]. Utilizing a branch of mathematics called graph theory, a network can be interpreted as a graph, where each protein is described as a node and the interaction between a pair of nodes is called an edge. A graph of a network is then just a set of nodes, $i \in 1, 2, \dots, N$ and edges, $e \in 1, 2, \dots, E$, such that it forms an ordered pair. The topology, or the structure, of the graph can be analyzed in various ways in order to understand how individual nodes interact in order to pass information from

one node to another. A node can represent anything that interacts with something else. Therefore, network analysis is a broad field including social media networks, author-collaborator networks, ecological networks, metabolic networks and intracellular networks, to name a few[10]. There are some general topological features that have been found to be common among all real networks (in comparison to random networks). One main feature is called “small-world” or “scale-free”[15], which is described by a power law distribution of the number of edges per node. These features have been used to classify networks and to examine whether certain network topologies, arising from experimental data, represent real networks (i.e., small-world vs. random). In this chapter, we used ideas from network analysis to help demonstrate that by virtue of the topology of the network, the majority of the signaling pathways cannot be linear.

What has also been of increasing interest in the area of Systems Biology with respect to networks has been the identification of network motifs. It has been postulated that biological networks are comprised of interacting smaller network motifs, which can give rise to different signaling landscapes given certain extracellular signals over time[7, 16]. Thus, understanding the structure and functions of these network motifs can provide a way to condense the complexity of the network, especially when studying the function of these networks in experiments. According to Barabasi and Oltvai[7], network motifs consist of particular subgraphs of a network graph that occur with greater frequency in comparison to other subgraphs. In general, for biological networks, motifs such as feed-forward and

feedback loops are prevalent. There are also cross-talk[17] and receptor trans-activation (or inhibition)[5], amongst others. The interaction of many different network motifs gives rise to complex (non-linear) network behavior. For example, cross-talk between calcium and cyclic adenosine monophosphate (cAMP) pathway gives rise to oscillations[18, 19]; while different types of feedback mechanisms can give rise to various types of attractor states[20]. Identification of these types of network motifs can provide information about functional behavior of a node within its context in the network. Knowledge of the complexity of real biological networks calls into question the validity of the Linear Pathway Hypothesis that has been the basis for experimental design in cell biology over many decades.

Using a signal flow algorithm and linear algebra techniques, we have been able to identify signaling network motifs that may give rise to complex behavior in a large CA1 hippocampal neuronal network. This complex behavior may be an explanation for the lack of consensus about A β -neuron interactions observed in *in vitro* experiments because experiments designed via LPH produce data too sparse to be discriminatory. In this chapter, we will identify network properties and motifs in a hippocampal neuronal network[21]. We will also demonstrate, on a significantly smaller network, the impact of these motifs on network dynamics and input inference based on LPH. Finally, we will make some associations between the behavior observed in the smaller network due to receptor trans-activation and feedback and the large network and how this information could guide experimental design toward discovering A β -neuron interactions.

4.2 Methods

4.2.1 Signal Flow Method

The Signal Flow Method is an algorithm that simulates the propagation of a signal through the network by the following mathematical equation (Eq. 4.2.1)[22, 23]:

$$x_i(t+1) = A(i,j) * x_j(t) \text{ (Eq. 4.2.1)}$$

where, $x_i(t+1)$ is the signal of node i at the current step $(t+1)$, $x_j(t)$ is the signal of node j at the previous step (t) . $A(i,j)$ is the Adjacency matrix, which is an $n \times n$ matrix, where each entry in the matrix is specified as such (Eq. 4.2.2):

$$A(i,j) = \begin{cases} 1, & \text{if } i \text{ is adjacent to } j \text{ (activation)} \\ 0, & \text{if } i \text{ is not adjacent to } j \\ -1, & \text{if } i \text{ is adjacent to } j \text{ (inhibition)} \end{cases} \text{ (Eq. 4.2.2)}$$

The signal for each simulation is initiated at the $A\beta$ node. $A\beta$ is connected to the specified receptor/channel or set of receptors/channels. As the signal propagates through the network, the signal at each node is calculated at each discrete step via Eq. 4.2.1. A discrete step is the next sequential movement in the network based on adjacency ($A(i,j)$ matrix). It is not directly related to time since there is no associated kinetics or selectivity of interactions; however, an indirect relationship to time can be

inferred because of the hierarchical and directional nature of the network[24]. Because of the lack of selectivity for the interactions, there are additive effects, such that, for example, if the signals through three nodes into the current node are all 1, then the current node will take on the signal value of 3. There are no units for the signal as it is a mathematical construct used solely for simulating the signal propagation through the network from a set of inputs to its associated set of outputs. The method makes no allowances for different dynamics of signals traveling through a network. Using the example from above, if the signals through three nodes represent signaling reactions that occur with different time constants (say on the order of milliseconds, seconds, and tens of seconds), then in the actual network inside the cell, those signals would not arrive at the intersecting node at the same time; however, in the signal flow model, so long as the number of steps to a node is the same, the signals arrive at the same time. This algorithm was coded and run in Matlab R2010b. The adjacency matrix was built in Visual Basic Application through Excel and imported into Matlab as a text file read into a matrix function. The interaction list used to build the adjacency matrix was from[21].

4.2.1.1 Characterizing receptor trans-activation

Receptor trans-activation (or inhibition) is characterized by the propagation of the signal through a receptor (or channel) that is not directly connected to the A β node during the simulation.

4.2.2 Identification of Feedback Motifs Via Path Length Analysis

Path length analysis[25] was used to identify and calculate the number of feedback loops (cycles) of length k originating and ending with node i . The calculation of paths of length k is defined as (Eq. 4.2.3):

$$N_{PL} = A(i, j)^k \text{ (Eq. 4.2.3)}$$

where, N_{PL} is the number of path lengths per node, $A(i, j)$ is the adjacency matrix (see Eq. 4.2.2) and k is the length of the path (1, 2,... k). In order to calculate the number of feedback loops per node, the diagonal of the path length matrix is given by (Eq. 4.2.4):

$$N_{FB} = \text{diag}(N_{PL}) = \text{diag}(A(i, j)^k) \text{ (Eq. 4.2.4)}$$

where, N_{FB} is the number of feedback loops per node, from node i to node i . Path length analysis was performed in Matlab R2010b.

4.2.3 Kinetic Model

A kinetic model of a small intracellular hippocampal signaling network[5] was developed utilizing reversible mass action kinetics given by Equation 4.2.5:

$$\frac{d[K]}{dt} = r_{K,f} - r_{K,b} \text{ (Eq. 4.2.5)}$$

where, $d[K]/dt$ is the rate of generation of protein K in $\text{nM}^{-1}\text{s}^{-2}$. $r_{K,f}$ and $r_{K,b}$ are the forward and back reaction rates, respectively. The reaction list, compound list, equations, kinetic parameters and initial conditions are given in Appendices 4A – 4E. The time range for the simulations was 0-100s. To identify those proteins in this small kinetic model that exhibited non-monotonic behavior, the sign of the slope of the concentration versus time curve ($d[K]/dt$) was recorded. Then, those proteins that exhibited a change of sign (change in the slope of the derivative) were those that exhibited non-linear dynamic behavior under specified initial conditions.

4.3 Results and Discussion

4.3.1 Intrinsic Topological Properties of CA1 Hippocampal Neuronal Signaling Network Challenge the Linear Pathway Hypothesis (LPH)

In this section, the general properties of the CA1 hippocampal neuronal signaling network were used to demonstrate why a Linear Pathway Hypothesis does not encompass the complexity of the system. Without encompassing this complexity, the LPH will likely give results that are confounded with other uncontrolled factors in an experiment.

The Linear Pathway Hypothesis (LPH) is insufficient for hypothesis generation because:

1. Power law or near power law distribution of degrees in the network exists (Figure 4.1). This is a property of real networks known as “scale-free” or “small-world”[10]. If a network consisted of primarily linear, non-intersecting pathways, then this “small-world” or “scale-free” property would not exist in such a network. The number of interactions would, instead, scale with the number of nodes (see Eq. 4.1). This is not true of a CA1 hippocampal neuronal signaling network, as demonstrated in **Figure 4.1**. In this figure, the top graph represents the number of in-coming interactions, or edges, also known as in-degree. In this graph, a power law distribution of the interactions is reported, where a large number of nodes have a small in-degree and a smaller amount of nodes have a large number of in-coming edges. The bottom graph shows the number of out-going interactions or edges, known as the out-degree. Again, a power law distribution is reported, similar to the top graph. Taken together, these graphs demonstrate that this CA1 hippocampal neuronal signaling network is scale-free, and therefore not amenable to the Linear Pathway Hypothesis.

$$\frac{N(N-1)}{2} = \frac{545(544)}{2} = 148,240 \text{ maximum interactions vs. 1235 actual interactions (Eq. 4.3.1)}$$

Ultimately, this means that the nodes in the network are highly interconnected. This makes pathways less distinguishable since many of them

intersect at proteins called “hub” molecules, which will be described in the next point.

2. The presence of hub proteins. This is a corollary of the small-world or scale-free property in that there are a few proteins in this network that act as hubs (nodes with very large number of interactions). The presence of these hubs readily suggests that there is cross-talk or some other type of interconnectivity across pathways of different receptor types. Ma’ayan et al[21] identifies the hub proteins in this network as being: PKA, PKC, $G_{\beta\gamma}$, Calmodulin, NMDAR, SRC, Calcium, CAMKII, PSD95, GRB2, $G_{\alpha i}$, MAPK, Calcineurin, Actin, Tubulin, and CREB. The presence of hub molecules in this neuronal network suggests, once again, a network that is not a set of linear pathways. The problem therein is that these hub proteins are highly studied in *in vitro* experiments studying the mechanisms of A β -neuron interaction[26-39] (see **Section 4.3.5**) and are likely associated with multiple different receptor-mediated pathways, thus making it nearly impossible to infer the pathway from which the signal originated.

3. As will be discussed further in the next section, there are network motifs that are naturally not congruent with LPH: such as receptor trans-activation, cross-talk and feedback/feedforward loops. The presence and high preponderance of (especially feedback/feedforward loops[21]) these network

motifs suggest a more interconnected network rather than a series of linear pathways.

4. The β index is a measure of the level of connectivity in a graph (Figure 4.2). The β index, given in Eq. 4.3.2, is calculated as the average number of links per node.

$$\beta = \frac{e}{v} = \frac{1235}{545} = 2.26 \text{ (4.3.2)}$$

The β index for trees and simple networks is less than one. On the other hand, a connected network with one cycle has a β index value of 1 and more complex networks have a value greater than 1[40, 41]. Examples of simple and complex networks are shown in **Figure 4.2**. Again, this network with a β index of 2.26 is a highly complex and interconnected graph, and therefore the LPH would not be a good assumption for hypothesis generation in such a system. This β index also gives us some indication that there are likely cycle (or loop) structures present in this network and we will discuss the implications of this in further detail in Sections 4.3.2 and 4.3.3.

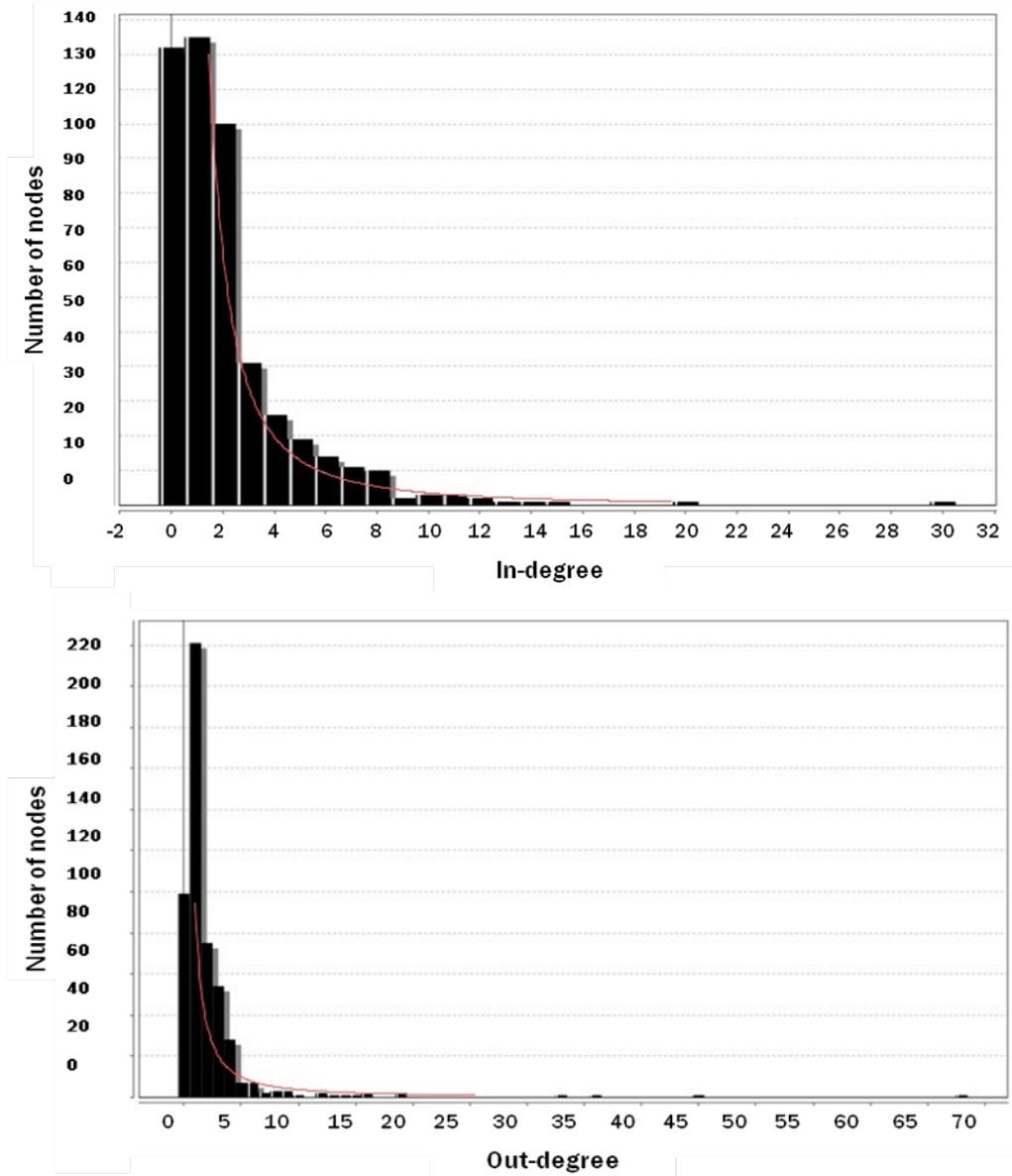


Figure 4.1: Histograms of the in- and out-degrees of nodes in the CA1 hippocampal neuronal network. *Top*, In-degree histogram where the abscissa is the number of incoming edges to each node (in-degree) and on the y-axis is the number of nodes. *Bottom*, similar to the top graph except that the abscissa is the number of outgoing edges (out-degree). In both graphs, the red curve represents a power law fit to the data. Graphical output generated from Network Analysis plugin in Cytoscape[4].

What consequence does knowing the topological properties of this CA1 hippocampal neuronal signaling network have on experimental design for inferring A β -neuron interactions? Firstly, a simplistic, reductionist hypothesis of a linear pathway between A β and a downstream measured protein is insufficient to characterize what is known about the system. Many factors are left uncontrolled and unmonitored in the experiment, thereby confounding the interpretation of the results. Without sufficient *a priori* knowledge in the design of the experiment, though one might ‘prove his or her hypothesis’, the rationale as to the processes that preceded the observed event may not be correct. And this could have an effect on reproducibility of the experimental results as well. Secondly, complex systems are known to produce complex, non-intuitive and sometimes unpredictable results[9]. This is typically referred to as emergent properties of the system[42]. These emergent properties are important because they usually give rise to the complex response of the system from an array of inputs and to the phenotypic response of the system to its environment[9]. These properties also become important as systems begin to interact and connect with other systems, such as neurons in a neural network in the brain. This is without taking into account the interplay between metabolic, signaling and regulatory networks. Therefore, it is necessary to begin to understand and to test the system as a system of interactions in order to identify this emergent behavior and to distinguish it from pathological behavior in the presence of a molecule such as A β . The first step in such an endeavor is to understand the intrinsic topological properties of the system and how that characterizes its complexity and interconnectedness. Given this information, the question the experimentalist should ask is: if protein x is measured in order to

infer $A\beta$'s interaction with protein s , in how many other pathways is protein x potentially involved (in-degree, for example)? Is protein x involved in other types of network motifs (receptor trans-activation or feedback)? If the answers to these questions are yes, then the experimentalist must decide how to design the experiment to control and/or monitor the behavior of protein x within its context in the system. An example of how an experimentalist might design an experiment with some of these questions in mind will be given in **Section 4.3.4**.

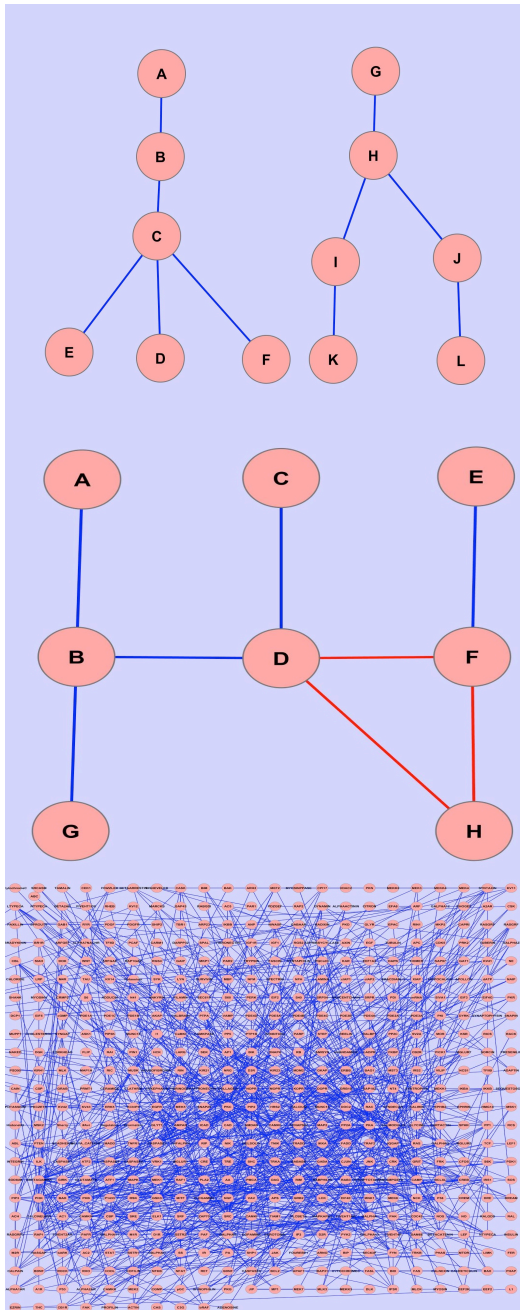


Figure 4.2: Example networks - trees, connected network with one cycle and a complex network. *Top*, a simple tree toy network with two trees consisting of 12 nodes and 10 edges. Its β index is 0.833. *Middle*, a toy connected network with one cycle (shown in red) with 8 nodes and 8 edges. Its β index is 1. *Bottom*, CA1 hippocampal neuronal signaling network with 545 nodes and 1235 edges (complex network). Its β index is 2.26. β index values were calculated according to equation 4.3.1. Network building and visualization done in Cytoscape[4].

4.3.2 Signal Flow Method is Used to Identify Signaling Motifs Based on Network Topology

The goal of this work is to identify signaling network motifs based on network topology analysis. In order to accomplish this goal, we used the Signal Flow Method to propagate a signal from the A β node through the network. At each discrete step, the signal has passed from one set of nodes to the next set in the pathway(s). Because networks are hierarchical, each discrete step is analogous to some sequential time point in chemical space[24]. However, a direct correlation with time would require the knowledge of the kinetics of the system. Also, without kinetic information, all paths can equally be followed by the signal and so there is no selectivity for each path. This is a disadvantage of this method. However, this method is advantageous because it allows for the determination of the flow of a signal as it starts from different interactions of A β with receptors or channels on the neuronal surface with just topographical information as its input. For example, nodes that are utilized in particular pathways can be observed and at what depth (or discrete step) the signal passes through. Our results in **Figures 4.3-4.7** demonstrate, using the Signal Flow Method, given a specific interaction of A β with a receptor or channel, the receptors that are trans-activated (or trans-inhibited). Receptor trans-activation (or inhibition) refers to the case in intracellular signaling when one receptor-mediated pathway activates (or inhibits) another receptor, and thereby modulates the function of that receptor-mediated pathway. In **Figure 4.3**, A β interacts with the integrin receptor.

Integrin was chosen because of recent work in our lab[43] and others[44, 45] that postulate interactions with integrins as being a target for A β induced neurotoxicity. The signal through three other receptors is shown here: the L-type calcium channel (LTYPECA), the N-methyl-D-aspartate receptor (NMDAR), and the metabotropic glutamate receptor 7 (MGLUR7). These receptors/channels have also been implicated in A β induced signaling[27, 46-48]. In this figure, starting with the top left graph, a signal of 1 is passed through the integrin receptor by way of A β . At the next discrete step and all subsequent steps thereof, the signal is 0. This is indicative of integrin not being directly involved in other network motifs that might regulate its function such as feedback/feedforward loops or receptor trans-activation. The possible involvement of any extracellular feedback mechanisms between its ligands and the receptor are not covered in this study nor are they present in the network. Moving to the top right graph, we see the signal passes through the LTYPECA at discrete step 3 and then at the next step the signal disappears. Two steps later, there is a sharp decrease in the signal. This is likely due to feedback mechanisms regulating the LTYPECA since it is between discrete steps 4 and 5 where feedback mechanisms, according to Ma'ayan et al[21], begin to appear.

For NMR (bottom left graph), again the signal of 1 goes through the receptor at discrete step 3 and at discrete step 4 returns to 0. Then at discrete step 5, we see a decrease in signal until discrete step 7 when there is an increase in the signal. Again, this is likely due to feedback mechanisms that are modulating NMR's function. Then in the bottom right graph, the MGLUR7 receives the signal at discrete step 6, but the

signal is 2 instead of 1. Since MGLUR7 receives this signal after the network has been fully traversed, this is indicative of it receiving the signal from two separate inputs that have received the signal of 1 in previous steps. Again, feedback mechanisms explain the increase in signal at the end of the simulation.

A β -INTEGRIN

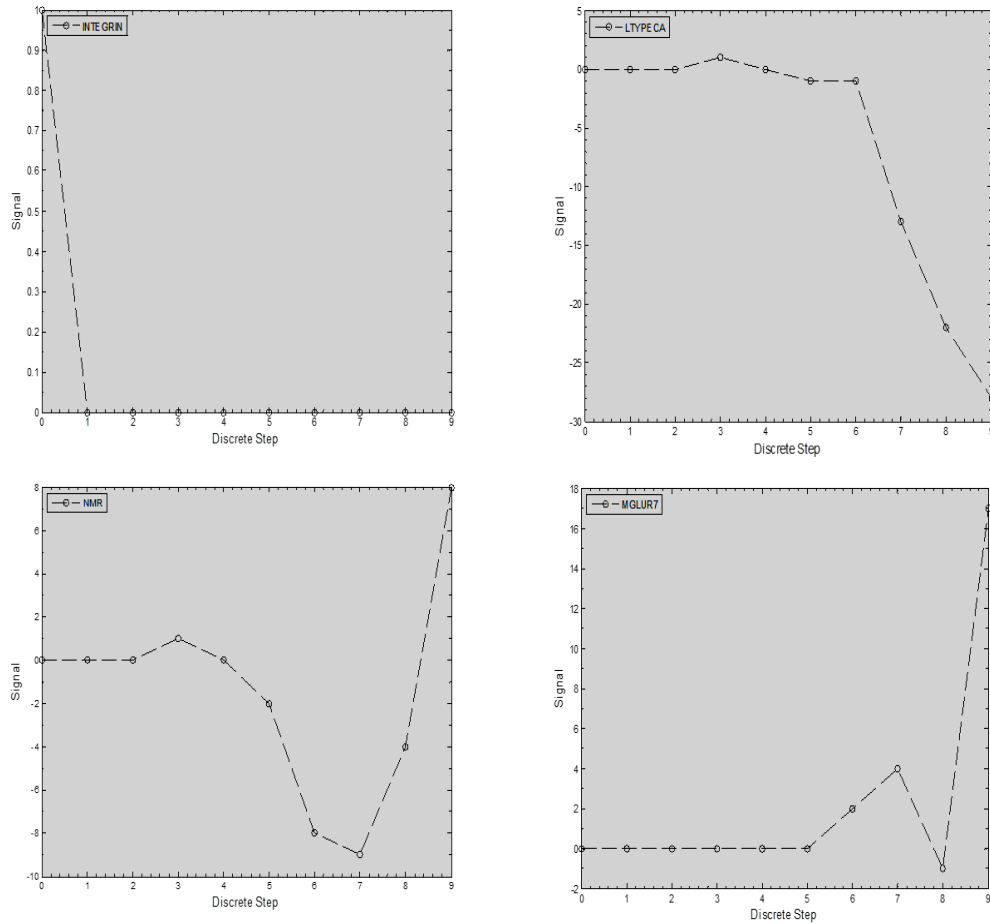


Figure 4.3: Signal through selected receptors for an interaction of A β with the integrin receptor.

Using the Signal Flow Method, a signal of 1 was initiated at the A β node and allowed to propagate through the network via Equation 4.2.1. The four selected receptors shown here are integrin, L-type calcium channel (LTYPECA), the N-methyl-D-aspartate receptor (NMR) and the metabotropic glutamate receptor 7 (MGLUR7). A β was the initial node and interacts only with the integrin receptor here. The curve in each graph represents the signal at each discrete step taken through the network. Ten discrete steps were simulated. Simulations were run and graphs were produced in Matlab.

In **Figure 4.4**, a signal is propagated from the A β node through the epidermal growth factor receptor (EGFR), which is a well-studied receptor tyrosine kinase. Receptor tyrosine kinases have also been implicated in A β -induced signaling and neurotoxicity[49]. Again, in the top left graph, we see the signal of 1 pass through EGFR, however, in this case, unlikely with integrin, at discrete step 4 there is a -1 signal that returns to EGFR. This would indicate some direct feedback from the EGFR pathway. From there, at discrete step 6, feedback mechanisms begin to regulate EGFR. Here, the integrin receptor receives no signal at any discrete step, which corroborates the behavior of integrin in **Figure 4.3**; that it is not regulated by any feedback mechanisms nor modulated by receptor trans-activation (or inhibition). LTYPECA in the left bottom graph receives a signal of -3 at discrete step 4. This likely means that there are three paths from the EGFR receptor that inhibit LTYPECA. From discrete step 4 on, feedback mechanisms are in play. MGLUR7 receives the signal at discrete step 4 and then at discrete step 6 feedback mechanisms come on. What this Signal Flow Method also elucidates for us is the ability of a signal from a receptor-mediated pathway, such as the one from EGFR, might potential self-regulate its receptor via feedback.

A β -EGFR

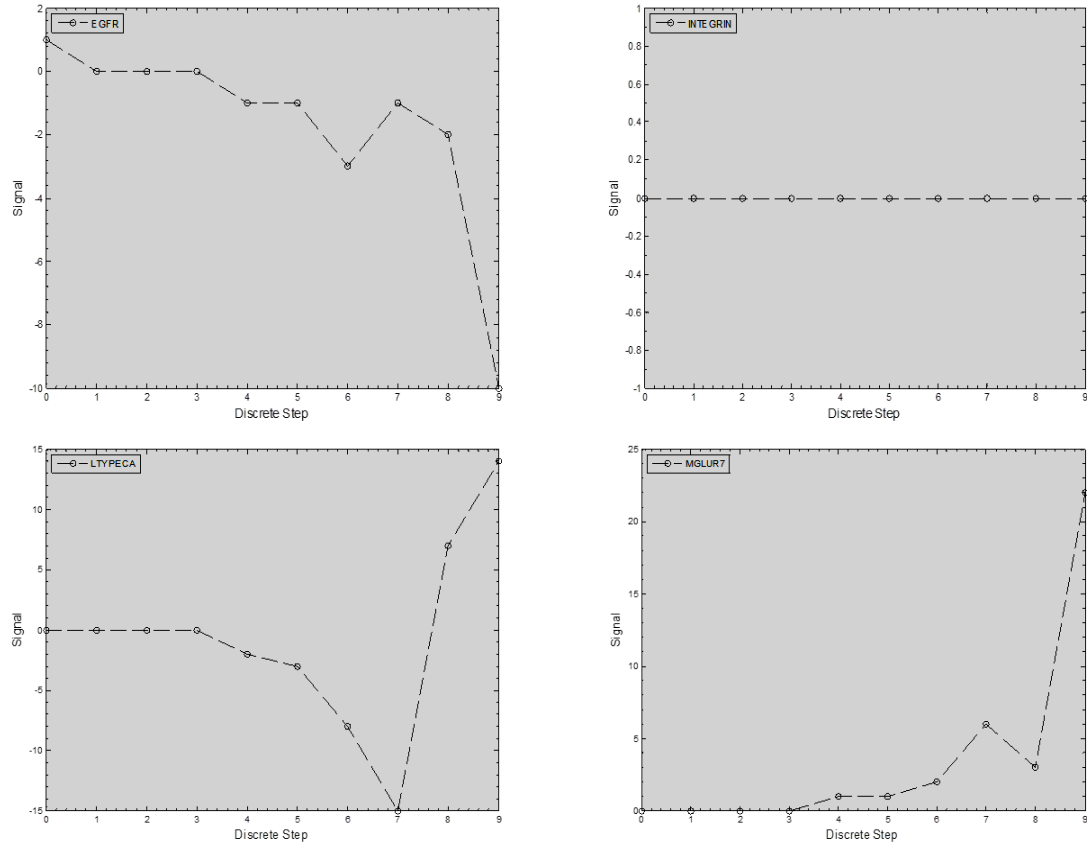


Figure 4.4: Signal through selected receptors for an interaction of A β with the EGF receptor.

Using the Signal Flow Method, a signal of 1 was initiated at the A β node and allowed to propagate through the network via Equation 4.2.1. The four selected receptors shown here are Epidermal growth factor receptor (EGFR), integrin, L-type calcium channel (LTYPECA), and the metabotropic glutamate receptor 7 (MGLUR7). A β was the initial node and interacts only with EGFR here. The curve in each graph represents the signal at each discrete step taken through the network. Ten discrete steps were simulated. Simulations were run and graphs were produced in Matlab (add in the particulars here).

A β has been frequently hypothesized to interact with the NMDA receptor[50, 51]. Support for this hypothesis was so widespread that a treatment for AD was created based on it called Memantine[52, 53]. However, Memantine, like many other drug treatments for AD, only alleviates symptoms rather than attenuating the disease progression. For this reason, however, we simulated the case of A β –NMDAR interaction (**Figure 4.5**). In the top left, NMR receives the signal of 1 initially and goes back down to 0 at subsequent steps until discrete step 3 where it receives a signal of -2. At discrete step 5 it goes back up to 0 and then after discrete step 6, feedback mechanisms begin to modulate NMR. Again, integrin is not modulated by NMR nor are there any feedback mechanisms. LTYPECA receives a signal of -4 at discrete step 4 indicating that there may be 4 paths by which LTYPECA is inhibited by NMR. Then after discrete step 6, feedback mechanisms increase the signal through LTYPECA. MGLUR7 receives the signal of 1 at discrete step 4, goes down to -1 and then from there has a sharp increase in the signal due to feedback.

In **Figure 4.6**, a signal is passed from the A β through the G-protein coupled receptor, metabotropic glutamate receptor 7 (MGLUR7). MGLUR7 has been demonstrated in some experiments to play a potential role in A β -induced signaling[54, 55]. Here the signal of 1 passes through MGLUR7 (top left graph), then the signal returns to 0 until discrete 6 where a signal of 2 passes through and then feedback mechanisms take over in subsequent steps. This suggests that there are two activating paths returning to MGLUR7 possibly through direct feedback from its own pathway. Integrin remains unaffected by MGLUR7 receptor-mediated pathways,

while LTYPECA and NMR see sharp decreases in signal after discrete step 4 and 5 and an increase at discrete step 9.

A β -NMDAR

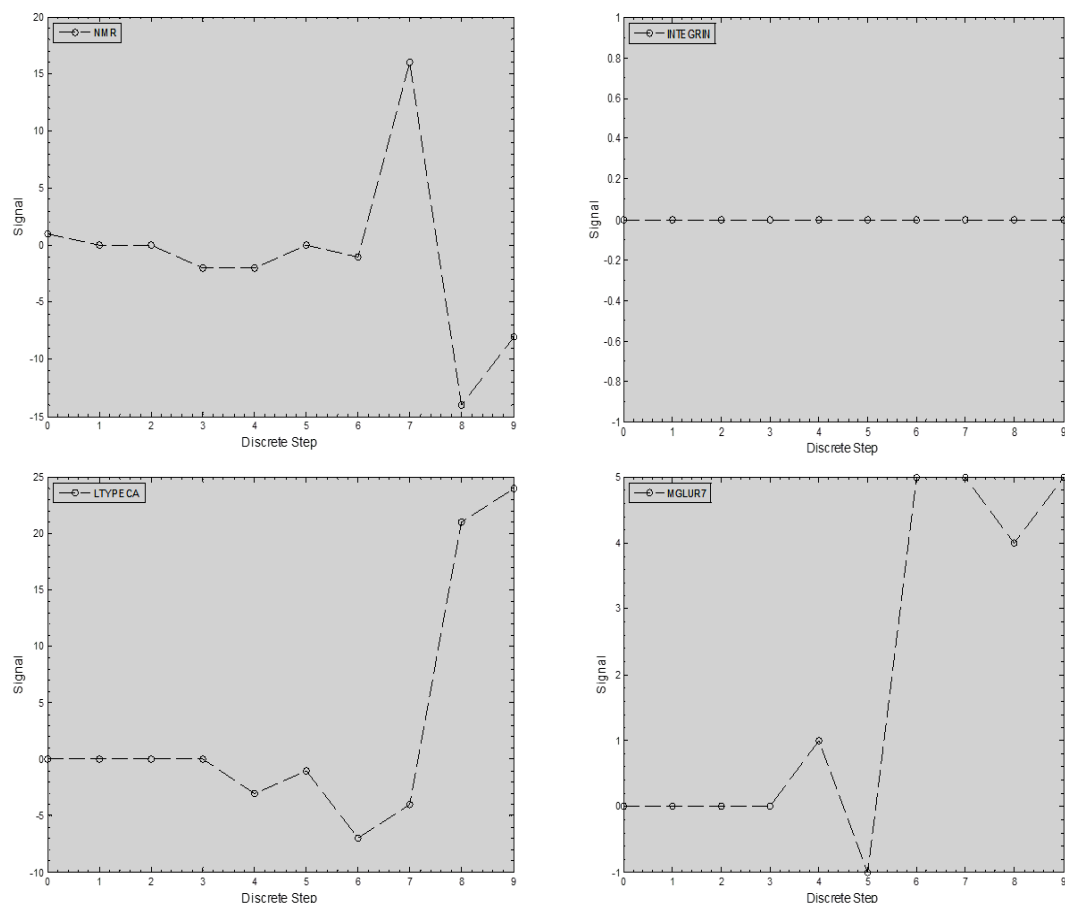


Figure 4.5: Signal through selected receptors for an interaction of A β with the NMDA receptor. Using the Signal Flow Method, a signal of 1 was initiated at the A β node and allowed to propagate through the network via Equation 4.2.1. The four selected receptors shown here are N-methyl-D-aspartate receptor (NMR), integrin, L-type calcium channel (LTYPECA), and the metabotropic glutamate receptor 7 (MGLUR7). A β was the initial node and interacts only with NMDAR here. The curve in each graph represents the signal at each discrete step taken through the network. Ten discrete steps were simulated. Simulations were run and graphs were produced in Matlab.

A β -MGLUR7

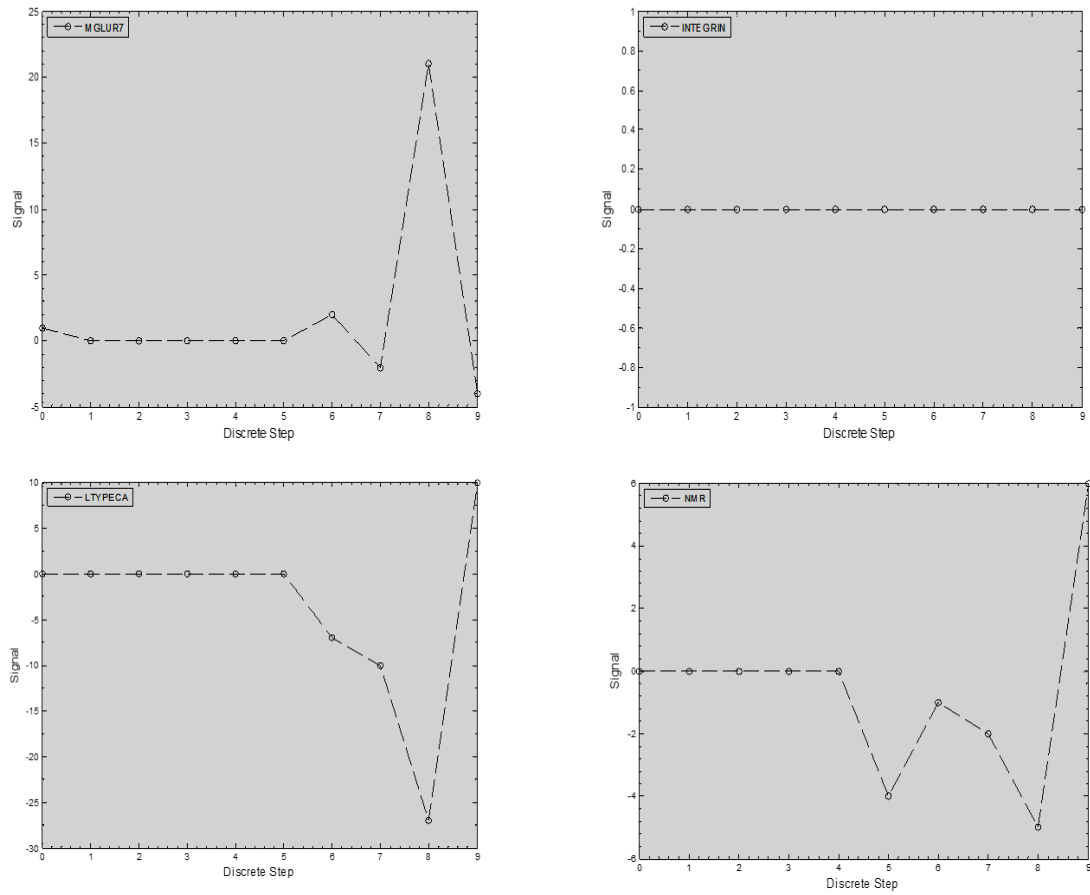


Figure 4.6: Signal through selected receptors for an interaction of A β with the MGLUR7 receptor. Using the Signal Flow Method, a signal of 1 was initiated at the A β node and allowed to propagate through the network via Equation 4.2.1. The four selected receptors shown here are Metabotropic glutamate receptor 7 (MGLUR7), integrin, L-type calcium channel (LTYPECA), and the N-methyl-D-aspartate receptor (NMR). A β was the initial node and interacts only with MGLUR7 here. The curve in each graph represents the signal at each discrete step taken through the network. Ten discrete steps were simulated. Simulations were run and graphs were produced in Matlab.

Finally in **Figure 4.7**, we have a signal passing through LTYPECA from A β . L-type calcium channels are the calcium channels that are frequently implicated in A β induced calcium dyshomeostasis[27, 46, 47]. LTYPECA received the signal and then goes back to 0 as the signal passes through other nodes in the pathway. Then, at discrete step 4 it receives an inhibiting signal of -2 and then subsequent feedback mechanisms begin to take effect. Integrin is unaffected. NMR receives a signal of -2 at discrete step three. Taken together with results from **Figure 4.5**, it would appear that NMR- and LTYPECA- mediated pathways inversely modulate each other. From there, NMR has a steady increase in the signal until discrete step 7 where there is a sharp increase and then subsequent decrease and then increase again in the last two steps. MGLUR7 receives a signal of -1 at discrete step 5 and then immediately following are the effects of feedback mechanisms.

A β -LTYPECA

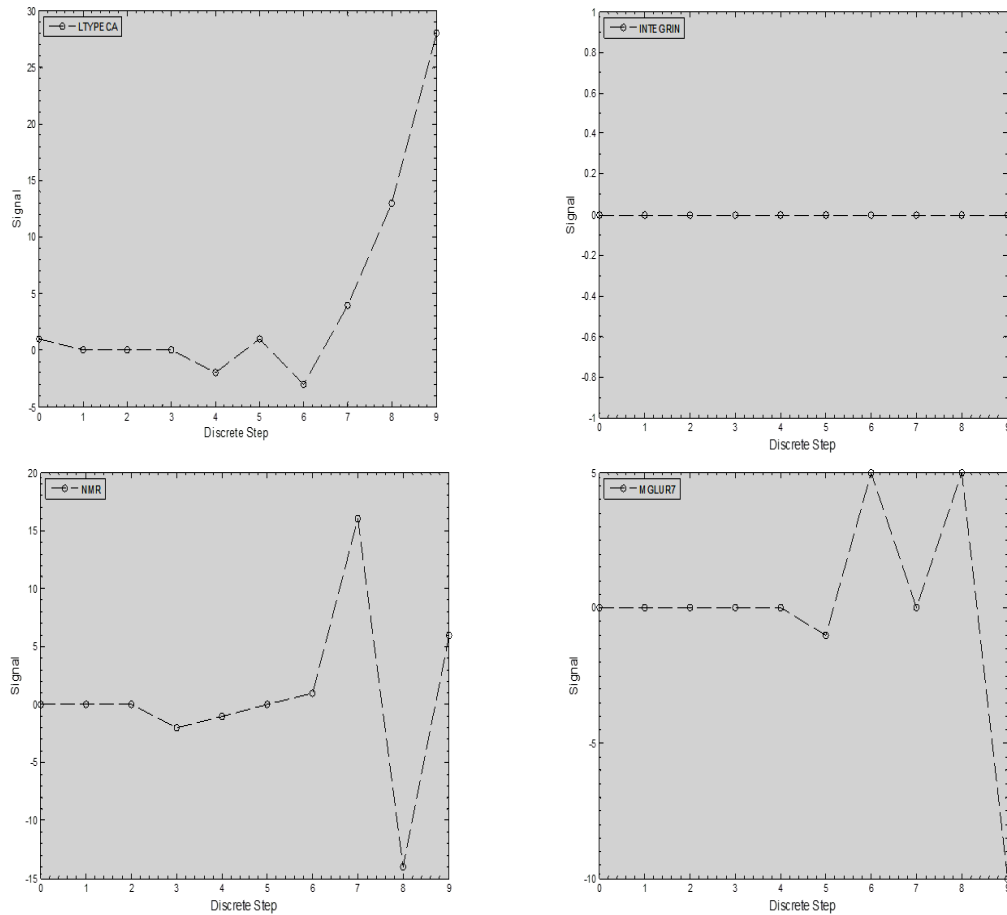


Figure 4.7: Signal through selected receptors for an interaction of A β with the LTYPECA channel. Using the Signal Flow Method, a signal of 1 was initiated at the A β node and allowed to propagate through the network via Equation 4.2.1. The four selected receptors shown here are L-type calcium channel (LTYPECA), integrin, the N-methyl-D-aspartate receptor (NMDAR) and the Metabotropic glutamate receptor 7 (MGLUR7). A β was the initial node and interacts only with the LTYPECA channel here. The curve in each graph represents the signal at each discrete step taken through the network. Ten discrete steps were simulated. Simulations were run and graphs were produced in Matlab.

In the last set of results, the presence of feedback mechanisms was observed in these simulations. Feedback loops are abundant in this network. In **Figure 4.8**, utilizing path length analysis described in **Section 4.2.2**, we show that 30% of all of the nodes in this network are involved in feedback loops that originate and end with the same node. Of that 30%, 19% of the nodes are involved in both positive and negative feedback loops, 7% in positive feedback loops only and 4% in negative feedback loops only. Seventy percent of nodes in the network are not involved in a feedback loop that originates and ends with the same node, however, some of these nodes might be intermediaries in feedback mechanisms, but the task to elucidate all of the feedback loops in the network is computationally expensive. The following table (**Table 4.1**) lists the nodes that are involved in the different feedback types (positive, negative, positive and negative). The nodes that are not involved in any feedback loops are listed in Appendix 4E. With respect to the LPH, if a node was chosen from this 30% of the network that is involved in feedback for experimental hypothesis testing, then it is likely that depending on when the measurement is taken, there could be discrepancies between measured activities. This would be especially true in the case of nodes that involved in both positive and negative feedback loops as their transient behavior may alternate between increasing and decreasing (see **Section 4.3.5**). The expected transient behavior of a node's activity, independent of other regulatory effects, when part of only positive or only negative feedback loops would be always increasing or always decreasing, respectively[56, 57]. Thus, their transient behavior would be more predictable and could be compared across times in terms of

direction of the trend (up or down) in comparison to the control. However, in terms of those nodes that are involved in both positive and negative feedback would not be as predictable unless measured with two or more time points. This is because the node may be involved in a different type of feedback mechanism (either positive or negative) depending on the path length (in effect, time). The importance of this with respect to experimental design will be discussed further in **Section 4.3.4**. Once the effects of kinetics are introduced to the system, the behavior of feedback loops becomes interesting. Positive feedback loops can introduce bistability (or switch-like behavior) into the system[58, 59], while negative feedback loops in biology are typically associated with processes that maintain homeostasis[58, 60]. The interplay between positive and negative feedback loops gives the cell a diversity response to external stimuli (bistability, switching, etc), while being able to maintain its response within the bounds of normal cellular behavior (homeostasis)[58, 60].

**Percentage of Nodes Involved in Feedback Loops in
CA1 Hippocampal Neuron
(none, positive, negative or both)**

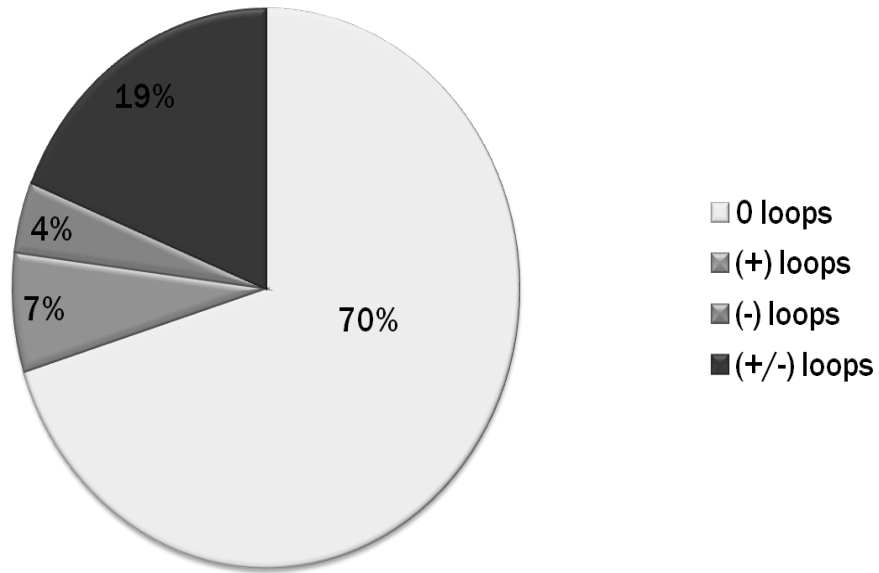


Figure 4.8: Percentage of nodes involved in feedback loops in a CA1 hippocampal neuronal network. In this pie chart, 70% of nodes in the neuronal network are not involved in feedback loops. Of the remaining 30%, 19% are involved in both positive and negative feedback loops, while 7% and 4% are involved in positive and negative feedback loops only, respectively. In this case, the feedback loops counted are only those that start and end with node i (node of interest). Feedback loops were counted using the path length analysis of **Section 4.2.2**.

Feedback Loops				
(+) loops	(-) loops	(+/-) loops		
BAX	AMPAR	AA	I1	RAS
BID	ASK1	ABL	IP3	RASGRP
CAMKI	CYTOCHROME C	AC1	IP3R	RCS
CAPRI	DOK	AC2	IRS1	RET
CASPASE9	GABA	AC5	LTYPECA	RIM
CDC42	GABABR	APAF1	MAPK	RTYPECA
CGMP	GAT1	BAD	MEK1	RYS
CJUN	ILK	BCLXL	MGLUR7	SHC
COOL	INHIBITOR2	BETA2AR	MUNC13	SHP1
CREB	MEK3	bRAF	NAIP	SNAP25
GALPHA11	P38	CALCINEURIN	NMR	SNAPIN
GALPHAQ	PROFILIN	CALCIUM	NTYPECA	SORCIN
GBETAGAMMA	RASGAP	CALMODULIN	P1433	SOS
GELSOLIN	RASGRF	CAMKII	PDE1A	SPINOPHILIN
IQGAP	RHO	CAMKIV	PDE1B	STEP
LCK	ROCK	CAMKK	PDE1C	SV2A
MGLUR1	SODIUM	CAMP	PDE2A	SYNAPSIN
NCK	SRCASM	CAMPGEFII	PDE3A	SYNAPTOTAGMIN
NO	SYNGAP	CASPASE3	PDE3B	SYNTAXIN
NOS	TIAM1	CASPASE8	PDE4D	VAV
PAK	GSK3	cGMP	PDE5A	
pGC		D1R	PDK1	
PIP5K		D2R	PI3K	
PKG		DAG	PIP2	
PTPA		DAPK	PIP3	
RAC		DARPP32	PKA	
RAL		DGK	PKB	
RALBP1		DOC2	PKC	
RALGDS		EGFR	PLA2	
RAP1		EPAC	PLCBETA	
RASGRP3		FAK	PLCGAMMA	
RIN1		FYN	PMCA	
RSK		GAB1	PP1	
SYK		GALPHA I	PP2A	
TAMALIN		GALPHAS	PQCaCh	
		GALPHA Z	PTEN	
		GRB2	RABPHILIN	
		HIPPOCALCIN	RAF1	

Table 4.1: List of nodes involved in feedback loops (positive, negative, and positive/negative) in a CA1 hippocampal signaling network.

4.3.3 Kinetic Model of Receptor Trans-activation and Feedback in a Small Hippocampal Network

Because cellular processes are ultimately dynamic, we ideally would want to model A β interactions with this CA1 hippocampal neuronal network system with kinetics. However, given the number of parameters and equations that would be required to model this system with even the most basic kinetic schema (mass action kinetics) and the unavailability of these parameters, we chose a similar system representing a subnetwork within the hippocampal neuronal signaling network. Yang and coworkers[5] performed a study on hippocampal neurons in order to deduce the pathways involved with cortisteroid-induced signaling. In this network, two of the salient network motifs that we identified in the last section are represented: receptor-transactivation (shown here by a GPCR-mediated pathway induced activation of the NMDA receptor-mediated pathway) and feedback (shown here by positive feedback between the tyrosine phosphate protein 2 (PYK2) and sarcoma (SRC)) (see **Figure 4.14**). Therefore, we were able to demonstrate with simple kinetics how the presence of these types of motifs can lead to either non-linear behavior in some of the nodes.

In **Figures 4.9-4.13**, we have graphs of predicted time-course profiles of proteins from a small hippocampal network[5]. For these simulations, we first calculated concentration versus time profiles for each protein in the network. Then, we calculated the sign change of the slope of the concentration vs. time curves. We

did this in order to identify which proteins exhibited non-linear dynamics under specific initial conditions. There are two ligands, corticosterone and $A\beta$. The corticosterone is the ligand associated with the network in[5], while we added the $A\beta$ as a ligand for the NMDAR (shown in **Figure 4.14** as NR2B/NR1) in order to test the effect of the NMDAR pathway on the rest of the network. To test the effect of corticosterone-induced signaling through a GPCR and $A\beta$ -induced signaling through NMDAR, each ligand was given the initial conditions specified in Appendix 4D. In **Figures 4.9-4.13**, each protein and its associated activated component (designated by the asterisk) represents examples of proteins which exhibited non-linear dynamics under a specific set of initial conditions designated by the colored oval. This colored oval has the same designation in **Figure 4.14**, which shows the network with each protein encircled by an oval that exhibits non-linear behavior under specified initial conditions. When simulations were run at baseline initial conditions (all concentrations at 1nM), the G-protein ($G_{i/o}/G_{i/o}^*$), phospholipase C (PLC/PLC*), sarcoma (SRC/SRC*), GTPases (Rho/Rho*), proto-oncogene, non-receptor tyrosine kinase (Abl/Abl*), and post-synaptic density 95 (PSD-95), all exhibited non-linear behavior; while protein kinase C (PKC/PKC*), protein kinase B (PKB/PKB*), and tyrosine phosphate protein 2 (Pyk2/Pyk2*) all exhibited non-linear dynamics when either corticosterone or $A\beta$ concentration was 10nM. When both $A\beta$ and corticosterone concentrations were initiated at 10nM, then the GPCR/GPCR*, NMDAR/NMDAR*, and Pyk2/Pyk2* exhibited non-linear behavior. What is seen here in this kinetic model is that when evaluating the effects of receptor trans-activation versus feedback on the dynamic behavior of individual nodes in the

pathways, we observe that feedback has more dynamic impact on the proteins not only involved in the feedback loop itself (Pyk2 \leftrightarrow SRC) but also on the adjacent proteins (Rho, Abl and PSD-95). On the other hand, the proteins in the NMDAR pathway (calcium/calmodulin dependent protein kinase II (CaMKII), serine/threonine specific protein kinase (Raf), mitogen-activated protein kinase (MEK), extracellular regulated kinase (ERK)) do not display any non-linear dynamics due to either receptor trans-activation nor feedback under any initial conditions tested.

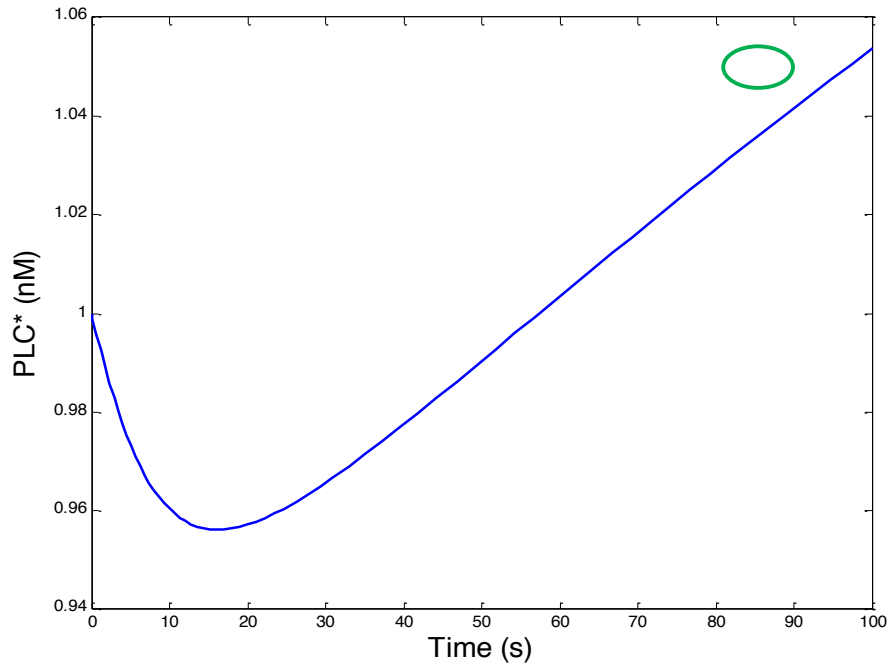
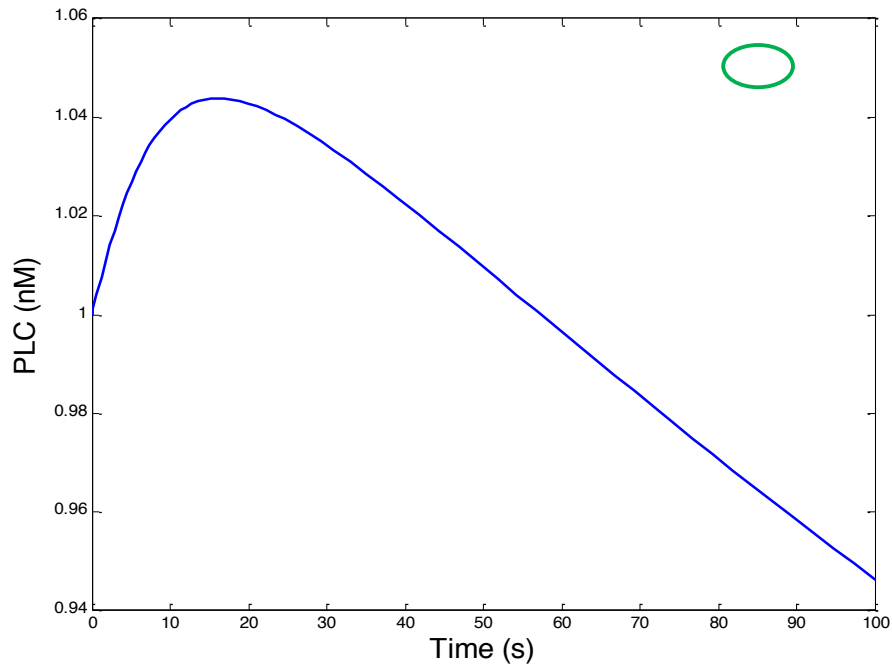


Figure 4.9: Time-course profiles of PLC and PLC* in hippocampal network from[5]. Protein concentrations (nM) in these profiles are for: PLC, PLC*, where the * represents the activated form of the protein. The simulated time is 100s. Legend shows initial concentrations of ligands and for other proteins in the network for this particular simulation.

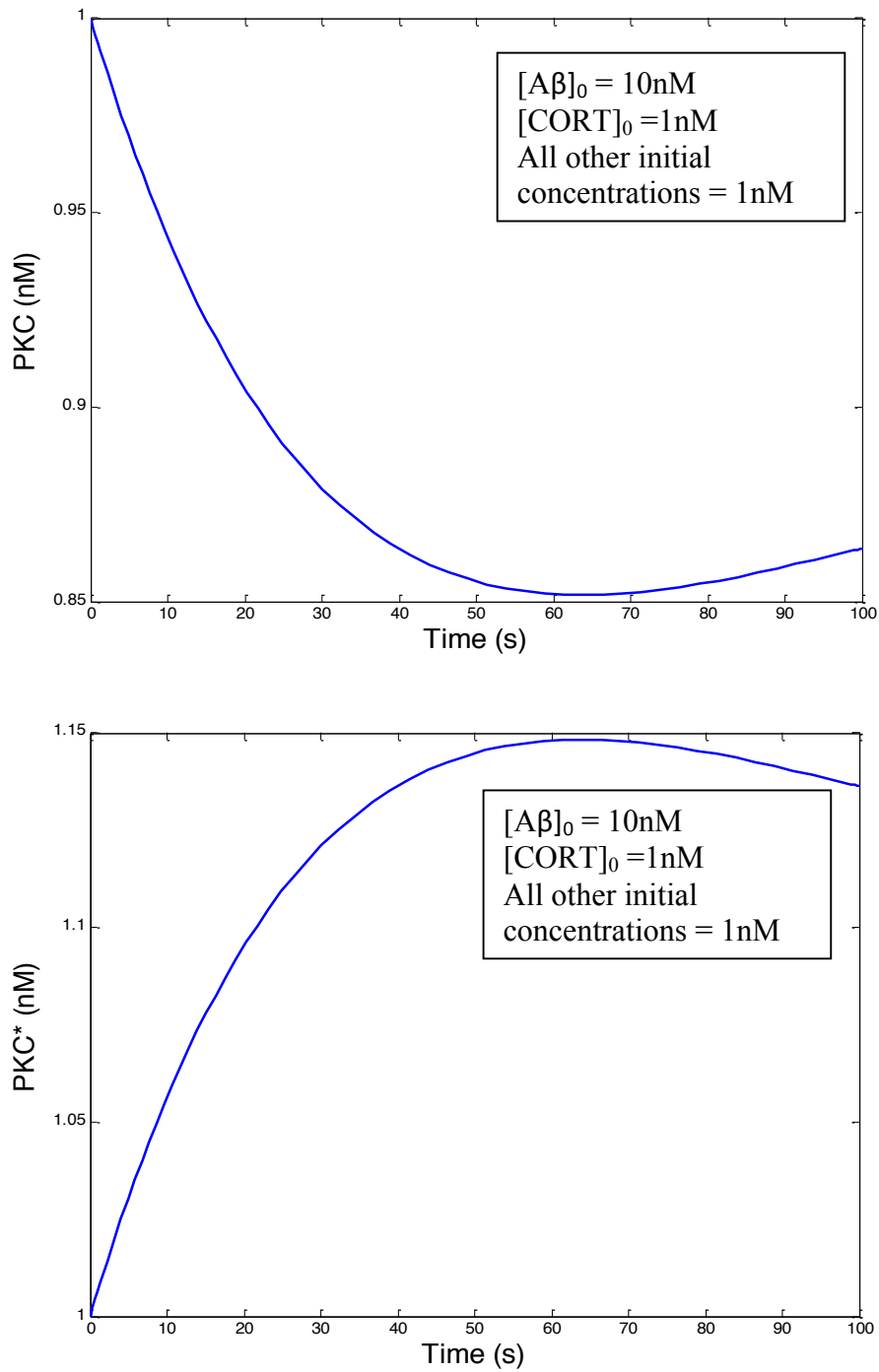


Figure 4.10: Time-course profiles of PKC and PKC* in hippocampal network from[5]. Protein concentrations (nM) in these profiles are for: PKC, PKC*, where the * represents the activated form of the protein. The simulated time is 100s. Legend shows initial concentrations of ligands and for other proteins in the network for this particular simulation.

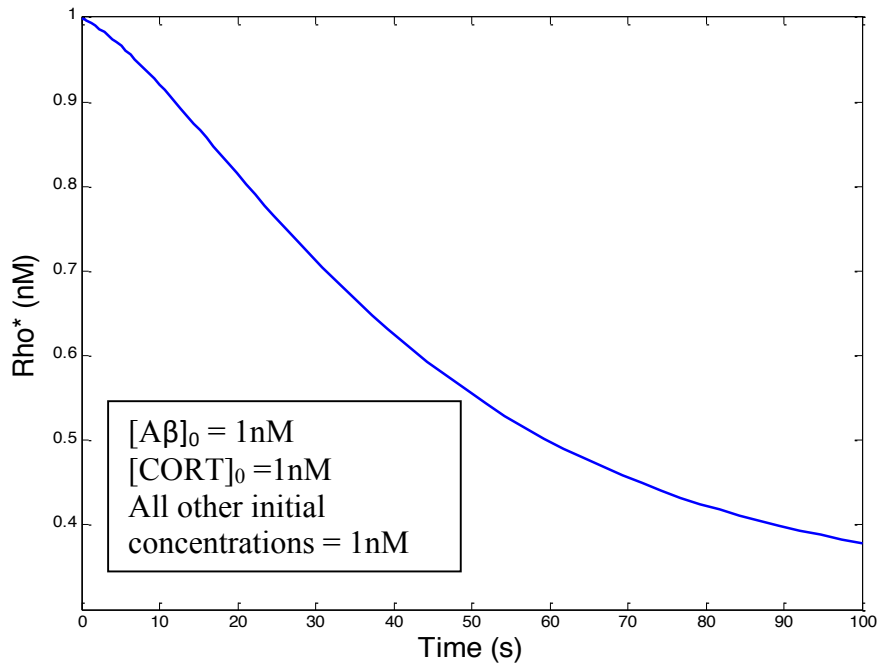
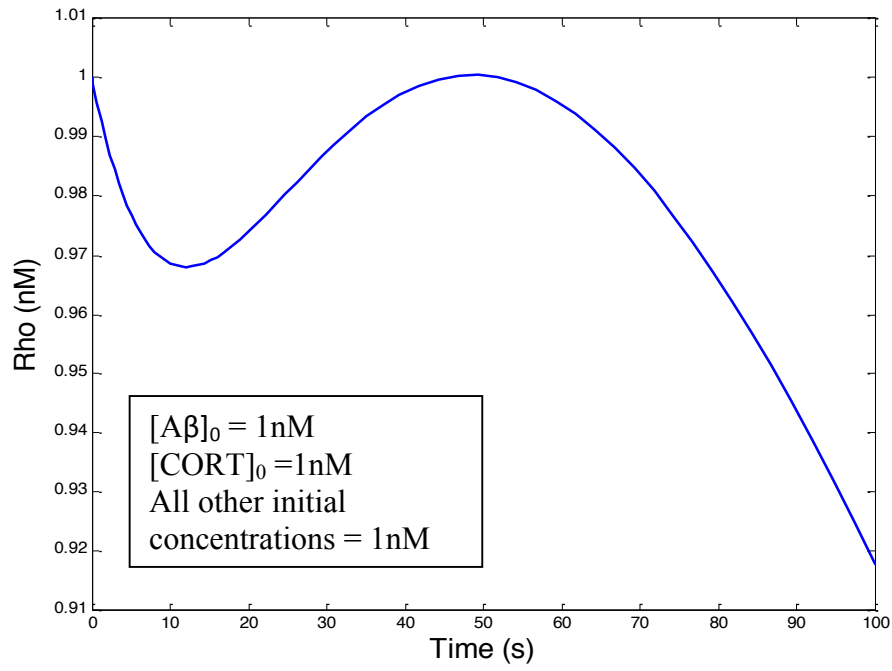


Figure 4.11: Time-course profiles of RHO and RHO* in hippocampal network from[5]. Protein concentrations (nM) in these profiles are for: RHO, RHO*, where the * represents the activated form of the protein. The simulated time is 100s. Legend shows initial concentrations of ligands and for other proteins in the network for this particular simulation.

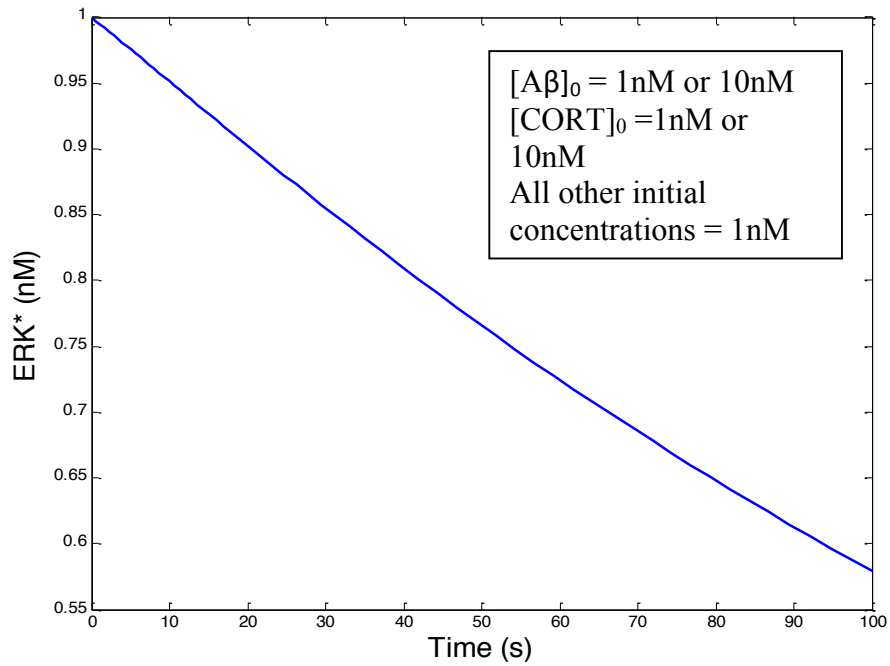
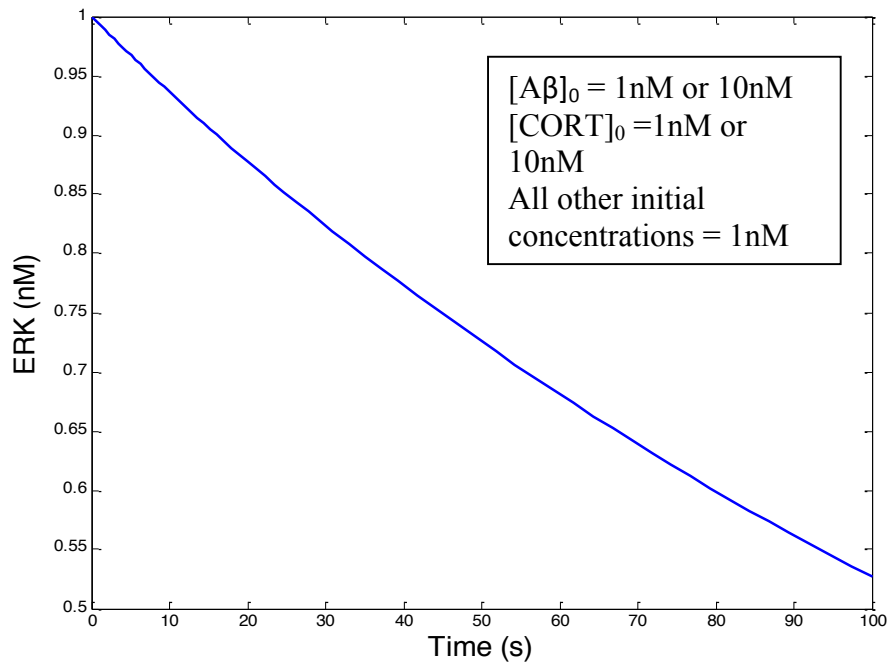


Figure 4.12: Time-course profiles of ERK and ERK* in hippocampal network from[5]. Protein concentrations (nM) in these profiles are for: ERK, ERK*, where the * represents the activated form of the protein. The simulated time is 100s. Legend shows initial concentrations of ligands and for other proteins in the network for this particular simulation.

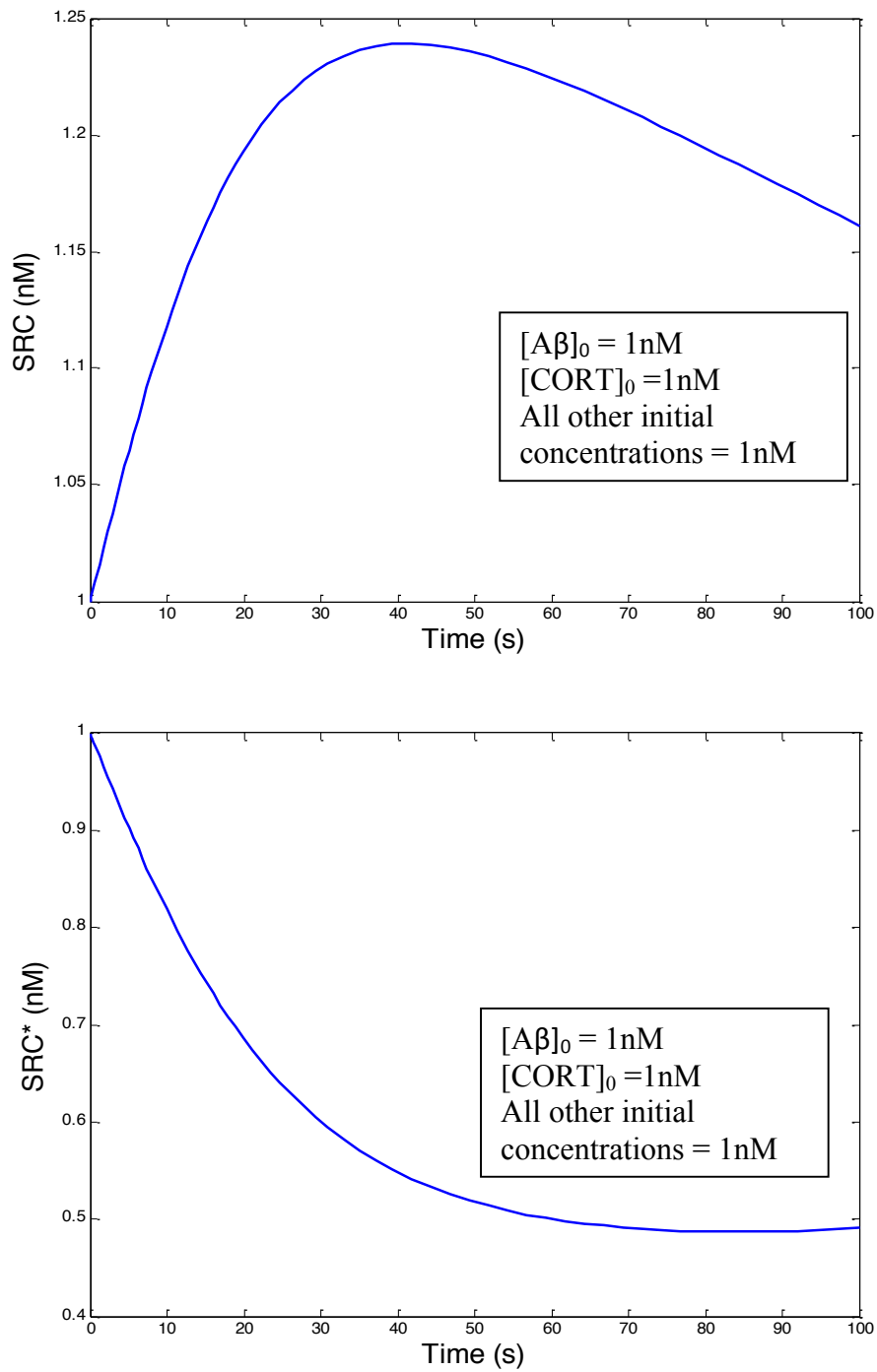


Figure 4.13: Time-course profiles of SRC and SRC* in hippocampal network from[5]. Protein concentrations (nM) in these profiles are for: SRC, and SRC*, where the * represents the activated form of the protein. The simulated time is 100s. Legend shows initial concentrations of ligands and for other proteins in the network for this particular simulation.

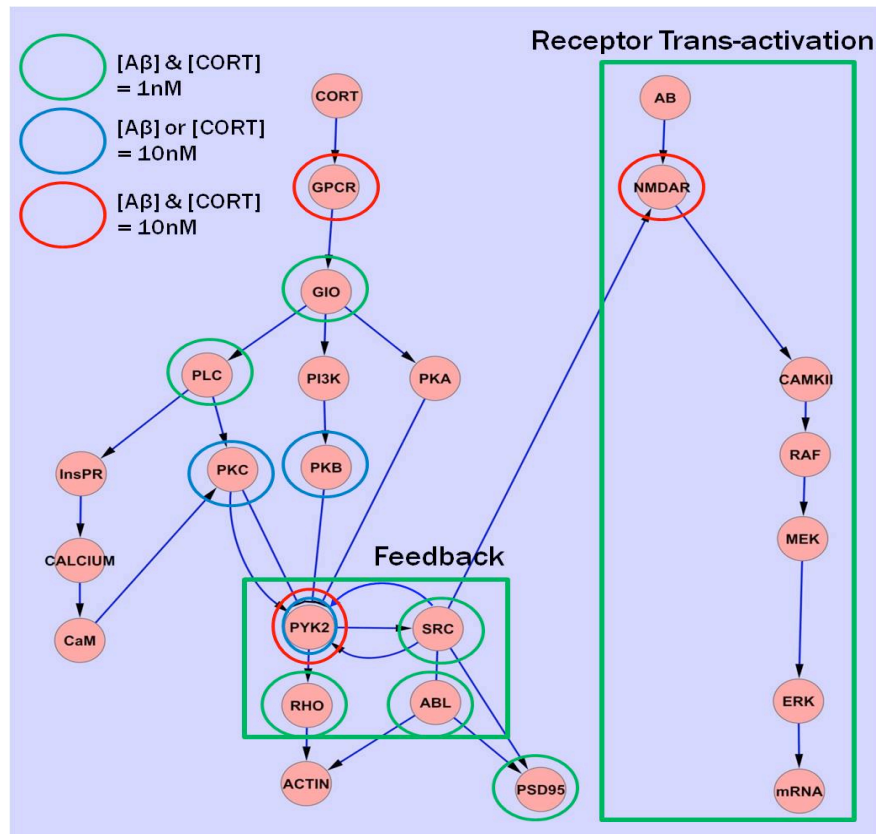


Figure 4.14: Proteins in Small Kinetic Model with sign change in derivative. The Small Kinetic Model was solved in Matlab for concentration versus time profiles. The sign change in the derivative of the ordinary differential equations used to solve for concentration over time was calculated using the `sgn` function in Matlab at each time point. Those proteins whose derivatives had a sign change at any point in time (from positive to negative or vice versa) are represented by the colored ovals in the figure. The green oval signifies that those proteins had a sign change in their derivative when all of the initial concentrations for all proteins were the baseline (1nM). The blue oval signifies proteins that had a sign change in the derivative when either A β or corticosterone initial concentrations were increased to 10nM. The red oval signifies proteins whose derivative had a sign change when both A β and corticosterone ligand initial concentrations were 10nM. Network drawing adapted from[5].

4.3.4 Experimental Rubric Based on Identified Feedback Loop in CA1 Hippocampal Network

As was mentioned in **Section 4.3.2**, 30% of the nodes in this network are involved in feedback mechanisms originating and ending with the same node. Most of these nodes are involved in what would be called “central signaling” and are likely targets for experimental design. Therefore, a guide for generating hypotheses and designing experiments should be recommended per what we know about a particular node’s involvement in specific network motifs. Ideally, such a guide would give an experimental design with the minimum set of nodes to measure along with the number of time points to do the measurements in order to perform discriminatory experiments. However, given that computational algorithms to analyze the topology of complex network graphs are computationally intractable for certain types of analysis (give some examples), we will present a simple rubric based on the path length analysis done to identify feedback loops on a per node basis in the network. The rubric in **Figure 4.15** shows four groups into which every node in this network can be categorized. Again, **Table 4.1** and Appendix 4E have a list where each node is separated into each category represented in this rubric. The idea of the rubric is to guide the experimentalist in the expected behavior of the node’s activity based on the category of feedback mechanisms in which it participates; such as no feedback, positive feedback only, negative feedback only and both positive and negative feedback. The first case would be nodes that participate in no feedback mechanisms. In this case, it would be expected that the activity of the node would either be on or off, and so a measurement at a single time point would be sufficient in an

experimental design. The next case is positive feedback, where the expected behavior would be that the activity of the node would be always increasing; at least until some other regulatory event takes place. In the case of negative feedback, the behavior would be similar to positive feedback but in the opposite direction. For these three cases, a single time point measurement may be sufficient to capture differences between the control and A β treatment. Even with positive and negative feedback loops, although the magnitude of the response may be time dependent, the overall trend would be predicted to either increase or decrease, respectively, thereby making comparisons across experimental conditions still possible. The fourth case involves those nodes where depending on the path length (k), the node might participate in either a positive or a negative feedback loop. With these nodes, it would be necessary to take measurements at more than one time point since its behavior (or activity) may change directions depending on what kind of loop it is involved in at that time. For example, at $k = 5$, PKC is involved in 5 positive feedback loops, whereas at $k = 7$ it is involved in 5 negative feedback loops. Further kinetic studies of such a network would be needed to elucidate the time scale associated with these path lengths. Nevertheless, this rubric does provide a very preliminary step toward experimental design based on an analysis of the system properties of an intracellular network in order to elucidate A β 's effects on neurons by categorizing the nodes based on their predicted time-course behavior due to feedback.

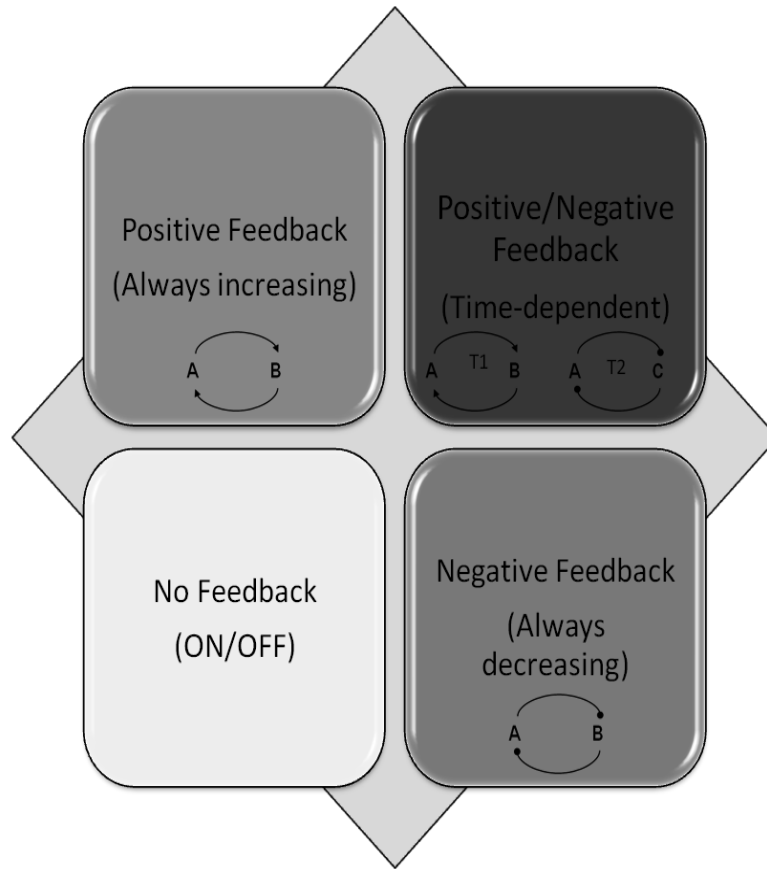


Figure 4.15: Experimental rubric based on feedback in CA1 hippocampal neuronal network. Given the path length analysis performed on this network, all of the nodes can be subdivided into these four rubric areas: nodes that are not involved in feedback at all which would represent an ON/OFF response (yellow), nodes involved in negative feedback only which would have a response that is always decreasing (green), nodes involved in positive feedback only which would have a response that is always increasing (blue) and nodes that involved in both positive and negative feedback loops whose response would be time-dependent (red). This rubric could act as general guidelines for how to measure any particular node with respect to time based on its involvement in feedback loops.

4.3.5 Network properties of Nodes from Literature-Derived Experimental Data of In Vitro Experiments with A β

We collected data from a literature survey of *in vitro* experiments done by exposing hippocampal or cortical primary culture neurons to A β exogenously for a period of no longer than 60 minutes. In Table 4.2, the nodes (or protein activity levels) that were measured in the experiments are listed along with the number of feedback loops per path length from the CA1 hippocampal neuronal network. The path lengths calculated were paths of length 3 to 10. Negative values indicate the number of negative feedback loops. Those rows that are highlighted in grey are nodes that do not participate at all in any feedback. Again, here the only feedback loops that are enumerated are those that originate and end with the same node. In general, as the path length increases, so does the number of feedback loops. Many of the nodes tend to go back and forth in their involvement in negative versus positive feedback loops. As was discussed in the last section on the experimental rubric, these types of nodes would likely need to be measured over time as their behavior will be time-dependent. This might be an indication of why the literature data lack consensus. Since there is no standard time when each experimental laboratory measures A β -induced signaling, for these nodes that are involved in both negative and positive feedback loops, the data could be inconsistent.

In **Table 4.3**, is the same list of measured nodes, but listed along with the number of in-, out- and total degrees. In-degrees are the incoming edges, whereas out-degrees are the outgoing edges into and out of a particular node. The total degree would then be the sum of the in- and out-degrees. This table is ranked by the in-degrees because in-degree is most likely indicative of number of pathways that the node is part of. The cAMP response element-binding (CREB) has the most incoming edges at 14, while brain neurotrophic factor (BDNF), calpain, and Fas ligand (FASL) has no incoming edges. The large number of incoming edges that CREB has would indicate that CREB is involved in many pathways and may be modulated by a variety of inputs. Therefore, the Linear Pathway Hypothesis would not be adequate enough to describe CREB's activity under experimental conditions. Alterations in any number of pathways could give rise to an increase or decrease in CREB activity. As is evident from **Tables 4.1-4.3**, most of the nodes in these experiments are not involved in a simple linear pathway from some receptor and thus such an assumption could lead to poor interpretation of experimental results, poor experimental reproducibility, or the inability to discriminate between experimental results (non-consensus).

Measured nodes in experiments	Number of Feedback Loops of Path Length k							
	k = 3	k = 4	k = 5	k = 6	k = 7	k = 8	k = 9	k = 10
AA	1	0	0	2	-2	11	-7	-19
BDNF	0	0	0	0	0	0	0	0
BETACATENIN	0	0	0	0	0	0	0	0
CALCIUM	-1	-1	6	-7	0	-25	5	73
CALPAIN	0	0	0	0	0	0	0	0
CASPASE3	2	1	1	4	5	20	28	-12
CASPASE7	0	0	0	0	0	0	0	0
CJUN	1	0	0	1	0	0	1	0
CREB	1	0	0	1	0	0	1	0
FASL	0	0	0	0	0	0	0	0
FYN	0	0	0	1	3	2	1	-11
GSK3	0	0	-1	-2	0	-8	-13	-39
JNK	0	0	0	0	0	0	0	0
MAPK	0	0	0	1	-2	6	0	-8
P53	0	0	0	0	0	0	0	0
PAK	2	2	0	4	8	4	7	29
PIP2	1	2	2	3	13	20	36	-10
PKB	0	-1	0	-3	0	2	-18	-16
PKC	1	-2	5	-7	-5	10	-43	14
PKR	0	0	0	0	0	0	0	0
RAC	1	1	0	2	4	2	3	11
STEP	0	0	0	0	-2	2	2	7
TAU	0	0	0	0	0	0	0	0
TRKA	0	0	0	0	0	0	0	0

Table 4.2: Number of feedback loops per path length of nodes measured in literature-derived experiments. In this table, these nodes were measured in the experiments listed in the references. For each node, the number of feedback loops of path length k of which it is involved in the network is listed. Negative signs represent the number of negative feedback loops because this network is signed. The nodes highlighted in grey are those that are not involved in feedback loops at all. The number of path lengths (k) shown here are 10. Path analysis was performed according to **Section 4.2.2** and simulated in Matlab.

Measured nodes in experiments	In-degree	Out-degree	Total
CREB	14	5	19
TAU	10	0	9
CALCIUM	8	19	27
BETACATENIN	7	2	9
PKB	7	6	13
FYN	6	6	12
PKC	6	36	42
CASPASE3	5	14	19
CJUN	5	2	7
GSK3	5	9	14
JNK	5	4	9
MAPK	5	15	20
CASPASE7	4	3	7
P53	4	0	4
PIP2	4	15	19
PAK	3	6	9
RAC	2	8	10
AA	1	1	2
PKR	1	3	4
STEP	1	2	3
TRKA	1	7	8
BDNF	0	1	1
CALPAIN	0	6	6
FASL	0	1	1

Table 4.3: Number of in-, out-, and total degrees for nodes measured in literature-derived experiments. In this table, the number of incoming edges (in-degree), outgoing edges (out-degree) and total degree is listed per node measured in literature-derived experiments. This list is ranked from most incoming edges to least with the cAMP response binding factor (CREB) having the greatest number of incoming edges (14) and brain-derived neurotrophic factor (BDNF), CALPAIN and Fas ligand (FASL) having the least (0). In-, out- and total degree were counted in Cytoscape[4].

4.4 Conclusions

In our present work, we present a variety of reasons to begin formulating new hypotheses for A β 's interactions with neurons based on the complex, interconnected, non-linear behavior of a real intracellular network. Based on our study, we demonstrated using network topological measures and features, as well as network motifs, that a CA1 hippocampal neuronal signaling network is not comprised of a series of non-interacting pathways, but rather comprised of hub proteins, receptor trans-activated or inhibited pathways, cross-talk and many feedback mechanisms, among other types of signal motifs. We also demonstrated that nodes that participate and are adjacent to feedback mechanisms can exhibit non-linear dynamic behavior, whereas nodes in a direct pathway from a receptor trans-activated pathway do not necessarily display non-linear behavior. From this conclusion, we recommend an experimental rubric based on feedback mechanisms and show that over half of the nodes measured in current literature-derived data (**Table 4.2**) participate in a feedback loop of some type; and that this may provide some indication as to inconsistencies in experimental results coming from different laboratories. By taking into account the context of interactions in which a particular node of interest participates, experiments can be designed that are more consistent with the underlying behavior of the system.

4.5 Future Work

In this work, we were able to identify the behavior of network motifs that are not consistent with a Linear Pathway Hypothesis. After testing some of the dynamic properties of two types of motifs that are abundant in this CA1 hippocampal neuronal network, we found that feedback mechanisms have a greater impact on the non-linear dynamic behavior of individual proteins over receptor trans-activation. From this analysis, we proposed an experimental rubric based on feedback mechanisms that would allow the experimentalist to determine how to make measurements on a particular protein based on what type of feedback mechanism in which it participates. For future work, we propose another method for experimental design based on hub proteins. According to Barabasi and Oltvat[7], real networks are very robust to random removal of nodes; however, when only a few hub nodes are removed, the network breaks down into isolated small clusters. This suggests that hub proteins are integral to network function (structure => function paradigm of biology) and that their high interconnectedness suggests that they are most often responding to extracellular cues. Thus, another experimental design could involve measuring input-hub response trends, which would consist of monitoring the behavior over time of hub proteins given a certain cue, under normal conditions and in the presence of A β .

A hub protein could be defined as a highly connected protein in the network. Referring back to **Figure 4.1**, where we are given a power law distribution of the interactions in this network, a hub protein would be one of the proteins represented in the tail of the distribution. The hub proteins for this network were listed in **Section**

4.3.1. Using our Signal Flow Method, we show some input-hub response behavior in **Figures 4.16-4.23**. The most highly connected hub protein in the network, PKA (47 total interactions), is shown in **Figure 4.16**. Four different inputs are activated and signal propagation through PKA is observed. The A β -LTYPECA (Ca²⁺ pathway) input propagates a signal through PKA at the earliest step (discrete step 2) in comparison to the other inputs. A β -MGLUR7 (GPCR pathway) propagates a signal to PKA at discrete step 4, while A β -EGFR (Receptor tyrosine kinase pathway) and A β -Integrin (Integrin pathway) receive the signal after discrete step 5 and then the signal appears to enter into a feedback mechanism. What is demonstrated here is that even utilizing the Signal Flow Method to analyze the movement of a signal through this network, it is evident that monitoring an input-hub response could yield potentially discriminating trends depending upon the input.

In order to further demonstrate this idea, we used the Signal Flow Method with the same inputs as was used for PKA on other hub proteins: PKC, G $\beta\gamma$, Calmodulin, NMDAR/NMR, SRC, and CREB (**Figures 4.16-4.23**). We chose these particular hubs because they have been measured previously in *in vitro* experiments with A β [48]. Again, there are clear differences in the trends of signal propagation through a particular hub node based on the input. In almost all of the cases, the A β -LTYPECA has the earliest propagation of the initial signal (usually before step 4). All of the other inputs tend to vary in how early the signal is propagated to the hub node. By the end of the simulation, all of the hub nodes shown in **Figures 4.16-4.23** begin to enter into feedback mechanisms. This is relevant to the experimental rubric

proposed in **Figure 4.15** in that at longer time scale it may be that these two experimental designs could be combined such that the input-hub response is measured according to what type of feedback mechanisms in which it is expected to participate (none, positive, negative, positive/negative).

PKA

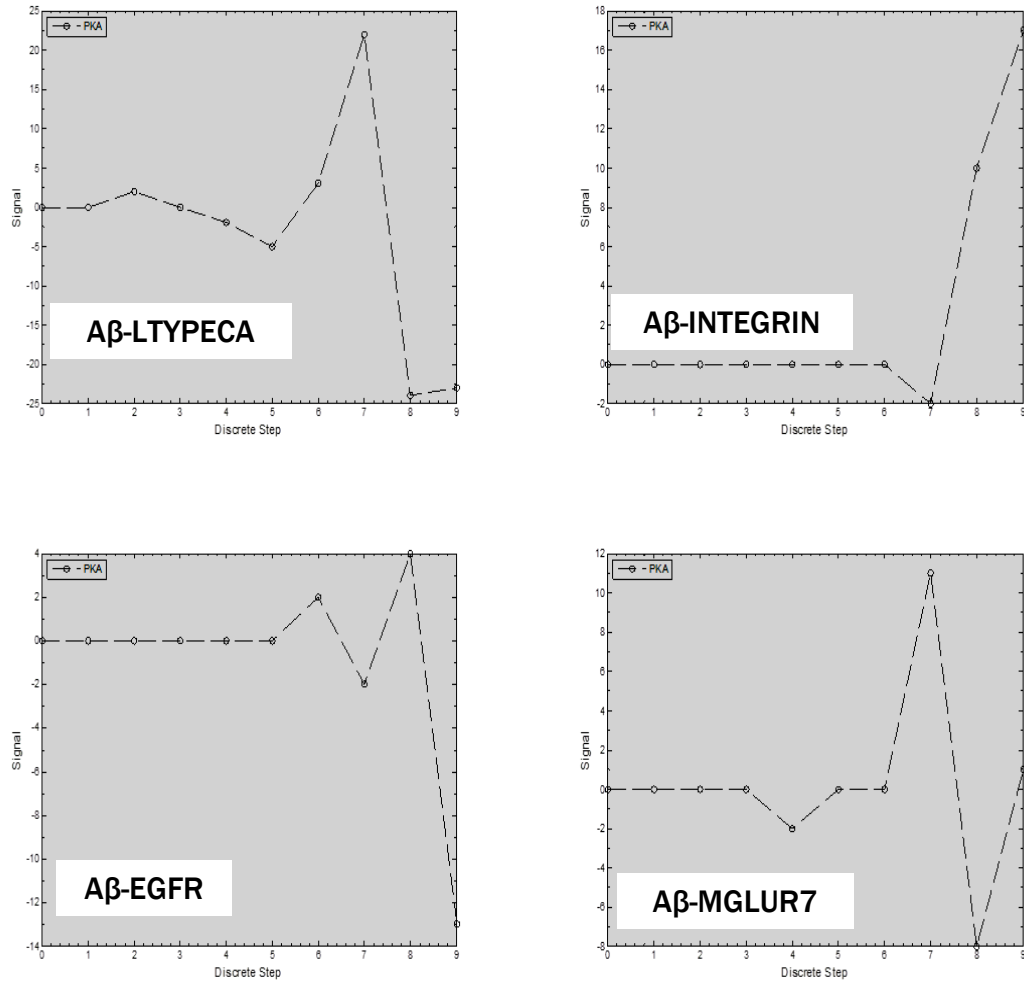


Figure 4.16: Signal through hub protein, Protein kinase A (PKA) given different inputs. The Signal Flow Method (section 4.2.1) was used to follow signal propagation through PKA starting from different inputs (Aβ-LTYPECA, Aβ-Integrin, Aβ-EGFR, and Aβ-MGLUR7). Aβ was the initial node and a signal of 1 is passed through this node at the first discrete step. The curve in each graph represents the signal at each discrete step taken through the network. Ten discrete steps were simulated. Simulations were run and graphs were produced in Matlab.

PKC

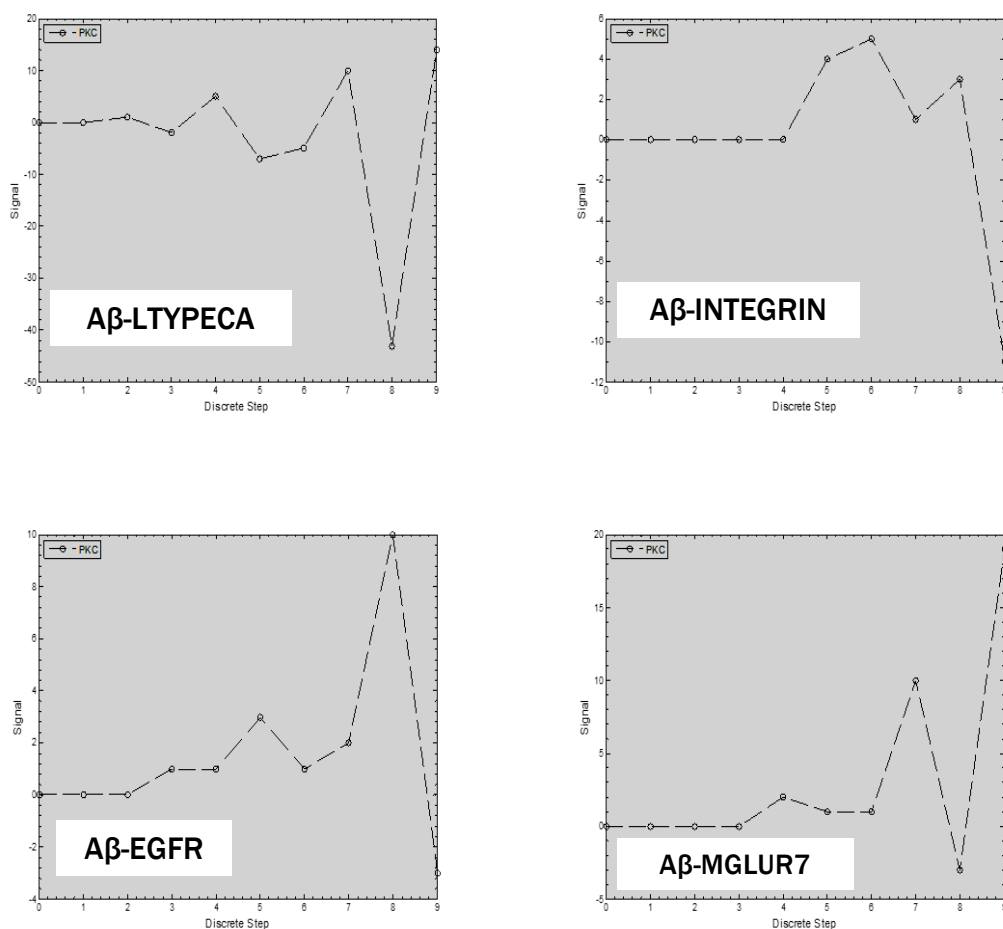


Figure 4.17: Signal through hub protein, Protein kinase C (PKC) given different inputs.

The Signal Flow Method (section 4.2.1) was used to follow signal propagation through PKC starting from different inputs (Aβ-LTYPECA, Aβ-Integrin, Aβ-EGFR, and Aβ-MGLUR7). Aβ was the initial node and a signal of 1 is passed through this node at the first discrete step. The curve in each graph represents the signal at each discrete step taken through the network. Ten discrete steps were simulated. Simulations were run and graphs were produced in Matlab.

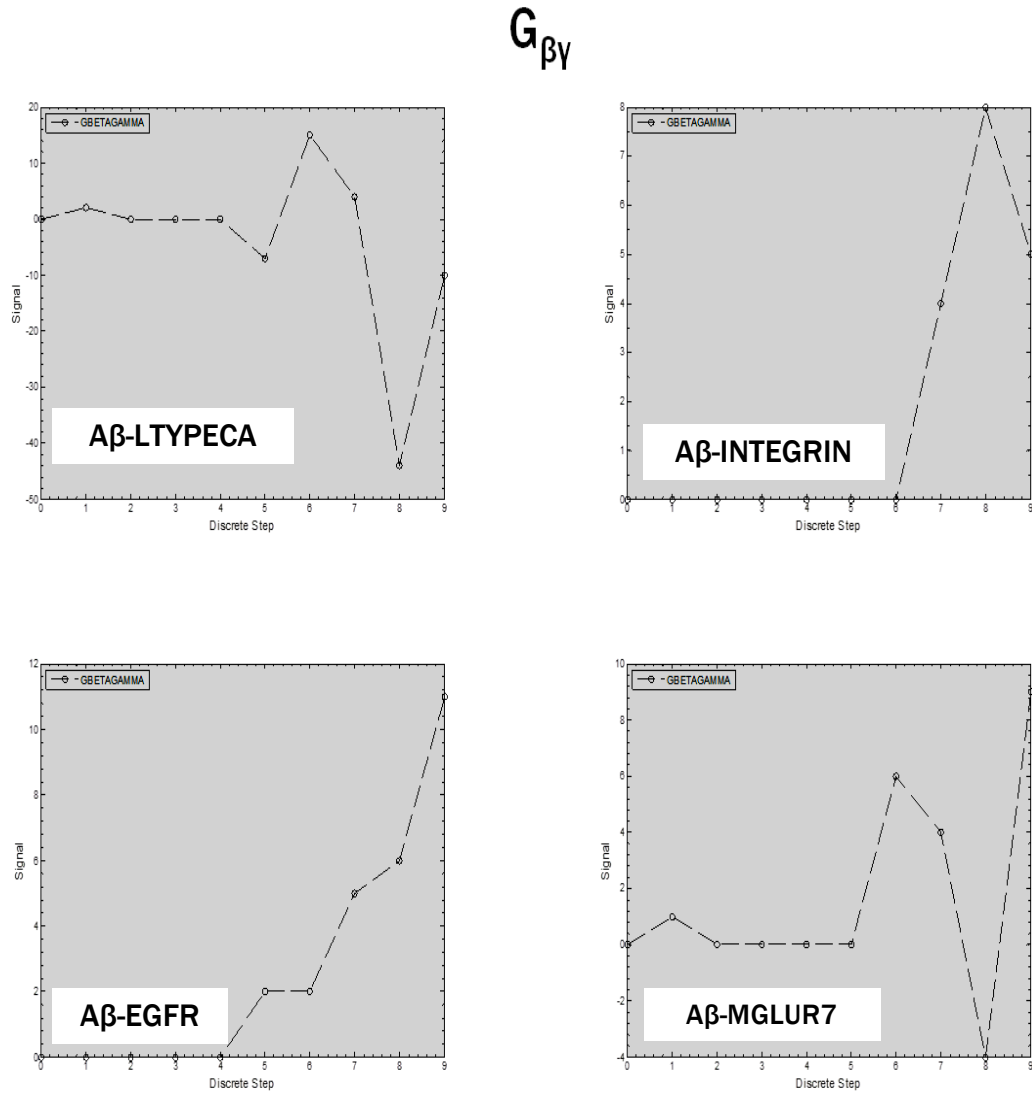


Figure 4.18: Signal through hub protein, G protein $\beta\gamma$ ($G_{\beta\gamma}$) given different inputs. The Signal Flow Method (section 4.2.1) was used to follow signal propagation through $G_{\beta\gamma}$ starting from different inputs (A β -LTYPECA, A β -Integrin, A β -EGFR, and A β -MGLUR7). A β was the initial node and a signal of 1 is passed through this node at the first discrete step. The curve in each graph represents the signal at each discrete step taken through the network. Ten discrete steps were simulated. Simulations were run and graphs were produced in Matlab.

Calmodulin

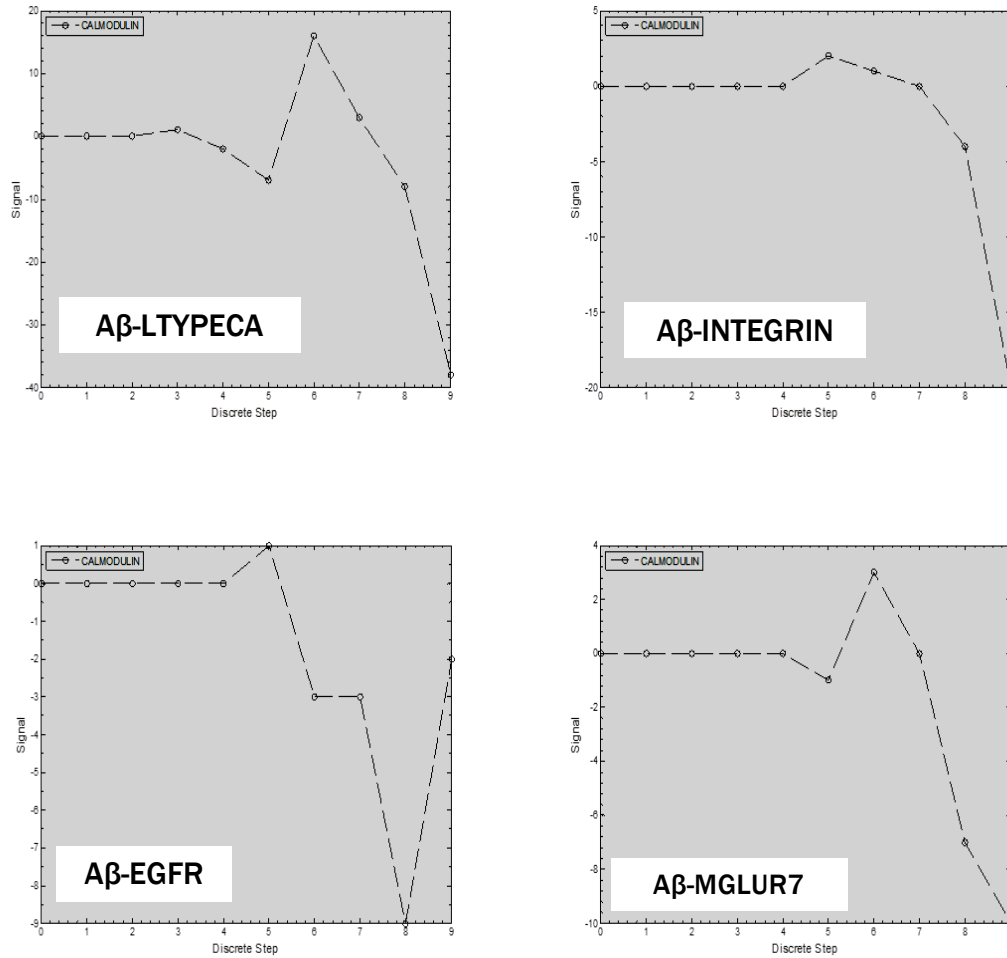


Figure 4.19: Signal through hub protein, Calmodulin, given different inputs. The Signal Flow Method (section 4.2.1) was used to follow signal propagation through Calmodulin starting from different inputs (Aβ-LTYPECA, Aβ-Integrin, Aβ-EGFR, and Aβ-MGLUR7). Aβ was the initial node and a signal of 1 is passed through this node at the first discrete step. The curve in each graph represents the signal at each discrete step taken through the network. Ten discrete steps were simulated. Simulations were run and graphs were produced in Matlab.

NMDAR

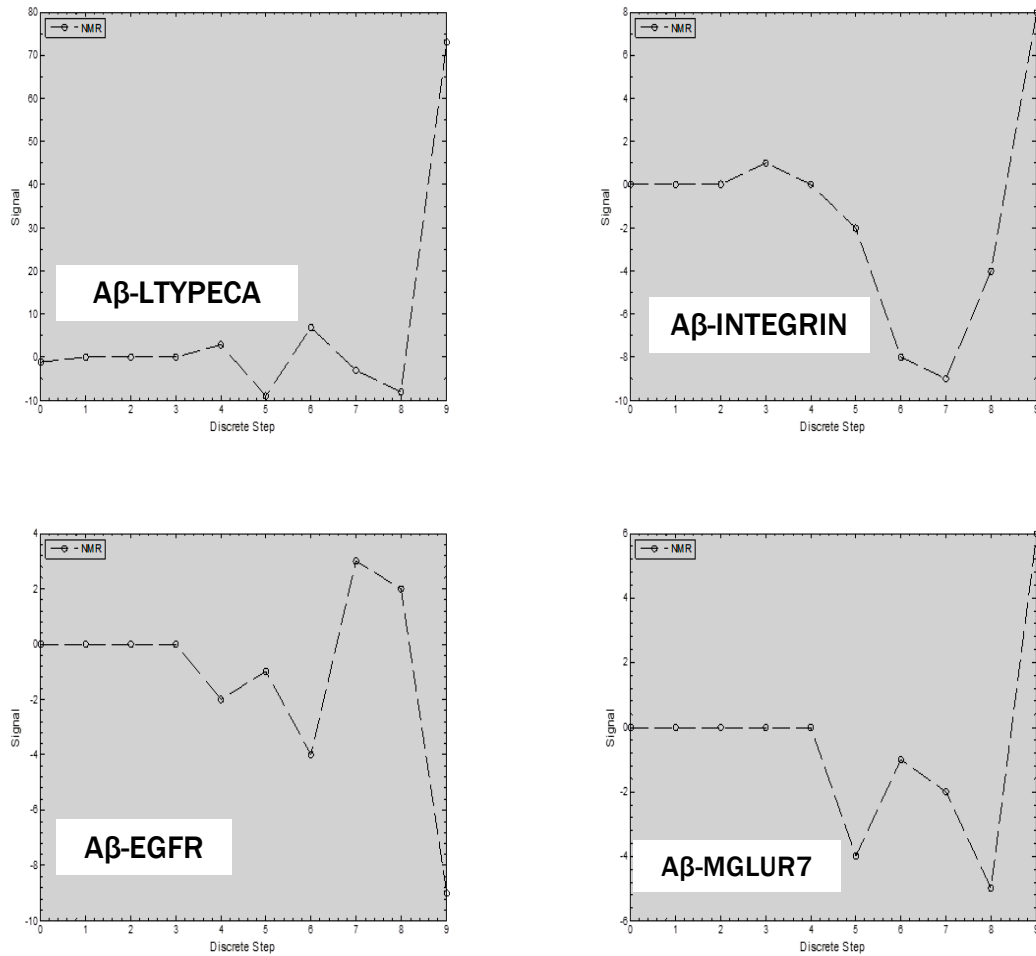


Figure 4.20: Signal through hub protein, N-methyl-D-aspartate receptor (NMDAR), given different inputs. The Signal Flow Method (section 4.2.1) was used to follow signal propagation through NMDAR starting from different inputs (Aβ-LTYPECA, Aβ-Integrin, Aβ-EGFR, and Aβ-MGLUR7). Aβ was the initial node and a signal of 1 is passed through this node at the first discrete step. The curve in each graph represents the signal at each discrete step taken through the network. Ten discrete steps were simulated. Simulations were run and graphs were produced in Matlab.

SRC

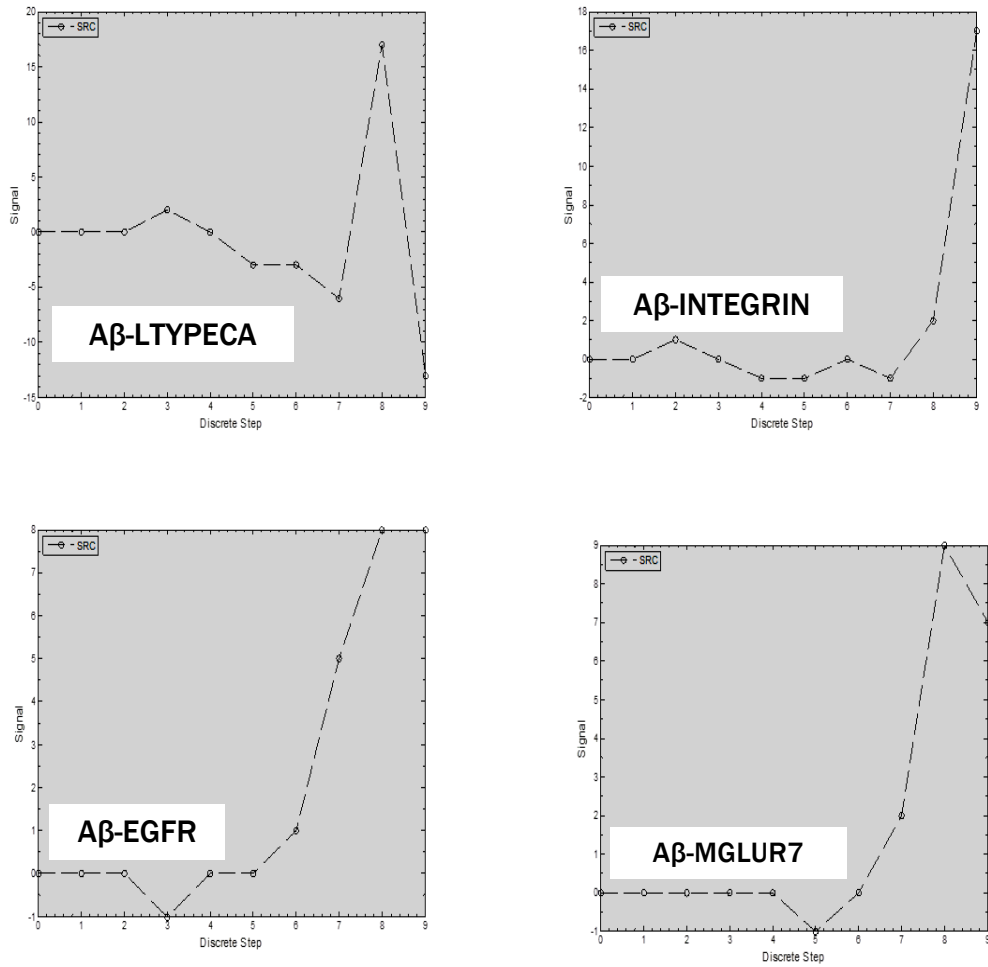


Figure 4.21: Signal through hub protein, proto-oncogene tyrosine-protein kinase (SRC) given different inputs. The Signal Flow Method (section 4.2.1) was used to follow signal propagation through SRC starting from different inputs (Aβ-LTYPECA, Aβ-Integrin, Aβ-EGFR, and Aβ-MGLUR7). Aβ was the initial node and a signal of 1 is passed through this node at the first discrete step. The curve in each graph represents the signal at each discrete step taken through the network. Ten discrete steps were simulated. Simulations were run and graphs were produced in Matlab.

CREB

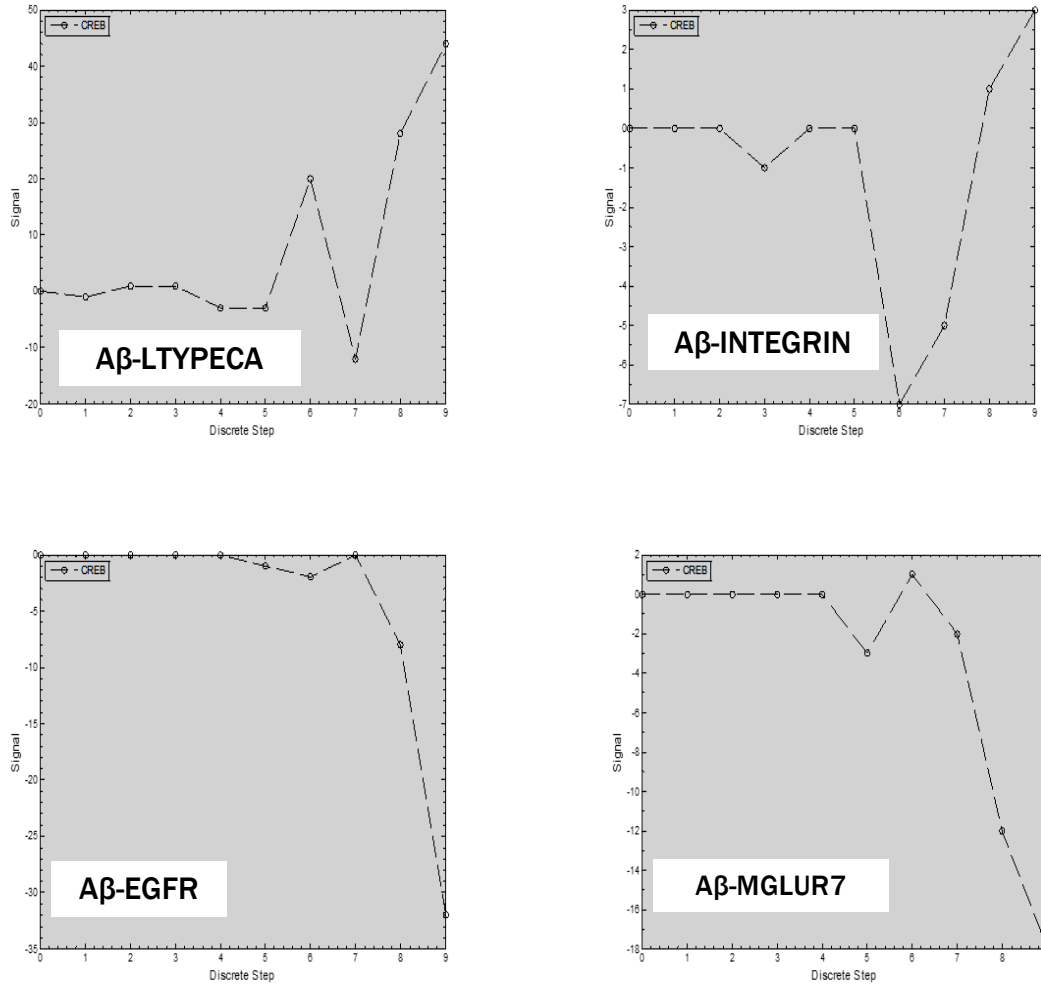


Figure 4.22: Signal through hub protein, cyclic adenosine monophosphate response element-binding (CREB) protein, given different inputs. The Signal Flow Method (section 4.2.1) was used to follow signal propagation through CREB starting from different inputs (Aβ-LTYPECA, Aβ-Integrin, Aβ-EGFR, and Aβ-MGLUR7). Aβ was the initial node and a signal of 1 is passed through this node at the first discrete step. The curve in each graph represents the signal at each discrete step taken through the network. Ten discrete steps were simulated. Simulations were run and graphs were produced in Matlab.

4.6 References

1. Demuro A, Parker I, Stutzmann G. Calcium Signaling and Amyloid Toxicity in Alzheimer Disease. *Journal of Biological Chemistry*. 2010;285(17):12463-8. doi: DOI 10.1074/jbc.R109.080895. PubMed PMID: ISI:000276787800001.
2. Kawahara M, Arispe N, Kuroda Y, Rojas E. Alzheimer's disease amyloid beta-protein forms Zn(2+)-sensitive, cation-selective channels across excised membrane patches from hypothalamic neurons. *Biophys J*. 1997;73(1):67-75. doi: S0006-3495(97)78048-2 [pii]
10.1016/S0006-3495(97)78048-2. PubMed PMID: 9199772; PubMed Central PMCID: PMCPMC1180909.
3. Arispe N, Pollard HB, Rojas E. beta-Amyloid Ca(2+)-channel hypothesis for neuronal death in Alzheimer disease. *Mol Cell Biochem*. 1994;140(2):119-25. PubMed PMID: 7898484.
4. Lopes C, Franz M, Kazi F, Donaldson S, Morris Q, Bader G. Cytoscape Web: an interactive web-based network browser. *Bioinformatics*. 2010;26(18):2347-8. doi: 10.1093/bioinformatics/btq430. PubMed PMID: WOS:000281714100059.
5. Yang S, Roselli F, Patchev A, Yu S, Almeida O. Non-receptor-tyrosine Kinases Integrate Fast Glucocorticoid Signaling in Hippocampal Neurons. *Journal of Biological Chemistry*. 2013;288(33):23725-39. doi: 10.1074/jbc.M113.470146. PubMed PMID: WOS:000330611400013.

6. Mullane K, Williams M. Alzheimer's therapeutics: Continued clinical failures question the validity of the amyloid hypothesis-but what lies beyond? *Biochemical Pharmacology*. 2013;85:289-305.
7. Barabasi A, Oltvai Z. Network biology: Understanding the cell's functional organization. *Nature Reviews Genetics*. 2004;5(2):101-U15. doi: 10.1038/nrg1272. PubMed PMID: WOS:000188602400012.
8. Albert R. Scale-free networks in cell biology. *Journal of Cell Science*. 2005;118:4947-56.
9. Van Regenmortel MHV. Reductionism and complexity in molecular biology. *EMBO Reports*. 2004;5(11):1016-20.
10. Albert R, Barabasi A. Statistical mechanics of complex networks. *Reviews of Modern Physics*. 2002;74(1):47-97. doi: 10.1103/RevModPhys.74.47. PubMed PMID: WOS:000174548700003.
11. Saez-Rodriguez J, Alexopoulos L, Epperlein J, Samaga R, Lauffenburger D, Klamt S, et al. Discrete logic modelling as a means to link protein signalling networks with functional analysis of mammalian signal transduction. *Molecular Systems Biology*. 2009;5. doi: 10.1038/msb.2009.87. PubMed PMID: WOS:000273359200002.
12. Margolin AA, Nemenman I, Basso K, Wiggins C, Stolovitzky G, Dalla Favera R, et al. ARACNE: an algorithm for the reconstruction of gene regulatory networks in a mammalian cellular context. *BMC Bioinformatics*. 2006;7 Suppl 1:S7. doi: 10.1186/1471-2105-7-S1-S7. PubMed PMID: 16723010; PubMed Central PMCID: PMC1810318.

13. Liang S, Fuhuman S, Somogyi R, editors. REVEAL, A General Reverse Engineering Algorithm For Inference of Genetic Network Architectures. Pacific Symposium on Biocomputing; 1998; Hawaii.
14. Jeong H, Neda Z, Barabasi A. Measuring preferential attachment in evolving networks. *Europhysics Letters*. 2003;61(4):567-72. doi: 10.1209/epl/i2003-00166-9. PubMed PMID: WOS:000180859600020.
15. Barabasi A, Albert R. Emergence of scaling in random networks. *Science*. 1999;286(5439):509-12. doi: 10.1126/science.286.5439.509. PubMed PMID: WOS:000083121200054.
16. Wang P, Lu J, Yu X. Identification of Important Nodes in Directed Biological Networks: A Network Motif Approach. *Plos One*. 2014;9(8). doi: 10.1371/journal.pone.0106132. PubMed PMID: WOS:000341127500112.
17. Rowland M, Fontana W, Deeds E. Crosstalk and Competition in Signaling Networks. *Biophysical Journal*. 2012;103(11):2389-98. doi: 10.1016/j.bpj.2012.10.006. PubMed PMID: WOS:000311963300018.
18. Siso-Nadal F, Fox JJ, Laporte SA, Hébert TE, Swain PS. Cross-talk between signaling pathways can generate robust oscillations in calcium and cAMP. *PLoS One*. 2009;4(10):e7189. doi: 10.1371/journal.pone.0007189. PubMed PMID: 19844582; PubMed Central PMCID: PMCPMC2760754.
19. Vajanapunich M, Schultz C, Tsien RY, Traynor-Kaplan AE, Pandol SJ. Cross-Talk between Calcium and cAMP-dependent Intracellular Signaling Pathways: Implications for Synergistic Secretion in T84 Colonic Epithelial Cells and Rat Pancreatic Acinar Cells. *Journal of Clinical Investigation*. 1995;96:386-93.

20. Choi M, Shi J, Jung SH, Chen X, Cho K-H. Attractor Landscape Analysis Reveals Feedback Loops in the p53 Network That Control the Cellular Response to DNA Damage. *Science Signaling*. 2012;5(251):1-13.
21. Ma'ayan A, Jenkins SL, Neves S, Hasseldine A, Grace E, Dubin-Thaler B, et al. Formation of regulatory patterns during signal propagation in a Mammalian cellular network. *Science*. 2005;309(5737):1078-83. doi: 309/5737/1078 [pii] 10.1126/science.1108876. PubMed PMID: 16099987; PubMed Central PMCID: PMC3032439.
22. Shmulevich I, Dougherty E, Mang W. From Boolean to probabilistic Boolean networks as models of genetic regulatory networks. *Proceedings of the Ieee*. 2002;90(11):1778-92. doi: 10.1109/JPROC.2002.804686. PubMed PMID: WOS:000179204700008.
23. Pliam JO. *An Algebraic Approach to Signal Flow Graph Theory*: University of Minnesota; 1992.
24. Liu YY, Slotine JJ, Barabási AL. Controllability of complex networks. *Nature*. 2011;473(7346):167-73. doi: 10.1038/nature10011. PubMed PMID: 21562557.
25. Stanley RP. *Topics in Algebraic Combinatorics* 2013. Available from: <http://www-math.mit.edu/~rstan/algcomb/algcomb.pdf>.
26. Sepulveda FJ, Parodi J, Peoples RW, Opazo C, Aguayo LG. Synaptotoxicity of Alzheimer beta amyloid can be explained by its membrane perforating property. *PLoS One*. 2010;5(7):e11820. doi: 10.1371/journal.pone.0011820. PubMed PMID: 20676404; PubMed Central PMCID: PMC3032439.

27. Fu H, Li W, Lao Y, Luo J, Lee NT, Kan KK, et al. Bis(7)-tacrine attenuates beta amyloid-induced neuronal apoptosis by regulating L-type calcium channels. *J Neurochem*. 2006;98(5):1400-10. doi: 10.1111/j.1471-4159.2006.03960.x. PubMed PMID: 16771827.
28. Snyder EM, Nong Y, Almeida CG, Paul S, Moran T, Choi EY, et al. Regulation of NMDA receptor trafficking by amyloid-beta. *Nat Neurosci*. 2005;8(8):1051-8. doi: nn1503 [pii] 10.1038/nn1503. PubMed PMID: 16025111.
29. Tong M, Arora M, Nichols RA. Role of Key Aromatic Residues in the Ligand-binding Domain of alpha7 Nicotinic Receptors in the Agonist Action of beta-Amyloid. *Journal of Biological Chemistry*. 2011;286(39):34373-81.
30. Alvarez AR, Godoy JA, Mullendorff K, Olivares GH, Bronfman M, Inestrosa NC. Wnt-3a overcomes beta-amyloid toxicity in rat hippocampal neurons. *Exp Cell Res*. 2004;297(1):186-96. doi: S0014482704000837 [pii] 10.1016/j.yexcr.2004.02.028. PubMed PMID: 15194435.
31. Berman D, Dall'Armi C, Voronov S, McIntire L, Zhang H, Moore A, et al. Oligomeric amyloid-beta peptide disrupts phosphatidylinositol-4,5-bisphosphate metabolism. *Nature Neuroscience*. 2008;11(5):547-54. doi: 10.1038/nn.2100. PubMed PMID: WOS:000255327300013.
32. Fogarty M, Downer E, Campbell V. A role for c-Jun N-terminal kinase 1 (JNK1), but not JNK2, in the beta-amyloid-mediated stabilization of protein p53 and induction of the apoptotic cascade in cultured cortical neurons. *Biochemical Journal*.

2003;371:789-98. doi: 10.1042/BJ20021660. PubMed PMID: WOS:000182733400016.

33. Um J, Nygaard H, Heiss J, Kostylev M, Stagi M, Vortmeyer A, et al. Alzheimer amyloid-beta oligomer bound to postsynaptic prion protein activates Fyn to impair neurons. *Nature Neuroscience*. 2012;15(9):1227-U85. doi: 10.1038/nn.3178. PubMed PMID: WOS:000308072600013.

34. Paula-Lima AC, Adasme T, SanMartin C, Sebollela A, Hetz C, Carrasco MA, et al. Amyloid-beta Peptide Oligomers Stimulate RyR-Mediated Ca²⁺ Release Inducing Mitochondrial Fragmentation in Hippocampal Neurons and Prevent RyR-Mediated Dendritic Spine Remodeling Produced by BDNF. *Antioxidants & Redox Signaling*. 2011;14(7):1209-23.

35. Shelat PB, Chalimoniuk M, Wang JH, Strosznajder JB, Lee JC, Sun AY, et al. Amyloid beta peptide and NMDA induce ROS from NADPH oxidase and AA release from cytosolic phospholipase A2 in cortical neurons. *J Neurochem*. 2008;106(1):45-55. doi: JNC5347 [pii] 10.1111/j.1471-4159.2008.05347.x. PubMed PMID: 18346200.

36. Bulbarelli A, Lonati E, Cazzaniga E, Re F, Sesana S, Barisani D, et al. TrkA pathway activation induced by amyloid-beta (Aβ). *Molecular and Cellular Neuroscience*. 2009;40(3):365-73. doi: 10.1016/j.mcn.2008.12.006. PubMed PMID: WOS:000263862000007.

37. Farias G, Godoy J, Hernandez F, Avila J, Fisher A, Inestrosa N. M1 muscarinic receptor activation protects neurons from beta-amyloid toxicity. A role for

- Wnt signaling pathway. *Neurobiology of Disease*. 2004;17(2):337-48. doi: 10.1016/j.nbd.2004.07.016. PubMed PMID: WOS:000224757500022.
38. Ma Q, Yang F, Calon F, Ubeda O, Hansen J, Weisbart R, et al. p21-activated kinase-aberrant activation and translocation in Alzheimer disease pathogenesis. *Journal of Biological Chemistry*. 2008;283(20):14132-43. doi: 10.1074/jbc.M708034200. PubMed PMID: WOS:000255728200067.
39. Morel M, Couturier J, Pontcharraud R, Gil R, Fauconneau B, Paccalin M, et al. Evidence of molecular links between PKR and mTOR signalling pathways in beta-amyloid neurotoxicity: Role p53, Redd1 and TSC2. *Neurobiology of Disease*. 2009;36(1):151-61.
40. Rodrigue J-P. *The Geography of Transport Systems* Hofstra University, New York, USA2015 [October 30, 2015]. Available from: <https://people.hofstra.edu/geotrans/eng/methods/betaindex.html>.
41. Analysis of Interdependence Structures: Networks University of Washington, Washington, USA2003 [cited 2015 October 30]. Available from: <https://faculty.washington.edu/krumme/207/networks.html>.
42. Bhalla U, Iyengar R. Emergent properties of networks of biological signaling pathways. *Science*. 1999;283(5400):381-7. doi: 10.1126/science.283.5400.381. PubMed PMID: WOS:000078067000046.
43. Venkatasubramaniam A. Engineering tools to analyze beta-amyloid's effect on cellular mechanisms linked to the neurodegeneration observed in Alzheimer's disease: University of Maryland, Baltimore County; 2014.

44. Bi X, Gall CM, Zhou J, Lynch G. Uptake and pathogenic effects of amyloid beta peptide 1-42 are enhanced by integrin antagonists and blocked by NMDA receptor antagonists. *Neuroscience*. 2002;112(4):827-40. PubMed PMID: 12088742.
45. Wang Q, Klyubin I, Wright S, Griswold-Prenner I, Rowan M, Anwyl R. alpha v integrins mediate beta-amyloid induced inhibition of long-term potentiation. *Neurobiology of Aging*. 2008;29(10):1485-93. doi: 10.1016/j.neurobiolaging.2007.03.018. PubMed PMID: WOS:000258817700005.
46. Kim S, Rhim H. Effects of Amyloid-beta Peptides on Voltage-Gated L-Type Ca(V)1.2 and Ca(V)1.3 Ca(2+) Channels. *Molecules and Cells*. 2011;32(3):289-94. doi: 10.1007/s10059-011-0075-x. PubMed PMID: WOS:000297627300011.
47. MacManus A, Ramsden M, Murray M, Henderson Z, Pearson HA, Campbell VA. Enhancement of (45)Ca(2+) influx and voltage-dependent Ca(2+) channel activity by beta-amyloid-(1-40) in rat cortical synaptosomes and cultured cortical neurons. Modulation by the proinflammatory cytokine interleukin-1beta. *J Biol Chem*. 2000;275(7):4713-8. PubMed PMID: 10671502.
48. Lacor P. Advances on the understanding of the origins of synaptic pathology in AD. *Current Genomics*. 2007;8(8):486-508. doi: 10.2174/138920207783769530. PubMed PMID: WOS:000254654000002.
49. Williamson R, Scales T, Clark BR, Gibb G, Reynolds CH, Kellie S, et al. Rapid tyrosine phosphorylation of neuronal proteins including tau and focal adhesion kinase in response to amyloid-beta peptide exposure: involvement of Src family protein kinases. *J Neurosci*. 2002;22(1):10-20. PubMed PMID: 11756483.

50. Kelly BL, Ferreira A. beta-Amyloid-induced dynamin 1 degradation is mediated by N-methyl-D-aspartate receptors in hippocampal neurons. *J Biol Chem.* 2006;281(38):28079-89. doi: 10.1074/jbc.M605081200. PubMed PMID: 16864575.
51. De Felice FG, Velasco PT, Lambert MP, Viola K, Fernandez SJ, Ferreira ST, et al. beta-amyloid Oligomers Induce Neuronal Oxidative Stress through an N-Methyl-D-aspartate Receptor-dependent Mechanism That Is Blocked by the Alzheimer Drug Memantine. *The Journal of Biological Chemistry.* 2007;282(15).
52. Reisberg B, Doody R, Stoffler A, Schmitt F, Ferris S, Mobius H, et al. Memantine in moderate-to-severe Alzheimer's disease. *New England Journal of Medicine.* 2003;348(14):1333-41. doi: 10.1056/NEJMoa013128. PubMed PMID: WOS:000181949100004.
53. Tucci P, Mhillaj E, Morgese MG, Colaianna M, Zotti M, Schiavone S, et al. Memantine prevents memory consolidation failure induced by soluble beta amyloid in rats. *Frontiers in Behavioral Neuroscience.* 2014;8(332).
54. Gu Z, Zhong P, Yan Z. Activation of muscarinic receptors inhibits beta-amyloid peptide-induced signaling in cortical slices. *J Biol Chem.* 2003;278(19):17546-56. doi: M209892200 [pii] 10.1074/jbc.M209892200. PubMed PMID: 12606559.
55. Gu Z, Cheng J, Zhong P, Qin L, Liu W, Yan Z. beta amyloid Selectively Impairs mGluR7 Modulation of NMDA Signaling in Basal Forebrain Cholinergic Neurons: Implication in Alzheimer's Disease. *The Journal of Neuroscience.* 2014;34(41).

56. Ferrell JE. Self-perpetuating states in signal transduction: positive feedback, double-negative feedback and bistability. *Curr Opin Cell Biol.* 2002;14(2):140-8. PubMed PMID: 11891111.
57. Tsai TY, Choi YS, Ma W, Pomerening JR, Tang C, Ferrell JE. Robust, tunable biological oscillations from interlinked positive and negative feedback loops. *Science.* 2008;321(5885):126-9. doi: 10.1126/science.1156951. PubMed PMID: 18599789; PubMed Central PMCID: PMC2728800.
58. Tyson JJ, Chen KC, Novak B. Sniffers, buzzers, toggles and blinkers: dynamics of regulatory and signaling pathways in the cell. *Current Opinion in Cell Biology.* 2003;15.
59. Thomas R. Laws for the dynamics of regulatory networks. *International Journal of Developmental Biology.* 1998;42.
60. Yasuda R, Nimchinsky EA, Scheuss V, Pologruto TA, Oertner TG, Sabatini B, et al. Imaging Calcium Concentration Dynamics in Small Neuronal Compartments *Science.* 2004;20.

Appendix 4A Reaction List

From Figure 8 in Yang et al, *Non-receptor-tyrosine Kinases Integrate Fast Glucocorticoid Signaling in Hippocampal Neurons*, J. Biol. Chem., 2013

	Equations	Reaction constants
1	$\text{CORT} + \text{GPCR} \leftrightarrow \text{GPCR}^*$	k1, k-1
2	$\text{GPCR}^* + \text{G}_{i/o} \leftrightarrow \text{G}_{i/o}^* + \text{GPCR}$	k2, k-2
3	$\text{G}_{i/o}^* + \text{PKA} \leftrightarrow \text{PKA}^* + \text{G}_{i/o}$	k3, k-3
4	$\text{G}_{i/o}^* + \text{PI3K} \leftrightarrow \text{PI3K}^* + \text{G}_{i/o}$	k4, k-4
5	$\text{G}_{i/o}^* + \text{PLC} \leftrightarrow \text{PLC}^* + \text{G}_{i/o}$	k5, k-5
6	$\text{PKA}^* + \text{PYK2}^* \leftrightarrow \text{PYK2} + \text{PKA}$	k6, k-6
7	$\text{PI3K}^* + \text{PKB} \leftrightarrow \text{PI3K} + \text{PKB}^*$	k7, k-7
8	$\text{PLC}^* + \text{PKC} \leftrightarrow \text{PKC}^* + \text{PLC}$	k8, k-8
9	$\text{PLC}^* + \text{InsPR} \leftrightarrow \text{InsPR}^* + \text{PLC}$	k9, k-9
10	$\text{InsPR}^* \rightarrow \text{Ca}^{2+}$	k10
11	$\text{Ca}^{2+} + \text{CaM} \leftrightarrow \text{CaM}^*$	k11, k-11
12	$\text{CaM}^* + \text{PKC} \leftrightarrow \text{PKC}^* + \text{CaM}$	k12, k-12
13	$\text{PKB}^* + \text{PYK2}^* \leftrightarrow \text{PYK2} + \text{PKB}$	k13, k-13
14	$\text{PKA}^* + \text{PYK2}^* \leftrightarrow \text{PYK2} + \text{PKA}$	k14, k-14
15	$\text{PYK2}^* + \text{Rho} \leftrightarrow \text{Rho}^* + \text{PYK2}$	k15, k-15
16	$\text{Rho}^* \rightarrow \text{Actin}$	k16
17	$\text{PYK2}^* + \text{Src} \leftrightarrow \text{PYK2} + \text{Src}^*$	k17, k-17
18	$\text{Src}^* + 2\text{PYK2} \leftrightarrow \text{Src} + 2\text{PYK2}^*$	k18, k-18
19	$\text{Src}^* + \text{Abl} \leftrightarrow \text{Src} + \text{Abl}^*$	k19, k-19
20	$\text{Abl} \rightarrow \text{Actin}$	k20
21	$\text{Src} + \text{PSD95} \leftrightarrow \text{Src} \text{ PSD95}$	k21, k-21
22	$\text{Abl} + \text{PSD95} \leftrightarrow \text{Abl} \text{ PSD95}$	k22, k-22
23	$\text{Src}^* + \text{NMDAR} \leftrightarrow \text{Src} + \text{NMDAR}^*$	k23, k-23
24	$\text{NMDAR}^* + \text{CaMKII} \leftrightarrow \text{NMDAR} + \text{CaMKII}^*$	k24, k-24
25	$\text{CaMKII}^* + \text{Raf} \leftrightarrow \text{CaMKII} + \text{Raf}^*$	k25, k-25
26	$\text{Raf}^* + \text{MEK} \leftrightarrow \text{Raf} + \text{MEK}^*$	k26, k-26
27	$\text{MEK}^* + \text{ERK} \leftrightarrow \text{ERK}^* + \text{MEK}$	k27, k-27
28	$\text{ERK}^* \rightarrow \text{mRNA}$	k28
29	$\text{AB} + \text{NMDAR} \leftrightarrow \text{NMDAR}^*$	k29, k-29

Appendix 4B List of Compounds

	List of compounds
1	CORT
2	GPCR
3	GPCR*
4	G _{i/o}
5	G _{i/o} *
6	PKA
7	PKA *
8	PI3K
9	PI3K*
10	PLC
11	PLC*
12	PYK2
13	PYK2*
14	PKB
15	PKB*
16	InsPR
17	InsPR*
18	Ca ²⁺
19	CaM
20	CaM*
21	PKC
22	PKC*
23	Rho
24	Rho*
25	Actin
26	Src
27	Src*
28	Abl
29	Abl*
30	Abl PSD95
31	Src PSD95
32	NMDAR
33	NMDAR*
34	CaMKII
35	CaMKII*
36	Raf
37	Raf*
38	MEK

39	MEK*
40	ERK
41	ERK*
42	mRNA
43	AB

Appendix 4C Reaction Equations

Equations
$\frac{d[GPCR]}{dt} = k_{-1}[GPCR^*] - k_1[GPCR][CORT] + k_2[G_{i/o}[GPCR^*] - k_{-2}[G_{i/o}^*][GPCR]$
$\frac{d[GPCR^*]}{dt} = k_1[GPCR][CORT] - k_{-1}[GPCR^*] + k_{-2}[G_{i/o}^*][GPCR] - k_2[G_{i/o}[GPCR^*]$
$\begin{aligned} \frac{d[G_{i/o}]}{dt} = & k_{-2}[G_{i/o}^*][GPCR] - k_2[G_{i/o}[GPCR^*] + k_3[G_{i/o}^*][PKA] - k_{-3}[PKA^*][G_{i/o}] \\ & + k_4[G_{i/o}^*][PI3K] - k_{-4}[PI3K^*][G_{i/o}] + k_5[G_{i/o}^*][PLC] - k_{-5}[PLC^*][G_{i/o}] \end{aligned}$
$\begin{aligned} \frac{d[G_{i/o}^*]}{dt} = & k_2[G_{i/o}[GPCR^*] - k_{-2}[G_{i/o}^*][GPCR] + k_{-3}[PKA^*][G_{i/o}] - k_3[G_{i/o}^*][PKA] + \\ & k_{-4}[PI3K^*][G_{i/o}] - k_4[G_{i/o}^*][PI3K] + k_{-5}[PLC^*][G_{i/o}] - k_5[G_{i/o}^*][PLC] \end{aligned}$
$\frac{d[PKA]}{dt} = k_{-3}[PKA^*][G_{i/o}] - k_3[G_{i/o}^*][PKA] + k_6[PKA^*][PYK2^*] - k_{-6}[PYK2][PKA]$
$\frac{d[PKA^*]}{dt} = k_3[G_{i/o}^*][PKA] - k_{-3}[PKA^*][G_{i/o}] + k_{-6}[PYK2][PKA] - k_6[PKA^*][PYK2^*]$
$\frac{d[PI3K]}{dt} = k_{-4}[PI3K^*][G_{i/o}] - k_4[G_{i/o}^*][PI3K] + k_7[PI3K^*][PKB] - k_{-7}[PKB^*][PI3K]$
$\frac{d[PI3K^*]}{dt} = k_4[G_{i/o}^*][PI3K] - k_{-4}[PI3K^*][G_{i/o}] + k_{-7}[PKB^*][PI3K] - k_7[PI3K^*][PKB]$
$\begin{aligned} \frac{d[PLC]}{dt} = & k_{-5}[PLC^*][G_{i/o}] - k_5[PLC][G_{i/o}^*] + k_8[PLC^*][PKC] - k_{-8}[PKC^*][PLC] \\ & + k_9[PLC^*][InsPR] - k_{-9}[InsPR^*][PLC] \end{aligned}$
$\begin{aligned} \frac{d[PLC^*]}{dt} = & k_5[PLC][G_{i/o}^*] - k_{-5}[PLC^*][G_{i/o}] + k_{-8}[PKC^*][PLC] - k_8[PLC^*][PKC] \\ & + k_{-9}[InsPR^*][PLC] - k_9[PLC^*][InsPR] \end{aligned}$
$\begin{aligned} \frac{d[PYK2]}{dt} = & k_6[PKA^*][PYK2^*] - k_{-6}[PYK2][PKA] + k_{13}[PKB^*][PYK2^*] \\ & - k_{-13}[PYK2][PKB] + k_{14}[PKA^*][PYK2^*] - k_{-14}[PYK2][PKA] + k_{15}[PYK2^*][Rho] \\ & - k_{-15}[Rho^*][PYK2] + k_{17}[PYK2^*][Src] - k_{-17}[PYK2][Src^*] + k_{-14}[PYK2][PKA] \\ & - k_{14}[PKA^*][PYK2^*] + k_{-15}[Rho^*][PYK2] - k_{15}[PYK2^*][Rho] \\ & + k_{-17}[PYK2][Src] - k_{17}[PYK2^*][Src] \\ & + k_{18} * 2[PYK2][Src^*] - k_{-18} * 2[PYK2^*][Src] \end{aligned}$

$\frac{d[PYK2^*]}{dt} = k_{-6}[PYK2][PKA] - k_6[PKA^*][PYK2^*] + k_{-13}[PYK2][PKB] - k_{13}[PKB^*][PYK2] \\ + k_{-14}[PYK2][PKA] - k_{14}[PKA^*][PYK2^*] + k_{-15}[Rho^*][PYK2] - k_{15}[PYK2^*][Rho] + k_{-17}[PYK2][Src^*] - k_{17}[PYK2^*][Src] \\ + k_{14}[PKA^*][PYK2^*] - k_{-14}[PYK2][PKA] + k_{15}[PYK2^*][Rho] - k_{-15}[Rho^*][PYK2] \\ + k_{17}[PYK2^*][Src] - k_{-17}[PYK2][Src] \\ + k_{-18} * 2[PYK2^*][Src] - k_{18} * 2[PYK2][Src^*]$
$\frac{d[PKC]}{dt} = k_{-8}[PKC^*][PLC] - k_8[PLC^*][PKC] + k_{-12}[PKC^*][CaM] - k_{12}[CaM^*][PKC]$
$\frac{d[PKC^*]}{dt} = k_8[PLC^*][PKC] - k_{-8}[PKC^*][PLC] + k_{12}[CaM^*][PKC] - k_{-12}[PKC^*][CaM]$
$\frac{d[PKB]}{dt} = k_{-7}[PI3K][PKB^*] - k_7[PI3K^*][PKB] + k_{13}[PKB^*][PYK2] \\ - k_{-13}[PYK2][PKB]$
$\frac{d[PKB^*]}{dt} = k_7[PI3K^*][PKB] - k_{-7}[PI3K][PKB^*] + k_{-13}[PKB][PYK2] \\ - k_{13}[PYK2][PKB^*]$
$\frac{d[InsPR]}{dt} = k_{-9}[InsPR^*][PLC] - k_9[PLC^*][InsPR]$
$\frac{d[InsPR^*]}{dt} = k_9[PLC^*][InsPR] - k_{-9}[InsPR^*][PLC] - k_{10}[InsPR]$
$\frac{d[Ca^{2+}]}{dt} = k_{10}[InsPR] + k_{-11}[CaM^*] - k_{11}[Ca^{2+}][CaM]$
$\frac{d[CaM]}{dt} = k_{-11}[CaM^*] - k_{11}[CaM][Ca^{2+}] + k_{12}[CaM^*][PKC] - k_{-12}[PKC^*][CaM]$
$\frac{d[CaM^*]}{dt} = k_{11}[CaM][Ca^{2+}] - k_{-11}[CaM^*] + k_{-12}[PKC^*][CaM] - k_{12}[CaM^*][PKC]$
$\frac{d[Rho]}{dt} = k_{-15}[Rho^*][PYK2] - k_{15}[PYK2^*][Rho]$
$\frac{d[Rho^*]}{dt} = k_{15}[PYK2^*][Rho] - k_{-15}[Rho^*][PYK2] - k_{16}[Rho^*]$
$\frac{d[Src]}{dt} = k_{-17}[PYK2][Src^*] - k_{17}[Src][PYK2^*] + k_{18} * 2[PYK2][Src^*] \\ - k_{-18} * 2[PYK2^*][Src] + k_{19}[Src^*][Abl] - k_{-19}[Src][Abl^*] \\ + k_{-21}[Src][PSD95] - k_{21}[Src][PSD95] + k_{23}[Src^*][NMDAR] \\ - k_{-23}[Src][NMDAR^*]$

$\frac{d[Src^*]}{dt} = k_{17}[Src[PYK2^*] - k_{-17}[PYK2[Src^*] + k_{-18} * 2[PYK2^*][Src]$ $- k_{18} * 2[PYK2[Src^*] + k_{-19}[Src[Abl^*] - k_{19}[Src^*][Abl]$ $+ k_{-23}[Src[NMDAR^*] - k_{23}[Src^*][NMDAR]$
$\frac{d[Abl]}{dt} = k_{-19}[Src[Abl^*] - k_{19}[Src^*][Abl] + k_{-22}[Abl_PSD95]$ $- k_{22}[Abl[PSD95] - k_{20}[Abl]$
$\frac{d[NMDAR]}{dt} = k_{-23}[Src[NMDAR^*] - k_{23}[Src^*][NMDAR] + k_{24}[NMDAR^*][CaMKII]$ $- k_{-24}[NMDAR[CaMKII^*] + k_{-29}[NMDAR^*] - k_{29}[AB[NMDAR]$
$\frac{d[NMDAR^*]}{dt} = k_{23}[Src^*][NMDAR] - k_{23}[Src^*][NMDAR] + k_{24}[NMDAR^*][CaMKII]$ $- k_{-24}[NMDAR[CaMKII] + k_{29}[AB[NMDAR] - k_{-29}[NMDAR^*]$
$\frac{d[Abl^*]}{dt} = k_{19}[Src^*][Abl] - k_{-19}[Src^*][Abl^*]$
$\frac{d[Actin]}{dt} = k_{20}[Abl]$
$\frac{d[Src_PSD95^*]}{dt} = k_{21}[Src[PSD95] - k_{-21}[Src_PSD95]$
$\frac{d[Abl_PSD95^*]}{dt} = k_{22}[Abl[PSD95] - k_{-22}[Abl_PSD95]$
$\frac{d[CaMKII]}{dt} = k_{-24}[NMDAR[CaMKII^*] - k_{24}[NMDAR^*][CaMKII]$ $+ k_{-25}[CaMKII[Raf^*] - k_{25}[CaMKII^*][Raf]$
$\frac{d[CaMKII^*]}{dt} = k_{24}[NMDAR^*][CaMKII] - k_{-24}[NMDAR[CaMKII^*]$ $+ k_{25}[CaMKII^*][Raf] - k_{-25}[CaMKII[Raf^*]$
$\frac{d[Raf]}{dt} = k_{-25}[CaMKII[Raf^*] - k_{25}[CaMKII^*][Raf] + k_{26}[Raf^*][MEK]$ $- k_{-26}[Raf[MEK]$
$\frac{d[Raf^*]}{dt} = k_{25}[CaMKII^*][Raf] - k_{-25}[CaMKII[Raf^*] + k_{-26}[Raf[MEK] - k_{26}[Raf^*][MEK]$
$\frac{d[MEK]}{dt} = k_{-26}[Raf[MEK^*] - k_{26}[Raf^*][MEK] + k_{27}[MEK^*][ERK] - k_{-27}[ERK^*][MEK]$
$\frac{d[MEK^*]}{dt} = k_{26}[Raf^*][MEK] - k_{-26}[Raf[MEK] + k_{-27}[ERK^*][MEK] - k_{27}[MEK^*][ERK]$
$\frac{d[ERK]}{dt} = k_{-27}[ERK^*][MEK] - k_{27}[MEK^*][ERK]$
$\frac{d[ERK^*]}{dt} = k_{27}[MEK^*][ERK] - k_{-27}[ERK^*][MEK] - k_{28}[ERK^*]$

$\frac{d[mRNA]}{dt} = k_{28}[ERK^*]$
$\frac{d[CORT]}{dt} = k_{-1}[GPCR^*] - k_1[CORT][GPCR]$
$\frac{d[AB]}{dt} = k_{-29}[NMDAR^*] - k_{29}[AB][NMDAR]$

Appendix 4D Initial Conditions

A β (nM)	Cortisterone (nM)
1	1
10	1
1	10
10	10

All other compounds were initiated at 1nM.

Appendix 4E Nodes in CA1 Hippocampal Neuron Not Involved in Feedback Loops

No loops											
AIR	BDNF	CITRON	ELK1	GLYCINE	KV12	MAP1	NT4	PSD95	SMAD4	DIABLO	VAMP
AZAR	BETAARRESTIN	CLATHRIN	ENKPHALIN	GLVR	KV14	MAP5	NWASP	PTP1B	SPAL		VDAC2
AB	BETACATENIN	COFILIN	EPH82	GLYT1	KV41	MCK	PS3	PKY2	SPECTRIN		VILIP
ACH	BIK	COLLAGEN	EPHRIN	GRAB	KV42	MLK	PA	RABGDI	SPHK		VITRONECTIN
ACTIN	BIM	CORTACTIN	ERBB	GRB10	KV43	MLK3	PAF	RACK	SPROUTY		VRK1
ADAPTIN	BIP	CPI17	ERK5	GRIT	L1	MNK1	PAFR	RADIXIN	SRC		WNT
ADDUCIN	BRIR	CRE	EZRIN	HCK	LAMINA	MOPR	PAR1	RAI	SRE		XIAP
ADENOSINE	BRADYKININ	CREM	FADD	HISTONEH3	LARG	MOR	PAR2	RAP1GAP	SRF		ZAP70
ADRISSCYCLASE	CSG	CRK	FAS	HMG14	LEF	MP1	PARP	RAP2	SRP54		
AKAP	CAD	CRMP2	FASCIN	HOMER	LEF1	mRNA	PAXILLIN	RB	SRPR		
ALPHA1AR	CADPR	CSK	FASL	HRS2	UMK	MSK1	PCAF	REELIN	SS		
ALPHA2AR	CAIN	CSP	FER	ICAD	LRP	MSK2	PD44A	RG2	SSTR1		
ALPHA27NACHR	CALBRAIN	D3R	FIBRINOGEN	IGF1	LYN	MST3	PD44B	RG4	SSTR2		
ALPHAHAECTININ	CALNEVIN	HATP	FIBRONECTIN	IGF1R	MIR	MTOR	PD44C	RHB	STAT		
AMISYN	CALPAIN	DCP1	FILAMIN	IKBA	M2R	MUNC18	PDGF	RHOGEF	SURVIVIN		
ANANDAMIDE	CALRETICULIN	DELTA_CATENIN	FIVERTIAR	IKBB	MAR	MUPP1	PDGFR	RIC	SYNAPTAPHYSIN		
ANKYRIN	CAMK1	DISHEVELED	FIVERTICR	IKK	MADD	MUSK	PDI	RICS	SYNDECAN		
ANP	CAMPASE	DLK	FIVERTIAR	IKB	MAP1A	MYOSIN	PDGEF	RIN	SYNAPTAPHILIN		
AP1	CARM1	DNAPK	FIVERT4R	INSULIN	MAP2	MYOSINPPASE	PERK	RIP	SYNPTROPHIN		
APC	CAS	DOPAMINE	FKBP	INTEGRIN	MAPK4PK2	MYOSIN	PHAP	S40	TAU		
APOLLON	CASK	DOPR	FLIP	IR	MARCKS	N41	PHAS	S6	TBR1		
APS	CASPASE6	DRE	FORKHEAD	IRS2	MBP	NAKED	PICK1	S60	TCF		
ARF	CASPASE7	DREAM	FOURBP1	JAK	MDM2	NASCENTCHAIN	PIN1	SEK	TFIIB		
AREGAP	CB1R	DYNAMIN	FRIZZLED	JIP	MEF2	NCAADHERIN	PKCZETA	SAM68	TFIID		
ARFGEF	CB2R	DYRK	FRK	JNK	MEK2	NCS1	PKD	S4P102	THC		
ARH2	CBL	EEF1A2	GABAAR	KAL	MEK4	NE	PKI	SAP97	TNFAIP3		
ARNO	CBP	EEF2	GALP	KALIRIN	MEK5	NEUROBROMIN	PKN	SEC61P	TNFR1		
ARPP38	CDK5	EEF2K	GALPHA12	KAR	MEK6	NFAT	PKR	SEC63P	TNIK		
ATF1	CEK1	EF46	GALPHA13	KCHIP4	MEK7	NF1	Potassium	SEK	TRADD		
ATF2	CERAMIDE	EGF	GALPHA40	KIR21	MEK1	NFKB	POTASSIUM	SEQUESTOSOME	TRAF2		
AXIN	CFOS	EIF2	GAP43	KIR23	MEK2	NFM	PP2C	SEROTONIN	TRE		
BAG1	CHLORIDE	EIF3	GDNF	KIR41	MEK3	NGF	PP5	SHANK	TRKB		
BAK	CHOLESTEROL	EIF4E	GIRK	KOPR	MEK4	NIK	PRESENILIN	SHP2	TRYPSIN		
BAP31	CIAP1	EIF4G	GKAP	KSR	MEK5	NOPR	PRK2	SIAH	TUBERIN		
BARK	CIAP2	EIF5	GLUTAMATE	KV11	MITF	NRG	PRMT1	SIVA1	TUBULIN		

Chapter 5: Conclusions and Future Work

5.1 Conclusions

“Grace builds on nature.” ~St. Thomas Aquinas

Alzheimer’s disease, being as complex as it is, certainly does not require that A β be the sole and primary cause of disease progression. However, it is clear that A β does play an important role in AD, and may well act as a trigger for processes leading to cognitive decline[1]. Therefore, understanding the mechanisms of A β ’s early action on neurons would be beneficial toward creating treatments that might cure or attenuate disease progression. In the work presented in the chapters of this dissertation, we worked to shed light on how to use computational modeling to discriminate between hypotheses and improve experimental design toward A β -neuron interaction discovery.

Starting with the hypotheses drawn from data produced by current experimental designs (see **Figure 5.1**); we sought in **Chapters 2 and 3** to develop tools for hypothesis discrimination (**Figure 5.2A**). With respect to hypothesis discrimination in **Chapter 2**, we developed a computational model neuron where were a priori hypotheses could be tested with experimentally testable results under three experimental conditions (**Figure 5.2B**). In the chapter, we tested two hypotheses

and generated results thereof: the block of the fast-inactivating potassium channel and the membrane conductance increase by $A\beta$. From our simulations, we were able to observe distinct behavior of the model outputs for each mechanism. This would therefore allow for distinguishing between these mechanisms under experimentally testable conditions. In this way, we provide information on the types of electrophysiology experiments that might further distinguish these two mechanisms. Importantly, this methodology can be readily extended to other amyloid-neuron interactions that involve an ion channel, ion-conducting receptor or membrane mechanism. This type of comparative modeling had not been done previously in the field with respect to generating hypotheses of $A\beta$ -neuron interactions.

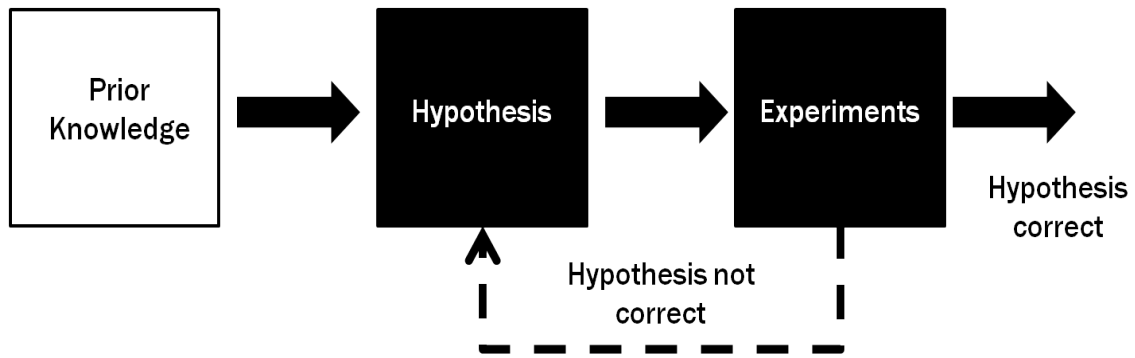
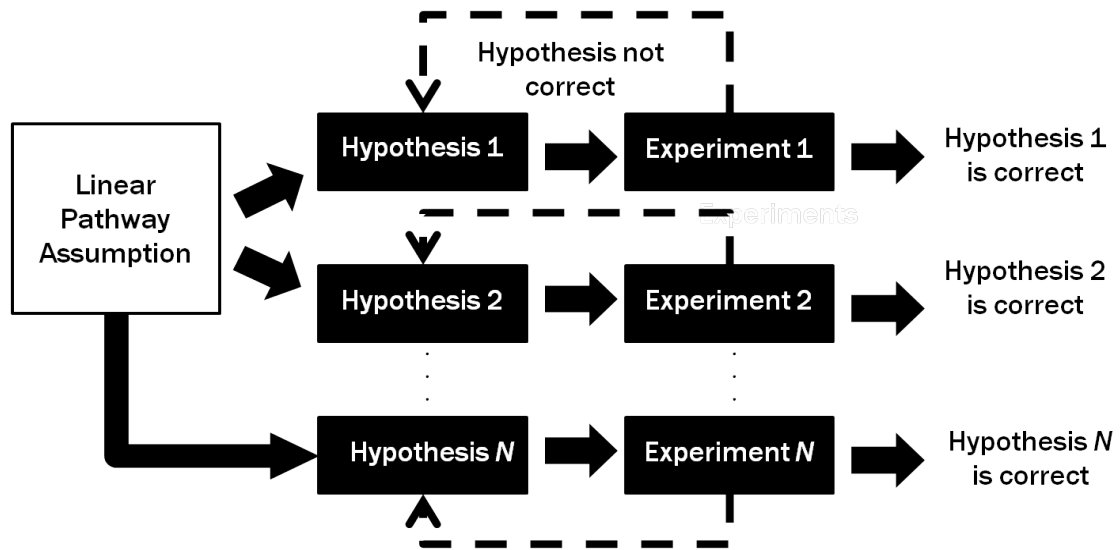


Figure 5.1: Flow chart of general experimental design. Given a set a prior knowledge in the field about the experimental system (white box), a hypothesis is formed. Experiments are designed based on this hypothesis in which the hypothesis of the experiment is proven either correct or incorrect. If proven correct by the particular set of experiments, the results of the experiments can be used to draw new conclusions about the system. If proven incorrect, then the hypothesis is revised, and experiment performed again. This loop continues until a hypothesis is proven correct.

In **Chapter 3**, our goal, as in **Chapter 2**, was to discriminate between hypotheses of A β -neuron interactions. In this case, we wanted to integrate literature-derived data and identify A β -neuron interactions through hypothesis discrimination (**Figure 5.3**). The premise behind our work was that intracellular signaling is complex, involving multiple intersecting pathways; therefore, a model that can discriminate between hypotheses of A β -induced signaling must include this complex. By starting with such a complex signaling model, we would be able to infer the correct set of A β -neuron interactions by comparing available literature data against model predictions and assessing the goodness-of-fit to the data. We made use of a reverse engineering algorithm, CellNOptR[2], which had never been used on a signaling network of the size and complexity as the one that we used[3]. The results of simulations were such that we were unable to identify a set of A β -neuron interactions that produce signals through the network that explains the data. From our investigation of the algorithm's results, we concluded that the dataset collected from the literature is not self-consistent. Here we will discuss a possible rationale for this lack of self-consistency in the data.

A typical experimental program usually includes a formulation of the hypothesis, testing the hypothesis via experimentation, and then interpretation of whether or not the hypothesis is correct. If it is incorrect, the hypothesis may be revised in light of new knowledge gained from the experiment (**Figure 5.1**). However, hypotheses come from a body of prior knowledge about the system. If revising this prior knowledge is not a part of the experimental feedback loop, then it

is possible that even revising the hypothesis will not give more consistent results (**Figure 5.2A**). This is a likely possibility for the lack of consensus on the mechanisms of A β -neuron interactions in current experimental literature. In **Chapter 3**, we explored, computationally, integration of a more complex network representation of intracellular signaling with literature-derived experimental data (**Figure 5.3**). By testing various hypotheses proposed in the literature for A β -neuron interactions, we attempted to discriminate between multiple hypotheses, *a posteriori*. However, by using the ‘pseudo-control’ of scrambled datasets and observing that CellNOptR consistently found better solutions on scrambled datasets than with the real dataset meant that the data that had been collected in the literature was not self-consistent. We propose that this is because the ‘experimental prior knowledge’ of the system used to formulate these hypotheses is limited and that the ‘experimental prior knowledge’ ought to be revised to reflect the complexity of the signaling network. We discussed this further in **Chapter 4**.



Which hypothesis do we accept?

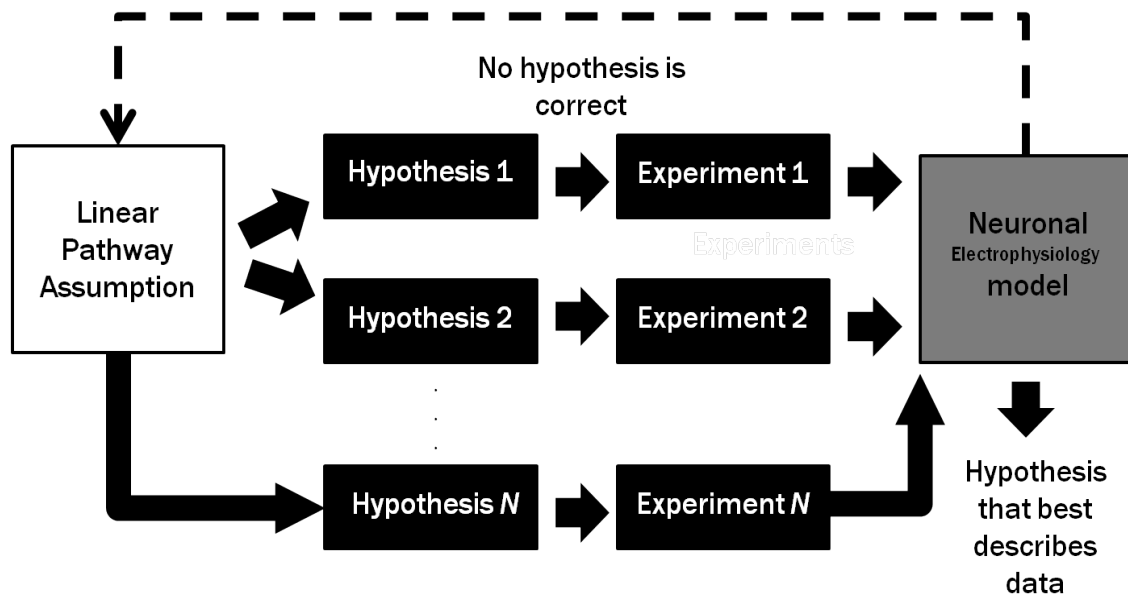


Figure 5.2: Flow charts of experimental design using the general approach and with a discriminatory step (Chapter 2). (A) Here, a linear pathway assumption (white box) is taken for prior knowledge of A β -neuron interactions and their subsequent effects on neuronal signaling. From this assumption, any number of hypotheses can be formed that correspond with a linear pathway assumption for A β -induced signaling. Next, each hypothesis is tested via experimentation according to the steps of the general experimental design approach described in **Figure 5.1**. If the results of each experiment, or even some experiments, are proven correct for that experimental preparation, then there exists a series of experimental results that are “correct”, but may not shed new light on the system, nor provide a consensus result. And in the same way as in **Figure 5.1**, when hypotheses are proven incorrect, they are revised, but not necessarily taking into account the results of the other experiments. The question is: which hypothesis do we accept? (B) Here, we have a similar schematic as in A, but with a discriminatory step (grey box). This step, in this case, consists of the neuronal electrophysiology model from **Chapter 2**. Using this neuronal electrophysiology model as a discriminatory step allows for testing multiple hypotheses and determining which one, under experimentally testable conditions, best explains the experimental data. If no hypothesis fits, then a feedback to the prior knowledge (linear pathway assumption) might indicate a need to adjust the basic assumptions about the system.

In **Chapter 4**, we provided a rationale for rejecting a linear pathway hypothesis for investigating A β -neuron interactions in favor of a more complex network representation (**Figure 5.4**). By performing network analysis on the CA1 hippocampal network, we were able to determine that this network is not comprised of a series of non-interacting pathways, but instead comprised of hub proteins, receptor trans-activated or inhibited pathways, cross-talk and feedback mechanisms. The ‘one disease/one pathway’ paradigm[4] produces an oversimplified ‘experimental prior knowledge’, which does not allow for adequate probing of the complex, underlying system. From our network analysis and kinetic modeling, we

identified motifs in which many of the proteins in the CA1 hippocampal neuron participate and examined their dynamic behavior. Based on this examination of dynamic behavior, we observed that feedback mechanisms exhibit non-linear dynamic behavior for both nodes participating in the feedback loop and those adjacent to the loop. We made recommendations for experiments based on a rubric for feedback mechanisms in the network. We also showed that over half of the proteins measured in our literature-derived dataset participate in a feedback mechanism. We believe this may be an explanation for the lack of self-consistency of the dataset, which was observed in **Chapter 3**. In order to use a Boolean modeling approach to represent a complex network with multiple feedback and feedforward control mechanisms, the data used to discriminate behavior must be selected outside of these loops. Alternatively, dynamic modeling approaches would have to be used; however, given the size of the network and the paucity of experimental parameters that adequately describe the kinetics of the signaling reactions, the ability to construct accurate dynamic models of the entire neuronal signaling network is impossible at this time.

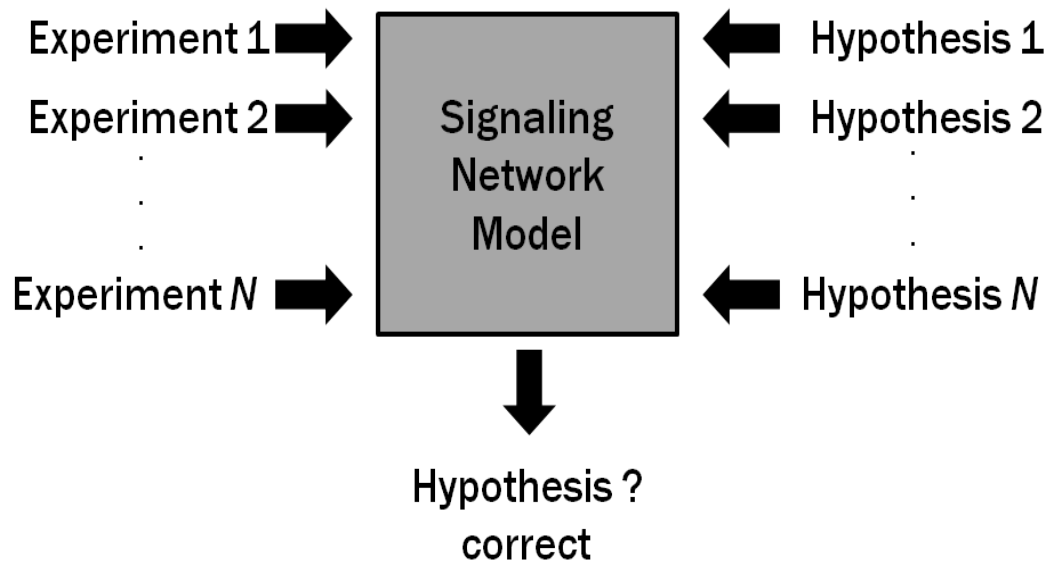


Figure 5.3: Flow chart of discriminatory step for discriminating between various hypotheses of A β -neuron interactions using a signaling network model (Chapter 3). In this flow chart, literature-derived experimental data and hypotheses for A β -neuron interactions are taken as inputs into a signaling network model. This is done according to the methods prescribed in Chapter 3 of this dissertation. By using a signaling network model on signaling data, given hypothesis of A β -neuron interaction, the hypothesis that produces the best fit to the data would, ideally, be determined. In this way, this type of model acts as a discriminatory step.

In conclusion, the search for a cure or a disease-ameliorating treatment for AD presses on. From the formulation of the Amyloid Cascade Hypothesis in 1992[5], there have been numerous experiments performed in order to understand A β 's action on neurons and its role in AD progression. From this hypothesis, multiple therapeutics have been designed to target A β and prevent the accumulation of fibrils and plaques; yet, these therapeutics have failed clinical trials[1, 4]. At last, after nearly thirty years of research, there is no consensus on the mechanisms underlying A β 's role in AD progression, or its mechanisms of neurotoxicity. Many researchers are now proposing that the Amyloid Cascade Hypothesis be abandoned because of the failure of clinical trials and the failure to demonstrate the link between A β plaque burden and cognitive decline[1, 6-9]. Though their arguments are compelling, the burden is still on these researchers to come up with another viable hypothesis, which can still explain A β 's neurotoxicity and the dependence of other features of AD, such as the hyper-phosphorylation of tau, on the presence of A β [10]. We suggest, instead, a two-fold computational approach to aid in the design of experiments. First, we have developed two computational tools, an electrophysiological neuronal model and an intracellular signaling model for discriminating between hypotheses for A β -neuron interactions, under experimentally testable conditions or utilizing existing experimental data. Second, by using network analysis to characterize and define network motifs present in a CA1 hippocampal network in terms of individual nodes, and in comparison to literature-derived data, we propose that experimental design move away from a linear pathway hypothesis (**Figure 5.2**) to a more complex

intracellular network, and to take this as a new ‘experimental prior knowledge’ (Figure 5.4). In this way, experimental hypotheses will take into account the actual underlying system; the measured component can be measured in a way consistent with its cellular context, and there can be greater control over experimental variables. Along with this, standardizations in experimental preparations, such as the use of the same A β species and aggregation states, measurement time point, and concentration, would also aid in bring consensus to a long-standing problem in AD research, which has hindered progress toward an adequate treatment for this disease.

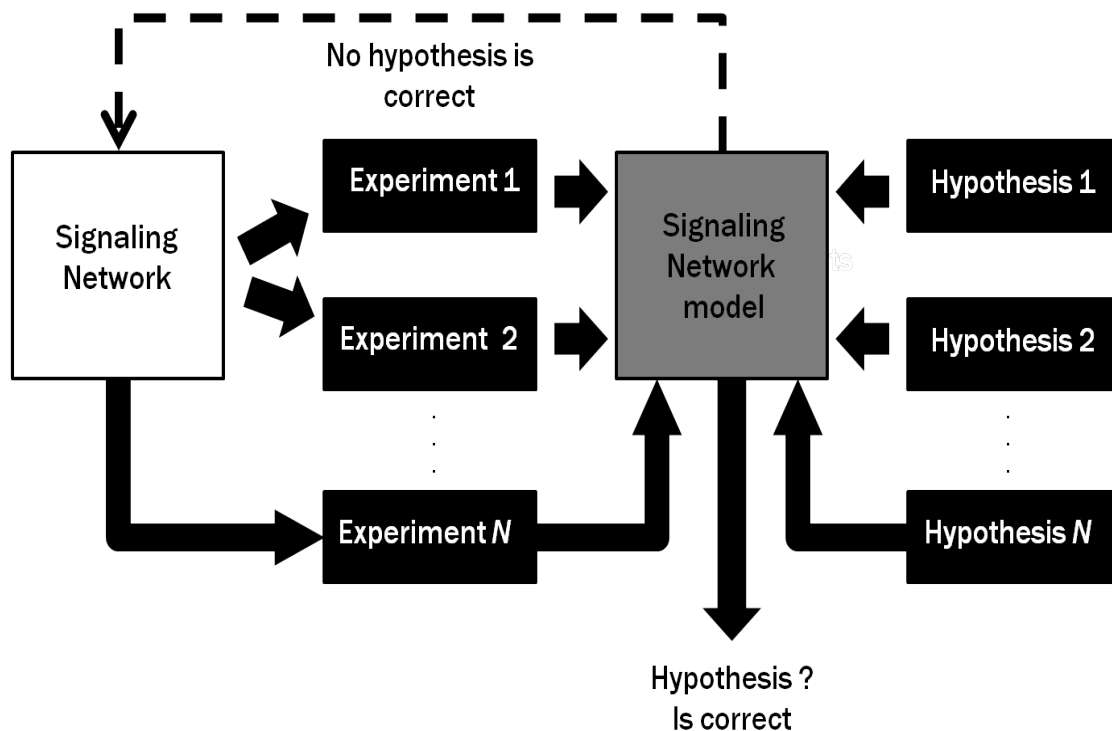


Figure 5.4: Flow chart of integrated methodology for experimentation and hypothesis discrimination. In Chapter 4, we justify a departure from a linear pathway assumption (Figure 5.2B) to a signaling network as prior knowledge (white box) for experimental design. Experiments are designed taking into account the cellular context of each protein to be part of the experiment. The signaling network model (Figure 5.3) is used as a discriminatory step (grey box) where experimental results are compared against N hypotheses for A β -neuron interactions. Again, as in Figure 5.3, ideally the hypothesis with the best fit to the data would be identified. If not, then the prior knowledge about the system could be revised.

5.2 Future Work

Much of what has been stated about the future work for this dissertation has been stated in the chapters, and so the details will not be reiterated here. Instead, we will present an outline of possible future work and the rationale behind this work. It is worthwhile to keep moving on toward understanding A β 's mechanism of action on neurons from an intracellular signaling perspective. In this way, once pathways are known, more experimentation to identify the kinetics of the system (and especially the parameters) can be done so that a kinetic model of the system can be developed. Then, the electrophysiological model in **Chapter 2** could be combined with such a kinetic model of A β -induced signaling in order to integrate the dynamics at the cell surface with the dynamics of changes in intracellular signaling.

In order to improve on the work toward inferring A β -neuron interactions from intracellular signaling data (pending that data is self-consistent), we also need to know what is the minimum dataset required to identify a network topology using a reverse-engineering algorithm such as CellNOptR. In **Chapter 3**, we described some preliminary work done in collaboration with the Erill lab in UMBC Biological Science Department to create a Bayesian algorithm to estimate the probability of finding a hypothetical network that is consistent with the experimental data given a partial dataset. Debugging and testing of this algorithm on a real experimental dataset and the CA1 hippocampal network would be needed in order to continue this work.

In **Chapter 4**, we proposed an experimental rubric based on feedback mechanisms that exist in the CA1 hippocampal network. By utilizing this rubric, an experimentalist, desiring to observe the effects of A β on a particular protein in a particular pathway would have more contextual knowledge of network motifs that might affect the dynamic behavior of the protein, such as feedback. However, there are other experimental designs that could be modeled using network analysis, and in particular the Signal Flow Method, of **Chapter 4**. One such design suggested was an input-hub protein response. Because these hub proteins are structurally highly connected in networks, it is likely that their response most often correspond to the dynamics of input signaling. Thus, monitoring these input-hub response trends could provide another experimental design with which the experimentalist can infer A β -neuron interactions. Using our Signal Flow Method, we can simulate trends for input-hub protein responses that the experimentalist might expect when monitoring these responses. In order to continue this work, it would be necessary to define all of the hub proteins in the network, and then simulate all input-hub response trends, similar to those shown in Figures 4.12-4.18 in **Chapter 4**.

5.3 References

1. Karran E, Mercken M, De Strooper B. The amyloid cascade hypothesis for Alzheimer's disease: an appraisal for the development of therapeutics. *Nat Rev Drug Discov.* 2011;10(9):698-712. doi: 10.1038/nrd3505. PubMed PMID: 21852788.

2. Saez-Rodriguez J, Alexopoulos L, Epperlein J, Samaga R, Lauffenburger D, Klamt S, et al. Discrete logic modelling as a means to link protein signalling networks with functional analysis of mammalian signal transduction. *Molecular Systems Biology*. 2009;5. doi: 10.1038/msb.2009.87. PubMed PMID: WOS:000273359200002.
3. Ma'ayan A, Jenkins SL, Neves S, Hasseldine A, Grace E, Dubin-Thaler B, et al. Formation of regulatory patterns during signal propagation in a Mammalian cellular network. *Science*. 2005;309(5737):1078-83. doi: 309/5737/1078 [pii] 10.1126/science.1108876. PubMed PMID: 16099987; PubMed Central PMCID: PMC3032439.
4. Mullane K, Williams M. Alzheimer's therapeutics: Continued clinical failures question the validity of the amyloid hypothesis-but what lies beyond? *Biochemical Pharmacology*. 2013;85:289-305.
5. Hardy JA, Higgins GA. Alzheimer's disease: the amyloid cascade hypothesis. *Science*. 1992;256(5054):184-5. PubMed PMID: 1566067.
6. Drachman DA. The amyloid hypothesis, time to move on: Amyloid is the downstream result, not cause, of Alzheimer's disease. *Alzheimers Dement*. 2014;10(3):372-80. doi: 10.1016/j.jalz.2013.11.003. PubMed PMID: 24589433.
7. Herrup K. The case for rejecting the amyloid cascade hypothesis. *Nature Neuroscience*. 2015;18(6):794-9. doi: 10.1038/nn.4017. PubMed PMID: WOS:000355218300006.
8. Reitz C. Alzheimer's Disease and the Amyloid Cascade Hypothesis: A Critical Review. *International Journal of Alzheimer's Disease*. 2012;2012.

9. Davis JN, Chisholm JC. The 'amyloid cascade hypothesis' of AD: decoy or real McCoy? *Trends Neurosci.* 1997;20(12):558-9. PubMed PMID: 9416666.
10. Williamson R, Scales T, Clark BR, Gibb G, Reynolds CH, Kellie S, et al. Rapid tyrosine phosphorylation of neuronal proteins including tau and focal adhesion kinase in response to amyloid-beta peptide exposure: involvement of Src family protein kinases. *J Neurosci.* 2002;22(1):10-20. PubMed PMID: 11756483.

Appendix

Location on computer for files related to each chapters in this dissertation

Computer located in Castellanos's lab (Room 335A)

Dell Precision T5500; Product key: BF4GB-93XGW-CQGQB-28GD4-W27QR

Username: NatashaWilson

Password: w@ashington

Chapter 1

C:\Users\Natasha Workstation\Desktop\Prophetic Project\It is time to
graduate Natasha\Papers\Chapter 1

Chapter 2

Literature and journal article preparations

C:\Users\Natasha Workstation\Desktop\Papers and Writing

Computational model

C:\Users\Natasha Workstation\Desktop\Oral Qualifiers Fall 2011\Neuron
model

Chapter 3

C:\Users\Natasha Workstation\Desktop\Prophetic Project\Computational

Chapter 4

Signal Flow Method

C:\Users\Natasha Workstation\Desktop\Prophetic
Project\Computational\Paper 1

Small Kinetic Model

C:\Users\Natasha Workstation\Desktop\Prophetic
Project\Computational\Paper 1\Small kinetic model

Chapter 5

C:\Users\Natasha Workstation\Desktop\Prophetic Project\It is time to
graduate Natasha\Papers\Chapter 5

Other information:

Proposal

C:\Users\Natasha Workstation\Desktop\Prophetic Project\Proposal

Experimental protocol

Calcium fluorescence and viability assays

C:\Users\Natasha Workstation\Desktop\Oral Qualifiers Fall
2011\Experiments

PKC fluorescence probe

C:\Users\Natasha Workstation\Desktop\Prophetic Project\Experiments

Undergraduate student work

C:\Users\Natasha Workstation\Desktop\Prophetic Project\Undergraduate
Projects

John Hopkins Cancer project

C:\Users\Natasha Workstation\Desktop\Prophetic Project\Cancer Project

